Optical Constants and Inelastic Electron-Scattering Data for 17 Elemental Metals

Wolfgang S. M. Werner[a)]
Institut für Allgemeine Physik, Vienna University of Technology, Wiedner Hauptstraße 8–10, A 1040 Vienna, Austria

Kathrin Glantschnig
Chair of Atomistic Modelling and Design of Materials, University of Leoben, Franz-Josefstraße 18, A 8700 Austria and Institut für Physik, Fachbereich Theoretische Physik, University of Graz, Universitätsplatz 5, A 8010 Graz, Austria

Claudia Ambrosch-Draxl
Chair of Atomistic Modelling and Design of Materials, University of Leoben, Franz-Josefstraße 18, A 8700 Austria

(Received 27 January 2009; accepted 16 September 2009; published online 10 December 2009)

Two new sets of optical data, i.e., values for the real (ε_1) and imaginary (ε_2) parts of the complex dielectric constant as well as the energy loss function (ELF) ($\mathrm{Im}\{-1/\varepsilon\}$), are presented for 16 elemental metals (Ti, V, Fe, Co, Ni, Cu, Zn, Mo, Pd, Ag, Ta, W, Pt, Au, Pb, and Bi) and 1 semimetal (Te) and are compared to available data in the literature. One data set is obtained from density functional theory (DFT) calculations and gives ε from the infrared to the soft x-ray range of wavelengths. The other set of optical constants, derived from experimental reflection electron energy-loss spectroscopy (REELS) spectra, provides reliable optical data from the near-ultraviolet to the soft x-ray regime. The two data sets exhibit very good mutual consistency and also, overall, compare well with optical data found in the literature, most of which were determined several decades ago. However, exceptions to this rule are also found in some instances, some of them systematic, where the DFT and REELS mutually agree significantly better than with literature data. The accuracy of the experimental data is estimated to be better than 10% for the ELF and ε_2 as well as for ε_1 for energies above 10 eV. For energies below 10 eV, the uncertainty in ε_1 in the experimental data may exceed 100%, which is a consequence of the fact that energy-loss measurements mainly sample the absorptive part of the dielectric constant. Electron inelastic-scattering data, i.e., the differential inverse inelastic mean free path (IMFP) as well the differential and total surface excitation probabilities are derived from the experimental data. Furthermore, the total electron IMFP is calculated from the determined optical constants by employing linear response theory for energies between 200 and 3000 eV. In the latter case, the consistency between the DFT and the REELS data is excellent (better than 5% for all considered elements over the entire energy range considered) and a very good agreement with earlier results is also obtained, except for a few cases for which the earlier optical data deviate significantly from those obtained here. © *2009 American Institute of Physics*. [doi:10.1063/1.3243762]

Key words: dielectric function; density functional theory; electron scattering.

CONTENTS

[a)]Electronic mail: werner@iap.tuwien.ac.at.

List of Tables

List of Figures

1. Introduction

The response of a solid to an external electromagnetic perturbation determines many important fundamental and technological properties of a material and its surface. The susceptibility of the solid to become polarized by incoming light or charged particles is described by the frequency- (ω) and momentum- (q) dependent dielectric function $\varepsilon(\omega,q)$ which can be measured by probing a surface with elementary particles such as photons[1–4] or electrons.[5,6] Energy-loss measurements with electrons mainly sample the energy loss function (ELF),

$$\mathrm{Im}\left\{-\frac{1}{\varepsilon}\right\}=\frac{\varepsilon_2}{\varepsilon_1^2+\varepsilon_2^2}, \tag{1}$$

where ε_1 and ε_2 are the real (dispersive) and imaginary (absorptive) parts of the dielectric function, respectively. These quantities are related to the index of refraction n and extinction coefficient k via

$$\varepsilon_1=n^2-k^2,$$

$$\varepsilon_2=2nk. \tag{2}$$

Since the rest mass of the photon is zero, conservation of energy and momentum requires that the particle be absorbed during an interaction with the solid-state electrons in the overwhelming majority of cases. This implies that optical spectra can be divided into regions of high opacity and transparency for which accurate simultaneous determination of the absorptive (imaginary) and dispersive (real) parts of the

dielectric function is not straightforward. Furthermore, to experimentally cover a wide wavelength range, different sources and monochromators as well as other optical components are needed. In the case of transmission experiments, accessing a wide wavelength range over which ε varies significantly generally also requires measurements on a series of samples with different thicknesses. Therefore, optical data found in the literature usually consist of a synthesis of various data sets employing a Kramers-Kronig analysis.[7] Investigating the dielectric response of a nanostructure down to small dimensions is also problematic since photons are rather difficult to focus. Measurements of the optical constants by means of light scattering have in the past not always been carried out under ultrahigh vacuum (UHV) conditions which implies that the investigated surfaces were not always well defined.

The drawbacks mentioned above for measurements of the optical response using photons can be avoided by using electrons as probing particles instead: First of all, they are easy to focus in the sub-nanometer range. Furthermore, electron scattering experiments are routinely carried out in UHV equipment where sample cleaning and monitoring facilities are available and it is easy to access the spectral range between the (near) infrared and soft x-ray regions in a single experiment. Both electron energy loss spectroscopy in transmission[5] and reflection[8,9] can be used for this purpose, the latter technique being the simplest from the experimental point of view, in particular, when applied to nanostructured surfaces.

An inherent drawback of using probing particles with a finite rest mass is that they experience multiple scattering since in this case energy and momentum conservation makes it highly unlikely for them to be absorbed during an interaction. Therefore, features due to multiple scattering need to be eliminated from the raw experimental data by means of an appropriate deconvolution procedure properly accounting for the physics governing the transport of the electrons from the source to the detector. The main processes that need to be considered in this connection are deflections arising in the course of an elastic interaction[10] as well as energy losses deep inside the solid ("volume" or "bulk" excitations[11]) and additional losses that may occur during the crossing of the vacuum-solid boundary ("surface" excitations[12]).

For electron energy-loss spectra measured in the transmission electron microscope (TEM), procedures for spectrum deconvolution have been developed several decades ago[1,5,6] and the measurement of optical data in the TEM is nowadays a matter of routine. Such measurements need to be carried out at high enough energies of several hundreds of a keV where the mean free path for inelastic scattering is of the order of the thickness of films that can be prepared in practice. In this energy regime the loss spectrum is dominated by volume energy losses, since the time it takes for an electron to cross the solid-vacuum boundary is too small to give rise to surface excitations to a significant extent.

Reflection electron energy-loss spectroscopy (REELS) represents an attractive alternative to energy-loss measurements in transmission since the experiment is extremely simple,[13,14] In many an UHV apparatus the required components are available, and REELS can therefore be conveniently combined with other surface characterization techniques. Owing to the energy dependence of the electron reflection coefficient, which decreases rapidly above several keV, energy-loss measurements in reflection are most easily carried out in the medium energy range (100 eV–10 keV). Then, the low-loss part of the spectrum is dominated by surface excitations, a fact which severely complicates data analysis, in particular, the elimination of plural scattering effects from the raw data.

Existing sources of optical constants[1–4] are often a synthesis of experimental and theoretical data and the reliability of these data sets below the soft x-ray regime is not well known. Self-consistent field calculations have been used for some decades to determine ε in the hard x-ray range for *free atoms*.[2–4] On the other hand, solid-state calculations based on density functional theory (DFT) beyond the ground state that allow one to access the soft x-ray range and below have only become available recently.[15–18] While DFT has become a standard tool for describing material properties in a parameter-free manner, as far as ground state properties are concerned, the treatment of excited states with the same reliability and hence predictive power as the ground state is still a challenge; nevertheless significant progress has been achieved during the past years such that theoretical spectroscopy has become an emerging field in solid-state theory.

In the present paper, two new sets of optical data for 17 elemental materials are presented. One is derived from DFT calculations made for energies between the infrared and soft x-ray regions. The other set is extracted from experimental energy-loss measurements in reflection between the visible and soft x-ray ranges. The method to extract the dielectric function from REELS is outlined and its consistency and accuracy are analyzed in detail. A comparison with earlier results compiled in Palik's books[1] is performed. Generally, very good consistency is found between the DFT calculations and the present measurements; while the overall agreement with Palik's data is satisfactory, significant differences are observed in several instances, some of these deviations being systematic. This comparison proves the reliability of DFT results which therefore represent a novel way to theoretically obtain information of the response of a solid to an electromagnetic perturbation. Furthermore the results demonstrate that REELS, owing to its experimental simplicity, is a very attractive alternative to the other experimental techniques to obtain information on optical constants of solids addressed above.

2. Density Functional Theory Calculations

DFT can be regarded as the *standard model* in computational solid-state science. Especially ground state properties such as equilibrium volumes, atomic positions, phonon frequencies, and elastic constants are obtained with high accuracy. Since the Hohenberg-Kohn theorem[19] is valid for the

ground state only, the interpretation of the Kohn-Sham (KS) eigenstates in terms of quasiparticle energies and wave functions should be handled with care. This is particularly true for semiconductors, which suffer from the band-gap problem. In contrast, for metals the KS band structure can be taken as a good approximation to the quasiparticle energies, where this approximation has proven successful for a variety of materials.

The electronic structure is obtained by solving the KS equations with the linearized augmented planewave method using the WIEN2K code.[20] It is based on a decomposition of the unit cell (with volume Ω) into two different volume types, the nonoverlapping muffin-tin spheres centered at the atomic positions and the interstitial region. In these areas appropriate basis sets are used.[21–23] In the interstitial region a plane wave basis is adopted to account for the moderate change of the wave functions in this part of the unit cell:

$$\phi_{\vec{k}+\vec{G}}(\vec{r}) = \frac{1}{\sqrt{\Omega}} e^{i(\vec{k}+\vec{G})\cdot\vec{r}}, \quad \vec{r} \in I. \tag{3}$$

The rapid oscillations of the wave functions close to the atom cores are described by atomiclike basis functions inside the muffin-tin spheres,

$$\phi_{\vec{k}+\vec{G}}(\vec{S}_\alpha + \vec{r}) = \sum_{lm} [A^\alpha_{lm}(\vec{k}+\vec{G}) u^\alpha_l(r,E_l) + B^\alpha_{lm}(\vec{k}+\vec{G}) \dot{u}^\alpha_l(r,E_l)] Y_{lm}(\hat{r}), \quad |\vec{r}| \leqslant R_\alpha, \tag{4}$$

where $\vec{S}_\alpha$ represents the position of the atomic nucleus α and $R_\alpha = R_{\mathrm{MT}}$ is the radius of the muffin-tin sphere. $u^\alpha_l(r,E_l)$ are the solutions of the radial Schrödinger equation for given linearization energies E_l, $\dot{u}^\alpha_l(r,E_l)$ denote the corresponding energy derivatives, and $Y_{lm}(\hat{r})$ represent spherical harmonics. The expansion coefficients $A^\alpha_{lm}(\vec{k}+\vec{G})$ and $B^\alpha_{lm}(\vec{k}+\vec{G})$ are obtained by the condition that the two basis sets match in value and slope at the sphere boundaries.

To improve the description of semicore states, local orbitals (LOs) can be introduced as additional basis functions. Their form is similar to that of the basis function inside the muffin-tin sphere,

$$\phi_{\mathrm{LO}}(\vec{S}_\alpha + \vec{r}) = \sum_{lm} [\tilde{A}^\alpha_{lm} u^\alpha_l(r,E_l) + \tilde{B}^\alpha_{lm} \dot{u}^\alpha_l(r,E_l) + \tilde{C}^\alpha_{lm} u^\alpha_l(r,E_{lo})] Y_{lm}(\hat{r}), \tag{5}$$

with the additional linearization energy E_{lo} corresponding to the semicore states. The variational parameters $\tilde{A}^\alpha_{lm}$, $\tilde{B}^\alpha_{lm}$, and $\tilde{C}^\alpha_{lm}$ are determined by the conditions that the basis set must be normalized and that the LO should be zero in value and slope at the sphere boundary. Thus, LOs are totally confined inside the atomic spheres.

For all elemental solids presented in this work, exchange and correlation effects were treated by the generalized gradient approximation (GGA) parametrized by Perdew *et al.*[24] Spin-polarized calculations were performed for the ferromagnetic elements Fe, Ni, and Co. For Au, Pb, Pd, Pt, and W, spin-orbit (SO) interaction was taken into account via a second variational scheme on top of the GGA calculation. In this procedure, the KS equations are solved neglecting SO coupling at first; the wave functions obtained in this way form the basis set for the eigenvalue problem including the SO part of the Hamiltonian.[25] Structural and convergence parameters used in the electronic structure and optical calculations are listed in Table 1.

We calculate the dielectric response within the random phase approximation, where the excited electron and the created hole are regarded to be independent (independent particle approximation). Due to the effective screening of the Coulomb interaction this approach is well suited for metals. The imaginary part of the interband dielectric function is given by

$$\frac{\hbar^2 e^2}{\pi m^2 \omega^2} \sum_{n,n'} \int_{\mathbf{k}} p_{n',n,\mathbf{k}} p_{n',n,\mathbf{k}} \times [f(\varepsilon_{n,\mathbf{k}}) - f(\varepsilon_{n',\mathbf{k}})] \delta(\varepsilon_{n',\mathbf{k}} - \varepsilon_{n,\mathbf{k}} - \omega) d\mathbf{k}, \tag{6}$$

where $p_{n',n,\mathbf{k}}$ is the momentum matrix element between bands n and n' for a $\mathbf{k}$ point in the irreducible wedge of the Brillouin zone (BZ) and $f(\varepsilon_{n,\mathbf{k}})$ is the occupation number of the corresponding single particle state with energy $\varepsilon_{n,\mathbf{k}}$. The intraband contributions ($n=n'$) are described by a Drude-like lineshape with a lifetime broadening of 0.1 eV. The same value is also used for the interband spectra. To obtain the real part of the dielectric function a Kramers-Kronig transformation is performed. The details regarding this framework are described in Ref. 17. The BZ integration is carried out by the improved tetrahedron method.[26]

In the following, a procedure for analyzing features in the optical spectra is presented, with silver serving as an example. Figure 1 shows the complex dielectric function for two different values of the intraband broadening Γ_{dr}. $\Gamma_{dr}=0.02$ eV corresponds to the experimentally determined lifetime τ of 31×10^{-15} s (Ref. 27) and $\Gamma_{dr}=0.1$ eV is a universal value chosen for all elemental metals in this work. The interband broadening Γ_{inter} was set to 0.1 eV. As can be seen from Fig. 1, the intraband broadening affects the low-energy region up to 2.6 eV. Because of a higher overlap between the interband and intraband contributions for $\Gamma_{dr}=0.1$ eV, the first minimum is narrowed and decreases in depth. The spectrum shows two interesting features in the energy range up to 25 eV, ie., a strong peak at 4 eV and a broad structure around 20 eV. To investigate the origin of these two structures, the oscillator strength of transitions contributing to a given energy range is calculated for each $\mathbf{k}$ point in the BZ by

$$\mathrm{O}_E(\mathbf{k}) = \sum_{n,n'} \int_{\omega=E_{\min}}^{E_{\max}} dE p_{n',n,\mathbf{k}} p_{n',n,\mathbf{k}} \delta(\varepsilon_{n',\mathbf{k}} - \varepsilon_{n,\mathbf{k}} - \omega), \tag{7}$$

where the sum runs over all band combinations n,n' for which the related transition energies lie within the energy range of interest, i.e., band energies fulfill

TABLE 1. Structural and convergence parameters: For each element, crystal structure and lattice parameters are given. The angles between the basis vectors different from 90° are $\gamma=120°$ for the trigonal Te lattice and $\gamma=110.33°$ for the monoclinic Bi case. In addition, the **k** meshes used in the calculation of the electronic structure and the optical spectra, the radius of the muffin-tin spheres R_{MT}, and the RK_{max} value, i.e., the product of the smallest muffin-tin radius and the plane wave cutoff, are listed

Material	Crystal structure	Lattice parameters			**k** mesh		R_{MT} (a.u.)	RK_{max}
		a (a.u.)	b (a.u.)	c (a.u.)	scf	Optic		
Ag	fcc	7.7290	7.7290	7.7290	34×34×34	58×58×58	2.5	11
Au	fcc	7.7101	7.7101	7.7101	31×31×31	58×58×58	2.5	11
Cu	fcc	6.8219	6.8219	6.8219	31×31×31	58×58×58	2.1	10
Ni	fcc	6.6518	6.6518	6.6518	34×34×34	58×58×58	2.25	11
Pb	fcc	9.3541	9.3541	9.3541	31×31×31	58×58×58	2.5	11
Pt	fcc	7.4077	7.4077	7.4077	31×31×31	58×58×58	2.5	11
Pd	fcc	7.3510	7.3510	7.3510	31×31×31	58×58×58	2.5	11
Fe	bcc	5.4235	5.4235	5.4235	34×34×34	58×58×58	2.33	10
Mo	bcc	5.9526	5.9526	5.9526	34×34×34	58×58×58	2.5	10
Ta	bcc	6.2361	6.2361	6.2361	31×31×31	53×53×53	2.5	11
V	bcc	5.7259	5.7259	5.7259	34×34×34	58×58×58	2.4	10.5
W	bcc	5.9715	5.9715	5.9715	34×34×34	58×58×58	2.5	11
Co	hcp	4.7432	4.7432	7.6912	29×29×15	62×62×33	2.3	11
Ti	hcp	5.5747	5.5747	8.8439	23×23×11	59×59×32	2.6	10
Zn	hcp	5.0359	5.0359	9.3481	34×34×16	70×70×32	2.4	10.5
Bi	Monoclinic	6.2437	12.6120	11.5595	20×9×20	42×18×42	2.5	11
Te	Trigonal	8.4229	8.4229	11.2042	19×19×12	40×40×26	2.5	11

$$E_{\min} \leqslant \epsilon_{n',\mathbf{k}} - \epsilon_{n,\mathbf{k}} \leqslant E_{\max}. \quad (8)$$

The resulting oscillator strengths $O_E(\mathbf{k})$ are visualized in Fig. 2 for selected planes in the BZ, depicted in the first row. In the second row, the oscillator strengths for transitions contributing to the feature around 4 eV are displayed, where dark gray areas correspond to high oscillator strengths. **K** points with k_z values smaller than $0.5\pi/a$ in a ring close to the BZ boundaries are dominant. High contributions are found in the region around the X points (see the first and third panels). They can be ascribed to transitions from valence bands of d character to p-like conduction bands. Moreover, **k** points in an area around the L point are involved in

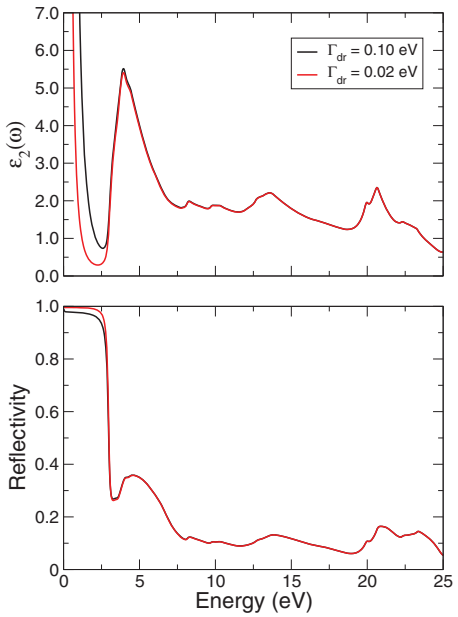

FIG. 1. (Color online) Imaginary part of the complex dielectric function and reflectivity of silver in the energy range of 0–25 eV for two different broadenings $\Gamma_{dr}=0.10$ eV (black line) and $\Gamma_{dr}=0.02$ eV (red line) of the intraband contributions. For the interband part of the spectrum a Lorentzian broadening of 0.10 eV was adopted.

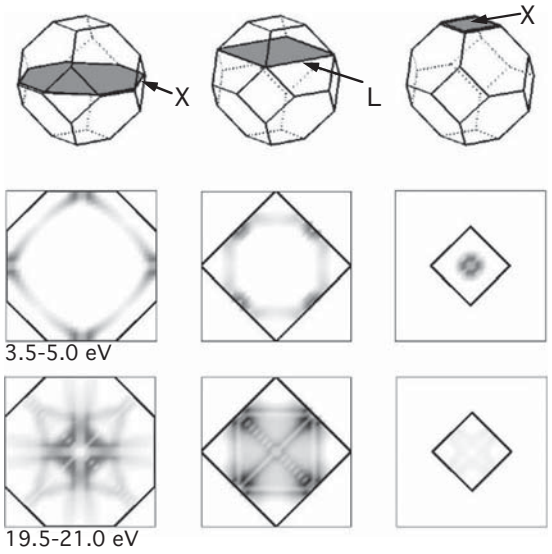

FIG. 2. Oscillator strengths for optical transitions of silver visualized for three planes in the BZ. From top to bottom: Position of the plane in the BZ; oscillator strength for transitions in the energy ranges of 3.5–5 and 19.5–21.5 eV, respectively. From left to right: $z=(1/34)(\pi/a)$, $z=0.5(\pi/a)$, and $z=(33/34)(\pi/a)$ planes. Dark areas correspond to regions with high oscillator strengths.

$p \rightarrow sd$ and $d \rightarrow pd$ transitions (middle panel).

A different situation is found for the features in the 19.5–21.5 eV range (bottom panels). They stem from a region of **k** points around the center of the BZ, with high oscillator strengths close to the k_z axis for small k_z values. As k_z increases, these areas move towards the BZ boundary and become strongest along $K-L$. The optical transitions creating this feature involve valence bands of d character and conduction bands of pf and f character.

3. Experiment

Loss spectra were acquired in UHV on a VG Microlab 310 F equipped with a hemispherical analyzer that was operated in the constant ΔE mode at 20 eV pass energy. The primary electrons were normally incident on the target. The detection angle was 60° with respect to the surface normal. According to the manufacturer, the full polar opening angle of our spectrometer amounts to 24°. The base pressure of the system during the measurements was $\sim 10^{-9}$ mbar. A single sample holder containing over 30 solids was used in order to ensure identical experimental conditions for the measurements of all samples. Of these samples, the following 17 elemental solids are considered in the present work: Ag, Au, Bi, Co, Cu, Fe, Mo, Ni, Ta, Te, Ti, Pb, Pd, Pt, V, W, and Zn.

REELS data were measured for energies of 50, 100, 150, 200, 300, 500, 700, 1000, 1500, 2000, 2500, 3000, and 3400 eV. The REELS spectra for primary energies below 300 eV contain significant intensity from low-energy secondary electrons whose tail can exceed kinetic energies of 100 eV and therefore interferes significantly with the loss spectrum for primary energies below ~300 eV. For this reason, only spectra measured with primary energies of 300 eV or more are considered in the present analysis. Count rates in the elastic peak were kept well below the saturation count rate of the channeltrons and the spectra were corrected for detector dead time. The samples were cleaned by means of 3 keV Ar^+ ion bombardment. This also served to amorphize some specimens such as silicon. Sample cleanliness was checked before and after the measurement of each sample by means of Auger electron spectroscopy. The primary beam current was stable throughout the measurements to within 2%. To minimize diffraction effects, the primary beam was scanned over a large area of the sample (0.5×0.5 μm^2). Three complete sets of data were acquired in the course of half a year to check the reproducibility of the experimental procedure. The results were found to agree within the experimental error imposed by counting statistics.

The raw REELS data were converted to loss spectra [corresponding to Eq. (22) below]. The spectra were first subjected to a Richardson-Lucy deconvolution to remove the experimental energy broadening caused by the thermal fluctuations of the electron gun and the finite resolution of the analyzer.[28] This is necessary to make a precise elimination of the elastic peak possible, as illustrated in Fig. 3.[28] It is assumed that the experimental broadening is symmetric and can be described by a Gaussian, with a width and position

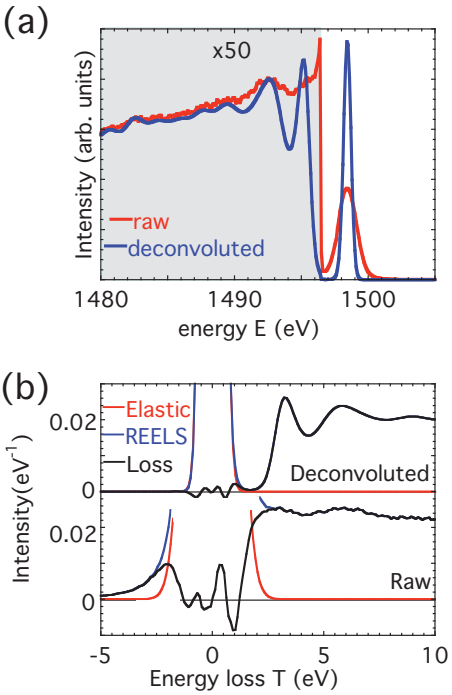

FIG. 3. (Color online) (a) Comparison of raw REELS data for 1500 eV electrons backscattered from a Au sample (red curve) with the corresponding data after a Richardson-Lucy deconvolution (blue curve). (b) Illustration of the elastic peak removal procedure for the data shown in (a). Blue curves: spectrum before elimination of the elastic peak; red curves: elastic peak; black curves: loss spectrum after removal of the elastic peak.

determined by fitting an appropriate portion of the elastic peak of the raw data. The spectrum is then subjected to a Richardson-Lucy deconvolution using a (normalized) Gaussian as (de)convolution kernel. In the resulting spectrum the elastic peak is always distinctly separated from the loss features and is then fitted by an asymmetric lineshape accounting for final state effects in the recoil process,[29]

$$f_0(T) = a_1 G(T) + a_2 \frac{\partial^3}{\partial T^3} G(T) + a_3 \frac{\partial^3}{\partial T^4} G(T) + a_4 \varrho(T), \quad (9)$$

where $G(T)$ is a Gaussian centered around the origin and $\varrho(T)$ represents the error function. The elastic peak is then subtracted from the spectrum which is subsequently divided by the elastic peak area giving the loss spectrum in absolute units [see Eq. (22) in the next section]. Figure 3(a) compares the REELS data for 1500 eV electrons backscattered from a Au sample before (blue curve) and after (red curve) deconvolution. The resulting loss spectrum is represented in Fig. 3(b) by the black solid curves. It should be noted that the fourth derivative in Eq. (9) needs to be included in the fitted peak shape to properly account for final state effects in the elastic recoil process at the low energies considered here and furthermore, that any attempt to fit the elastic peak with a symmetric function leads to much larger misfits than the ones shown in the lower panel of Fig. 3(b). The latter also demonstrates the necessity for a deconvolution prior to the elastic peak elimination: Owing to the large dynamic range of REELS data which is caused by the fact that the elastic

peak is much sharper than any other features in the spectrum, it overlaps with the loss features unless the broadening can be reduced significantly during the experiment. Then only a comparably small energy range of the elastic peak can be used to fit its shape and the resulting fit is generally worse than after deconvolution, leading to spurious oscillations in the loss spectrum around zero energy loss. It can be seen in the lower panel of Fig. 3(b) that these oscillations may be comparable in intensity to the real loss features, which complicates quantitative interpretation of the loss spectra.

4. Extracting Optical Constants From REELS

The procedure to extract the dielectric function from (reflection) electron energy-loss spectra consists of two steps: eliminating multiple scattering from the spectra to reveal the single-scattering loss distribution in an inelastic interaction and subsequent determination of the optical constants from the latter. Since in a reflection experiment the momentum transfer is not fixed by the geometry, as in transmission electron energy-loss measurements,[5] the single-scattering loss distribution represents an average over the BZ and therefore the second step cannot be achieved with a Kramers-Kronig analysis, as is usually done in a transmission experiment. Furthermore, since the reflection coefficient is very small for the typical energies used in the TEM, a reflection experiment is usually performed at much lower energies where it is no longer admissible to neglect surface excitations. Therefore, the procedure to eliminate multiple scattering also needs to be modified to take into account the effects of surface excitations.

In the following, the fundamental parameters for the electron-solid interaction in the relevant energy range are presented and the procedure to eliminate multiple scattering to retrieve the single-scattering loss distributions as well as the method to extract the dielectric function from them are outlined. Finally, a detailed consistency check and an error analysis are performed.

4.1. Electron-solid interaction parameters

When an electron hits the surface of a solid, it interacts strongly with the ionic and electronic subsystems of the solid. Therefore its degrees of freedom are subject to fluctuations. Changes in the direction of motion (referred to as elastic collision in the following) are mainly brought about by interaction with the screened Coulomb field of the nucleus that is assumed to be static during the interaction. Energy losses of the probing particle (referred to as *inelastic* collisions in the following) mainly occur via polarization of the solid-state electrons as a response of the loosely bound solid-state electrons to the incoming probing particle representing a strong perturbation. The incoming particle is decelerated by the polarization field it induces in the solid. In a semi-infinite solid with a planar surface, two types of inelastic excitations exist: bulk or volume excitations (denoted by the subscript "b" in the following) taking place deep inside the solid where the influence of the vacuum-solid boundary can be neglected and surface excitations (subscript "s") that take place in a narrow depth region z_s near the surface ($z_s = v/\omega_s$, where v is the electron speed and ω_s is the surface plasmon frequency) both in vacuum and inside the solid. These surface modes are governed by the boundary conditions of Maxwell's equations at the interface of two media with different dielectric susceptibilities and have a somewhat lower characteristic frequency than volume excitations ($\omega_s = \omega_b/\sqrt{2}$ for a free-electron material with a planar surface).

Since energy and momentum conservation governs the kinematics of the interaction, any change in the direction of motion is always accompanied by a change in the speed of the electron and vice versa. However, the recoil energy loss suffered during an elastic collision is typically of the order of some 10 meV which is much smaller than the energy loss during an inelastic collision, which is typically of the order of 10 eV. Furthermore, the scattering angles during an inelastic collision are much smaller than deflections caused by elastic collisions: milliradians for inelastic scattering compared to scattering angles of the order of π for elastic scattering. Therefore, to a good approximation, deflections and energy losses can be treated as independent processes. Note that this follows immediately from energy and momentum conservation and by considering the fact that the masses of the interaction partners in an inelastic collision are very similar, while they are very different for an elastic interaction.

When coherent scattering (diffraction) is neglected, elastic-scattering processes are completely specified by the differential cross section for elastic scattering $d\sigma_e(\theta_s)/d\Omega$, i.e., the distribution of polar scattering angles θ_s in an individual interaction. This quantity can be calculated by means of the partial-wave expansion method.[10,30] Usually a static atomic potential is used for such calculations, which is justified by the fact that solid-state effects mainly affect the small-angle scattering part of the cross section which is immaterial for the momentum relaxation process (see Ref. 31 for a detailed discussion). Inelastic scattering is described by the differential inelastic mean free path (DIIMFP) for bulk scattering $W_b(T)$, i.e., the distribution of energy losses per unit path length. Surface excitations are most conveniently expressed via the so-called differential surface excitation probability (DSEP) $W_s(T)$, i.e., the distribution of energy losses in a single surface crossing.

While calculations of the elastic-scattering cross section have been performed over several decades, only in the very recent past has the advent of density functional calculations made *ab initio* calculations for the inelastic-interaction characteristics possible. To date, empirical data for the susceptibility of any given solid to become polarized by an incoming charged particle have been used instead. The relationship between the inelastic-interaction characteristics and the macroscopic response function of a solid is provided by linear response theory. The DIIMFP is expressed in terms of the dielectric function $\varepsilon(\omega,q)$ of the solid via the well known formula[11]

$$W_b(\omega) = \frac{1}{\pi E}\int_{q_-}^{q_+} \mathrm{Im}\left\{\frac{-1}{\varepsilon(\omega,q)}\right\}\frac{dq}{q}, \tag{10}$$

where a quadratic dispersion is usually assumed such that the momentum transfer q is limited by q_- and q_+ given by

$$q_\pm = \sqrt{2E} \pm \sqrt{2(E-\omega)}. \tag{11}$$

Note that atomic units are used in this section and $T=\omega$ is used interchangeably throughout this work to denote the energy loss or the corresponding characteristic frequency. The differential inverse mean free path normalized to unity area is related to the unnormalized DIIMFP via $w_b(T)=\lambda_i W_b(T)$, where λ_i is the (total) inelastic mean free path (IMFP), i.e., the average distance the particle travels in between successive inelastic collisions, measured along its trajectory.

For the DSEP, the expression by Tung *et al.* that includes the recoil term[32] is employed in the present work,

$$W_s(\omega,\theta,E) = P_s^+(\omega,\theta,E) + P_s^-(\omega,\theta,E), \tag{12}$$

where the quantity $P_s^\pm(\omega,\theta,E)$ is defined as

$$P_s^\pm(\omega,\theta,E) = \frac{1}{\pi E\cos\theta}\int_{q_-}^{q_+}\frac{|q_s^\pm|dq}{q^3} \times \mathrm{Im}\left[\frac{(\varepsilon(\omega,q)-1)^2}{\varepsilon(\omega,q)(\varepsilon(\omega,q)+1)}\right] \tag{13}$$

and

$$q_s^\pm = \left[q^2 - \left(\frac{\omega+q^2/2}{\sqrt{2E}}\right)^2\right]^{1/2}\cos\theta \pm \left(\frac{\omega+q^2/2}{\sqrt{2E}}\right)\sin\theta. \tag{14}$$

The normalized DSEP is calculated via $w_s(T,\theta) = W_s(T,\theta)/\langle n_s(\theta,E)\rangle$, where $\langle n_s(\theta,E)\rangle$ is obtained by integrating Eq. (13) over the energy loss and represents the average number of surface excitations experienced during a single surface crossing.

To avoid confusion, it is noted that although the same symbol ("W" in W_b and W_s) is used to denote the distribution of energy losses in a surface and bulk excitation, the physical meaning of these quantities is quite different. While the DIIMFP is the volume-scattering probability per unit path length and energy, the DSEP represents the surface excitation probability (SEP) per unit energy, since this quantity is obtained by integrating over the path the electron takes through the surface-scattering zone.[32] The normalized distribution of energy losses $w_b(T)$ and $w_s(T)$ are physically equivalent quantities and both have the dimension of reciprocal energy, which is the reason why the same symbol is chosen for these quantities.

Examples of the DIIMFP and DSEP for Si and Pt are given in Fig. 4. The DIIMFP is shown for two energies (1000 and 3000 eV), while the DSEP is given for 1000 eV for two different surface-crossing angles of 0° and 70°. It is seen that for the considered energy-loss range, being significantly smaller than the probing energy, the shape of the DIIMFP hardly depends on the energy, or, in other words, that the normalized distribution of energy losses is independent of the incoming energy $w_b(T,E)\simeq w_b(T)$ to a good approximation. The same holds for the DSEP (not shown). On the other hand, the angular dependence of the normalized DSEP is seen to be very weak as well, $w_s(T,E,\theta)\simeq w_s(T)$. Of course the *total* SEP $\langle n_s(E,\theta)\rangle$ exhibits a pronounced angular and energy dependence, while the energy dependence of the IMFP, $\lambda_i(E)$, which governs the total bulk scattering probability, is appreciable as well.

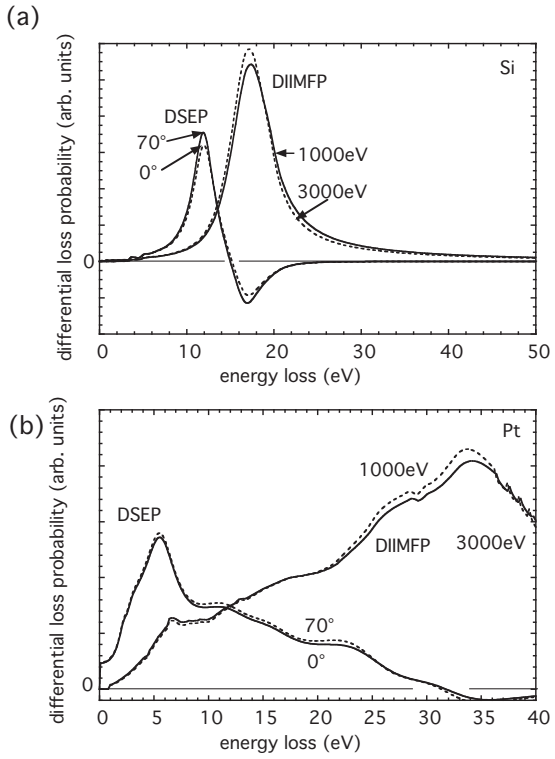

FIG. 4. DIIMFP and DSEP for medium energy electrons in Al and Pt. The DIIMFP is presented for 1000 eV (solid curves) and 3000 eV (dashed curves) while the DSEP is shown for 1000 eV for two different angles of surface crossing (0°, solid curves; 70°, dashed curves). (a) Al; (b) Pt.

4.2. Multiple scattering

Owing to their finite rest mass, electrons suffer intense multiple scatering when traveling through a solid. This is in contrast to the case of photon transport in matter where the vanishing rest mass makes it highly unlikely for the photon *not* to be absorbed during an interaction. The energy and direction of motion of a charged particle are changed repeatedly by multiple-scattering processes. For noncrystalline materials, where coherent scattering can be neglected (see Ref. 33 for the limitations of the standard model for particle transport where diffraction effects are neglected), the fluctuations after multiple scattering can be expressed in terms of the fluctuation distributions for a single collision by solving a linearized Boltzmann-type kinetic equation.[34] This was done in the so-called quasielastic approximation, valid for energy losses significantly smaller than the incoming energy ($T/E \ll 1$), where the interaction characteristics are taken to be

independent of the energy. Green's function of the problem can then be expressed in terms of the (n_b-1)-fold self-convolution of the DIIMFP, $w_b^{(n_b)}(T)$, and the (n_s-1)-fold self-convolution of the DSEP, $w_s^{(n_s)}(T)$, weighted with the collision statistics A_{n_b,n_s}, i.e., the number of times a given scattering process occurs for the considered boundary conditions [Eq. (12) in Ref. 34]. The resulting REEL spectrum $Y(E)$ is then found by superposition,[8]

$$Y(E)=\sum_{n_b=0}^{\infty}\sum_{n_s=0}^{\infty}A_{n_b,n_s}w_b^{(n_b)}(T')\otimes w_s^{(n_s)}(T'')\otimes f_0(E+T'+T''), \tag{15}$$

where the energy distribution at the source is given by $f_0(E)$ and the symbol "⊗" denotes a convolution over the energy loss T. The partial intensities A_{n_b,n_s} represent the number of electrons that arrive in the detector after being (n_b,n_s)-fold inelastically scattered in the solid. Since the width of the surface-scattering zone v/ω_s is smaller than, or of the order of, the elastic mean free path λ_e, the electron path in the surface-scattering zone is rectilinear to a good approximation. A most beneficial consequence of this fact is that the partial intensities for volume and surface scatterings are uncorrelated to a good approximation,[35]

$$A_{n_b,n_s}=A_{n_b}\times A_{n_s}. \tag{16}$$

Although (small) effects of deflections in the surface-scattering zone have been experimentally observed for a rather pathological case,[36] implying that Eq. (16) is not strictly true, this approach nonetheless has proven to constitute an effective approximation.[35–38]

The volume partial intensities A_{n_b} are given by an integral over all possible lengths of the paths, s, taken by the particle in the solid,

$$A_{n_b}=\int_0^{\infty}W_{n_b}(s)Q(s)ds. \tag{17}$$

Here $Q(s)$ is the distribution of path lengths and $W_n(s)$ is the stochastic process for multiple scattering, which, in the quasielastic regime, is given by[39]

$$W_n(s)=\left(\frac{s}{\lambda_i}\right)^n\frac{e^{-s/\lambda_i}}{n!}. \tag{18}$$

The path length distribution (PLD) $Q(s)$ can be calculated analytically[34] or using a MC technique.[31,34]

Since there exists a unique straight line path connecting any two points in space, the part of the PLD relevant for surface excitations resembles a δ function, and $Q_s(s)\approx\delta(s-v/\omega_s\cos\theta_i)$ when the passage through the surface-scattering zone is approximately rectilinear. In this case an equation similar to Eq. (17) for the surface partial intensities can readily be integrated giving

$$A_{n_s}=\frac{\langle n_s\rangle^{n_s}}{n_s!}e^{-\langle n_s\rangle}. \tag{19}$$

The quantity $\langle n_s(E,\theta)\rangle$ represents the average number of surface excitations in a single surface crossing, which is given in terms of a material parameter a_s, the so-called surface excitation parameter, by the formula[32]

$$\langle n_s(E,\theta)\rangle=\frac{a_s}{\sqrt{E}\cos\theta}, \tag{20}$$

and θ is the off-normal polar angle of surface crossing. Plural surface scattering is usually assumed to be described by the Poisson stochastic process. The fact that the normalized DSEP does not significantly depend on the energy and surface-crossing angle (see Fig. 4) was utilized in Eq. (19), allowing one to combine the effect of surface excitations along the in- and outgoing parts of the trajectory by writing[8]

$$\langle n_s\rangle=\langle n_s(\theta_i)\rangle+\langle n_s(\theta_o)\rangle, \tag{21}$$

where the θ_i and θ_o indicate the incident and outgoing polar directions of surface crossing.

Finally, for quantitative analysis of REELS, the elastic peak needs to be removed and the energy scale converted into an energy-loss scale. Furthermore, the spectrum is divided by the area of the elastic peak. These transformations then give the reduced loss spectrum $y(T)$ which is used in the following analysis in the compact form:

$$y(T)=\sum_{n_b=0}^{\infty}\sum_{n_s=0}^{\infty}\alpha_{n_b,n_s}w_b^{(n_b)}(T')\otimes w_s^{(n_s)}(T''), \tag{22}$$

where the reduced partial intensities $\alpha_{n_b,n_s}=A_{n_b,n_s}/A_{n_b=0,n_s=0}$ have been introduced and the zero-order partial intensity is taken to be zero, $\alpha_{n_b=0,n_s=0}=0$, to account for the fact that the elastic peak has been removed from the spectrum.

4.3. Deconvolution of multiple scattering from loss spectra

To extract the dielectric function from an energy-loss spectrum, the single-scattering loss distributions $w_b(T)$ and $w_s(T)$ need to be retrieved, i.e., a method to eliminate multiple scattering from Eq. (22) is needed. Recalling the convolution theorem, it is immediately obvious that in Fourier space, the spectrum is given by a bivariate power series in the variables $w_b(T)$ and $w_s(T)$. This result implies that a unique solution of these quantities cannot be found by reverting the series equation (22) since a single equation with two unknowns has no unique solution. However, when *two* loss spectra $y_1(T)$ and $y_2(T)$, with a different sequence of partial intensities $\alpha_{n_bn_s}$ and β_{n_b,n_s}, are measured, reversion of the bivariate power series becomes possible using the formula[8,40]

$$w(T) = \sum_{k=0}^{N}\sum_{l=0}^{N} a_{k,l} Y_{k,l}(T) - \int_{T'=0}^{T} \sum_{k=0}^{N}\sum_{l=0}^{N} b_{k,l} Y_{k,l}(T-T') w(T') dT', \quad (23)$$

where the quantity $Y_{k,l}(T)$ is the (k,l)-th order cross convolution of the two REELS spectra,

$$Y_{k,l}(T) = y_1^{(k)}(T-T') \otimes y_2^{(l)}(T'). \quad (24)$$

Since $w(T=0) \equiv 0$, the integration on the right hand side of Eq. (23) can always be carried out over the energy-loss range for which the loss distribution is already known. For more details on the (trivial) numerical treatment of the Volterra integral equation of the second kind see, e.g., Ref. 41.

The expansion coefficients $a_{k,l}$ and $b_{k,l}$ are entirely determined by the reduced partial intensities of the two spectra,[8,40] which, together with the two loss spectra, are therefore the only input parameters of the procedure. The reduced volume partial intensities can always be calculated with sufficient accuracy when a reasonable estimate for the IMFP is used, such as the TPP-2M predictive formula.[42] While a similar guideline has been published for the surface excitation parameter,[43] it is not needed to know the absolute value of this parameter at all, since the expansion coefficients turn out to scale with the value of a_s in Eq. (20).[40] Thus, apart from the functional form of the dependence of the SEP on the energy and surface-crossing direction, such as Eq. (20), no information on surface excitations whatsoever is needed as input to the procedure. Note, finally, that the equations to retrieve the surface and volume single-scattering loss distributions are identical and given by Eq. (23); merely the expansion coefficients are different.[40]

Calculation of the expansion coefficients in Eq. (23) is quite tedious, as explained in Refs. 8 and 44. Therefore, in Appendix A, the synopsis of a recently developed simplified deconvolution procedure[45] is given which is equivalent to the procedure employed here and can be used for the same purpose with considerably less numerical effort.

4.4. Retrieval of optical data from the single-scattering distributions

The final step in the analysis is the retrieval of the dielectric function from the single-scattering loss distributions. This is achieved by fitting the theoretical expressions for the DIIMFP and DSEP to the corresponding experimental results using a suitable model for the dielectric function.

The electromagnetic response of the solid is described in terms of the fit parameters f_i, ω_i, and γ_i using a model for the dielectric function in terms of a set of Drude-Lindhard oscillators for the evaluation of the theoretical expressions for the DIIMFP and DSEP,[46]

$$\varepsilon_1(\omega,q) = 1 - \sum_i \frac{f_i(\omega^2 - \omega_i(q)^2)}{(\omega^2 - \omega_i(q)^2)^2 + \omega^2\gamma_i^2},$$

$$\varepsilon_2(\omega,q) = \sum_i \frac{f_i\gamma_i\omega}{(\omega^2 - \omega_i(q)^2)^2 + \omega^2\gamma_i^2}, \quad (25)$$

where $\omega = T$ is the energy loss and q is the momentum transfer. In the above expressions, f_i represents the oscillator strength, γ_i is the damping coefficient, and ω_i is the energy of the i-th oscillator. A quadratic dispersion,

$$\omega_i(q) = \omega_i + \alpha q^2/2, \quad (26)$$

was used for the transition described by the i-th oscillator. The value of the dispersion coefficient α was chosen to be unity, except for those oscillators with an energy higher than the most loosely bound core electrons (semicore transitions), for which $\alpha = 0.5$ was used. Those values of the Drude-Lorentz parameters in the above equation that minimize the deviation between the experimental data and the theoretical expressions for the DIIMFP and DSEP (as described below) are taken to parametrize the dielectric function. Note that a dielectric function of the form of Eq. (25) implicitly satisfies the Kramers-Kronig dispersion relationships as well as the perfect screening ps-sum rule.

The (normalized) distributions $w_b(T)$ and $w_s(T)$ obtained from the experimental data are simultaneously fitted to the above theoretical expressions by minimizing the function

$$X_b\chi^2_{\mathrm{DIIMFP}}(p_b,f_i,\omega_i,\gamma_i) + X_s\chi^2_{\mathrm{DSEP}}(p_s,f_i,\omega_i,\gamma_i). \quad (27)$$

Here the function χ^2 is the least-squares difference between theory and experiment, defined in the usual way, and X_b and X_s are weight factors chosen as $X_b = 1.0$ and $X_s = 0.01$, emphasizing the DIIMFP in the fitting procedure. The reason for this choice of X_s is that, although the experimental single-scattering loss distributions for surface scattering are reasonably described by Eq. (12), they differ in detail for some materials (see Sec. 5.1 below), while the theoretical expression for the DIIMFP does match the experimental results in much better detail. In consequence, the overall agreement of the simultaneous fit of experiment to theory is significantly improved by reducing the weight of the surface term in the fitting procedure. As discussed further below, the physical reason for this behavior is related to the approximation of depth-independent surface-scattering characteristics, made in the model of Tung *et al.* The fit parameters p_b and p_s are multiplicative scaling factors for the DIIMFP and the DSEP that compensate for an eventual mismatch of the surface excitation parameter and IMFP used as input. Using the TPP-2M formula[42] to estimate the IMFP, the value of p_b deviated from unity by less than 5% for all cases studied, while the returned value of p_s scales with the value of the surface excitation parameter a_s, as expected.

4.5. Consistency test and error analysis

In the above procedure to measure the dielectric function, the following of assumptions have been introduced that should be investigated in some detail in order to judge the reliability of the method and to arrive at a meaningful error estimate for the resulting optical constants.

(i) An essential assumption that makes the outlined procedure possible at all is that the partial intensities for surface and volume scatterings are uncorrelated [Eq. (16)].

(ii) The model to calculate the reduced volume partial intensities via Eq. (17) on the basis of state-of-the-art calculations for the elastic-scattering cross section is assumed to be accurate enough for the present purpose.

(iii) The functional form of the energy and angular dependence of the surface-scattering probability is supposed to be known. In the present work, it is assumed to be given by Eq. (20). The scaling properties of the deconvolution coefficients in Eq. (23) with respect to the parameter a_s make any knowledge concerning the value of this parameter immaterial for the determination of the optical constants.[8,40,44]

(iv) The shapes of the normalized DIIMFP and DSEP are supposed not to depend on the primary energy of the reflected electrons and the surface-crossing direction.

(v) In the theoretical relationships between the DIIMFP and the DSEP and the dielectric function [Eqs. (10) and (13)], it is assumed that the dispersion of the oscillators in the Drude-Lorentz expansion used as model dielectric function [Eq. (25)] is of the form $\omega_i(q)=\omega_i+\alpha q^2/2$ and that an appropriate value of α can be chosen.

The first four assumptions above pertain to the deconvolution of multiple scattering providing the single-scattering loss distributions that will be discussed first, while the last assumption concerns the extraction of optical constants from the single-scattering loss distributions and will be dealt with at the end of this section.

In Fig. 5, the calculation of the reduced volume partial intensities is illustrated. This is achieved most easily by means of a MC simulation for the PLD $Q(s)$, such as the algorithm described in Ref. 31. The only input parameter for such calculations is the differential elastic-scattering cross section for the considered energy and the geometrical configuration employed in the experiment. The relevant portion of the differential elastic-scattering cross section for Au is shown in Fig. 5(a) for several energies. It is seen that the cross section exhibits deep minima at scattering angles varying with the energy. These minima are more pronounced for high-atomic-number elements and low energies. For energies in excess of some tens of a keV, these oscillations disappear and the differential cross section approaches a Rutherford shape. It has been known for some time[47] that if the experimental configuration corresponds to scattering angles coinciding with a deep minimum in the cross section, the shape of the loss spectrum changes significantly. The explanation is that when the value of the cross section is small for the considered scattering geometry, the probability for the electron to be backscattered into the detector after a single elastic collision is also small and plural elastic scattering predominates for the electron to experience the required net directional change. In consequence, the path length traveled in the solid is larger than for a case where the differential elastic cross section is larger. This can be clearly observed in Fig. 5(b) where the PLDs for 700 and 3400 eV, corresponding to a maximum and a minimum in the differential cross section, respectively, demonstrates the expected differences: For 700 eV, the PLD decreases monotonically with the traveled path length, while for 3400 eV it exhibits a maximum. As a consequence, the sequence of partial intensities for different energies also becomes qualitatively different, as can be seen in Figure 5(c) where the partial intensities calculated from the PLDs of Fig. 5(b) with Eq. (17) are shown for four energies.

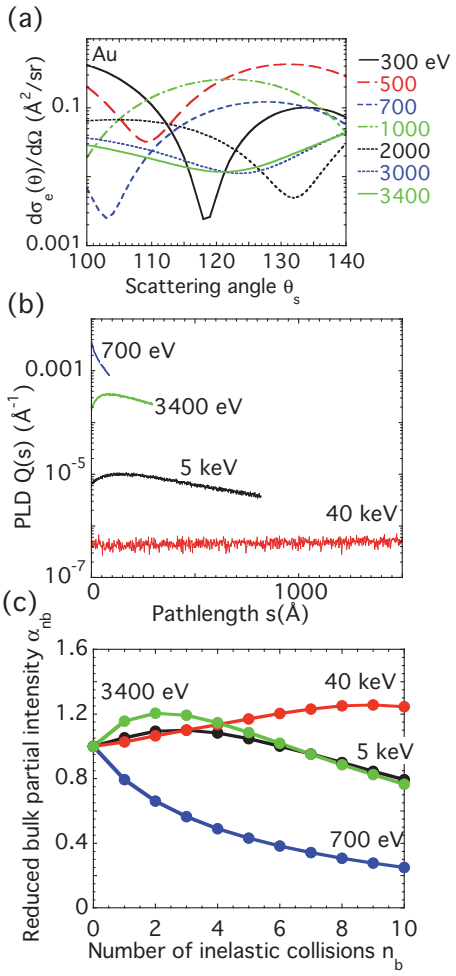

FIG. 5. (Color online) (a) Elastic scattering cross section of Au for several energies in the range of scattering angles between 100° and 140°. (b) PLD $Q(s)$ calculated by means of a MC simulation for Au for 700 and 3400 eV for the geometrical configuration used in the present work and for 5 and 40 keV for the experimental setup of Ref. 58. (c) Reduced partial intensities for volume scattering calculated by means of Eq. (17) for the PLDs shown in (b).

Let us now address the uncertainty of the reduced volume partial intensities obtained in this way. It is easy to see from Eq. (17) that the absolute value of the partial intensities scales with the value used for the IMFP. This is in fact the basis of the so-called elastic peak ($n_s=n_b\equiv 0$) electron spectroscopy (EPES) technique to measure the IMFP.[34,48–51]

However, the reduced partial intensities are virtually unaffected by the choice of the IMFP value. This can be seen by employing the common rules of error propagation to Eq. (17). For the reduced partial intensities one finds that an uncertainty $\Delta\lambda$ in the IMFP leads to an error in the first-order reduced partial intensity given by

$$\frac{\Delta\alpha_1}{\alpha_1} = \left|\frac{\Delta\lambda}{\lambda}\right| |1-\alpha_1|. \tag{28}$$

In Fig. 5(b) it is seen that the width of the PLD is large compared to the value of the IMFP. The IMFP, on the other hand, governs the width of the Poisson distribution [Eq. (18)] for any value of n. Taking into account Eq. (17), it follows that the difference between the reduced partial intensities of subsequent order is always considerably smaller than unity, implying that α_1 is always quite close to unity (the zero-order partial intensity is unity per definition, $\alpha_0 \equiv 1$). In consequence, the error in the partial intensities due to an uncertainty in the IMFP is always negligible if a reasonable estimate of the IMFP is available. For example, for $0.9 < \alpha_1 < 1$, the error in the partial intensities will be at least *ten times* smaller than the error in the IMFP, as follows from Eq. (28).

The second input parameter for calculation of the partial intensities is the elastic-scattering cross section based on a static atomic potential. The accuracy of this quantity has been studied in detail by Jablonski and co-workers.[10,48,52] One of the main conclusions of these works was that the cross sections calculated in this way are appropriate and reliable for the description of elastic scattering in solids, except for scattering angles close to a deep minimum in the cross section. Also, the effects of absorption can reach up to 30% in the vicinity of a deep minimum[53,54] adding to the uncertainty in this range of scattering angles. Moreover, for experimental geometries where the net scattering angle coincides with a deep minimum, most electrons experience plural elastic deflections before reaching the detector leading to a violation of assumption (i) above, since in these cases the part of the trajectory in the surface-scattering zone is likely to be nonrectilinear. This expectation has indeed been proven experimentally.[36] Finally, near a deep minimum the derivative of the cross section is relatively high implying that in MC calculations, the solid angle of acceptance of the analyzer needs to be accurately known.

The above discussion may be summarized by stating that quantitative interpretation of REELS may be problematic when, for a particular element and energy and for a particular experimental scattering geometry, there is a deep minimum in the differential elastic-scattering cross section. On the other hand, it is clear that for the deconvolution procedure to yield numerically stable results, the spectra need to be sufficiently different. In other words, the employed combination of energies and/or surface-crossing directions should be chosen in such a way that the sequence of partial intensities for the two considered spectra is sufficiently different. The extent to which the spectra differ is to first order determined by the determinant[40]

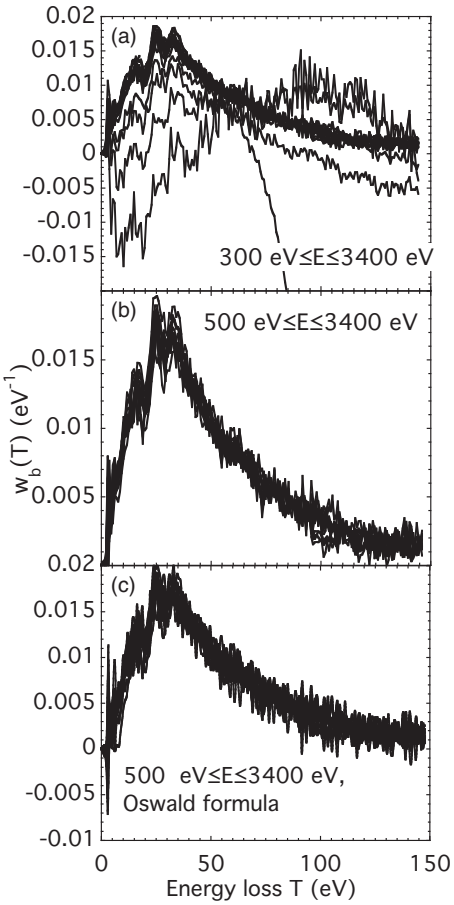

FIG. 6. (a) Results of the deconvolution procedure equation (23) applied to all possible energy combinations between 300 and 3400 eV. Note that the scattering geometry employed in the present work corresponds to a deep minimum in the elastic-scattering cross section at 300 eV (see Fig. 5). (b) Same as (a) for energies larger than 300 eV, thus avoiding the deep minimum in the scattering cross section at 300 eV. (c) Same as (b) but using Oswald's formula for the energy and angular dependence of the surface excitation parameter equation (30) instead of Eq. (20).

$$\Delta = \alpha_{1,0}\beta_{0,1} - \alpha_{0,1}\beta_{1,0}, \tag{29}$$

where α_{n_b,n_s} and β_{n_b,n_s} represent the partial intensities of the two spectra. The above considerations are fully supported by the outcome of the consistency test shown in Fig. 6. The result of the deconvolution procedure equation (23) for the DIIMFP of Au is shown for all possible combinations of incident energies between 300 and 3400 eV for which $\Delta \geqslant 0.1$ in Fig. 6(a). Note from Fig. 5 that the differential cross section at 300 eV exhibits a deep minimum at the scattering angle of 120° employed in our experiment. Comparison with the results in Fig. 6(b) where this deep minimum is avoided by disregarding the spectrum for an incident energy of 300 eV shows that the consistency is dramatically improved. A statistical analysis of the rms deviation from the average of these results leads to an error estimate for the DIIMFP of $\leqslant$10%. In Fig. 6(c) a similar result is shown, from an analysis in which the energy and angular dependence given by Eq. (20) is replaced with the formula proposed by Oswald,[49]

$$\langle n_s(E,\theta)\rangle = \frac{1}{a_s^*\sqrt{E}\cos\theta + 1}. \quad (30)$$

It is seen that in this case the consistency of results is slightly worse, in particular, for small energy losses, where negative excursions are seen in the DIIMFP in Fig. 6(c), which are not physically realistic. The analysis so far demonstrates that when deep minima in the cross section are avoided, results consistent to within $\lesssim$10% are obtained for the considered experimental spectra.

The assumption that the shapes of the DIIMFP and DSEP are approximately independent of the energy and surface-crossing direction was studied in detail earlier[8] by analyzing model spectra with Eq. (23) and comparing the results with experimental data. The results verified the model for the dynamic interaction of an energetic electron with a surface, summarized by Eqs. (10) and (13) in great detail. It was found that this approximation leads to small spurious replicas of the DIIMFP and DSEP when the loss features are very sharp, such as for free-electron materials, such as Al and Si. For solids with a broad loss distribution, such as those studied in the present work, the approximation (iv) mentioned above consitutes an appropriate approach.

While the consistency for different incident energies is apparent from the above, the question remains whether the same level of consistency is also obtained when analyzing different geometrical configurations. Furthermore, Yubero and co-workers suggested that there may be an influence of interference effects between the in- and outgoing parts of the trajectory on the energy-loss spectrum when the field set up during the penetration of the electron into the solid affects the surface crossing on its way out.[55–57] The magnitude of the interference effect is predicted to scale reciprocally with the speed of the incoming electron and should be negligible at energies above several keV. Figure 7 compares the result of the deconvolution for a set of spectra taken at rather low energies of 700 and 3400 eV [Fig. 7(a)], measured in the present work, with the spectra of Ref. 58 measured for incident energies of 5 and 40 keV [Fig. 7(b)]. The shape of the loss spectra is seen to significantly depend on the energy: For 700 eV the spectrum is decreasing more or less monotonically with energy loss, while for energies above ~3 keV an increase is seen at small energy losses and a flat energy-loss dependence is observed at higher energies. Note that the shape of these spectra can be explained perfectly by considering the collision statistics imposed by elastic scattering, as follows from the partial intensities shown in Fig. 5(a). Considering the fact that these sets of spectra were measured at opposite sides of the world on different samples using a different spectrometer in a different energy range and with different geometrical setups, the consistency between the single-scattering loss distributions shown in the lower panel of Fig. 7 is remarkable and gives confidence in the experimental procedure as well as the method of analysis employed. It also suggests that the difference in shape of loss spectra taken at different energies is indeed caused by the influence of elastic scattering rather than by interference effects, for which no experimental evidence whatsoever can be found in the literature.

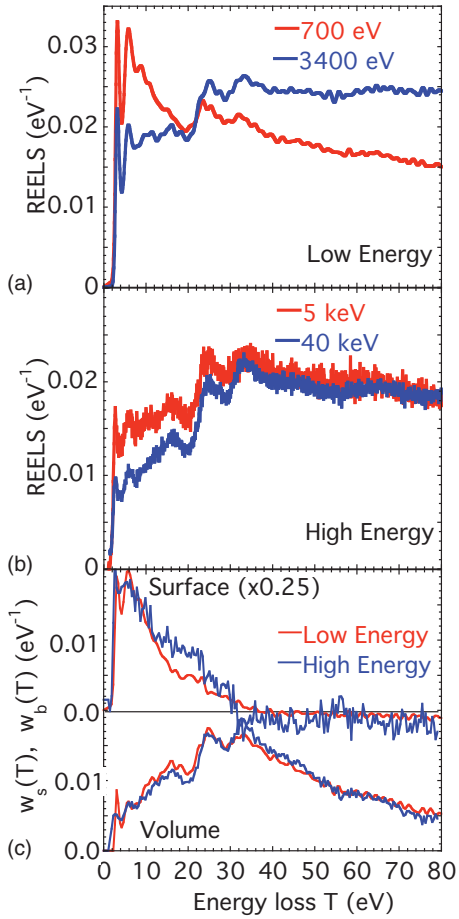

FIG. 7. (Color online) Comparison of deconvolution of REELS spectra for Au measured in significantly different energy ranges, corresponding to the PLDs and partial intensities shown in Figs. 5(b) and 5(c). (a) Loss spectra for 700 and 3400 eV electrons, measured in the present work. (b) Measurements of Ref. 58 for 5 and 40 keV. (c) Comparison of the single-scattering loss distributions obtained with Eq. (23) using the partial intensities shown in Fig. 5(c).

In concluding this section, the model for the dielectric function and, in particular, the choice of the dispersion constant α deserve to be discussed. First of all, it should be noted that the physical significance of the fit parameters describing the oscillators in the Drude-Lorentz expansion of the dielectric function, Eq. (25), is limited in that the characteristic frequencies ω_i and damping constants γ_i in the low-energy region (i.e., for energies clearly below the ionization edges of the semicore states) do not necessarily reflect the correct energies describing the inter- and intraband transitions, etc. The values of the fit parameters, together with the Drude-Lorentz expansion, should rather be regarded as a convenient numerical representation of the data. Also, in this energy-loss range, the choice of the dispersion constant is immaterial, as can be seen from Eq. (11) which shows that for low-energy losses $\omega \ll E$ the range of momentum transfers over which the averaging is performed is small. Indeed, changing the dispersion constant α between unity and 0.5

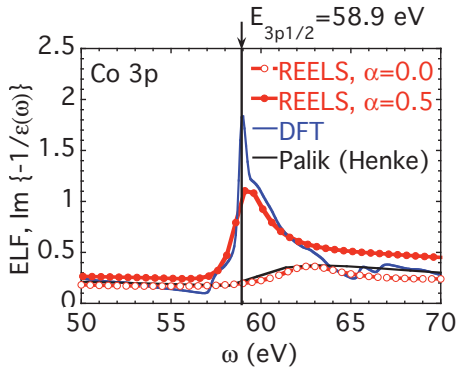

FIG. 8. (Color online) Influence of the chosen dispersion constant α in the retrieval of the dielectric function from the single-scattering loss distributions for the Co $3p$ semicore transition. Dashed red curve with open circles: ELF values of ε retrieved from REELS using $\alpha=0.0$ in Eq. (26); solid red curve with filled circles: ELF values of ε retrieved from REELS using $\alpha=0.5$; black curve: Palik's data (Ref. 1) for the ELF [that were taken from Henke's work (Ref. 2)]. Blue curves: results of DFT calculations. Note that the DFT calculations accurately reproduce the position of the semicore edge binding energy $E_{3p_{3/2}}=58.9$ eV derived from photoemission data (Ref. 59), as do the REELS data when a value of $\alpha=0.5$ is used for the dispersion constant.

during the retrieval of ε from the single-scattering loss distributions does not lead to any significant change in the resulting values for ε for $\omega \lesssim 50$ eV.

For the semicore transitions, i.e., the ionization edges of the core states with the lowest binding energy, the situation is different. This is illustrated in Fig. 8 that compares the value of the ELF function for the Co $3p$ edge retrieved from REELS data with the present procedure using different values of the dispersion constant α with DFT calculations and

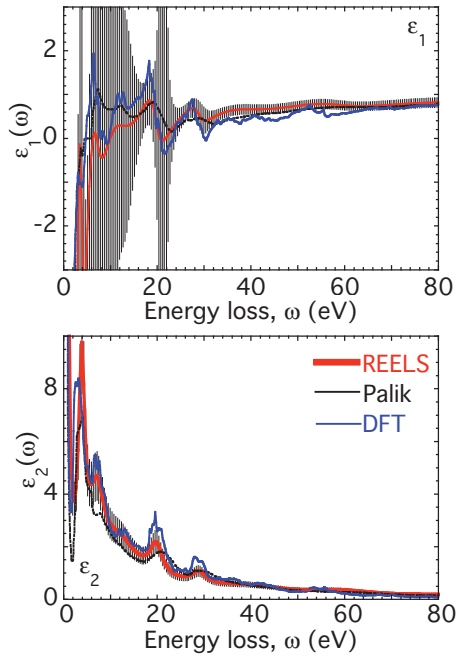

FIG. 9. (Color online) Comparison of the dispersive (ε_1) and absorptive (ε_2) parts of ε for Au derived from the present REELS measurements (red curves with error bars), DFT calculations (blue curves), and Palik's data (black curves).

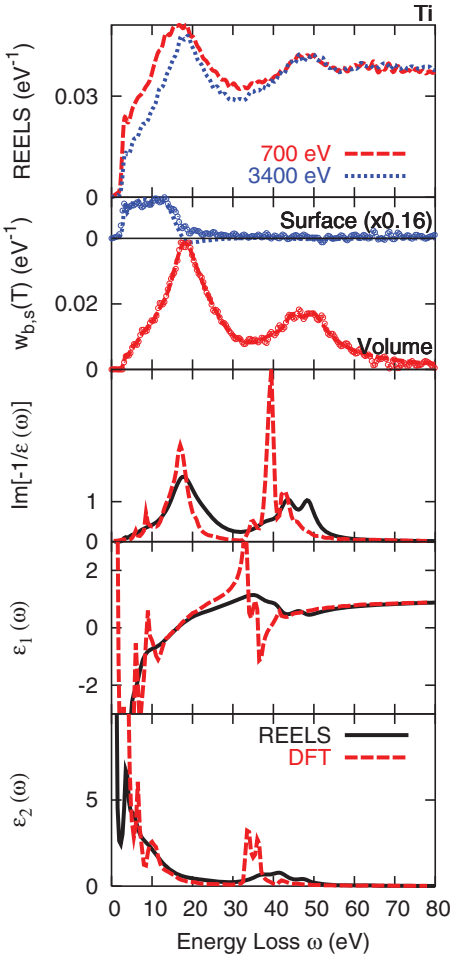

FIG. 10. (Color online) REELS data and optical constants derived from them for Ti. Upper panel: deconvoluted REELS data at the employed energies, as indicated in the legend; second panel from above: DIIMFP $[w_b(T)]$ and DSEP $[w_s(T)]$ (data points) as well as the best fit of these data to the Drude-Lorentz model of Eq. (25) (solid curves); lower three panels: comparison of the loss function $\mathrm{Im}\{-1/\varepsilon\}$ as well as the dispersive (ε_1) and absorptive (ε_2) parts of the dielectric function extracted from REELS (red curves) with results from DFT calculations (blue curves) and Palik's data set (black curves).

with the optical constants taken from Palik's book.[1] For this larger energy-loss range, the entire BZ is sampled by Eq. (11) and the influence of dispersion becomes more important. At this stage it should be noted that the employed Drude-Lorentz expansion model for the dielectric function only roughly accounts for the effects of dispersion through a single parameter, the dispersion constant α, which is a fundamental weakness of this model. Three effects of dispersion play a role in electron energy-loss spectra: the dispersion of (1) the initial and (2) the final state and (3) the fact that the scattered electron itself can transfer momentum to the solid. It should be clear that the details of these phenomena are difficult to describe with a single dispersion parameter in ε, which complicates the choice of α. Therefore, the retrieval was performed for different values of α and the results were compared with other results for the dielectric function. It was found that for $\alpha=0.5$ the characteristic energies ω for the semicore transitions compare best to the binding energies

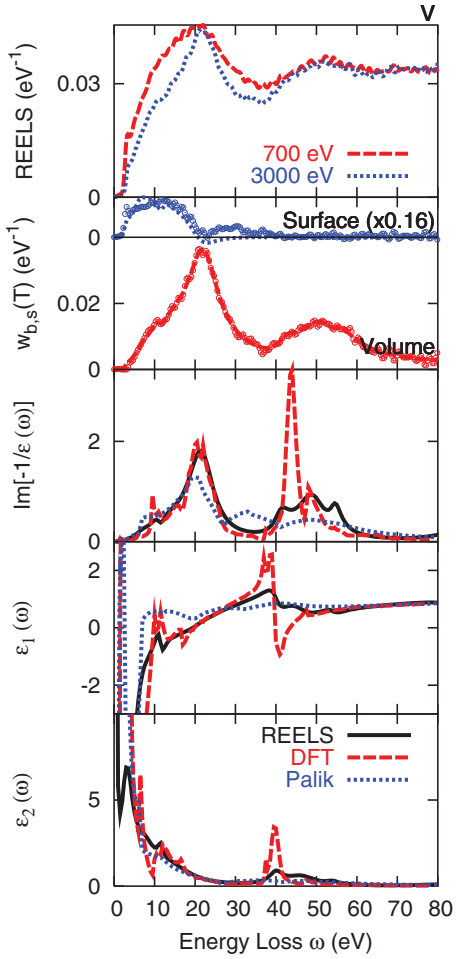

FIG. 11. (Color online) Same as Fig. 10 for V.

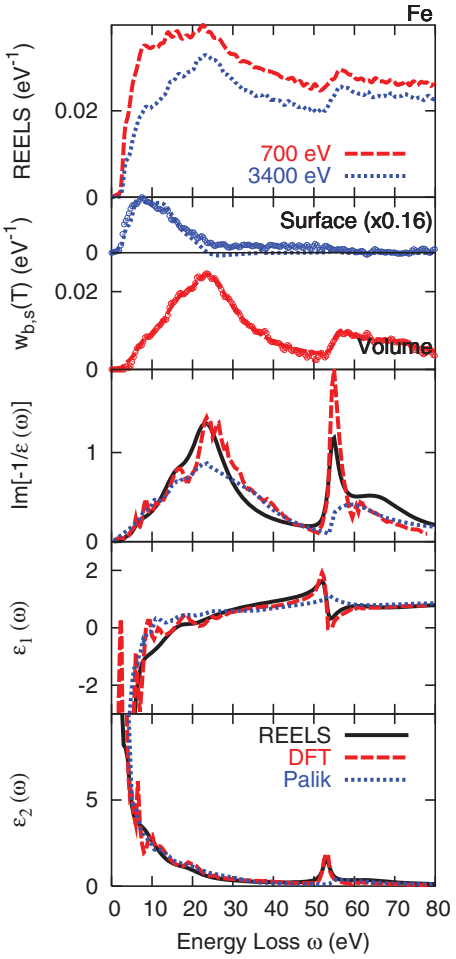

FIG. 12. (Color online) Same as Fig. 10 for Fe.

derived from photoemission data found in the literature.[59] This value of α also gives very good agreement with the DFT calculations for the semicore transitions, as can be seen in Fig. 8. For $\alpha=0$, the retrieved ELF agrees closely with the data found in Palik's books. In this energy region Palik's data were taken from Henke's work,[2] which is a synthesis of empirical and theoretical data for *free* atoms, and therefore is not expected to be representative for the semicore ionization edges in a solid. The same is true for the more recent compilation by Chantler,[3,4] which gives ε values very close to those obtained by Henke for most of the transitions considered in the present work. Therefore, although our approach introduces a small systematic uncertainty in the retrieved dielectric function for energies beyond the semicore edges, we have chosen a value of $\alpha=0.5$ throughout this work for all transitions involving semicore levels, while for lower energies α was taken to be unity.

In the above, the error in the retrieved DIIMFP was derived from a statistical analysis of data derived from different energy combinations and was estimated to be $\lesssim$10%. Assuming that the resulting error in the ELF $\mathrm{Im}\{-1/\varepsilon(0,\omega)\}$ is of the same order of magnitude, the common rules of error propagation can be used to estimate the uncertainty in ε_1 and ε_2. The results of this analysis are shown for Au in Fig. 9 which again also shows Palik's data and the results of DFT calculations. The uncertainty in ε_1 is seen to be rather large below 20 eV. This is a fundamental characteristic of the derivation of optical data from absorption measurements that mainly sample ε_2. Within the estimated uncertainty, the three data sets agree satisfactorily both for the real as well as the imaginary parts of ε. It should be noted again at this point that the employed procedure determines in the first place the ELF, $\mathrm{Im}\{-1/\varepsilon(0,\omega)\}$, for which the uncertainty is estimated to amount to $\lesssim$10%.

5. Results and Discussion

5.1. Optical constants

The results of the data analysis according to the procedure outlined above are given in Figs. 10–32. A comparison of the optical constants $\mathrm{Im}\{-1/\varepsilon\}$, ε_1, and ε_2 as a function of frequency or energy loss ω derived from REELS, DFT calculations, and Palik's data are presented in Figs. 10–26. In Figs. 27–32 the refractive index n and extinction coefficient k derived from the same data are shown as a function of the photon wavelength. Numerical values corresponding to the data in the lower three panels of Figs. 10–32 are given in the Appendixes.

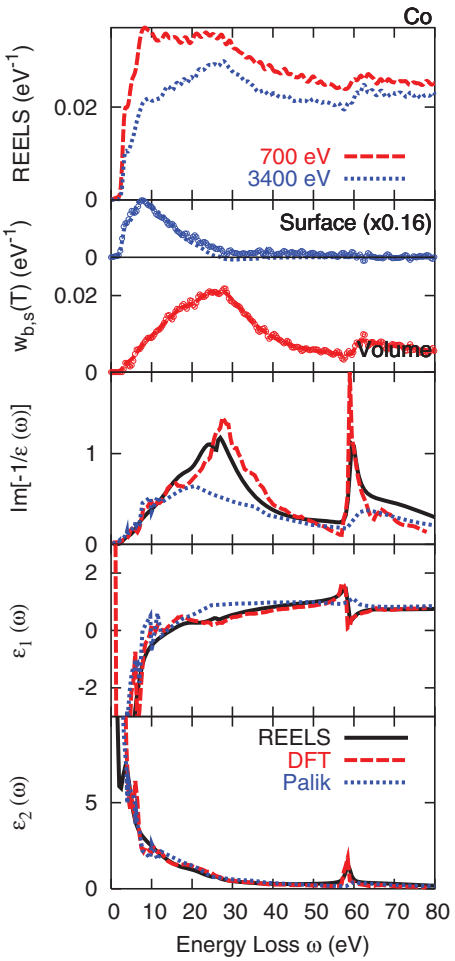

FIG. 13. (Color online) Same as Fig. 10 for Co.

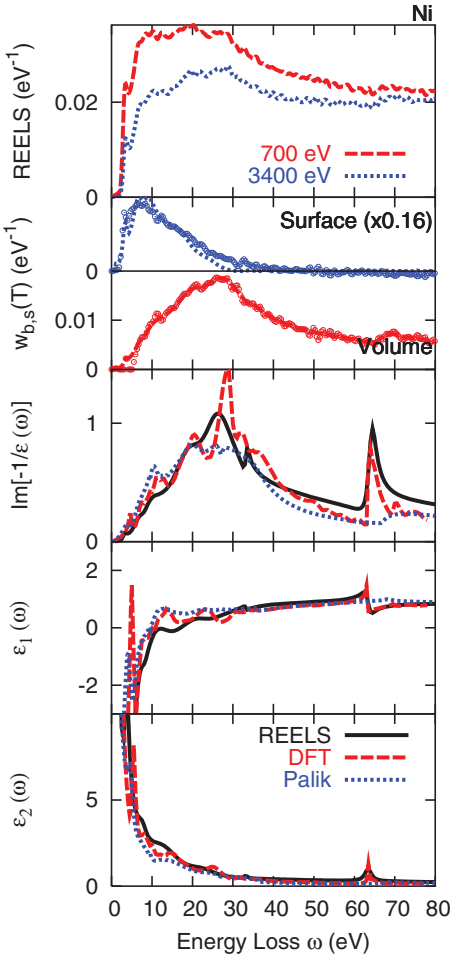

FIG. 14. (Color online) Same as Fig. 10 for Ni.

In Figs. 10–26, the upper panels display the pair of energy-loss spectra used for the analysis. The raw data were subjected to a Richardson-Lucy deconvolution, and subsequently the elastic peak was fitted to a function of the form given by Eq. (9) and removed from the spectra, which were finally divided by the elastic peak area to give the loss spectrum in absolute units.

The primary energies chosen for the analysis are indicated. These were selected according to the guidelines given in the previous section, i.e., those energy combinations were selected for which the contributions of surface excitations are sufficiently different. This is indicated by the value of the determinant Δ [Eq. (29)] using Eq. (20) to estimate the surface excitation parameter. On the other hand, energies close to a deep minimum in the differential elastic-scattering cross section were avoided. Values of Δ for all energy combinations were in the range $\Delta \approx 0.2-0.4$. For most materials the overall shape of the two spectra is very similar, in particular, for energy losses in excess of $\sim$30 eV where the effects of multiple inelastic scattering dominate. Significant differences in the high-energy-loss tail can be observed for some materials, such as Ag, Au, W, Pd, Pt, Mo, Ta, Pb, and Bi, which is attributable to the influence of elastic scattering on the shape of energy-loss spectra measured in reflection, as discussed in detail in the previous section (see Figs. 5 and 7). The fact that such differences mainly occur for materials with high atomic number, for which the effects of elastic scattering are most pronounced, supports these considerations.

The influence of surface excitations on REELS is evident in the differences of the spectral pair at energies $\lesssim$20 eV: for the lower energy of the pair, the corresponding features are significantly enhanced as compared to the region of higher energy losses. For some materials, such as, Ti, the spectral pair is very similar, and at first sight the attempted separation of the distribution of individual losses inside the solid and during the surface crossing may seem questionable. However, it should be kept in mind that the sequence of partial intensities is generally different for the spectral pair allowing a stable decomposition of the spectra to be made.

The second panel from the top in Figs. 15–26 shows the result of the partial-intensity analysis [Eq. (23)] to retrieve the energy-loss distributions for single surface- and volume-scattering processes, represented by the blue (surface) and red (bulk) data points. The results for the DIIMFP are in absolute units; the units for the DSEP are arbitrary since a value of $a_s \equiv 1$ was chosen throughout for the calculation of the SEP with Eq. (20), as the normalized DSEP scales with SEP and accurate values for this quantity are not known for all materials under study.[43]

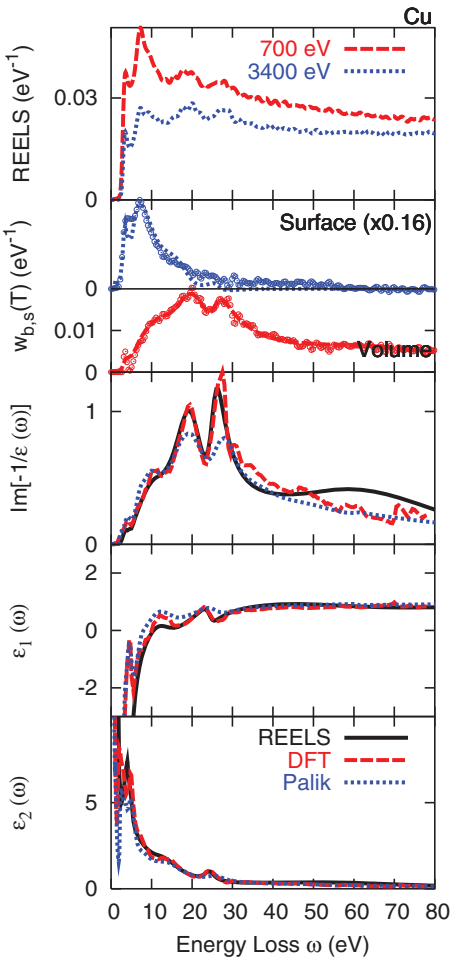

FIG. 15. (Color online) Same as Fig. 10 for Cu.

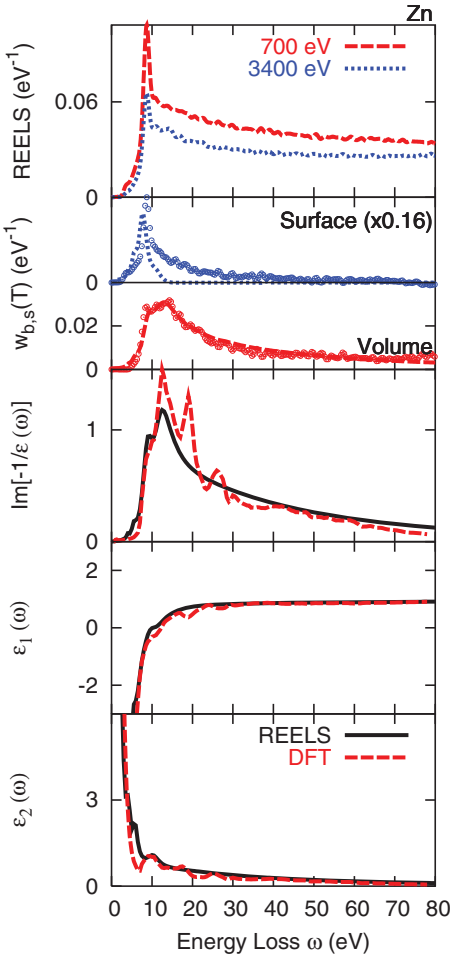

FIG. 16. (Color online) Same as Fig. 10 for Zn.

Comparison with the loss spectra in the upper panels clearly shows that the contribution of plural inelastic scattering becomes significant above ~20 eV and that the low-energy-loss regions in the loss spectra are dominated by surface excitations. These observations emphasize the need for spectral decomposition before information on the optical constants can be retrieved from loss spectra.

The solid curves drawn through the data points represent the results of a simultaneous fit of the volume and surface single-scattering loss distributions (DIIMFP and DSEP, respectively) to the theoretical expressions for these quantities, Eqs. (10) and (13), using a Drude-Lorentz model for the optical constants. For the bulk single-scattering loss distributions this procedure always leads to a very good match of the experimental data and the fitted loss distribution. The only exceptions to this statement are the sharp low-loss features in the DIIMFP at about 5 eV in Cu, Ag, and Au, which almost, but not quite,[60] coincide with the surface plasmon loss feature, representing the dominant structure in the DSEP. It should be emphasized that the fact that these features are attributed to volume scattering (and are therefore observable in the DIIMFP after deconvolution) rather than surface excitations not only follows from a partial-intensity analysis on a spectral pair taking into account the collision statistics, as in Figs. 15, 19, and 24, but can also be demonstrated directly experimentally by covering the surface with a small amount of another material and observing the changes in the (double) peak structure.[60] We also note that ε_1 increases rapidly with increasing energy loss in this region so that the conditions for prominent surface and volume energy losses are satisfied for similar energy-loss values.

The fit of the data for the DSEP is slightly worse than for the DIIMFP for the same optimum values of the fitted Drude-Lorentz parameters, in particular, for materials with a pronounced "begrenzungs" effect that display a slight negative excursion in the DSEP at the energy of the volume plasmon. This effect is caused by the coupling of the surface and the bulk plasmon,[12,35] i.e., the polarization of the surface dipoles leads to a decrease in the polarization for frequencies corresponding to volume excitations. Since, per definition, the DSEP describes the influence of the surface on the electron energy loss it consists of the "pure" surface term and the begrenzungs term and becomes (slightly) negative whenever the magnitude of the former exceeds the latter. This effect can be clearly identified in the present data set for Ti, V, W, Mo, Ta, Pb, Te, and Bi. Since the absolute value of the intensity of the DSEP for these materials near the energy of the volume plasmon is quite small, the deviation of the fit from

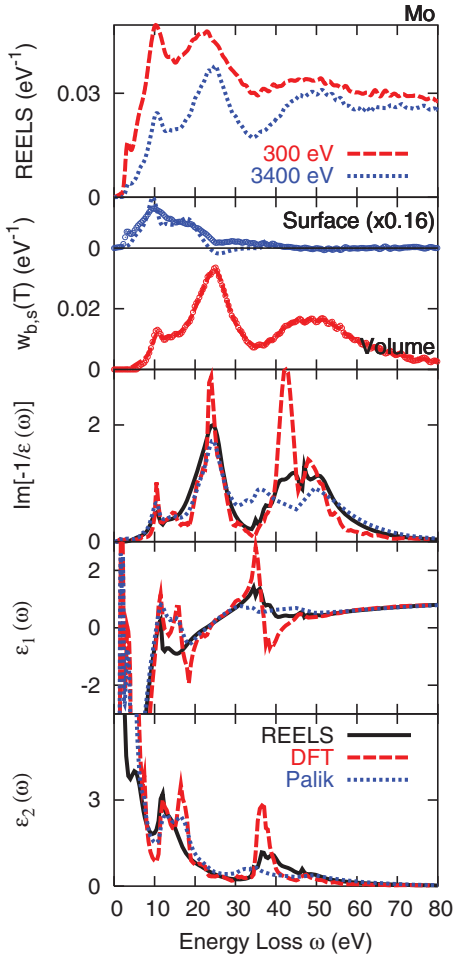

FIG. 17. (Color online) Same as Fig. 10 for Mo.

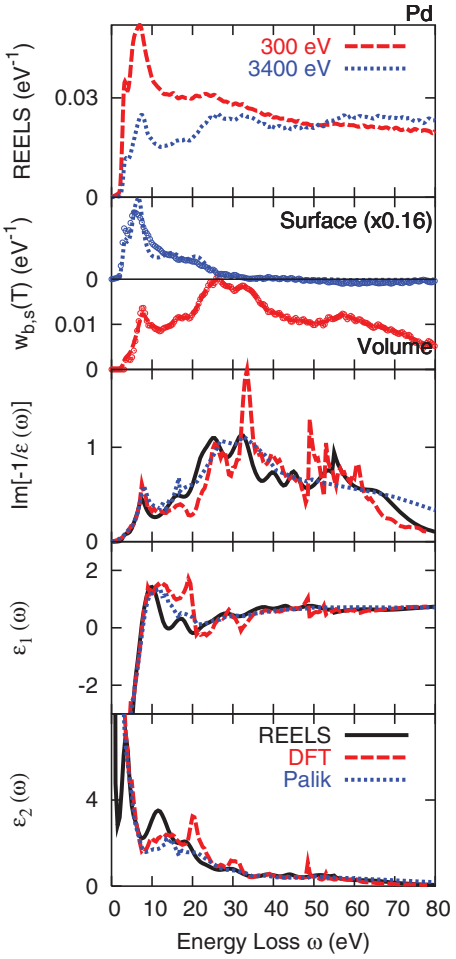

FIG. 18. (Color online) Same as Fig. 10 for Pd.

the data points is nonetheless moderate. It should be noted that for materials with a pronounced begrenzungs effect, such as the free-electron materials, the predicted negative excursion is satisfactorily reproduced by the deconvoluted DSEP.[35] The second reason why the fitted dielectric function matches the volume data better than the surface data is that the theoretical expression for the DIIMFP [Eq. (10)] is exact, while the model for the DSEP is based on the approximation that the actual shape of the trajectory the electron takes has no influence on the normalized DSEP, allowing one to integrate the effect of surface excitations over depth along a V-shaped trajectory. This approach then gives rise to the expression in Eq. (13) in the framework of the model of Tung *et al.*[32] Indeed, in a recent work,[61] this model has been studied in detail and it was found that the assumption of simple rectilinear surface crossing gives rise to changes in the shape of the DSEP similar to the deviations between the fitted function and the data points observed here. However, the influence of the actual trajectory shape on the *collision statistics* was found to be negligible, which implies that the basis of the deconvolution procedure, i.e., Eq. (16), retains its validity and the procedure should thus return the correct shape of the volume single-scattering loss distribution. This is the reason why the DSEP was given a relative weight of 0.01 in the fitting procedure.

The sets of Drude-Lorentz parameters giving the best fits of the experimental single-scattering loss distributions to the theoretical expressions for these quantities [Eqs. (10) and (13)] is given in Appendix B. The corresponding optical constants, i.e., $\mathrm{Im}(-1/\varepsilon)$, ε_1, and ε_2, are displayed in the lower three panels of Figs. 15–26. For comparison, the results of the DFT calculations and the corresponding data taken from Palik are also included in these figures. In general, the three data sets agree reasonably well for all examined cases in view of the experimental uncertainties involved in the analysis of the present experimental data and the data sets of Palik. The important exception to this rule are the strong deviations observed in all cases for the semicore edges, where Palik's data are consistently different from the other two data sets. The DFT and REELS results show a very good mutual agreement for Fe, Co, and Ni, while for the other materials the DFT and REELS data for the semicore edges agree satisfactorily but differ in detail. Palik's data, on the other hand, always essentially deviate from the DFT and REELS results. This can be attributed to the fact that most of Palik's data in this energy range have been taken from Henke's tables[2] which are based on atomic calculations.

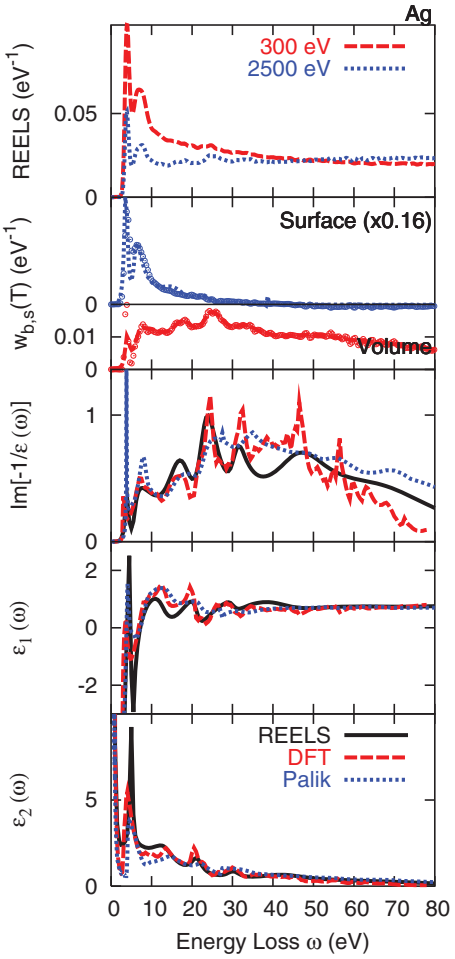

FIG. 19. (Color online) Same as Fig. 10 for Ag.

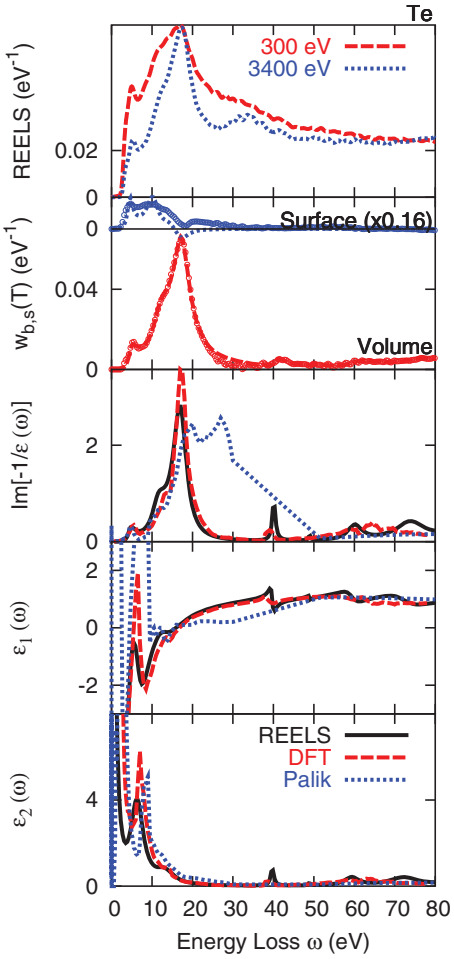

FIG. 20. (Color online) Same as Fig. 10 for Te.

For energy losses below the semicore edges ($\lesssim$50 eV), the three data sets are consistent within the involved errors, although for most materials the DFT and REELS data agree in more detail with each other than with Palik's data. For example, for the position of the peaks below 30 eV in the ELF for Ag, Pd, and Au (Figs. 19, 18, and 24), the DFT and REELS data are accurately consistent, while the peaks appear a bit shifted in Palik's data. For Fe, Co, and Ni (Figs. 12–14) the strong deviations of the latter in this energy range are particularly dramatic.

When comparing ε_1 and ε_2 instead of the ELF, similar general observations can be made. It should be kept in mind, however, that for the REELS data, the volume single-scattering loss function that is used in the fit procedure is essentially governed by the ELF rather than the real and imaginary parts of the dielectric function. Consequently, small deviations in the retrieved ELF for small energy losses can lead to large uncertainties in ε_1 and ε_2 (see Fig. 9). Therefore, for energies below ~5 eV, where the loss function assumes small values, the uncertainty in the real and imaginary parts of the dielectric function derived from REELS becomes appreciable (that may exceed 100% in the case of ε_1). Indeed, the deviations of the REELS data from the other data sets in this energy range generally seem to be more significant than for the ELF, as expected. This is even more apparent when the refractive index and the extinction coefficient derived from the three data sets are plotted against the photon wavelength, as shown in Figs. 27–32 where the REELS data deviate from the other data sets for wavelengths above ~0.2 μm. The DFT results generally agree quite well with Palik's data for wavelengths ranging from the soft x-ray regime up to the near infrared. The origin of the rather large uncertainty in the REELS data from the near-UV to the infrared regime (i.e., energy losses between 0.1 and 5 eV) lies in the dynamic range of the REELS spectrum, i.e., the fact that tails of the elastic peak in this energy-loss range assumes values comparable to the loss features which makes their separation problematic. The only way to improve this situation seems to be the use of a better monochromated primary beam.

An additional test of the consistency of the derived data is provided by the sum rules for optical constants. The data presented here were subjected to two sum rule tests: The f-sum rule or Thomas-Reiche-Kuhn sum rule,

$$Z_{\text{eff}} = \frac{2}{\pi\Omega_p^2}\int_0^{\omega_{\max}} \omega\,\text{Im}\{-1/\varepsilon(\omega)\}d\omega, \tag{31}$$

where $\hbar\Omega_p = \sqrt{4\pi n_a e^2/m_e}$ is the generalized plasmon energy and n_a is the atomic density. The expectation value of the

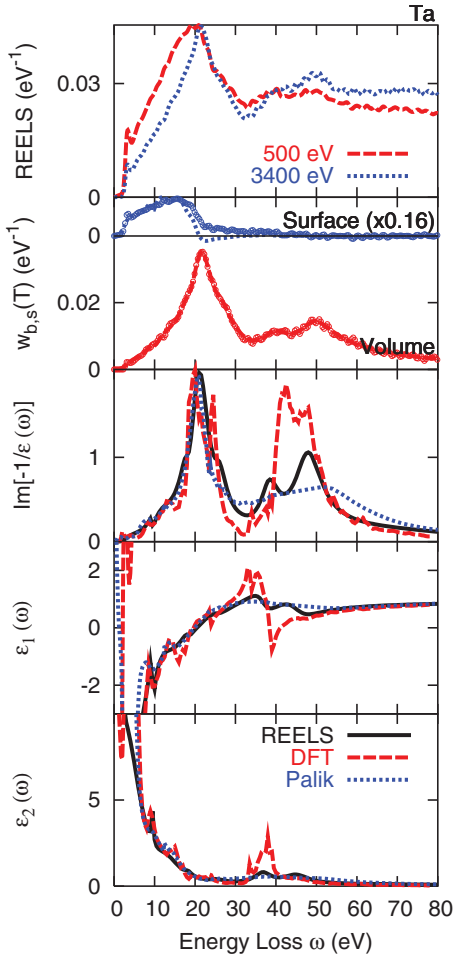

FIG. 21. (Color online) Same as Fig. 10 for Ta.

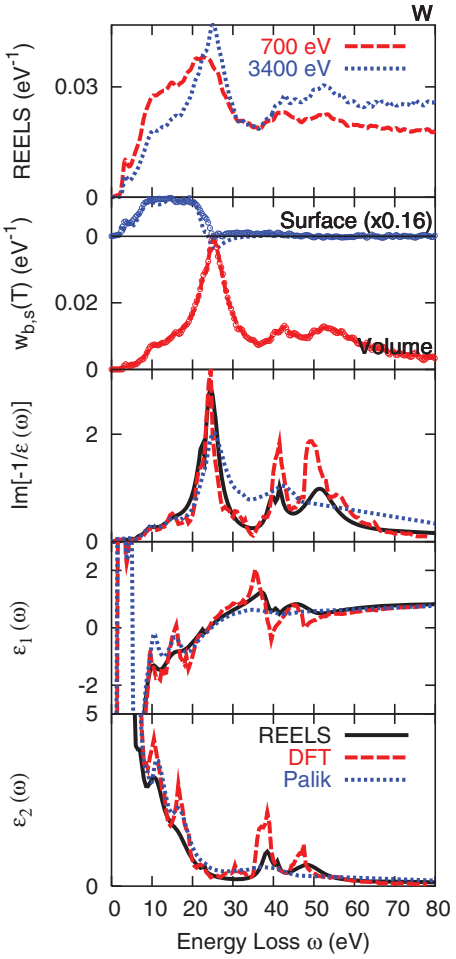

FIG. 22. (Color online) Same as Fig. 10 for W.

f-sum rule is the total number of electrons per atom and should approach Z, the atomic number, for sufficiently large values of $\omega_{\max} \gtrsim E_c$, where E_c is the largest binding energy for the inner-shell levels. Therefore, the main contribution to the f-sum rule comes from energies beyond the range of interest here ($\sim$1–80 eV). The ps-sum rule for metals, on the other hand, emphasizes energy losses below 100 eV, and is therefore more relevant in the present context:

$$P_{\text{eff}} = \frac{2}{\pi}\int_0^{\omega_{\max}} \frac{1}{\omega}\,\text{Im}\{-1/\varepsilon(\omega)\}d\omega. \tag{32}$$

The expectation value of the ps-sum rule is unity when $\omega_{\max}$ is significantly larger than $\sim$100 eV. Since the DFT and REELS data provide values of the optical constants over a limited energy range ($\lesssim$100 eV), they were complemented by Henke's data above 80 eV in order to perform the sum rule tests.

The results are summarized in Table 2. It is seen that the deviations from the expectation value for the f-sum rule is of the same order of magnitude for the three data sets, of the order of 3%–5%, but except for Pd and Pt, the REELS and DFT data yield values of Z_{eff} consistently closer to the atomic number of the considered element. Since the used optical data are essentially identical for energies above 80 eV, this suggests that the REELS and DFT data are generally superior to Palik's data in the UV regime. As far as the REELS data are concerned this is not surprising since electron energy-loss measurements mainly sample the UV regime. A similar conclusion can be drawn from the results for the ps-sum rule, which is most sensitive to the UV regime, where the REELS data exhibit deviations typically of the order of 2% and never in excess of 4%, while Palik's data show much larger deviations from the expected value.

The analysis so far can be summarized by stating that the DFT calculations for the 17 examined materials agree satisfactorily with earlier optical data available in the literature, as compiled in Palik's books, for wavelengths ranging from the near infrared to the soft x-ray region. In the UV regime, these data differ in detail, however. The DFT data exhibit significantly more fine structure in the optical constants, a result probably caused simply by the finite energy resolution of the experiments and the fact that detailed optical measurements in this regime are more difficult. Indeed, the number of earlier measurements (or calculations which are mostly for free atoms) in the UV range is generally far smaller than measurements in the near UV to infrared range, indicating the need for simple experimental methods that produce reliable data in the UV range.

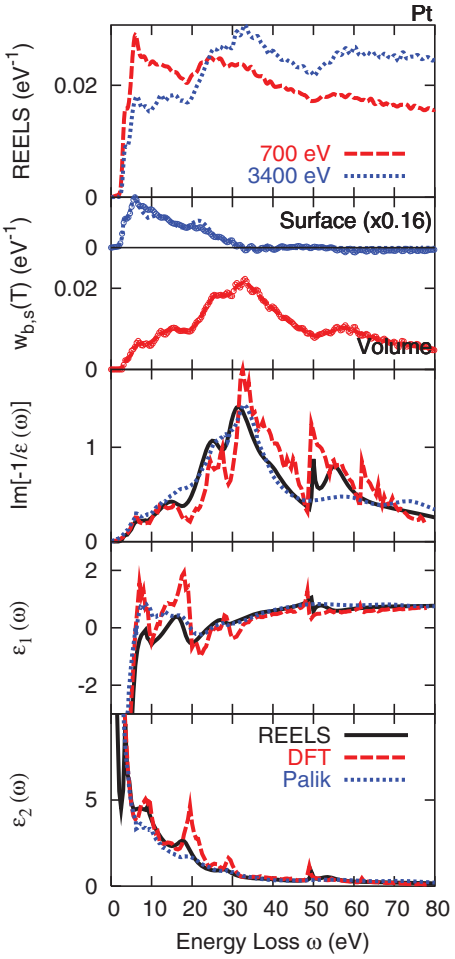

FIG. 23. (Color online) Same as Fig. 10 for Pt.

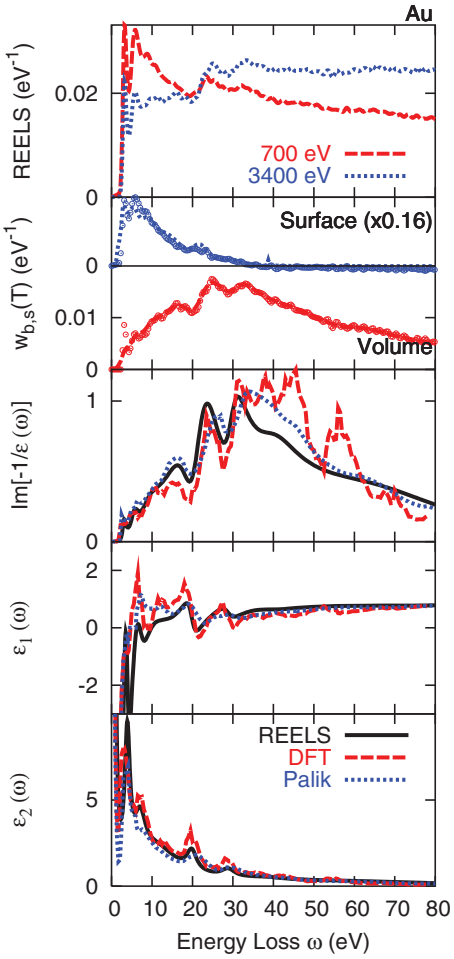

FIG. 24. (Color online) Same as Fig. 10 for Au.

Important deviations between DFT and Palik's data are mainly seen for the semicore ionization edges in the far UV where the DFT calculations predict much more pronounced peaks in the optical data than Palik's data. It is believed that this result reflects the difference between solid-state calculations, such as the present DFT calculations, and atomic calculations, such as the far UV values for the optical constants in Palik's data sets.

The assessment of the uncertainties associated with optical constants derived from electron energy-loss measurements in reflection, together with a comparison with the DFT results and Palik's data, leads us to conclude that the energy-loss measurements provide accurate values (with an uncertainty better than 10%) for the optical constants in the range between the near-UV and the soft x-ray regime. Thus, such measurements can provide useful information to further improve theoretical techniques to calculate the optical response, in particular, for energy losses in the UV regime and beyond.

5.2. Inelastic electron-scattering data

Calculation of the inelastic-interaction characteristics of charged particles with solids within the framework of linear response theory represents an important example where optical constants, in particular, in the UV regime, are of paramount importance.[42,62–69] In calculations of the stopping power of charged particles in matter[66–69] the relevant transport process is dominated by momentum relaxation rather than by energy fluctuations,[31] such as scattering of ions in solids, inelastic electron backscattering, x-ray production by electron bombardment, and emission of secondary electrons. When energy fluctuations dominate the particle transport, i.e., when discrete (multiple) energy losses are observable in the corresponding spectra, the quantities of relevance are the total IMFP λ_i, the DIIMFP $w_b(T)$, the DSEP $w_s(T)$, and the integral SEP $\langle n_s \rangle$.

The DSEP and DIIMFP are graphically represented in the second panel from the top in Figs. 10–26. These quantities can also be derived from the corresponding Drude-Lorentz parameters given in Appendix B using Eqs. (10) and (13).

Accurate knowledge of the DIIMFP and DSEP is essential for a detailed analysis of the shape of a photoelectron line in an electron spectrum as well as the inelastic background accompanying it.[70,71] The inelastic background in an x-ray photoelectron spectrum is in fact similar to the REELS spectrum recorded at the same energy, apart from the fact that the collision statistics, i.e., the partial intensities, are generally essentially different for an emission geometry compared to the case of a reflection geometry. Therefore, the present op-

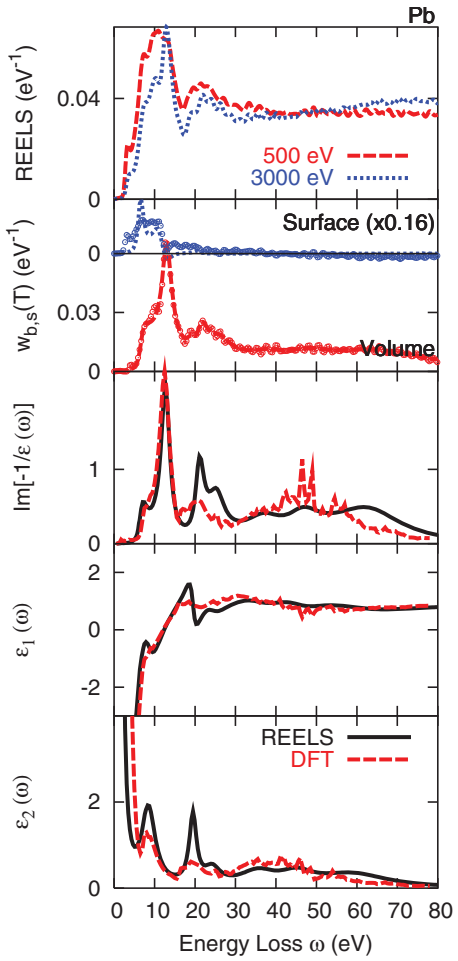

FIG. 25. (Color online) Same as Fig. 10 for Pb.

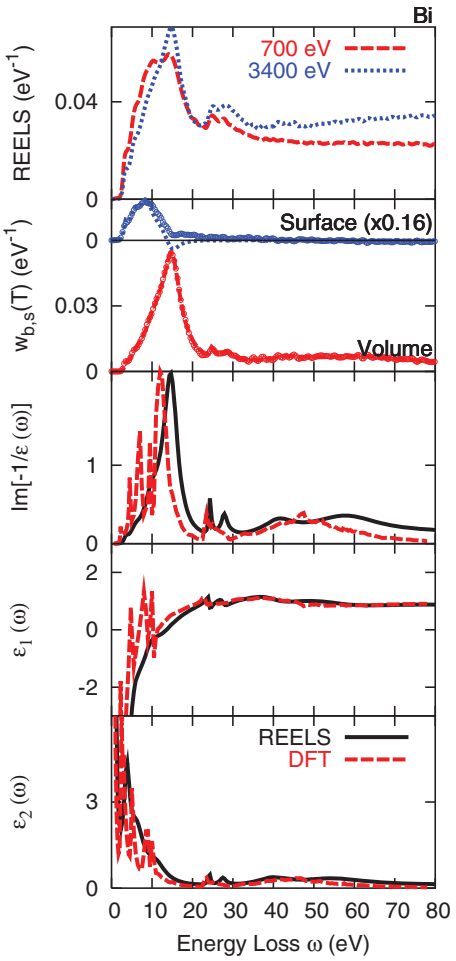

FIG. 26. (Color online) Same as Fig. 10 for Bi.

tical constants in Appendixes A and B are believed to be useful in peak-shape analysis[31,70,72] where multiple inelastic scattering needs to be eliminated from an experimental spectrum in order to reveal the intrinsic photoemission lineshape which contains important information on the electronic structure of a solid. It should be noted that even for a very common material, such as Au, for which quite a large number of data have been published for the optical constants (see Ref. 73 and references therein), the present opical data, in particular, those for the ELF, are believed to lead to an improvement in inelastic background analysis. This can be seen by comparing the peaks in the ELF in Fig. 24 for Au with the corresponding REELS data in the upper panel. The two interband transitions at around 25 and 35 eV in Palik's optical constants are clearly located at a slightly higher energy loss than the corresponding peaks in the REELS. In the ELF and ε_2 derived from REELS, on the other hand, the location of these peaks is obviously consistent with the REELS itself. While the chosen example may not lead to dramatical differences in the background analysis, it is nonetheless important to conclude that in general an analysis of REELS spectra such as in the present work can provide, in a straightforward way, data needed in background analysis.

The quantity of foremost importance for quantitative analysis of electron spectra is the total IMFP. It is not only needed to convert measured intensities of a certain element in an electron spectrum into chemical composition,[74] but is also essential for nanoscale calibration in the depth dimension,[75] which can be established accurately by means of data for electron-beam attenuation provided a reliable value for the IMFP is available. Figure 33 shows a comparison of IMFP values derived from four sets of optical constants. The four materials chosen for this figure are those for which the deviations between Palik's data for the ELF and the two other data sets are the largest (Fe, Co) as well as Ti and Pd for which the optical data used by Tanuma and co-workers,[42,65,68,69,76] deviate significantly from the present results. For all other materials considered here a very good agreement between the IMFP results from the four sets of optical constants was found. In Fig. 33, IMFP values calculated with Penn's algorithm[63] are shown as solid lines for energies between 100 and 10 000 eV using the optical constants calculated with DFT, those derived from REELS, and those taken from Palik's and Tanuma's[77] data sets. Above 80 eV the REELS and DFT data have again been complemented by Henke's data.[2] In addition, the data points represent results of EPES (Ref. 48) measurements of the IMFP.[51,78] The first apparent feature of this figure is the fact

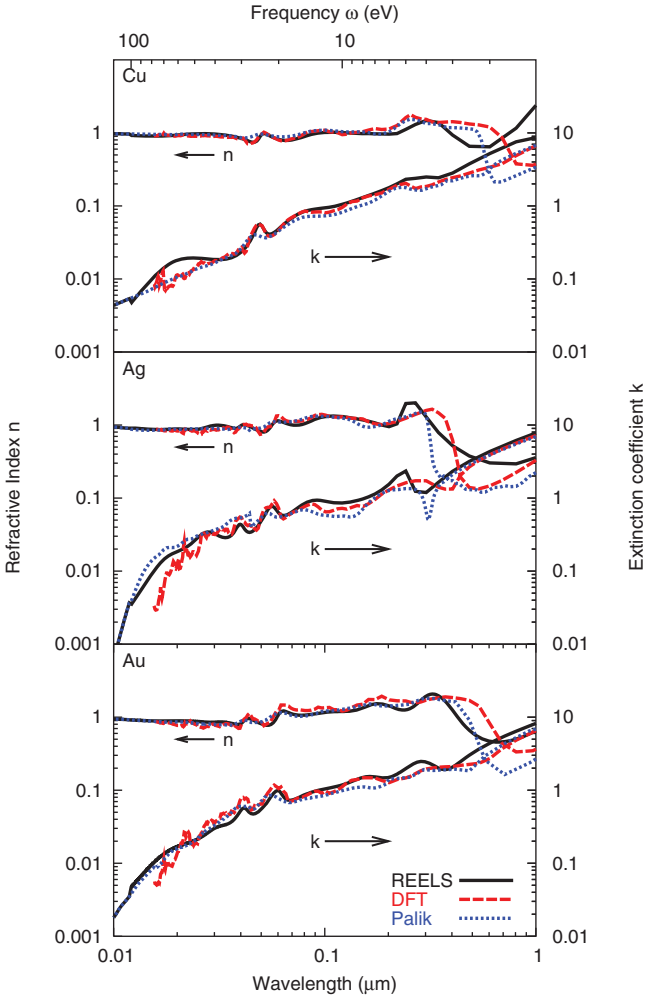

FIG. 27. (Color online) Comparison of values for the refractive index n and extinction coefficient k derived from REELS (black full curves) and DFT (red dashed curves) with the values given in Palik's book (blue dotted curves) as a function of the photon wavelength for Cu, Ag, and Au.

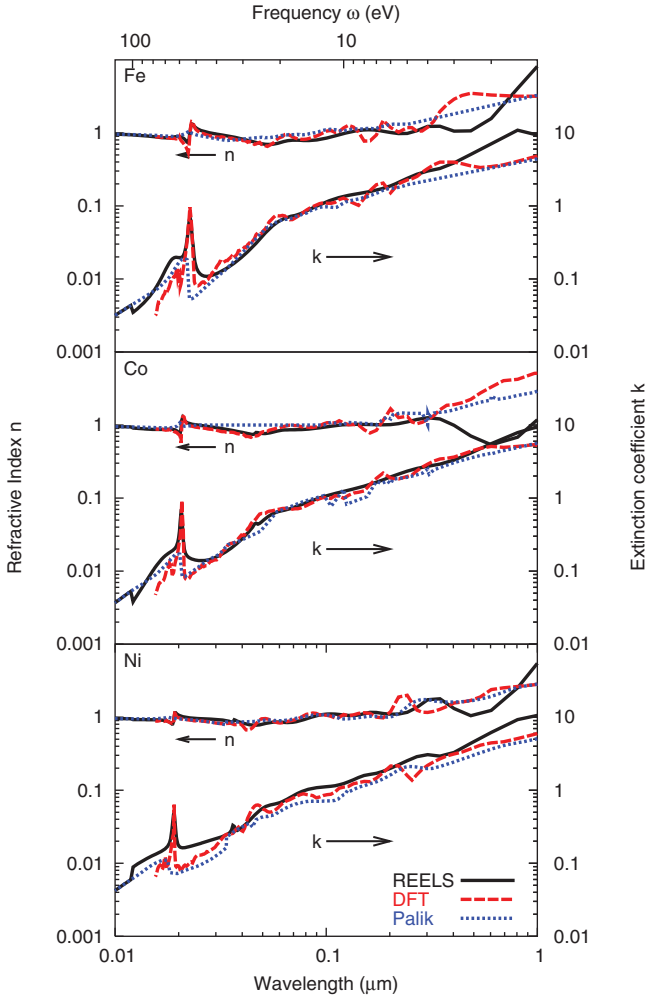

FIG. 28. (Color online) Same as Fig. 27 for Fe, Co, and Ni.

that the DFT and REELS results for the IMFP are indistinguishably similar, leading to the very important conclusion that DFT nowadays provides accurate enough optical data to calculate the reference length used in in-depth nanoscale calibration by means of electron-beam attenuation. The importance of this finding can only be appropriately appreciated after familiarizing oneself with the serious problems related to IMFP measurements in the past three decades, as outlined in an excellent review by Powell and Jablonski.[48]

In view of the significant differences for the ELF for Co according to Palik's data on one hand and the REELS and DFT results on the other hand, in particular, in the UV range, the difference of ~20% in the corresponding IMFP values sets a rather moderate upper limit to the uncertainty of IMFP values in use nowadays. It should be emphasized again that for all other materials examined here a much better mutual agreement in the IMFP values of typically better than 5% is found.

The IMFP values derived from the REELS data have been fitted to an equation of the form

$$\lambda_i(E) = k_1 E^{p_1} + k_2 E^{p_2}. \tag{33}$$

The resulting fit parameters are given in Table 3.

As a final result of this work, values of the total surface excitation parameter have been derived from the REELS spectra. This was done by fitting the REELS spectra to Eq. (15) using a single quantity, the zero-order partial intensity, or the average number of surface excitations in a single surface crossing $\langle n_s(E) \rangle$ as a free parameter. The values for the DIIMFP and DSEP derived from the deconvolution of REELS spectra were used in the fitting procedure, along with the appropriate volume partial intensities. The higher-order surface partial intensities were calculated according to the Poisson stochastic process. A result of the fitting procedure for all considered energies is shown for Cu, Fe, Ag, and Au in Fig. 34. In spite of the fact that the shape of the loss spectra is significantly different, as a result of the energy dependence of the shape of the *elastic cross section*, as discussed above, the fit is satisfactory in all cases, indicating that the approximations involved in Eq. (15) and, in particular, in Eq. (16) are reasonable and lead to a detailed understanding of the electrodynamical interaction of electrons with plane surfaces in the considered energy range.

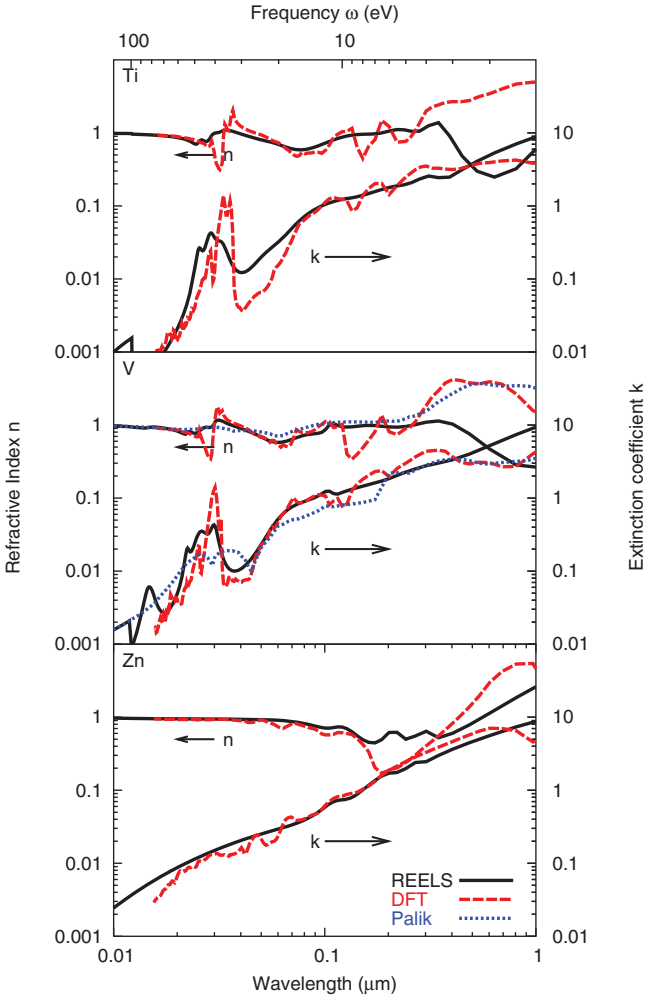

FIG. 29. (Color online) Same as Fig. 27 for Ti, V, and Zn.

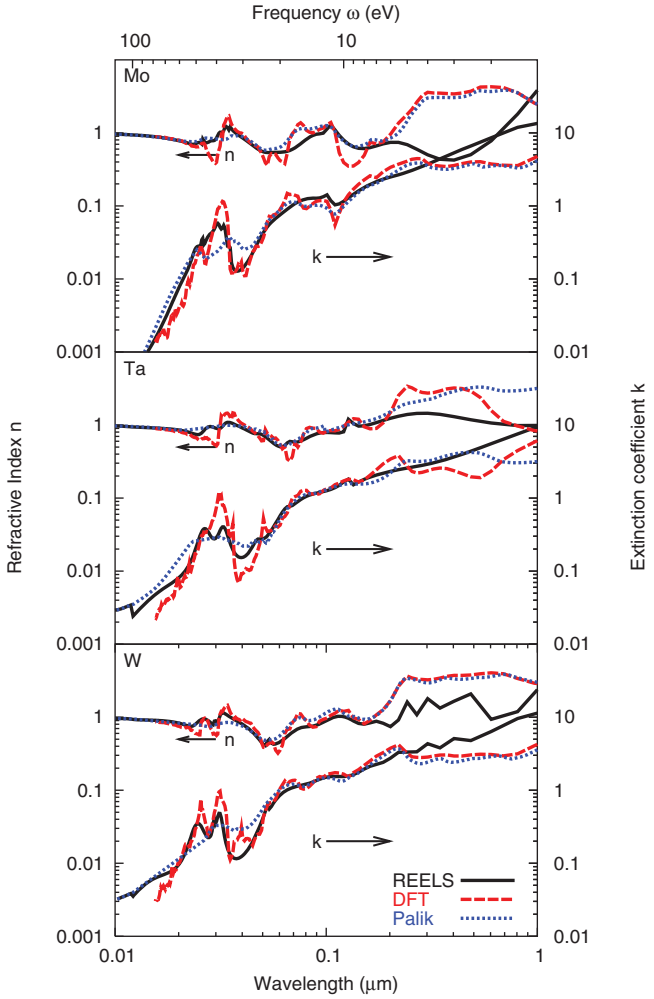

FIG. 30. (Color online) Same as Fig. 27 for Mo, Ta, and W.

For each energy, such a fit gives the zero-order surface partial intensity, being equal to the average number of surface excitations for a single surface crossing, $\langle n_s(E)\rangle$. The energy dependence of this quantity is compared with results from other sources in Fig. 35. The filled circles are the present results, and the solid lines represent a fit of the energy dependence of the zero-order partial-intensity Eq. (20) using the surface excitation parameter a_s as a free parameter. For all studied cases, the energy dependence of the zero-order partial intensity is seen to be well described by Eq. (20). Therefore, the magnitude of surface excitations can be accurately predicted by using the values of the surface excitation parameter given in Table 4, in combination with Eq. (20). The dashed curves in Fig. 35 were derived in a very similar way in Ref. 43 but using Palik's data to calculate the DIIMFP and DSEP. The resulting fit was also considerably worse than the ones shown in Fig. 34. Thus the differences in the resulting values of the zero-order partial intensities are attributed to the systematic error caused by using Palik's data. The present results for the surface excitation parameter are therefore believed to be significantly more reliable than the earlier ones. The dashed-dotted lines are theoretical calculations by Chen[79] using Palik's optical data as input.

6. Summary

Two new sets of optical constants have been presented for 16 elemental metals (Ti, V, Fe, Co, Ni, Cu, Zn, Mo, Pd, Ag, Ta, W, Pt, Au, Pb, and Bi) and one semimetal (Te) and are compared with existing data in the literature. Values are given for the real (ε_1) and imaginary (ε_2) parts of the complex dielectric constant as well as the ELF ($\mathrm{Im}\{-1/\varepsilon\}$). These values have been calculated from the Drude-Lorentz expansion coefficients derived from experimental results for the DIIMFP (and DSEP) which are also given in graphical and tabular forms. The method to determine such data using DFT calculations has been given and a detailed analysis of the experimental determination of optical constants from REELS spectra is also described, along with an analysis of the reliability of the results. The latter analysis showed that accurate results can be expected for optical constants ranging from the visible to the soft x-ray regime of wavelengths. In principle such measurements can also provide optical constants in the infrared regime; however, in this case the use of a monochromated electron source is mandatory since the thermal spread in the source energy distribution cannot be adequately eliminated numerically. The agreement between

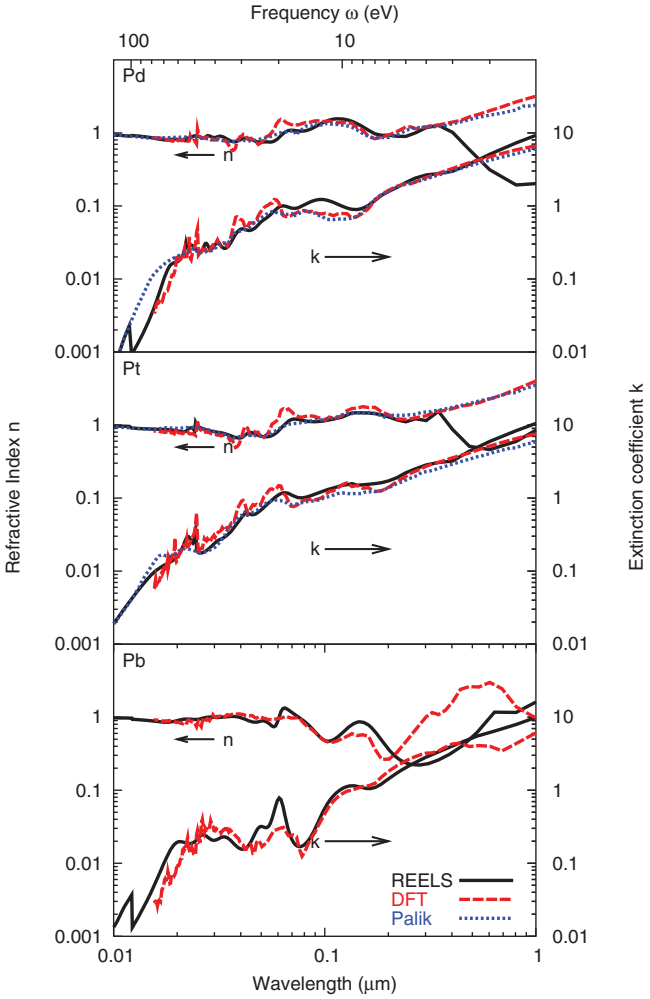

FIG. 31. (Color online) Same as Fig. 27 for Pd, Pt, and Pb.

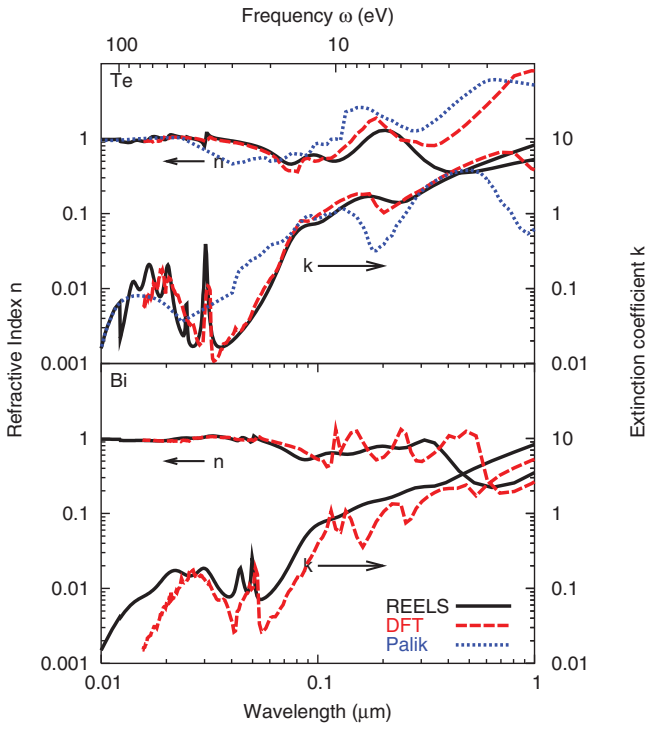

FIG. 32. (Color online) Same as Fig. 27 for Te and Bi.

the DFT and REELS results is satisfactory for all studied materials, while larger deviations are observed with Palik's data.

The experimental data for the optical constants were derived from a particular pair of energy-loss spectra for each material, selected according to outlined criteria that the sequence of partial intensities be sufficiently different for the two spectra while at the same time avoiding measurements where the combination of primary energy and scattering angle corresponding to a deep minimum in the elastic-scattering cross section. A detailed consistency check for many different pairs of spectra with arbitrary energy combinations demonstrates that this is essential to appropriately separate surface and bulk contributions contained in an energy-loss spectrum. Further consistency checks also support other key assumptions that need to be made in order to perform the analysis:

(i) The collision statistics (partial intensities) for surface and bulk scattering are uncorrelated.

(ii) Calculation of the volume partial intensities using elastic-scattering cross sections for free atoms on the basis of a Boltzmann-type kinetic equation (i.e., neglecting coherent scattering and diffraction) is adequate for the present purpose.

(iii) The functional form of the energy and angular dependence of the surface-scattering probability is appropriately described by Eq. (20) rather than by Eq. (30). Plural surface scattering is described by the Poisson stochastic process.

TABLE 2. Results of sum-rule checks on the three sets of optical data discussed in the present work

		f sum			ps sum		
		REELS	DFT	Palik	REELS	DFT	Palik
Ti	22	20.8	20.7	–	1.023	0.979	–
V	23	22.3	22.0	21.0	1.029	0.990	1.016
Fe	26	25.9	25.2	24.0	1.012	1.007	0.944
Co	27	27.3	26.7	24.2	1.035	1.016	0.845
Ni	28	29.9	27.8	26.7	1.000	1.017	1.011
Cu	29	30.6	29.5	28.3	1.037	1.016	0.995
Zn	30	16.2	29.4	–	1.021	1.034	–
Mo	42	40.1	40.3	39.7	1.022	0.991	1.013
Pd	46	43.0	43.2	45.6	1.026	0.997	1.143
Ag	47	46.6	44.5	50.6	1.018	1.005	1.148
Te	52	55.4	53.7	69.1	1.027	0.991	1.378
Ta	73	69.9	70.9	70.5	1.041	1.007	1.025
W	74	71.5	72.7	77.7	1.039	1.012	0.986
Pt	78	74.4	76.0	75.2	1.028	1.012	1.105
Au	79	74.5	75.2	75.0	1.008	0.992	1.107
Pb	82	79.9	77.9	–	1.024	1.009	–
Bi	83	80.8	72.6	–	1.018	1.003	–

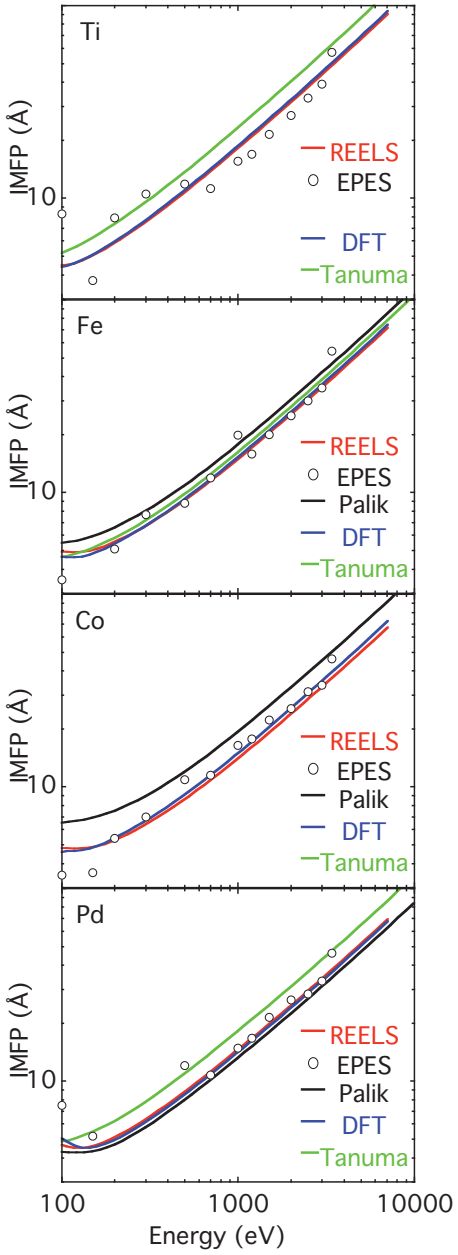

FIG. 33. (Color online) Comparison of IMFP values for Ti, Fe, Co, and Pd taken from different sources.

(iv) The shapes of the normalized DIIMFP and DSEP are independent of the energy of the reflected electrons and the surface crossing direction to a good approximation.

(v) The dispersion of the characteristic frequency of any electronic transition, as well as the dispersion of the involved initial and final states, can appropriately be described by a *single* dispersion parameter α in a Drude-Lorentz expansion of the dielectric constant using oscillator energies of the form $\omega_i(q)=\omega_i+\alpha q^2/2$. This follows from the fact that the results show no pronounced variation around a reasonable choice of this parameter of $\alpha=0.5$.

TABLE 3. Fit parameters in Eq. (33) describing the IMFP values derived from the REELS measurements

	k_1	p_1	k_2	p_2
Ti	0.046	0.85	4.2	−0.17
V	0.043	0.85	6.1	−0.23
Fe	0.043	0.84	16.9	−0.40
Co	0.042	0.83	22.3	−0.45
Ni	0.041	0.83	24.0	−0.45
Cu	0.040	0.84	14.1	−0.34
Zn	0.042	0.86	4.7	−0.11
Mo	0.038	0.85	3.5	−0.13
Pd	0.045	0.83	15.7	−0.42
Ag	0.048	0.82	29.3	−0.52
Te	0.050	0.87	12.5	−0.36
Ta	0.035	0.85	3.9	−0.10
W	0.034	0.84	5.0	−0.16
Pt	0.039	0.83	10.5	−0.31
Au	0.044	0.83	14.0	−0.35
Pb	0.048	0.85	16.2	−0.42
Bi	0.054	0.84	13.6	−0.35

The uncertainty in the experimental data has been analyzed and is estimated to amount to about 10% for the ELF

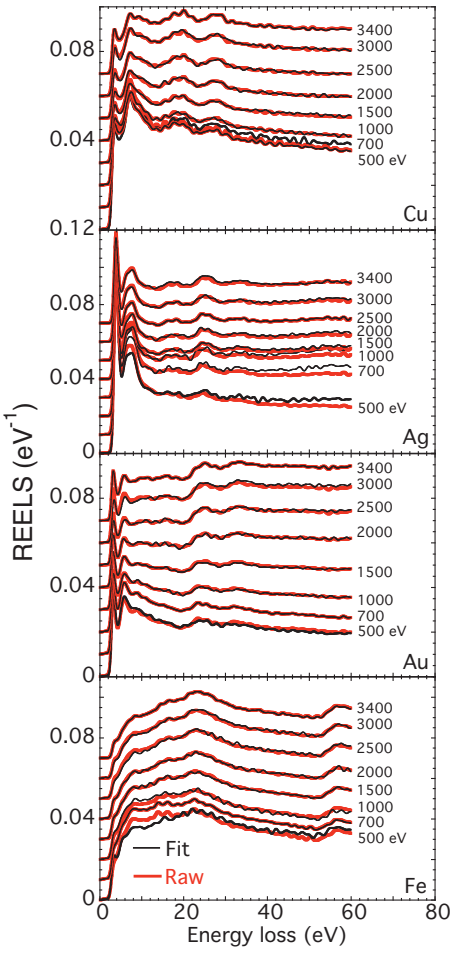

FIG. 34. (Color online) Comparison of REELS spectra with fitted spectra for determination of the surface excitation parameter.

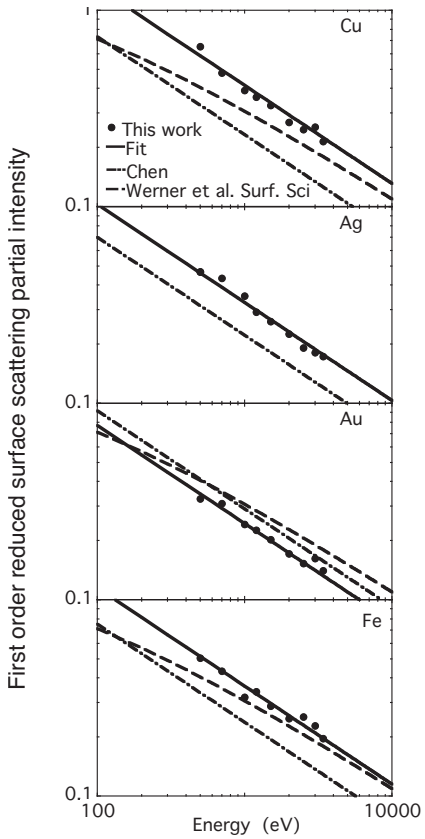

FIG. 35. First-order reduced surface partial intensities (data points) derived from the REELS spectra. Solid line: fit of these data to Eq. (20); dashed line: results of Ref. 43 based on Oswald's energy and angular dependence of the average number of surface excitations, Eq. (30); dashed-dotted line: theoretical results by Chen (Ref. 79) based on the optical constants of Palik (Ref. 73).

and ε_2 as well as for ε_1 for energies above 10 eV. For energies below 10 eV, the uncertainty in ε_1 in the present data may exceed 100%, which is a consequence of the fact that energy-loss measurements mainly sample the absorptive part of the dielectric constant. Below ~3–5 eV, the uncertainty in the present REELS data (for ε_1 as well as for ε_2) is additionally increased as a result of the large dynamic range of REELS experiments, leading to difficulties in the separation of the elastic peak from the energy-loss portion of the spectra. The accuracy of the DFT results is difficult to estimate quantitatively, but the comparison with the experimental results and Palik's data shows that for energies below 10 eV, where, for the reasons mentioned above, the experimental data are known to be less reliable, the agreement between DFT and Palik's data is comparable to the agreement of all three data sets at higher energies.

The above may be summarized by stating that the REELS data provide optical constants with an experimental accuracy of about 10% for energies between the near-ultraviolet regime and the (far) soft x-ray regime of energies, while the DFT results provide similarly reliable data for energies ranging from the infrared to the soft-x-ray regime.

Electron-scattering data derived from the optical constants have also been compared with literature values, again showing very good agreement. In particular, values for the electron IMFP derived from REELS and DFT show a very good consistency and agree better than 5% for the majority of all cases studied for energies between 50 and 5000 eV. An important conclusion in this context is that nanoscale calibration by means of electron-beam attenuation is nowadays possible on the basis of DFT calculations without the need for an experimental calibration of the electron attenuation length.

TABLE 4. Values for the surface excitation parameter a_s in units of a_{NFE} $=2.896\ \text{eV}^{-1/2}$ derived from the REELS measurements, compared with the theoretical values of Chen (Ref. 79)

Metal	a_s	Chen (Ref. 79)
Ti	2.8	–
V	3.3	–
Fe	3.8	2.51
Co	3.8	–
Ni	4.1	–
Cu	4.3	2.45
Zn	4.8	–
Mo	3.9	–
Pd	2.9	–
Ag	3.4	2.34
Te	3.8	–
Ta	3.3	–
W	3.4	–
Pt	2.7	–
Au	2.6	3.06
Pb	3.1	–
Bi	3.2	–

7. Acknowledgments

Support by the Austrian Science Foundation FWF (Project Nos. P16227 and P20891-N20) is gratefully acknowledged.

8. Appendix A: Deconvolution Algorithm For REELS Spectra

In the present work, multiple-scattering contributions in REELS spectra were eliminated by the deconvolution procedure equation (23). Calculation of the coefficients needed using this Padé expansion is very tedious as described in Refs. 8 and 44. A simplified deconvolution procedure was recently developed[45] which leads to the same results and may be used for the same purpose while the numerical effort is dramatically reduced. Therefore, for completeness, a synopsis of this simplified deconvolution procedure is given below.

The simplified algorithm for retrieval of the DIIMFP and DSEP can be summarized as follows: Let $y_1(T)$ and $y_2(T)$ be the measured spectra with the reduced volume partial intensities α_n and β_n, respectively. In the first step, the intermediate spectra $y_1^*(T)$ and $y_2^*(T)$ are derived by

$$y_1^*(T) = y_1(T) - \int_0^T y_1(T-T')y_1^*(T')dT',$$

$$y_2^*(T) = y_2(T) - \int_0^T y_2(T-T')y_2^*(T')dT'. \quad \text{(A1)}$$

The DIIMFP and DSEP can then be retrieved by means of the series expansion

$$w(T) = u_{10}y_1^*(T) + u_{01}y_2^*(T) + u_{11}y_1^* \otimes y_2^*(T) + u_{20}y_1^* \otimes y_1^*(T) + u_{02}y_2^* \otimes y_2^*(T), \quad \text{(A2)}$$

where the expansion coefficients are different for the surface and bulk (subscripts "s" and "b," below) single-scattering loss distributions. To bring the expressions for the expansion coefficients into a more tractable form, it is useful to introduce the shorthand notation

$$\mu = \frac{1}{\sqrt{E_1}}\left(\frac{1}{\cos\theta_1^i} + \frac{1}{\cos\theta_1^o}\right),$$
$$\nu = \frac{1}{\sqrt{E_2}}\left(\frac{1}{\cos\theta_2^i} + \frac{1}{\cos\theta_2^o}\right),$$

where the indices "1" and "2" refer to the two spectra $y_1(T)$ and $y_2(T)$ and the superscript i and o indicate the ingoing and outgoing polar direction of surface crossing. Furthermore, by writing

$$\alpha_{k,l} = \alpha_k\frac{\mu^l}{l!},$$
$$\beta_{k,l} = \beta_k\frac{\nu^l}{l!}$$

where the subscript "k" in α_k and β_k indicate the fact that these quantities represent the *bulk* partial intensities, the expressions for the expansion coefficients read

$$\Delta = \alpha_1\nu - \beta_1\mu,$$
$$u_{10}^b = \nu/\Delta,$$
$$u_{01}^b = -\mu/\Delta,$$
$$u_{10}^s = -\beta_1/\Delta,$$
$$u_{01}^s = \alpha_1/\Delta, \quad \text{(A3)}$$

$$u_{02}^b = \frac{\mu}{\Delta^3}\left\{(\beta_2 - \beta_1^2)\mu^2 + \left(\frac{\alpha_1^2}{2} + \alpha_1\beta_1 - \alpha_2\right)\mu\nu - \frac{\alpha_1^2}{2}\nu^2\right\},$$
$$u_{11}^b = \frac{\mu\nu}{\Delta^3}\{\beta_1^2\mu - 2\beta_2\mu - \alpha_1^2\nu + 2\alpha_2\nu\},$$
$$u_{20}^b = -\frac{\nu}{\Delta^3}\left\{(\alpha_2 - \alpha_1^2)\nu^2 + \left(\frac{\beta_1^2}{2} + \alpha_1\beta_1 - \beta_2\right)\nu\mu - \frac{\beta_1^2}{2}\mu^2\right\}, \quad \text{(A4)}$$

$$u_{02}^s = \frac{1}{\Delta^3}\left\{\mu^2\left(\alpha_2\beta_1 + \alpha_1\left[\beta_1^2 - \beta_2 - \frac{\alpha_1\beta_1}{2}\right]\right) - \mu\nu\alpha_1^2\beta_1 + \nu^2\frac{\alpha_1^3}{2}\right\},$$
$$u_{11}^s = \frac{\mu\nu}{\Delta^3}\{\beta_1(\alpha_1^2 - 2\alpha_2 - \alpha_1\beta_1) + 2\alpha_1\beta_2\},$$

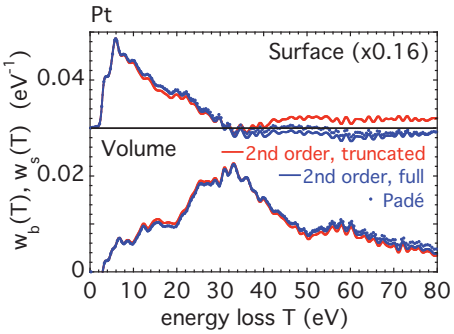

FIG. 36. (Color online) Comparison of the Padé approximation [Eq. (23), dots] for the DIIMFP and DSEP for Pt with the second-order truncated [Eq. (A6), red curves] and the full second-order [Eq. (A2), blue curves] expansion.

$$u_{20}^s = -\frac{1}{\Delta^3}\left\{\nu^2\left(\alpha_1\beta_2 + \beta_1\left[\alpha_1^2 - \alpha_2 - \frac{\alpha_1\beta_1}{2}\right]\right) - \mu\nu\beta_1^2\alpha_1 + \mu^2\frac{\beta_1^3}{2}\right\}. \quad \text{(A5)}$$

Equation (A2) can also be truncated after the mixed second-order term, giving for the deconvoluted single-scattering loss distributions

$$w(T) = u_{10}y_1^*(T) + u_{01}y_2^*(T) + u_{11}y_1^* \otimes y_2^*(T). \quad \text{(A6)}$$

In this case, the expansion coefficients for the mixed second-order term are given by

$$u_{11}^b = \frac{\mu\nu(\alpha_1 - \beta_1)}{(\alpha_1\nu)^2 - (\beta_1\mu)^2},$$
$$u_{11}^s = \frac{\alpha_1\beta_1(\nu - \mu)}{(\alpha_1\nu)^2 - (\beta_1\mu)^2}, \quad \text{(A7)}$$

while u_{01} and u_{10} are still given by Eq. (A3). The above deconvolution scheme [Eqs. (A1), (A6), and (A7)] is extremely simple and yet accurate enough for most practical purposes.

In Fig. 36 the red curves are the single-scattering loss distributions for Pt obtained by means of Eq. (A6) that are compared with the results for the DIIMFP and DSEP obtained with the second-order Padé approximation equation (23), calculating the coefficients in the usual way.[44] Considering the complexity of the calculation of the former Padé coefficients in comparison to the simplicity of the coefficients u_{kl}, the agreement between the resulting single-scattering loss functions is remarkable. The agreement can be even further improved by taking into account the quadratic terms in the intermediate spectra, leading to the full second-order expansion [blue curves, Eq. (A2)]. The latter is also shown in these figures and is seen to agree excellently with the results of the Padé approximation.

9. Appendix B: Values of the Drude-Lorentz Parameters for the Dielectric Function

This appendix contains values of the Drude-Lorentz parameters for the dielectric function as given in Tables 5–10.

TABLE 5. Drude-Lorentz parameters for Ti ($E_{3p1/2}$=32.6 eV), V ($E_{3p3/2}$=37.3 eV), and Fe ($E_{3p1/2}$=52.7 eV)

Ti			V			Fe		
ω_i (eV)	γ_i (eV)	A_i (eV^2)	ω_i (eV)	γ_i (eV)	A_i (eV^2)	ω_i (eV)	γ_i (eV)	A_i (eV^2)
0.000	0.027	116.1	0.000	0.027	143.3	0.000	8.0	0.049
1.0	0.5	7.8	1.0	9.8	0.2	1.1	0.5	168.5
3.7	1.2	22.3	3.6	3.6	73.6	3.9	2.0	31.5
5.5	3.0	36.5	8.2	7.3	108.3	8.9	10.5	225.2
9.9	10.5	197.8	11.5	1.5	14.2	19.0	8.4	58.1
22.8	10.8	28.7	15.4	11.1	145.9	32.8	148.6	19.1
37.2	6.5	112.6	40.1	4.0	106.8	44.0	231.9	1278.6
41.7	5.1	116.5	46.3	8.9	214.8	53.1	2.1	150.1
47.5	4.1	49.8	54.1	3.3	29.6	63.3	16.8	246.8
80.6	37.1	0.1	82.1	11.8	95.7			

TABLE 6. Drude-Lorentz parameters for Co ($E_{3p1/2}$=58.9 eV), Ni ($E_{3p3/2}$=66.2 eV), and Cu ($E_{3p3/2}$=75.1 eV)

Co			Ni			Cu		
ω_i (eV)	γ_i (eV)	A_i (eV^2)	ω_i (eV)	γ_i (eV)	A_i (eV^2)	ω_i (eV)	γ_i (eV)	A_i (eV^2)
0.000	0.027	133.4	0.000	0.027	32.0	0.000	0.027	86.3
1.0	0.5	19.0	1.0	0.5	127.3	1.0	0.5	19.8
4.0	3.6	71.8	3.9	1.6	44.7	1.0	0.5	21.9
10.1	12.8	133.3	6.2	7.9	111.2	4.0	1.7	30.2
15.1	32.3	407.5	7.7	2.3	13.3	4.8	0.5	2.5
20.8	7.7	38.3	13.6	10.8	237.3	7.2	11.3	157.7
26.1	1.2	3.2	22.9	8.8	83.7	14.2	10.1	130.9
58.6	1.4	91.8	33.2	0.9	4.6	16.9	68.2	108.6
66.1	37.1	645.3	40.5	32.4	160.1	24.3	3.0	40.0
			63.4	1.9	86.2	59.4	55.1	1022.4
			79.6	109.5	1843.5			

TABLE 7. Drude-Lorentz parameters for Zn ($E_{3d5/2}$=10.1 eV), Mo ($E_{4p3/2}$=35.5 eV), and Pd ($E_{4p3/2}$=50.9 eV)

Zn			Mo			Pd		
ω_i (eV)	γ_i (eV)	A_i (eV^2)	ω_i (eV)	γ_i (eV)	A_i (eV^2)	ω_i (eV)	γ_i (eV)	A_i (eV^2)
0.000	0.8	85.9	0.000	0.027	177.0	0.000	0.027	138.9
0.9	0.5	0.002	1.0	0.5	114.1	3.7	2.6	59.9
4.2	0.5	3.6	5.9	4.9	88.8	6.1	1.9	8.3
5.9	1.4	9.5	11.8	1.0	15.4	12.1	7.4	281.0
10.4	3.5	14.3	14.0	7.3	201.5	18.8	5.3	121.6
23.6	26.4	16.1	21.7	9.6	56.5	23.7	5.2	32.8
35.7	114.7	1257.7	34.7	0.5	6.9	29.9	7.5	119.3
			36.6	1.9	55.4	38.9	5.7	68.3
			39.2	3.4	102.0	44.0	3.7	40.7
			43.0	6.1	94.9	52.0	10.6	217.3
			46.6	0.5	5.7	54.8	0.5	3.4
			49.4	6.6	73.9	64.6	15.3	176.4
			56.4	20.6	99.9			

TABLE 8. Drude-Lorentz parameters for Ag ($E_{4p3/2}$=58.3 eV), Te ($E_{4d5/2}$=40.4 eV), and Ta ($E_{4f7/2}$=21.6 eV)

Ag			Te			Ta		
ω_i (eV)	γ_i (eV)	A_i (eV^2)	ω_i (eV)	γ_i (eV)	A_i (eV^2)	ω_i (eV)	γ_i (eV)	A_i (eV^2)
0.000	0.065	98.4	0.000	0.027	102.3	0.000	0.027	139.3
1.0	93.8	103.9	1.0	2.3	19.8	1.0	7.9	138.2
4.9	0.7	23.8	6.6	3.7	92.5	5.4	7.2	161.8
10.3	22.0	318.3	9.0	405.0	0.1	9.5	0.5	8.6
13.2	6.3	89.6	13.4	5.6	44.2	13.7	7.5	92.5
21.2	3.3	63.5	39.7	0.9	29.4	18.3	1.9	6.5
30.2	3.7	43.3	48.9	0.5	3.5	25.5	3.6	12.3
43.0	16.7	313.3	59.4	4.2	95.8	36.8	4.9	108.4
65.7	38.8	519.9	72.4	8.6	236.1	45.1	7.6	180.6
			86.0	10.8	177.8	70.4	70.0	411.2

TABLE 9. Drude-Lorentz parameters for W ($E_{4f7/2}$=31.4 eV), Pt ($E_{5p3/2}$=51.7 eV), and Au ($E_{5p3/2}$=57.2 eV)

W			Pt			Au		
ω_i (eV)	γ_i (eV)	A_i (eV^2)	ω_i (eV)	γ_i (eV)	A_i (eV^2)	ω_i (eV)	γ_i (eV)	A_i (eV^2)
0.000	0.027	168.0	0.000	0.2	179.1	0.000	0.2	113.1
1.0	0.5	54.3	3.5	0.8	16.6	4.0	1.5	44.6
2.7	0.9	47.4	4.5	0.9	7.5	7.3	3.3	54.8
3.9	0.5	25.5	9.0	0.5	2.1	12.8	11.8	184.9
5.0	0.8	33.4	9.1	11.5	367.4	18.9	71.0	728.1
7.0	2.5	37.9	9.7	0.5	1.0	19.9	2.9	65.7
11.1	6.0	164.2	18.2	4.9	121.3	28.9	3.9	50.0
16.7	7.7	125.1	18.7	36.1	18.5	38.7	13.0	74.7
22.9	0.6	2.9	26.4	55.5	486.5	64.3	51.9	544.0
38.4	3.1	98.4	28.2	4.0	36.9			
41.1	0.9	11.1	38.9	6.0	12.1			
48.5	8.9	221.9	39.2	25.0	3.3			
80.2	65.1	495.5	49.6	0.5	14.5			
			53.5	5.7	87.2			
			72.4	47.6	421.4			

TABLE 10. Drude-Lorentz parameters for Pb ($E_{5d5/2}$=18.1 eV) and Bi ($E_{5d5/2}$=23.8 eV)

Pb			Bi		
ω_i (eV)	γ_i (eV)	A_i (eV^2)	ω_i (eV)	γ_i (eV)	A_i (eV^2)
0.000	0.4	161.7	0.000	0.087	108.4
1.9	0.5	6.3	3.9	1.8	23.6
8.7	4.2	64.5	6.6	4.5	50.2
19.5	2.1	66.1	11.3	6.2	44.8
24.4	4.8	42.9	24.1	0.6	6.6
35.9	10.9	126.8	27.5	1.9	13.2
37.9	48.6	0.6	40.2	9.6	99.3
45.4	9.7	120.1	55.8	21.7	326.8
59.9	21.6	400.8	84.2	48.4	373.1

TABLE 11. Values of the real (ε_1) and imaginary (ε_2) parts of the complex dielectric constant and the ELF ($\mathrm{Im}\{-1/\varepsilon(\omega)\}$) of Ti calculated with DFT and derived from REELS data. The last two columns contain values for the volume and surface single-scattering loss distributions the DIIMFP (w_b) and the DSEP (w_s)

Ti									
DFT				REELS					
E (eV)	ε_1	ε_2	ELF	E (eV)	ε_1	ε_2	ELF	w_b (meV^{-1})	w_s (arb. un.)
0.50	5.812	51.273	0.019	0.50	−447.600	28.594	0.000	0.0	1.2
0.75	6.799	49.843	0.020	0.75	−189.661	16.723	0.000	0.0	1.9
1.00	9.039	39.345	0.024	1.00	−109.799	19.374	0.002	0.1	2.5
1.25	9.622	38.053	0.025	1.25	−74.201	9.230	0.002	0.1	3.1
1.50	3.674	39.479	0.025	1.50	−49.772	4.557	0.002	0.1	3.7
1.75	−1.163	33.160	0.030	1.75	−34.555	3.018	0.003	−0.2	4.8
2.00	−3.570	27.125	0.036	2.00	−24.626	2.496	0.004	−0.4	8.3
2.25	−4.749	23.926	0.040	2.25	−17.761	2.422	0.008	−0.9	17.5
2.50	−4.804	19.609	0.048	2.50	−12.773	2.638	0.016	−1.2	33.5
2.75	−3.433	17.267	0.056	2.75	−9.016	3.144	0.034	−0.6	51.6
3.00	−2.755	16.906	0.058	3.00	−6.197	4.025	0.074	1.1	62.7
3.25	−3.440	16.717	0.057	3.25	−4.395	5.352	0.112	2.9	63.8
3.50	−4.892	15.876	0.058	3.50	−4.024	6.719	0.110	4.0	60.2
3.75	−5.655	14.873	0.059	3.75	−4.737	6.945	0.098	4.3	56.6
4.00	−8.458	14.037	0.052	4.00	−4.994	6.007	0.098	4.3	55.3
4.25	−9.576	9.965	0.052	4.25	−4.481	5.080	0.111	4.2	56.2
4.50	−8.658	6.784	0.056	4.50	−3.749	4.570	0.131	4.4	58.3
4.75	−7.080	4.875	0.066	4.75	−3.120	4.367	0.152	5.0	59.9
5.0	−5.583	3.795	0.083	5.0	−2.686	4.306	0.167	6.0	60.4
5.5	−3.065	2.833	0.163	5.5	−2.292	4.170	0.184	7.7	60.3
6.0	−0.546	3.494	0.279	6.0	−2.099	3.796	0.202	7.6	63.7
6.5	−1.970	6.058	0.149	6.5	−1.825	3.366	0.230	7.7	66.4
7.0	−3.447	3.264	0.145	7.0	−1.509	3.039	0.264	9.7	62.1
7.5	−2.567	2.263	0.193	7.5	−1.235	2.822	0.297	12.0	56.8
8.0	−1.733	1.244	0.273	8.0	−1.034	2.670	0.326	12.1	59.3
8.5	−0.470	1.195	0.724	8.5	−0.902	2.545	0.349	11.5	63.6
9.0	0.601	1.972	0.464	9.0	−0.821	2.422	0.370	12.4	63.0
9.5	−0.283	2.461	0.401	9.5	−0.773	2.290	0.392	14.1	61.3
10.0	−0.443	2.571	0.378	10.0	−0.739	2.146	0.417	15.0	63.8
10.5	−0.661	2.409	0.386	10.5	−0.709	1.993	0.445	14.8	70.7
11.0	−0.970	2.266	0.373	11.0	−0.674	1.836	0.480	15.6	73.8
11.5	−1.108	1.716	0.411	11.5	−0.632	1.681	0.521	18.5	69.9
12.0	−0.958	1.317	0.497	12.0	−0.581	1.531	0.571	20.4	65.7
12.5	−0.731	1.055	0.641	12.5	−0.523	1.391	0.630	20.0	69.0
13.0	−0.498	0.966	0.818	13.0	−0.458	1.262	0.700	20.1	75.2
13.5	−0.368	0.892	0.959	13.5	−0.390	1.145	0.782	22.2	72.8
14.0	−0.322	0.829	1.048	14.0	−0.319	1.040	0.878	24.8	63.1
14.5	−0.230	0.759	1.206	14.5	−0.248	0.947	0.988	26.9	55.6
15.0	−0.165	0.683	1.383	15.0	−0.178	0.864	1.110	28.4	54.0
15.5	−0.069	0.651	1.519	15.5	−0.108	0.792	1.240	29.3	53.5
16.0	−0.084	0.550	1.777	16.0	−0.041	0.728	1.368	30.9	47.5
16.5	0.008	0.447	2.234	16.5	0.023	0.673	1.484	34.4	36.5
17.0	0.103	0.388	2.408	17.0	0.084	0.625	1.571	38.2	23.9
17.5	0.187	0.342	2.250	17.5	0.142	0.584	1.617	38.8	18.4
18.0	0.258	0.321	1.891	18.0	0.196	0.548	1.616	37.2	22.2
18.5	0.322	0.279	1.540	18.5	0.247	0.518	1.572	37.7	20.8
19.0	0.386	0.261	1.204	19.0	0.294	0.492	1.497	39.0	11.3
19.5	0.444	0.238	0.938	19.5	0.338	0.470	1.404	37.4	8.6
20.0	0.509	0.228	0.732	20.0	0.377	0.450	1.306	34.6	13.8
20.5	0.538	0.218	0.648	20.5	0.413	0.433	1.210	32.8	15.4
21.0	0.570	0.201	0.551	21.0	0.445	0.417	1.121	30.9	13.9
21.5	0.617	0.163	0.399	21.5	0.474	0.402	1.040	29.3	13.6

TABLE 11. Values of the real (ε_1) and imaginary (ε_2) parts of the complex dielectric constant and the ELF ($\mathrm{Im}\{-1/\varepsilon(\omega)\}$) of Ti calculated with DFT and derived from REELS data. The last two columns contain values for the volume and surface single-scattering loss distributions the DIIMFP (w_b) and the DSEP (w_s)—Continued

Ti									
DFT				REELS					
E (eV)	ε_1	ε_2	ELF	E (eV)	ε_1	ε_2	ELF	w_b (meV^{-1})	w_s (arb. un.)
22.0	0.670	0.147	0.312	22.0	0.501	0.387	0.966	28.6	10.1
22.5	0.721	0.136	0.252	22.5	0.526	0.372	0.897	27.7	6.1
23.0	0.769	0.129	0.212	23.0	0.549	0.357	0.831	25.5	8.1
23.5	0.814	0.124	0.183	23.5	0.573	0.341	0.767	23.6	10.0
24.0	0.859	0.121	0.161	24.0	0.596	0.325	0.705	22.5	8.3
24.5	0.898	0.124	0.151	24.5	0.620	0.310	0.646	21.0	8.0
25.0	0.933	0.123	0.139	25.0	0.644	0.296	0.589	18.6	11.0
25.5	0.969	0.119	0.125	25.5	0.669	0.282	0.535	17.5	11.5
26.0	1.008	0.117	0.114	26.0	0.694	0.270	0.487	18.2	6.4
26.5	1.046	0.112	0.101	26.5	0.720	0.259	0.443	17.1	4.8
27.0	1.090	0.107	0.089	27.0	0.747	0.250	0.404	14.9	7.2
27.5	1.133	0.103	0.079	27.5	0.773	0.243	0.370	14.3	6.7
28.0	1.185	0.098	0.069	28.0	0.800	0.238	0.341	14.1	6.0
28.5	1.241	0.093	0.060	28.5	0.827	0.234	0.316	13.1	5.2
29.0	1.305	0.089	0.052	29.0	0.855	0.232	0.296	12.0	3.2
29.5	1.383	0.085	0.044	29.5	0.882	0.233	0.279	11.2	4.1
30.0	1.479	0.091	0.041	30.0	0.910	0.235	0.266	10.3	8.1
30.5	1.585	0.102	0.040	30.5	0.938	0.240	0.256	9.4	9.1
31.0	1.719	0.108	0.036	31.0	0.967	0.249	0.249	9.3	5.5
31.5	1.915	0.123	0.033	31.5	0.995	0.260	0.246	9.7	2.1
32.0	2.204	0.154	0.032	32.0	1.024	0.275	0.245	9.1	2.9
32.5	2.771	0.254	0.033	32.5	1.052	0.295	0.247	8.0	6.5
33.0	4.014	1.617	0.086	33.0	1.079	0.320	0.253	7.7	6.4
33.5	2.453	3.220	0.197	33.5	1.103	0.351	0.262	8.4	2.9
34.0	0.520	3.144	0.310	34.0	1.124	0.389	0.275	9.3	1.2
34.5	0.340	1.949	0.498	34.5	1.138	0.433	0.292	9.2	3.6
35.0	0.677	1.662	0.516	35.0	1.143	0.484	0.314	8.9	4.3
35.5	0.936	1.835	0.432	35.5	1.136	0.538	0.341	9.2	2.8
36.0	0.640	2.725	0.348	36.0	1.113	0.591	0.372	8.7	5.4
36.5	−1.133	2.471	0.334	36.5	1.076	0.635	0.407	8.3	6.9
37.0	−1.064	0.861	0.460	37.0	1.029	0.665	0.443	9.5	2.7
37.5	−0.581	0.568	0.860	37.5	0.982	0.679	0.476	9.7	2.0
38.0	−0.324	0.408	1.502	38.0	0.942	0.680	0.504	8.3	7.7
38.5	−0.142	0.327	2.573	38.5	0.915	0.676	0.523	8.3	9.4
39.0	−0.021	0.272	3.652	39.0	0.898	0.677	0.536	10.3	3.3
39.5	0.065	0.213	4.298	39.5	0.884	0.690	0.549	11.5	−0.5
40.0	0.179	0.139	2.702	40.0	0.864	0.715	0.569	10.8	3.0
40.5	0.306	0.114	1.065	40.5	0.825	0.749	0.604	10.4	5.7
41.0	0.441	0.124	0.589	41.0	0.760	0.777	0.658	12.0	1.8
41.5	0.570	0.252	0.649	41.5	0.675	0.780	0.733	13.6	−0.3
42.0	0.415	0.336	1.178	42.0	0.588	0.747	0.827	12.7	4.8
42.5	0.393	0.307	1.237	42.5	0.520	0.684	0.927	12.3	7.1
43.0	0.377	0.262	1.242	43.0	0.482	0.607	1.010	13.7	2.9
43.5	0.385	0.211	1.093	43.5	0.473	0.533	1.050	15.8	−1.2
44.0	0.416	0.169	0.841	44.0	0.484	0.471	1.034	16.8	−0.6
44.5	0.453	0.143	0.632	44.5	0.506	0.426	0.973	16.4	2.2
45.0	0.497	0.133	0.503	45.0	0.534	0.397	0.897	15.6	4.5
45.5	0.514	0.145	0.510	45.5	0.560	0.385	0.834	15.7	6.2
46.0	0.517	0.141	0.491	46.0	0.578	0.388	0.802	17.3	4.6
46.5	0.529	0.124	0.422	46.5	0.579	0.402	0.809	18.4	0.9
47.0	0.543	0.110	0.359	47.0	0.558	0.414	0.858	16.8	3.6
47.5	0.563	0.102	0.311	47.5	0.519	0.409	0.936	15.3	7.3

TABLE 11. Values of the real (ε_1) and imaginary (ε_2) parts of the complex dielectric constant and the ELF ($\mathrm{Im}\{-1/\varepsilon(\omega)\}$) of Ti calculated with DFT and derived from REELS data. The last two columns contain values for the volume and surface single-scattering loss distributions the DIIMFP (w_b) and the DSEP (w_s)—Continued

Ti									
DFT				REELS					
E (eV)	ε_1	ε_2	ELF	E (eV)	ε_1	ε_2	ELF	w_b (meV^{-1})	w_s (arb. un.)
48.0	0.574	0.096	0.285	48.0	0.480	0.377	1.012	16.3	5.4
48.5	0.590	0.089	0.251	48.5	0.458	0.328	1.035	17.2	3.0
49.0	0.600	0.085	0.232	49.0	0.455	0.277	0.976	17.0	1.2
49.5	0.608	0.072	0.192	49.5	0.466	0.232	0.856	17.1	1.3
50.0	0.627	0.063	0.160	50.0	0.484	0.196	0.718	17.1	–
50.5	0.643	0.060	0.144	50.5	0.504	0.167	0.592	16.1	–
51.0	0.662	0.064	0.145	51.0	0.525	0.145	0.489	15.0	–
51.5	0.661	0.064	0.146	51.5	0.545	0.128	0.407	15.6	–
52.0	0.667	0.057	0.127	52.0	0.564	0.114	0.343	16.6	–
52.5	0.680	0.049	0.105	52.5	0.582	0.102	0.293	15.3	–
53.0	0.692	0.047	0.097	53.0	0.598	0.093	0.253	12.8	–
53.5	0.706	0.048	0.096	53.5	0.613	0.084	0.221	11.0	–
54.0	0.706	0.049	0.098	54.0	0.627	0.078	0.195	10.5	–
54.5	0.714	0.043	0.083	54.5	0.640	0.072	0.173	11.0	–
55.0	0.725	0.040	0.076	55.0	0.652	0.067	0.155	10.4	–
55.5	0.731	0.041	0.077	55.5	0.663	0.062	0.140	9.2	–
56.0	0.736	0.037	0.069	56.0	0.674	0.058	0.127	8.3	–
56.5	0.747	0.034	0.060	56.5	0.684	0.055	0.116	7.3	–
57.0	0.757	0.038	0.065	57.0	0.693	0.051	0.106	7.1	–
57.5	0.759	0.042	0.073	57.5	0.702	0.049	0.098	7.6	–
58.0	0.758	0.039	0.067	58.0	0.710	0.046	0.091	8.0	–
58.5	0.763	0.033	0.056	58.5	0.718	0.044	0.084	7.7	–
59.0	0.771	0.029	0.049	59.0	0.726	0.041	0.078	6.4	–
59.5	0.779	0.028	0.047	59.5	0.733	0.039	0.073	5.5	–
60.0	0.784	0.028	0.045	60.0	0.739	0.038	0.068	5.2	–
60.5	0.791	0.025	0.041	60.5	0.746	0.036	0.064	4.7	–
61.0	0.799	0.025	0.039	61.0	0.752	0.034	0.060	5.5	–
61.5	0.807	0.028	0.043	61.5	0.758	0.033	0.057	6.4	–
62.0	0.809	0.032	0.049	62.0	0.764	0.031	0.054	5.3	–
62.5	0.812	0.035	0.053	62.5	0.769	0.030	0.051	4.2	–
63.0	0.809	0.036	0.055	63.0	0.774	0.029	0.048	4.2	–
63.5	0.812	0.029	0.045	63.5	0.779	0.028	0.046	4.6	–
64.0	0.819	0.028	0.042	64.0	0.784	0.027	0.044	3.9	–
64.5	0.824	0.031	0.046	64.5	0.789	0.026	0.041	2.0	–
65.0	0.825	0.032	0.047	65.0	0.793	0.025	0.039	1.1	–
65.5	0.827	0.031	0.046	65.5	0.797	0.024	0.038	2.4	–
66.0	0.829	0.031	0.045	66.0	0.801	0.023	0.036	3.2	–
66.5	0.833	0.031	0.044	66.5	0.805	0.022	0.034	3.1	–
67.0	0.835	0.033	0.047	67.0	0.809	0.022	0.033	3.5	–
67.5	0.832	0.032	0.046	67.5	0.813	0.021	0.032	4.0	–
68.0	0.834	0.028	0.040	68.0	0.816	0.020	0.030	3.1	–
68.5	0.837	0.025	0.036	68.5	0.820	0.020	0.029	0.8	–
69.0	0.841	0.024	0.034	69.0	0.823	0.019	0.028	0.5	–
69.5	0.844	0.023	0.032	69.5	0.826	0.018	0.027	2.6	–
70.0	0.847	0.022	0.030	70.0	0.830	0.018	0.026	3.0	–
70.5	0.850	0.022	0.030	70.5	0.833	0.017	0.025	1.0	–

TABLE 12. Values of the real (ε_1) and imaginary (ε_2) parts of the complex dielectric constant and the ELF ($\mathrm{Im}\{-1/\varepsilon(\omega)\}$) of V calculated with DFT and derived from REELS data. The last two columns contain values for the volume and surface single-scattering loss distributions the DIIMFP (w_b) and the DSEP (w_s)

V									
DFT				REELS					
E (eV)	ε_1	ε_2	ELF	E (eV)	ε_1	ε_2	ELF	w_b (meV^{-1})	w_s (arb. un.)
0.50	−209.448	52.784	0.001	0.50	−562.518	32.050	0.000	0.1	0.6
0.75	−80.837	21.302	0.003	0.75	−245.332	10.631	0.000	0.1	1.0
1.00	−35.526	14.875	0.010	1.00	−134.086	5.797	0.000	0.1	1.3
1.25	−13.731	12.682	0.036	1.25	−82.588	4.446	0.001	0.2	1.6
1.50	−0.230	14.499	0.069	1.50	−54.671	4.209	0.001	0.2	1.9
1.75	5.941	19.382	0.047	1.75	−37.947	4.441	0.003	−0.1	2.7
2.00	5.912	23.941	0.039	2.00	−27.262	4.904	0.006	−0.4	5.1
2.25	3.891	22.714	0.043	2.25	−20.172	5.476	0.013	−1.2	11.9
2.50	5.740	22.225	0.042	2.50	−15.399	6.061	0.022	−2.5	25.2
2.75	7.038	25.386	0.037	2.75	−12.203	6.563	0.034	−3.7	42.7
3.00	4.130	30.735	0.032	3.00	−10.098	6.892	0.046	−3.5	54.5
3.25	−4.903	32.995	0.030	3.25	−8.720	6.987	0.056	−1.7	54.8
3.50	−11.641	26.728	0.031	3.50	−7.781	6.843	0.064	0.4	49.2
3.75	−13.812	21.725	0.033	3.75	−7.069	6.507	0.070	1.7	44.4
4.00	−15.732	16.148	0.032	4.00	−6.452	6.056	0.077	2.2	42.8
4.25	−14.030	11.544	0.035	4.25	−5.866	5.568	0.085	2.3	44.2
4.50	−12.191	8.189	0.038	4.50	−5.294	5.098	0.094	2.4	46.9
4.75	−9.981	6.249	0.045	4.75	−4.738	4.680	0.106	2.8	49.6
5.0	−8.197	5.364	0.056	5.0	−4.210	4.326	0.119	3.3	51.2
5.5	−5.954	3.761	0.076	5.5	−3.275	3.808	0.151	4.9	51.5
6.0	−3.185	3.171	0.157	6.0	−2.534	3.490	0.188	6.1	51.9
6.5	−3.799	6.461	0.115	6.5	−1.987	3.294	0.223	7.1	54.5
7.0	−4.655	3.741	0.105	7.0	−1.608	3.152	0.252	8.2	55.5
7.5	−3.820	2.521	0.120	7.5	−1.352	3.015	0.276	9.4	55.0
8.0	−3.038	1.771	0.143	8.0	−1.170	2.859	0.300	10.6	55.2
8.5	−2.275	1.235	0.184	8.5	−1.017	2.684	0.326	11.8	57.5
9.0	−1.480	0.860	0.293	9.0	−0.865	2.506	0.357	12.2	61.5
9.5	−0.522	0.662	0.932	9.5	−0.695	2.348	0.392	12.4	63.7
10.0	0.437	1.571	0.591	10.0	−0.505	2.241	0.425	13.6	61.8
10.5	−0.077	1.867	0.535	10.5	−0.312	2.235	0.439	14.9	59.4
11.0	0.014	1.681	0.595	11.0	−0.231	2.401	0.413	14.8	62.3
11.5	0.563	1.795	0.507	11.5	−0.538	2.502	0.382	13.7	68.4
12.0	0.120	2.396	0.416	12.0	−0.765	2.139	0.415	13.9	68.8
12.5	−0.170	2.243	0.443	12.5	−0.680	1.824	0.481	14.9	65.5
13.0	−0.340	2.089	0.466	13.0	−0.551	1.651	0.545	15.1	65.7
13.5	−0.405	1.840	0.518	13.5	−0.450	1.544	0.597	16.2	65.0
14.0	−0.364	1.645	0.579	14.0	−0.378	1.464	0.640	18.5	58.5
14.5	−0.290	1.506	0.640	14.5	−0.328	1.392	0.681	19.1	57.4
15.0	−0.207	1.416	0.691	15.0	−0.292	1.321	0.722	18.4	63.2
15.5	−0.127	1.376	0.721	15.5	−0.264	1.247	0.767	19.9	58.9
16.0	−0.069	1.390	0.718	16.0	−0.239	1.170	0.820	21.8	49.9
16.5	−0.069	1.559	0.640	16.5	−0.213	1.091	0.883	21.5	52.4
17.0	−0.587	1.343	0.625	17.0	−0.185	1.012	0.957	21.8	56.1
17.5	−0.493	0.974	0.817	17.5	−0.152	0.934	1.044	24.9	46.3
18.0	−0.340	0.778	1.080	18.0	−0.116	0.859	1.144	27.7	34.5
18.5	−0.186	0.685	1.360	18.5	−0.076	0.788	1.258	27.6	35.3
19.0	−0.097	0.666	1.470	19.0	−0.033	0.722	1.382	27.5	38.3
19.5	−0.078	0.566	1.735	19.5	0.011	0.662	1.511	29.7	30.9
20.0	0.047	0.511	1.939	20.0	0.056	0.607	1.634	32.5	21.7
20.5	0.130	0.468	1.984	20.5	0.102	0.557	1.737	35.2	14.1
21.0	0.226	0.474	1.719	21.0	0.148	0.512	1.802	36.7	8.2
21.5	0.217	0.503	1.677	21.5	0.193	0.472	1.816	35.5	10.1

TABLE 12. Values of the real (ε_1) and imaginary (ε_2) parts of the complex dielectric constant and the ELF ($\mathrm{Im}\{-1/\varepsilon(\omega)\}$) of V calculated with DFT and derived from REELS data. The last two columns contain values for the volume and surface single-scattering loss distributions the DIIMFP (w_b) and the DSEP (w_s)—Continued

V									
DFT				REELS					
E (eV)	ε_1	ε_2	ELF	E (eV)	ε_1	ε_2	ELF	w_b (meV^{-1})	w_s (arb. un.)
22.0	0.201	0.425	1.922	22.0	0.237	0.436	1.772	34.5	12.8
22.5	0.297	0.364	1.647	22.5	0.279	0.404	1.674	35.5	5.6
23.0	0.349	0.354	1.432	23.0	0.321	0.375	1.538	35.7	−1.4
23.5	0.389	0.330	1.268	23.5	0.361	0.349	1.383	33.4	2.4
24.0	0.427	0.326	1.131	24.0	0.400	0.326	1.223	30.5	10.5
24.5	0.424	0.294	1.104	24.5	0.438	0.306	1.072	28.9	11.4
25.0	0.485	0.244	0.827	25.0	0.474	0.288	0.935	27.5	8.8
25.5	0.522	0.250	0.746	25.5	0.510	0.272	0.814	24.2	14.0
26.0	0.542	0.211	0.623	26.0	0.544	0.257	0.711	21.4	18.4
26.5	0.588	0.170	0.453	26.5	0.577	0.245	0.623	20.7	15.4
27.0	0.644	0.146	0.334	27.0	0.609	0.233	0.549	19.6	14.5
27.5	0.702	0.132	0.259	27.5	0.640	0.224	0.487	17.6	16.7
28.0	0.760	0.133	0.224	28.0	0.670	0.215	0.435	16.1	16.7
28.5	0.799	0.137	0.209	28.5	0.700	0.208	0.390	15.4	15.3
29.0	0.840	0.138	0.191	29.0	0.729	0.202	0.353	14.6	14.9
29.5	0.871	0.139	0.178	29.5	0.757	0.197	0.322	12.8	17.3
30.0	0.913	0.134	0.157	30.0	0.786	0.193	0.296	11.0	19.5
30.5	0.959	0.137	0.146	30.5	0.814	0.191	0.273	10.0	20.0
31.0	0.998	0.145	0.143	31.0	0.842	0.190	0.255	9.7	19.3
31.5	1.034	0.153	0.140	31.5	0.870	0.189	0.239	10.3	14.0
32.0	1.065	0.161	0.139	32.0	0.898	0.191	0.226	10.6	8.0
32.5	1.106	0.153	0.122	32.5	0.927	0.193	0.216	9.0	10.1
33.0	1.161	0.158	0.115	33.0	0.956	0.198	0.208	8.1	13.1
33.5	1.212	0.172	0.115	33.5	0.986	0.204	0.201	9.2	8.4
34.0	1.256	0.191	0.118	34.0	1.017	0.213	0.197	9.3	4.6
34.5	1.296	0.185	0.108	34.5	1.050	0.225	0.195	8.2	7.5
35.0	1.377	0.159	0.083	35.0	1.083	0.240	0.195	7.7	7.8
35.5	1.497	0.152	0.067	35.5	1.119	0.260	0.197	7.6	4.3
36.0	1.657	0.160	0.058	36.0	1.156	0.286	0.202	6.4	7.0
36.5	1.901	0.188	0.051	36.5	1.194	0.321	0.210	4.8	13.5
37.0	2.447	0.358	0.058	37.0	1.232	0.366	0.222	4.8	13.0
37.5	1.990	1.571	0.244	37.5	1.268	0.427	0.239	5.7	7.6
38.0	2.003	1.007	0.200	38.0	1.295	0.508	0.262	5.8	6.4
38.5	2.531	1.331	0.163	38.5	1.302	0.610	0.295	6.1	7.4
39.0	2.556	2.668	0.195	39.0	1.270	0.731	0.340	7.4	5.9
39.5	1.250	3.425	0.258	39.5	1.180	0.844	0.401	8.1	3.1
40.0	−0.517	3.353	0.291	40.0	1.037	0.907	0.478	7.9	1.3
40.5	−0.751	2.460	0.372	40.5	0.889	0.893	0.563	7.7	3.3
41.0	−0.934	1.523	0.477	41.0	0.785	0.821	0.637	8.1	6.5
41.5	−0.840	0.786	0.594	41.5	0.737	0.737	0.678	9.2	3.7
42.0	−0.454	0.518	1.091	42.0	0.729	0.669	0.684	10.4	−1.5
42.5	−0.230	0.417	1.840	42.5	0.739	0.626	0.668	10.4	−1.3
43.0	−0.095	0.359	2.605	43.0	0.753	0.604	0.648	9.9	1.4
43.5	0.006	0.301	3.322	43.5	0.764	0.598	0.636	10.6	0.6
44.0	0.097	0.254	3.433	44.0	0.765	0.603	0.635	11.5	−0.7
44.5	0.175	0.218	2.788	44.5	0.757	0.614	0.646	10.9	2.4
45.0	0.243	0.189	1.992	45.0	0.737	0.624	0.669	10.5	3.4
45.5	0.308	0.170	1.374	45.5	0.708	0.630	0.702	11.7	0.4
46.0	0.363	0.145	0.950	46.0	0.672	0.627	0.742	12.9	−0.3
46.5	0.446	0.126	0.584	46.5	0.634	0.613	0.789	12.8	0.7
47.0	0.549	0.144	0.446	47.0	0.598	0.590	0.836	12.4	0.6
47.5	0.645	0.359	0.658	47.5	0.567	0.557	0.881	12.9	0.5

TABLE 12. Values of the real (ε_1) and imaginary (ε_2) parts of the complex dielectric constant and the ELF ($\mathrm{Im}\{-1/\varepsilon(\omega)\}$) of V calculated with DFT and derived from REELS data. The last two columns contain values for the volume and surface single-scattering loss distributions the DIIMFP (w_b) and the DSEP (w_s)—Continued

V									
DFT				REELS					
E (eV)	ε_1	ε_2	ELF	E (eV)	ε_1	ε_2	ELF	w_b (meV^{-1})	w_s (arb. un.)
48.0	0.433	0.304	1.087	48.0	0.545	0.520	0.916	13.2	2.5
48.5	0.443	0.269	1.003	48.5	0.532	0.480	0.935	12.9	5.6
49.0	0.446	0.222	0.895	49.0	0.527	0.440	0.934	14.0	2.3
49.5	0.465	0.200	0.780	49.5	0.529	0.403	0.911	14.9	−2.4
50.0	0.480	0.182	0.691	50.0	0.537	0.370	0.870	13.6	–
50.5	0.492	0.166	0.613	50.5	0.550	0.341	0.815	12.9	–
51.0	0.504	0.151	0.545	51.0	0.566	0.319	0.755	14.1	–
51.5	0.521	0.129	0.448	51.5	0.585	0.303	0.699	14.8	–
52.0	0.542	0.112	0.366	52.0	0.603	0.295	0.654	14.3	–
52.5	0.568	0.110	0.330	52.5	0.619	0.297	0.629	13.8	–
53.0	0.579	0.106	0.305	53.0	0.627	0.308	0.632	13.9	–
53.5	0.597	0.099	0.271	53.5	0.616	0.323	0.667	13.5	–
54.0	0.615	0.102	0.262	54.0	0.586	0.327	0.726	12.3	–
54.5	0.612	0.110	0.284	54.5	0.552	0.304	0.766	12.2	–
55.0	0.624	0.095	0.237	55.0	0.534	0.263	0.742	13.2	–
55.5	0.634	0.094	0.228	55.5	0.536	0.222	0.660	13.0	–
56.0	0.635	0.089	0.217	56.0	0.548	0.188	0.561	12.1	–
56.5	0.645	0.078	0.185	56.5	0.565	0.163	0.471	12.2	–
57.0	0.653	0.069	0.161	57.0	0.582	0.143	0.399	12.2	–
57.5	0.671	0.059	0.130	57.5	0.599	0.128	0.341	11.6	–
58.0	0.687	0.059	0.124	58.0	0.616	0.116	0.297	12.2	–
58.5	0.700	0.062	0.125	58.5	0.630	0.107	0.261	12.4	–
59.0	0.708	0.062	0.122	59.0	0.644	0.099	0.232	9.9	–
59.5	0.717	0.062	0.120	59.5	0.657	0.092	0.208	8.1	–
60.0	0.729	0.063	0.117	60.0	0.669	0.086	0.189	9.0	–
60.5	0.736	0.071	0.130	60.5	0.681	0.081	0.172	9.7	–
61.0	0.737	0.074	0.134	61.0	0.692	0.076	0.158	8.3	–
61.5	0.737	0.075	0.137	61.5	0.702	0.073	0.146	6.8	–
62.0	0.743	0.070	0.125	62.0	0.711	0.069	0.135	6.8	–
62.5	0.751	0.075	0.132	62.5	0.720	0.066	0.126	6.8	–
63.0	0.746	0.072	0.128	63.0	0.729	0.063	0.118	6.0	–
63.5	0.756	0.071	0.123	63.5	0.738	0.061	0.112	5.6	–
64.0	0.757	0.074	0.128	64.0	0.745	0.059	0.105	5.2	–
64.5	0.761	0.079	0.135	64.5	0.753	0.057	0.100	5.2	–
65.0	0.751	0.083	0.145	65.0	0.760	0.055	0.095	6.4	–
65.5	0.741	0.068	0.124	65.5	0.768	0.054	0.091	6.1	–
66.0	0.748	0.052	0.092	66.0	0.774	0.053	0.088	4.1	–
66.5	0.764	0.049	0.084	66.5	0.781	0.052	0.084	3.2	–
67.0	0.768	0.052	0.088	67.0	0.787	0.051	0.082	3.9	–
67.5	0.771	0.048	0.081	67.5	0.794	0.050	0.079	5.5	–
68.0	0.774	0.049	0.082	68.0	0.800	0.050	0.077	6.5	–
68.5	0.777	0.040	0.066	68.5	0.806	0.049	0.075	5.3	–
69.0	0.788	0.036	0.058	69.0	0.811	0.049	0.074	3.1	–
69.5	0.799	0.046	0.071	69.5	0.817	0.049	0.073	2.6	–
70.0	0.793	0.047	0.075	70.0	0.822	0.049	0.072	4.4	–
70.5	0.794	0.042	0.067	70.5	0.828	0.049	0.072	5.6	–

TABLE 13. Values of the real (ε_1) and imaginary (ε_2) parts of the complex dielectric constant and the ELF ($\mathrm{Im}\{-1/\varepsilon(\omega)\}$) of Fe calculated with DFT and derived from REELS data. The last two columns contain values for the volume and surface single-scattering loss distributions the DIIMFP (w_b) and the DSEP (w_s)

Fe									
DFT				REELS					
E (eV)	ε_1	ε_2	ELF	E (eV)	ε_1	ε_2	ELF	w_b (meV^{-1})	w_s (arb. un.)
0.50	−121.135	68.667	0.004	0.50	157.124	35.710	0.001	−0.1	0.9
0.75	−44.593	43.976	0.011	0.75	186.611	90.339	0.002	−0.1	1.4
1.00	−21.687	35.929	0.020	1.00	158.602	242.890	0.003	−0.2	1.8
1.25	−12.071	29.833	0.029	1.25	−85.798	233.642	0.004	−0.2	2.3
1.50	−6.571	25.884	0.036	1.50	−102.565	89.018	0.005	−0.2	2.7
1.75	−2.809	23.737	0.042	1.75	−69.923	40.072	0.006	−0.2	2.6
2.00	−1.020	22.815	0.044	2.00	−47.877	22.358	0.008	−0.4	3.9
2.25	0.299	22.856	0.044	2.25	−33.944	14.618	0.011	−0.8	8.1
2.50	−0.271	24.683	0.041	2.50	−24.733	10.850	0.015	−1.4	16.7
2.75	−3.785	24.655	0.040	2.75	−18.384	8.988	0.021	−1.8	29.0
3.00	−7.452	22.970	0.039	3.00	−13.936	8.183	0.031	−1.3	40.2
3.25	−9.978	19.331	0.041	3.25	−10.913	7.985	0.044	−0.2	46.1
3.50	−12.033	15.646	0.040	3.50	−9.058	8.014	0.055	0.7	48.9
3.75	−11.333	10.479	0.044	3.75	−8.074	7.874	0.062	0.9	51.2
4.00	−9.111	7.753	0.054	4.00	−7.491	7.355	0.067	0.7	54.6
4.25	−7.145	6.103	0.069	4.25	−6.907	6.583	0.072	0.5	59.0
4.50	−5.305	5.326	0.094	4.50	−6.204	5.807	0.080	0.5	63.8
4.75	−4.149	5.558	0.116	4.75	−5.443	5.169	0.092	0.8	68.1
5.0	−3.737	5.352	0.126	5.0	−4.705	4.692	0.106	1.5	71.3
5.5	−3.006	4.113	0.158	5.5	−3.456	4.112	0.143	3.1	74.2
6.0	−0.875	3.585	0.263	6.0	−2.551	3.824	0.181	4.5	74.6
6.5	−2.031	6.103	0.148	6.5	−1.933	3.670	0.213	5.7	76.4
7.0	−2.930	3.661	0.166	7.0	−1.529	3.562	0.237	6.1	81.6
7.5	−2.009	2.515	0.243	7.5	−1.275	3.458	0.255	6.1	85.8
8.0	−1.017	1.957	0.402	8.0	−1.120	3.336	0.269	7.3	83.8
8.5	0.015	2.088	0.479	8.5	−1.026	3.189	0.284	8.5	79.9
9.0	0.244	2.619	0.378	9.0	−0.962	3.021	0.301	8.4	78.8
9.5	0.236	2.981	0.333	9.5	−0.909	2.837	0.320	8.4	77.4
10.0	−0.275	2.997	0.331	10.0	−0.856	2.646	0.342	9.0	75.3
10.5	−0.401	2.562	0.381	10.5	−0.798	2.457	0.368	9.6	73.3
11.0	−0.214	2.275	0.436	11.0	−0.732	2.275	0.398	10.3	69.9
11.5	−0.014	2.336	0.428	11.5	−0.659	2.104	0.433	11.0	67.4
12.0	−0.064	2.316	0.431	12.0	−0.581	1.949	0.471	11.3	67.7
12.5	−0.202	2.216	0.448	12.5	−0.499	1.809	0.514	12.1	65.2
13.0	−0.254	2.036	0.484	13.0	−0.416	1.685	0.559	12.7	63.7
13.5	−0.236	1.857	0.530	13.5	−0.334	1.577	0.607	12.7	67.0
14.0	−0.198	1.707	0.578	14.0	−0.254	1.484	0.655	14.2	64.2
14.5	−0.155	1.569	0.631	14.5	−0.179	1.406	0.700	16.5	54.8
15.0	−0.089	1.439	0.692	15.0	−0.108	1.340	0.741	17.2	50.2
15.5	−0.005	1.334	0.750	15.5	−0.045	1.287	0.776	17.3	50.5
16.0	0.083	1.255	0.793	16.0	0.009	1.243	0.804	18.0	49.9
16.5	0.170	1.197	0.819	16.5	0.053	1.208	0.826	19.1	45.2
17.0	0.261	1.159	0.821	17.0	0.087	1.177	0.845	19.7	39.6
17.5	0.361	1.153	0.790	17.5	0.109	1.147	0.864	19.4	37.9
18.0	0.438	1.200	0.736	18.0	0.122	1.116	0.886	19.3	38.1
18.5	0.474	1.305	0.677	18.5	0.128	1.079	0.914	19.9	36.8
19.0	0.371	1.383	0.674	19.0	0.132	1.036	0.950	20.4	33.7
19.5	0.235	1.318	0.735	19.5	0.135	0.986	0.995	20.8	30.8
20.0	0.217	1.264	0.768	20.0	0.143	0.932	1.048	20.7	31.5
20.5	0.162	1.229	0.800	20.5	0.155	0.876	1.107	21.3	30.7
21.0	0.068	1.158	0.860	21.0	0.172	0.821	1.167	23.2	24.3
21.5	0.049	1.015	0.983	21.5	0.194	0.768	1.224	24.0	22.1

TABLE 13. Values of the real (ε_1) and imaginary (ε_2) parts of the complex dielectric constant and the ELF ($\mathrm{Im}\{-1/\varepsilon(\omega)\}$) of Fe calculated with DFT and derived from REELS data. The last two columns contain values for the volume and surface single-scattering loss distributions the DIIMFP (w_b) and the DSEP (w_s)—Continued

Fe									
DFT				REELS					
E (eV)	ε_1	ε_2	ELF	E (eV)	ε_1	ε_2	ELF	w_b (meV^{-1})	w_s (arb. un.)
22.0	0.070	0.914	1.087	22.0	0.220	0.718	1.272	23.4	25.0
22.5	0.084	0.818	1.210	22.5	0.248	0.673	1.308	23.5	25.4
23.0	0.127	0.717	1.353	23.0	0.278	0.632	1.326	24.3	21.3
23.5	0.208	0.651	1.395	23.5	0.308	0.594	1.326	24.7	16.0
24.0	0.272	0.635	1.329	24.0	0.338	0.561	1.307	24.5	14.6
24.5	0.308	0.589	1.334	24.5	0.368	0.531	1.272	23.6	16.0
25.0	0.386	0.606	1.173	25.0	0.397	0.504	1.225	23.3	13.6
25.5	0.342	0.624	1.233	25.5	0.425	0.480	1.168	23.5	10.1
26.0	0.333	0.568	1.309	26.0	0.452	0.457	1.106	22.8	11.6
26.5	0.357	0.493	1.330	26.5	0.478	0.437	1.042	21.8	12.7
27.0	0.418	0.479	1.184	27.0	0.503	0.419	0.978	21.0	12.5
27.5	0.459	0.448	1.088	27.5	0.527	0.403	0.916	19.6	13.3
28.0	0.491	0.474	1.017	28.0	0.550	0.388	0.857	18.6	13.0
28.5	0.469	0.439	1.063	28.5	0.572	0.374	0.801	18.7	9.8
29.0	0.523	0.413	0.930	29.0	0.593	0.361	0.750	18.4	7.8
29.5	0.538	0.426	0.904	29.5	0.613	0.349	0.702	17.5	8.3
30.0	0.550	0.404	0.869	30.0	0.632	0.338	0.658	16.7	9.4
30.5	0.569	0.407	0.831	30.5	0.650	0.328	0.618	15.8	11.0
31.0	0.573	0.393	0.814	31.0	0.668	0.319	0.582	14.9	10.9
31.5	0.576	0.389	0.805	31.5	0.685	0.310	0.548	14.7	8.4
32.0	0.587	0.349	0.750	32.0	0.702	0.302	0.517	13.7	9.5
32.5	0.623	0.339	0.674	32.5	0.718	0.294	0.489	12.5	12.6
33.0	0.637	0.329	0.641	33.0	0.733	0.287	0.463	12.3	12.2
33.5	0.664	0.323	0.593	33.5	0.748	0.281	0.440	11.9	11.9
34.0	0.678	0.346	0.598	34.0	0.762	0.275	0.418	11.3	12.7
34.5	0.672	0.328	0.586	34.5	0.776	0.269	0.398	11.2	10.7
35.0	0.680	0.318	0.564	35.0	0.790	0.264	0.380	10.8	9.8
35.5	0.697	0.305	0.527	35.5	0.804	0.259	0.363	9.8	11.7
36.0	0.709	0.308	0.515	36.0	0.817	0.254	0.347	9.7	11.5
36.5	0.717	0.301	0.498	36.5	0.830	0.250	0.333	9.7	10.3
37.0	0.725	0.295	0.481	37.0	0.842	0.246	0.319	9.4	10.2
37.5	0.744	0.291	0.455	37.5	0.855	0.242	0.307	9.6	8.4
38.0	0.749	0.304	0.466	38.0	0.867	0.239	0.295	9.9	6.1
38.5	0.738	0.305	0.479	38.5	0.879	0.236	0.284	9.0	8.0
39.0	0.731	0.283	0.461	39.0	0.891	0.233	0.274	7.7	11.6
39.5	0.743	0.271	0.433	39.5	0.903	0.230	0.265	7.1	12.4
40.0	0.746	0.256	0.412	40.0	0.916	0.228	0.256	7.1	11.4
40.5	0.757	0.238	0.378	40.5	0.928	0.226	0.248	7.0	10.9
41.0	0.775	0.231	0.353	41.0	0.940	0.225	0.240	6.8	10.6
41.5	0.789	0.223	0.332	41.5	0.953	0.223	0.233	6.7	9.3
42.0	0.796	0.218	0.320	42.0	0.965	0.222	0.226	6.1	9.8
42.5	0.811	0.204	0.291	42.5	0.979	0.222	0.220	5.1	12.6
43.0	0.826	0.202	0.279	43.0	0.992	0.221	0.214	5.2	11.7
43.5	0.837	0.190	0.258	43.5	1.006	0.221	0.209	6.3	7.5
44.0	0.859	0.183	0.237	44.0	1.020	0.222	0.204	5.9	8.5
44.5	0.873	0.179	0.225	44.5	1.036	0.223	0.199	4.7	12.2
45.0	0.896	0.172	0.206	45.0	1.052	0.225	0.194	4.8	10.9
45.5	0.920	0.170	0.194	45.5	1.069	0.227	0.190	5.1	7.8
46.0	0.942	0.177	0.193	46.0	1.087	0.231	0.187	4.3	9.7
46.5	0.956	0.178	0.189	46.5	1.107	0.235	0.183	3.9	11.9
47.0	0.976	0.177	0.180	47.0	1.129	0.241	0.180	4.4	8.9
47.5	0.997	0.174	0.170	47.5	1.154	0.248	0.178	4.5	6.9

TABLE 13. Values of the real (ε_1) and imaginary (ε_2) parts of the complex dielectric constant and the ELF ($\mathrm{Im}\{-1/\varepsilon(\omega)\}$) of Fe calculated with DFT and derived from REELS data. The last two columns contain values for the volume and surface single-scattering loss distributions the DIIMFP (w_b) and the DSEP (w_s)—Continued

Fe									
DFT				REELS					
E (eV)	ε_1	ε_2	ELF	E (eV)	ε_1	ε_2	ELF	w_b (meV^{-1})	w_s (arb. un.)
48.0	1.027	0.170	0.157	48.0	1.182	0.258	0.176	3.5	10.5
48.5	1.060	0.169	0.147	48.5	1.213	0.270	0.175	3.0	11.9
49.0	1.104	0.170	0.136	49.0	1.250	0.288	0.175	3.9	6.6
49.5	1.156	0.174	0.127	49.5	1.293	0.312	0.176	4.5	5.0
50.0	1.225	0.179	0.117	50.0	1.345	0.347	0.180	3.1	–
50.5	1.323	0.195	0.109	50.5	1.408	0.399	0.186	2.3	–
51.0	1.487	0.224	0.099	51.0	1.483	0.482	0.198	2.9	–
51.5	1.728	0.453	0.142	51.5	1.565	0.620	0.219	4.0	–
52.0	1.921	0.820	0.188	52.0	1.622	0.858	0.255	4.3	–
52.5	1.768	1.514	0.280	52.5	1.534	1.228	0.318	3.4	–
53.0	1.146	1.848	0.391	53.0	1.093	1.546	0.431	3.1	–
53.5	−0.010	1.834	0.545	53.5	0.531	1.399	0.625	4.3	–
54.0	−0.002	0.856	1.168	54.0	0.314	1.012	0.901	5.6	–
54.5	0.010	0.572	1.748	54.5	0.332	0.728	1.137	6.5	–
55.0	0.203	0.419	1.933	55.0	0.409	0.563	1.163	7.4	–
55.5	0.302	0.349	1.641	55.5	0.485	0.470	1.031	8.2	–
56.0	0.369	0.298	1.326	56.0	0.549	0.416	0.878	9.0	–
56.5	0.420	0.257	1.058	56.5	0.600	0.384	0.757	9.5	–
57.0	0.466	0.224	0.839	57.0	0.641	0.365	0.671	9.3	–
57.5	0.506	0.198	0.671	57.5	0.673	0.354	0.612	9.0	–
58.0	0.543	0.177	0.543	58.0	0.698	0.348	0.572	9.4	–
58.5	0.576	0.154	0.434	58.5	0.718	0.346	0.545	9.6	–
59.0	0.619	0.135	0.337	59.0	0.733	0.345	0.526	9.3	–
59.5	0.677	0.129	0.271	59.5	0.744	0.347	0.515	8.6	–
60.0	0.757	0.218	0.351	60.0	0.751	0.348	0.508	8.7	–
60.5	0.672	0.199	0.405	60.5	0.755	0.350	0.506	8.9	–
61.0	0.712	0.180	0.334	61.0	0.756	0.352	0.505	8.5	–
61.5	0.701	0.243	0.442	61.5	0.756	0.352	0.507	8.3	–
62.0	0.671	0.214	0.432	62.0	0.753	0.352	0.509	8.0	–
62.5	0.675	0.192	0.390	62.5	0.749	0.351	0.512	8.3	–
63.0	0.689	0.181	0.356	63.0	0.744	0.348	0.515	9.3	–
63.5	0.694	0.182	0.354	63.5	0.739	0.344	0.518	9.2	–
64.0	0.693	0.178	0.348	64.0	0.733	0.338	0.519	8.2	–
64.5	0.698	0.170	0.329	64.5	0.728	0.332	0.518	7.4	–
65.0	0.701	0.168	0.323	65.0	0.723	0.324	0.516	6.9	–
65.5	0.700	0.162	0.314	65.5	0.718	0.315	0.512	7.1	–
66.0	0.700	0.152	0.297	66.0	0.714	0.305	0.506	7.5	–
66.5	0.704	0.143	0.276	66.5	0.711	0.295	0.498	7.3	–
67.0	0.711	0.133	0.254	67.0	0.709	0.285	0.488	7.3	–
67.5	0.719	0.126	0.237	67.5	0.708	0.275	0.476	7.6	–
68.0	0.730	0.122	0.223	68.0	0.708	0.264	0.463	7.4	–
68.5	0.736	0.127	0.228	68.5	0.708	0.254	0.448	7.3	–
69.0	0.734	0.124	0.225	69.0	0.710	0.244	0.433	7.9	–
69.5	0.738	0.122	0.218	69.5	0.711	0.234	0.418	7.8	–
70.0	0.735	0.117	0.211	70.0	0.714	0.225	0.402	7.1	–
70.5	0.741	0.109	0.194	70.5	0.716	0.216	0.386	7.0	–

TABLE 14. Values of the real (ε_1) and imaginary (ε_2) parts of the complex dielectric constant and the ELF ($\mathrm{Im}\{-1/\varepsilon(\omega)\}$) of Co calculated with DFT and derived from REELS data. The last two columns contain values for the volume and surface single-scattering loss distributions the DIIMFP (w_b) and the DSEP (w_s)

Co									
DFT				REELS					
E (eV)	ε_1	ε_2	ELF	E (eV)	ε_1	ε_2	ELF	w_b (meV^{-1})	w_s (arb. un.)
0.50	−107.960	51.266	0.004	0.50	−501.815	36.182	0.000	0.0	0.7
0.75	−21.595	33.538	0.021	0.75	−203.650	27.709	0.001	−0.1	1.1
1.00	7.463	45.855	0.021	1.00	−119.311	42.469	0.003	−0.1	1.4
1.25	−2.923	54.923	0.018	1.25	−91.209	22.506	0.003	−0.1	1.8
1.50	−8.233	43.145	0.022	1.50	−61.840	10.778	0.003	−0.1	2.1
1.75	−8.132	40.200	0.024	1.75	−42.714	7.132	0.004	−0.2	2.0
2.00	−14.932	33.796	0.025	2.00	−30.446	5.951	0.006	−0.3	3.2
2.25	−15.453	26.390	0.028	2.25	−22.251	5.691	0.011	−0.6	7.1
2.50	−14.114	19.689	0.034	2.50	−16.616	5.842	0.019	−1.0	15.7
2.75	−11.590	16.011	0.041	2.75	−12.702	6.183	0.031	−1.1	29.5
3.00	−9.627	13.889	0.049	3.00	−10.014	6.574	0.046	−0.2	43.2
3.25	−8.842	13.049	0.053	3.25	−8.222	6.902	0.060	1.4	50.8
3.50	−9.154	11.116	0.054	3.50	−7.070	7.079	0.071	2.4	53.0
3.75	−8.455	8.557	0.059	3.75	−6.335	7.056	0.078	2.5	53.3
4.00	−7.090	6.923	0.071	4.00	−5.833	6.841	0.085	2.2	54.4
4.25	−5.789	5.745	0.086	4.25	−5.427	6.480	0.091	1.8	57.6
4.50	−4.495	4.929	0.111	4.50	−5.042	6.043	0.098	1.6	62.3
4.75	−3.055	4.560	0.151	4.75	−4.648	5.589	0.106	1.5	67.5
5.0	−2.177	5.233	0.163	5.0	−4.245	5.160	0.116	1.5	71.5
5.5	−1.739	4.616	0.190	5.5	−3.453	4.444	0.140	2.7	72.8
6.0	−0.747	6.263	0.157	6.0	−2.747	3.931	0.171	5.0	69.7
6.5	−3.518	5.088	0.133	6.5	−2.163	3.574	0.205	6.0	74.4
7.0	−2.770	3.164	0.179	7.0	−1.702	3.321	0.238	5.9	84.7
7.5	−1.747	2.384	0.273	7.5	−1.348	3.132	0.269	6.5	89.3
8.0	−0.833	2.161	0.403	8.0	−1.079	2.981	0.297	7.4	89.0
8.5	−0.445	2.412	0.401	8.5	−0.878	2.848	0.321	8.1	86.8
9.0	−0.338	2.381	0.412	9.0	−0.726	2.725	0.343	8.8	82.9
9.5	−0.170	2.199	0.452	9.5	−0.609	2.606	0.364	9.0	80.9
10.0	0.170	2.123	0.468	10.0	−0.517	2.489	0.385	8.9	79.8
10.5	0.180	2.434	0.409	10.5	−0.442	2.373	0.407	9.4	75.3
11.0	−0.024	2.292	0.436	11.0	−0.377	2.258	0.431	10.3	69.1
11.5	0.177	2.121	0.468	11.5	−0.319	2.147	0.456	10.9	65.8
12.0	0.141	2.176	0.458	12.0	−0.266	2.039	0.482	11.1	64.5
12.5	0.033	2.105	0.475	12.5	−0.215	1.937	0.510	11.7	62.4
13.0	−0.018	1.904	0.525	13.0	−0.166	1.840	0.539	12.6	61.1
13.5	0.015	1.778	0.562	13.5	−0.118	1.749	0.569	13.7	58.5
14.0	0.111	1.614	0.617	14.0	−0.071	1.665	0.600	14.9	52.6
14.5	0.173	1.543	0.640	14.5	−0.026	1.587	0.630	14.7	50.5
15.0	0.263	1.476	0.657	15.0	0.018	1.517	0.659	13.7	52.7
15.5	0.320	1.436	0.663	15.5	0.061	1.453	0.687	14.3	50.5
16.0	0.373	1.386	0.673	16.0	0.102	1.395	0.713	16.0	44.3
16.5	0.455	1.404	0.645	16.5	0.140	1.345	0.736	16.6	40.3
17.0	0.457	1.402	0.645	17.0	0.175	1.300	0.755	16.3	38.4
17.5	0.486	1.394	0.640	17.5	0.206	1.262	0.772	17.2	35.0
18.0	0.474	1.425	0.632	18.0	0.232	1.228	0.786	17.8	34.7
18.5	0.441	1.411	0.646	18.5	0.251	1.199	0.799	16.7	38.1
19.0	0.405	1.390	0.663	19.0	0.264	1.172	0.812	17.0	34.2
19.5	0.375	1.357	0.685	19.5	0.271	1.144	0.828	18.7	26.5
20.0	0.353	1.312	0.711	20.0	0.271	1.113	0.848	18.5	27.8
20.5	0.341	1.272	0.734	20.5	0.268	1.078	0.874	17.1	33.9
21.0	0.326	1.232	0.759	21.0	0.265	1.036	0.906	17.6	33.5
21.5	0.316	1.190	0.785	21.5	0.265	0.990	0.943	19.5	26.6

TABLE 14. Values of the real (ε_1) and imaginary (ε_2) parts of the complex dielectric constant and the ELF ($\mathrm{Im}\{-1/\varepsilon(\omega)\}$) of Co calculated with DFT and derived from REELS data. The last two columns contain values for the volume and surface single-scattering loss distributions the DIIMFP (w_b) and the DSEP (w_s)—Continued

Co									
DFT				REELS					
E (eV)	ε_1	ε_2	ELF	E (eV)	ε_1	ε_2	ELF	w_b (meV^{-1})	w_s (arb. un.)
22.0	0.304	1.157	0.808	22.0	0.269	0.941	0.982	20.3	21.9
22.5	0.286	1.121	0.837	22.5	0.279	0.892	1.021	19.8	22.5
23.0	0.253	1.062	0.891	23.0	0.294	0.844	1.057	19.6	24.0
23.5	0.276	1.003	0.927	23.5	0.313	0.799	1.084	20.0	22.9
24.0	0.281	0.994	0.932	24.0	0.337	0.759	1.100	20.9	18.3
24.5	0.253	0.977	0.959	24.5	0.364	0.724	1.102	21.1	16.1
25.0	0.191	0.901	1.062	25.0	0.396	0.699	1.084	20.7	17.4
25.5	0.196	0.808	1.170	25.5	0.427	0.692	1.046	20.9	15.3
26.0	0.228	0.737	1.239	26.0	0.420	0.714	1.041	20.9	12.7
26.5	0.264	0.700	1.251	26.5	0.372	0.662	1.148	20.4	13.1
27.0	0.268	0.673	1.283	27.0	0.392	0.594	1.173	20.5	13.7
27.5	0.263	0.601	1.397	27.5	0.424	0.554	1.139	21.3	10.6
28.0	0.315	0.554	1.365	28.0	0.452	0.526	1.093	21.9	4.2
28.5	0.346	0.528	1.326	28.5	0.478	0.503	1.045	21.5	2.4
29.0	0.365	0.482	1.320	29.0	0.501	0.483	0.997	19.8	8.4
29.5	0.426	0.452	1.170	29.5	0.523	0.465	0.950	18.6	11.3
30.0	0.463	0.462	1.081	30.0	0.543	0.449	0.904	18.4	7.8
30.5	0.472	0.472	1.058	30.5	0.562	0.433	0.860	18.0	6.6
31.0	0.471	0.441	1.059	31.0	0.580	0.420	0.818	17.5	6.7
31.5	0.495	0.424	0.999	31.5	0.598	0.407	0.778	17.3	5.2
32.0	0.509	0.404	0.958	32.0	0.615	0.395	0.740	16.9	4.8
32.5	0.535	0.388	0.889	32.5	0.631	0.384	0.704	15.9	6.3
33.0	0.562	0.385	0.829	33.0	0.646	0.373	0.670	15.1	6.2
33.5	0.572	0.388	0.812	33.5	0.661	0.363	0.638	15.1	4.5
34.0	0.581	0.382	0.790	34.0	0.676	0.354	0.609	14.6	5.5
34.5	0.581	0.380	0.789	34.5	0.690	0.346	0.581	13.7	7.1
35.0	0.583	0.369	0.775	35.0	0.704	0.338	0.555	13.3	6.3
35.5	0.583	0.354	0.761	35.5	0.717	0.331	0.531	12.7	6.0
36.0	0.593	0.328	0.715	36.0	0.729	0.324	0.509	11.5	7.7
36.5	0.613	0.317	0.664	36.5	0.742	0.318	0.488	10.6	10.4
37.0	0.621	0.313	0.647	37.0	0.754	0.312	0.469	10.6	10.3
37.5	0.625	0.301	0.625	37.5	0.766	0.307	0.451	11.3	5.2
38.0	0.633	0.281	0.586	38.0	0.777	0.302	0.435	11.5	2.1
38.5	0.650	0.265	0.537	38.5	0.788	0.298	0.419	10.1	6.6
39.0	0.672	0.256	0.495	39.0	0.799	0.294	0.405	8.8	11.7
39.5	0.685	0.252	0.473	39.5	0.809	0.290	0.392	9.0	10.1
40.0	0.700	0.242	0.441	40.0	0.820	0.286	0.380	9.8	4.9
40.5	0.719	0.245	0.424	40.5	0.830	0.283	0.369	9.9	2.9
41.0	0.726	0.248	0.422	41.0	0.840	0.281	0.358	9.2	4.7
41.5	0.732	0.243	0.409	41.5	0.849	0.278	0.349	8.5	5.5
42.0	0.741	0.239	0.395	42.0	0.859	0.277	0.340	8.3	5.6
42.5	0.749	0.238	0.385	42.5	0.868	0.275	0.332	7.7	8.9
43.0	0.752	0.237	0.381	43.0	0.877	0.273	0.324	7.5	10.0
43.5	0.757	0.226	0.362	43.5	0.886	0.272	0.317	8.2	5.6
44.0	0.768	0.219	0.344	44.0	0.894	0.272	0.311	7.8	5.2
44.5	0.780	0.212	0.324	44.5	0.903	0.271	0.305	6.7	8.2
45.0	0.793	0.213	0.316	45.0	0.911	0.271	0.300	6.4	7.8
45.5	0.800	0.211	0.308	45.5	0.919	0.271	0.295	6.5	6.5
46.0	0.811	0.209	0.298	46.0	0.927	0.271	0.291	6.6	5.7
46.5	0.821	0.215	0.298	46.5	0.935	0.272	0.287	6.4	6.6
47.0	0.817	0.218	0.305	47.0	0.943	0.273	0.283	5.6	9.9
47.5	0.820	0.205	0.286	47.5	0.951	0.274	0.280	5.6	8.7

TABLE 14. Values of the real (ε_1) and imaginary (ε_2) parts of the complex dielectric constant and the ELF ($\mathrm{Im}\{-1/\varepsilon(\omega)\}$) of Co calculated with DFT and derived from REELS data. The last two columns contain values for the volume and surface single-scattering loss distributions the DIIMFP (w_b) and the DSEP (w_s)—Continued

Co									
DFT				REELS					
E (eV)	ε_1	ε_2	ELF	E (eV)	ε_1	ε_2	ELF	w_b (meV^{-1})	w_s (arb. un.)
48.0	0.834	0.203	0.275	48.0	0.959	0.276	0.277	6.2	4.4
48.5	0.839	0.200	0.269	48.5	0.967	0.277	0.274	6.1	3.5
49.0	0.847	0.199	0.263	49.0	0.975	0.279	0.271	5.7	5.2
49.5	0.853	0.194	0.254	49.5	0.983	0.282	0.269	5.8	6.6
50.0	0.862	0.189	0.243	50.0	0.992	0.284	0.267	5.9	–
50.5	0.872	0.184	0.232	50.5	1.000	0.287	0.265	5.9	–
51.0	0.886	0.181	0.221	51.0	1.009	0.290	0.263	5.9	–
51.5	0.898	0.178	0.213	51.5	1.019	0.294	0.261	5.4	–
52.0	0.911	0.178	0.207	52.0	1.029	0.298	0.260	5.1	–
52.5	0.924	0.176	0.199	52.5	1.040	0.302	0.258	5.6	–
53.0	0.935	0.171	0.189	53.0	1.053	0.308	0.256	5.8	–
53.5	0.960	0.162	0.171	53.5	1.067	0.314	0.254	5.4	–
54.0	0.985	0.159	0.159	54.0	1.083	0.321	0.252	5.1	–
54.5	1.021	0.158	0.148	54.5	1.103	0.331	0.249	4.7	–
55.0	1.061	0.160	0.139	55.0	1.127	0.343	0.247	4.5	–
55.5	1.115	0.163	0.129	55.5	1.158	0.360	0.245	5.0	–
56.0	1.191	0.171	0.118	56.0	1.198	0.385	0.243	5.5	–
56.5	1.321	0.188	0.106	56.5	1.253	0.425	0.243	4.9	–
57.0	1.640	0.287	0.103	57.0	1.328	0.500	0.248	3.7	–
57.5	1.582	0.978	0.283	57.5	1.421	0.655	0.268	3.2	–
58.0	1.392	1.355	0.359	58.0	1.445	0.998	0.323	3.9	–
58.5	0.086	1.798	0.555	58.5	0.995	1.417	0.473	5.3	–
59.0	0.148	0.482	1.897	59.0	0.403	1.117	0.792	5.3	–
59.5	0.425	0.430	1.175	59.5	0.365	0.721	1.104	4.4	–
60.0	0.466	0.377	1.050	60.0	0.455	0.537	1.083	5.4	–
60.5	0.506	0.325	0.899	60.5	0.533	0.453	0.925	7.4	–
61.0	0.548	0.281	0.742	61.0	0.589	0.409	0.795	7.6	–
61.5	0.580	0.258	0.641	61.5	0.629	0.385	0.707	7.0	–
62.0	0.602	0.236	0.566	62.0	0.658	0.369	0.648	8.5	–
62.5	0.623	0.222	0.509	62.5	0.679	0.358	0.607	10.2	–
63.0	0.631	0.201	0.459	63.0	0.695	0.351	0.578	8.7	–
63.5	0.652	0.175	0.384	63.5	0.707	0.344	0.557	6.8	–
64.0	0.685	0.159	0.321	64.0	0.716	0.339	0.541	7.3	–
64.5	0.721	0.156	0.287	64.5	0.722	0.335	0.528	8.0	–
65.0	0.741	0.159	0.277	65.0	0.727	0.330	0.518	7.6	–
65.5	0.776	0.212	0.327	65.5	0.731	0.326	0.509	7.1	–
66.0	0.735	0.203	0.348	66.0	0.733	0.322	0.501	7.4	–
66.5	0.759	0.204	0.330	66.5	0.735	0.317	0.495	7.9	–
67.0	0.731	0.221	0.379	67.0	0.736	0.313	0.489	8.0	–
67.5	0.719	0.205	0.366	67.5	0.737	0.308	0.483	7.1	–
68.0	0.719	0.190	0.343	68.0	0.737	0.304	0.478	6.0	–
68.5	0.723	0.186	0.333	68.5	0.737	0.299	0.472	5.9	–
69.0	0.716	0.178	0.327	69.0	0.737	0.294	0.467	6.7	–
69.5	0.715	0.163	0.303	69.5	0.737	0.289	0.461	7.4	–
70.0	0.721	0.150	0.276	70.0	0.737	0.284	0.455	7.2	–
70.5	0.728	0.139	0.253	70.5	0.737	0.278	0.449	7.0	–

TABLE 15. Values of the real (ε_1) and imaginary (ε_2) parts of the complex dielectric constant and the ELF ($\mathrm{Im}\{-1/\varepsilon(\omega)\}$) of Ni calculated with DFT and derived from REELS data. The last two columns contain values for the volume and surface single-scattering loss distributions the DIIMFP (w_b) and the DSEP (w_s)

Ni									
DFT				REELS					
E (eV)	ε_1	ε_2	ELF	E (eV)	ε_1	ε_2	ELF	w_b (meV^{-1})	w_s (arb. un.)
0.50	−158.422	79.503	0.003	0.50	33.880	58.369	0.013	0.1	0.5
0.75	−61.253	52.551	0.008	0.75	119.796	146.571	0.004	0.1	0.7
1.00	−38.025	43.332	0.013	1.00	−22.964	256.452	0.004	0.2	1.0
1.25	−26.202	32.429	0.019	1.25	−112.616	114.300	0.004	0.2	1.2
1.50	−18.963	26.763	0.025	1.50	−79.874	46.863	0.005	0.3	1.5
1.75	−14.840	23.273	0.031	1.75	−53.413	24.412	0.007	0.0	2.4
2.00	−14.053	21.248	0.033	2.00	−36.711	15.339	0.010	−0.4	4.7
2.25	−13.486	15.632	0.037	2.25	−25.791	11.169	0.014	−1.1	11.7
2.50	−10.674	12.483	0.046	2.50	−18.275	9.221	0.022	−2.6	26.9
2.75	−8.490	10.728	0.057	2.75	−12.903	8.505	0.036	−4.2	50.0
3.00	−7.375	9.830	0.065	3.00	−9.046	8.631	0.055	−3.9	68.9
3.25	−6.702	8.230	0.073	3.25	−6.503	9.397	0.072	−0.9	72.3
3.50	−5.608	6.892	0.087	3.50	−5.365	10.469	0.076	2.1	66.4
3.75	−4.513	5.867	0.107	3.75	−5.591	11.101	0.072	2.9	61.7
4.00	−3.434	5.090	0.135	4.00	−6.390	10.605	0.069	2.0	61.9
4.25	−2.354	4.507	0.174	4.25	−6.746	9.269	0.071	0.4	65.5
4.50	−1.142	4.098	0.226	4.50	−6.452	7.853	0.076	−0.7	69.9
4.75	0.609	4.338	0.226	4.75	−5.809	6.728	0.085	−1.1	73.2
5.0	1.483	6.323	0.150	5.0	−5.081	5.917	0.097	−0.7	74.9
5.5	−1.126	8.154	0.120	5.5	−3.774	4.923	0.128	1.3	76.3
6.0	−3.203	5.108	0.141	6.0	−2.777	4.383	0.163	3.2	79.6
6.5	−2.102	3.420	0.212	6.5	−2.042	4.089	0.196	4.5	82.8
7.0	−1.139	2.926	0.297	7.0	−1.559	3.958	0.219	5.7	81.1
7.5	−0.447	2.955	0.331	7.5	−1.360	3.845	0.231	6.6	79.0
8.0	−0.417	3.033	0.324	8.0	−1.280	3.553	0.249	6.6	81.3
8.5	−0.352	2.862	0.344	8.5	−1.088	3.192	0.281	6.9	81.7
9.0	−0.351	2.633	0.373	9.0	−0.825	2.921	0.317	8.2	76.5
9.5	−0.173	2.354	0.423	9.5	−0.575	2.749	0.349	9.2	72.9
10.0	−0.036	2.399	0.417	10.0	−0.370	2.644	0.371	9.3	73.7
10.5	−0.150	2.127	0.468	10.5	−0.217	2.581	0.385	10.1	70.3
11.0	0.065	1.856	0.538	11.0	−0.114	2.540	0.393	11.2	62.8
11.5	0.291	1.816	0.537	11.5	−0.054	2.505	0.399	11.4	60.7
12.0	0.377	1.847	0.520	12.0	−0.031	2.466	0.405	10.4	65.4
12.5	0.416	1.803	0.527	12.5	−0.034	2.414	0.414	9.8	67.9
13.0	0.505	1.741	0.530	13.0	−0.054	2.344	0.426	10.6	63.3
13.5	0.653	1.777	0.496	13.5	−0.078	2.257	0.442	11.4	58.5
14.0	0.587	1.926	0.475	14.0	−0.101	2.155	0.463	11.8	56.1
14.5	0.491	1.916	0.490	14.5	−0.114	2.042	0.488	12.3	54.1
15.0	0.431	1.908	0.499	15.0	−0.116	1.924	0.518	12.5	54.0
15.5	0.288	1.862	0.524	15.5	−0.105	1.806	0.552	12.4	54.7
16.0	0.216	1.727	0.570	16.0	−0.081	1.693	0.589	12.9	52.7
16.5	0.193	1.602	0.615	16.5	−0.047	1.587	0.629	13.8	50.5
17.0	0.194	1.491	0.659	17.0	−0.005	1.492	0.670	14.3	49.0
17.5	0.211	1.397	0.700	17.5	0.042	1.408	0.709	14.9	46.2
18.0	0.234	1.319	0.735	18.0	0.092	1.337	0.745	15.4	44.7
18.5	0.246	1.257	0.766	18.5	0.142	1.277	0.774	15.4	45.8
19.0	0.257	1.189	0.804	19.0	0.190	1.229	0.795	15.5	44.5
19.5	0.272	1.106	0.853	19.5	0.233	1.191	0.808	16.1	41.1
20.0	0.313	1.025	0.892	20.0	0.270	1.162	0.816	16.6	39.5
20.5	0.371	0.964	0.903	20.5	0.298	1.140	0.821	17.0	37.3
21.0	0.434	0.925	0.886	21.0	0.317	1.121	0.826	17.4	33.0
21.5	0.498	0.905	0.848	21.5	0.327	1.102	0.834	17.0	31.7

TABLE 15. Values of the real (ε_1) and imaginary (ε_2) parts of the complex dielectric constant and the ELF ($\mathrm{Im}\{-1/\varepsilon(\omega)\}$) of Ni calculated with DFT and derived from REELS data. The last two columns contain values for the volume and surface single-scattering loss distributions the DIIMFP (w_b) and the DSEP (w_s)—Continued

Ni									
DFT				REELS					
E (eV)	ε_1	ε_2	ELF	E (eV)	ε_1	ε_2	ELF	w_b (meV^{-1})	w_s (arb. un.)
22.0	0.557	0.907	0.801	22.0	0.328	1.079	0.848	16.3	33.0
22.5	0.602	0.928	0.758	22.5	0.324	1.051	0.869	16.3	31.9
23.0	0.634	0.966	0.723	23.0	0.318	1.015	0.897	16.8	28.5
23.5	0.632	1.027	0.706	23.5	0.315	0.973	0.931	17.3	24.8
24.0	0.612	1.048	0.711	24.0	0.315	0.926	0.968	17.6	22.3
24.5	0.564	1.111	0.716	24.5	0.322	0.876	1.006	17.6	22.1
25.0	0.460	1.125	0.761	25.0	0.334	0.827	1.039	17.8	22.5
25.5	0.361	1.092	0.826	25.5	0.352	0.780	1.065	18.4	20.8
26.0	0.273	1.014	0.919	26.0	0.373	0.737	1.080	18.7	18.2
26.5	0.223	0.922	1.024	26.5	0.398	0.697	1.081	18.5	18.3
27.0	0.200	0.810	1.164	27.0	0.425	0.662	1.070	18.3	18.7
27.5	0.210	0.711	1.294	27.5	0.453	0.631	1.046	18.2	16.9
28.0	0.245	0.624	1.389	28.0	0.481	0.604	1.014	18.3	15.5
28.5	0.275	0.551	1.454	28.5	0.508	0.580	0.975	18.6	14.4
29.0	0.323	0.471	1.443	29.0	0.536	0.559	0.932	18.2	14.1
29.5	0.411	0.426	1.215	29.5	0.563	0.542	0.888	16.9	14.5
30.0	0.494	0.413	0.996	30.0	0.589	0.526	0.843	16.2	12.8
30.5	0.548	0.445	0.894	30.5	0.616	0.514	0.799	16.7	9.9
31.0	0.564	0.480	0.875	31.0	0.642	0.503	0.756	17.2	6.6
31.5	0.546	0.500	0.912	31.5	0.670	0.497	0.714	16.5	5.5
32.0	0.542	0.476	0.914	32.0	0.701	0.496	0.672	14.9	9.0
32.5	0.540	0.455	0.912	32.5	0.738	0.513	0.635	13.7	13.7
33.0	0.556	0.426	0.868	33.0	0.746	0.589	0.652	13.6	13.4
33.5	0.582	0.414	0.811	33.5	0.629	0.566	0.791	13.8	9.1
34.0	0.607	0.415	0.767	34.0	0.647	0.488	0.743	13.3	8.1
34.5	0.613	0.423	0.763	34.5	0.679	0.461	0.685	13.3	6.8
35.0	0.607	0.420	0.770	35.0	0.703	0.449	0.646	13.5	4.6
35.5	0.614	0.410	0.752	35.5	0.721	0.441	0.617	12.7	7.5
36.0	0.611	0.406	0.755	36.0	0.737	0.436	0.595	12.3	7.8
36.5	0.606	0.395	0.754	36.5	0.750	0.431	0.576	12.8	3.0
37.0	0.607	0.377	0.738	37.0	0.761	0.426	0.560	12.5	2.3
37.5	0.612	0.360	0.714	37.5	0.772	0.422	0.546	11.3	5.5
38.0	0.619	0.344	0.687	38.0	0.781	0.419	0.533	10.9	5.8
38.5	0.627	0.331	0.658	38.5	0.790	0.415	0.522	11.2	3.1
39.0	0.637	0.317	0.626	39.0	0.797	0.412	0.511	11.3	1.8
39.5	0.645	0.305	0.599	39.5	0.805	0.409	0.502	10.6	3.5
40.0	0.655	0.293	0.569	40.0	0.811	0.405	0.493	10.1	4.3
40.5	0.667	0.281	0.536	40.5	0.818	0.402	0.484	9.7	4.3
41.0	0.681	0.274	0.508	41.0	0.824	0.399	0.476	9.8	3.1
41.5	0.693	0.270	0.488	41.5	0.829	0.396	0.469	10.4	0.2
42.0	0.701	0.264	0.470	42.0	0.834	0.392	0.462	10.1	0.5
42.5	0.710	0.260	0.454	42.5	0.839	0.389	0.455	9.0	3.3
43.0	0.719	0.256	0.439	43.0	0.844	0.386	0.448	8.7	3.0
43.5	0.728	0.253	0.425	43.5	0.849	0.383	0.442	9.2	0.9
44.0	0.736	0.250	0.415	44.0	0.853	0.380	0.435	9.4	0.5
44.5	0.738	0.251	0.413	44.5	0.858	0.377	0.429	9.2	0.2
45.0	0.743	0.242	0.396	45.0	0.862	0.374	0.423	8.8	0.5
45.5	0.751	0.237	0.383	45.5	0.866	0.371	0.418	8.4	2.4
46.0	0.760	0.235	0.372	46.0	0.870	0.368	0.412	8.2	2.2
46.5	0.765	0.234	0.366	46.5	0.874	0.365	0.407	8.2	0.6
47.0	0.770	0.231	0.357	47.0	0.878	0.362	0.401	8.2	0.4
47.5	0.776	0.231	0.352	47.5	0.882	0.359	0.396	8.2	0.5

TABLE 15. Values of the real (ε_1) and imaginary (ε_2) parts of the complex dielectric constant and the ELF ($\mathrm{Im}\{-1/\varepsilon(\omega)\}$) of Ni calculated with DFT and derived from REELS data. The last two columns contain values for the volume and surface single-scattering loss distributions the DIIMFP (w_b) and the DSEP (w_s)—Continued

Ni									
DFT				REELS					
E (eV)	ε_1	ε_2	ELF	E (eV)	ε_1	ε_2	ELF	w_b (meV^{-1})	w_s (arb. un.)
48.0	0.779	0.230	0.348	48.0	0.886	0.356	0.391	8.1	–0.3
48.5	0.785	0.231	0.345	48.5	0.890	0.354	0.386	7.5	1.6
49.0	0.783	0.231	0.347	49.0	0.894	0.351	0.381	6.8	4.9
49.5	0.781	0.228	0.345	49.5	0.898	0.349	0.376	7.5	1.5
50.0	0.780	0.222	0.337	50.0	0.902	0.346	0.371	8.5	–
50.5	0.780	0.214	0.327	50.5	0.906	0.344	0.367	7.5	–
51.0	0.781	0.203	0.312	51.0	0.910	0.342	0.362	6.0	–
51.5	0.788	0.191	0.290	51.5	0.914	0.340	0.358	6.5	–
52.0	0.803	0.182	0.269	52.0	0.918	0.338	0.353	7.9	–
52.5	0.818	0.186	0.264	52.5	0.923	0.336	0.349	7.9	–
53.0	0.820	0.190	0.269	53.0	0.927	0.335	0.344	7.0	–
53.5	0.820	0.188	0.266	53.5	0.932	0.333	0.340	7.1	–
54.0	0.824	0.180	0.253	54.0	0.937	0.331	0.336	7.9	–
54.5	0.831	0.176	0.244	54.5	0.942	0.330	0.331	7.4	–
55.0	0.839	0.172	0.234	55.0	0.948	0.329	0.327	6.4	–
55.5	0.849	0.169	0.225	55.5	0.954	0.328	0.322	6.8	–
56.0	0.858	0.172	0.224	56.0	0.961	0.328	0.318	7.3	–
56.5	0.860	0.176	0.228	56.5	0.968	0.328	0.313	6.8	–
57.0	0.864	0.173	0.223	57.0	0.977	0.328	0.309	6.4	–
57.5	0.869	0.167	0.213	57.5	0.986	0.328	0.304	6.6	–
58.0	0.877	0.161	0.203	58.0	0.997	0.330	0.299	6.2	–
58.5	0.889	0.155	0.190	58.5	1.009	0.332	0.295	5.9	–
59.0	0.910	0.149	0.175	59.0	1.024	0.337	0.290	6.4	–
59.5	0.933	0.156	0.174	59.5	1.041	0.343	0.285	6.5	–
60.0	0.950	0.172	0.185	60.0	1.063	0.352	0.281	5.9	–
60.5	0.958	0.180	0.190	60.5	1.090	0.368	0.278	5.8	–
61.0	0.971	0.183	0.187	61.0	1.124	0.393	0.277	6.4	–
61.5	0.996	0.183	0.179	61.5	1.166	0.436	0.281	5.8	–
62.0	1.045	0.182	0.162	62.0	1.215	0.515	0.296	4.9	–
62.5	1.148	0.197	0.145	62.5	1.246	0.664	0.333	5.5	–
63.0	1.466	0.330	0.146	63.0	1.153	0.901	0.421	6.1	–
63.5	0.583	1.258	0.654	63.5	0.815	1.017	0.599	5.7	–
64.0	0.596	0.413	0.785	64.0	0.551	0.814	0.843	5.5	–
64.5	0.650	0.395	0.684	64.5	0.519	0.597	0.954	5.4	–
65.0	0.649	0.331	0.624	65.0	0.561	0.473	0.878	5.0	–
65.5	0.660	0.279	0.544	65.5	0.608	0.405	0.758	5.4	–
66.0	0.679	0.241	0.464	66.0	0.648	0.366	0.661	6.4	–
66.5	0.697	0.214	0.402	66.5	0.678	0.341	0.592	6.4	–
67.0	0.715	0.194	0.353	67.0	0.703	0.325	0.542	6.0	–
67.5	0.732	0.180	0.316	67.5	0.722	0.313	0.506	6.6	–
68.0	0.748	0.167	0.284	68.0	0.738	0.305	0.478	7.3	–
68.5	0.768	0.157	0.255	68.5	0.751	0.298	0.456	7.2	–
69.0	0.793	0.152	0.234	69.0	0.762	0.292	0.439	7.2	–
69.5	0.825	0.185	0.259	69.5	0.771	0.287	0.425	7.7	–
70.0	0.798	0.221	0.322	70.0	0.778	0.283	0.413	7.7	–
70.5	0.768	0.205	0.324	70.5	0.785	0.280	0.403	7.3	–

TABLE 16. Values of the real (ε_1) and imaginary (ε_2) parts of the complex dielectric constant and the ELF ($\mathrm{Im}\{-1/\varepsilon(\omega)\}$) of Cu calculated with DFT and derived from REELS data. The last two columns contain values for the volume and surface single-scattering loss distributions the DIIMFP (w_b) and the DSEP (w_s)

Cu									
DFT				REELS					
E (eV)	ε_1	ε_2	ELF	E (eV)	ε_1	ε_2	ELF	w_b (meV^{-1})	w_s (arb. un.)
0.50	−299.196	61.762	0.001	0.50	−288.397	34.594	0.000	−0.1	0.6
0.75	−130.859	18.836	0.001	0.75	−91.601	49.326	0.005	−0.1	0.9
1.00	−69.909	8.228	0.002	1.00	−73.064	86.333	0.007	−0.1	1.2
1.25	−40.759	4.587	0.003	1.25	−80.642	41.391	0.005	−0.2	1.5
1.50	−23.639	3.677	0.006	1.50	−55.729	17.567	0.005	−0.2	1.8
1.75	−13.577	6.510	0.029	1.75	−38.032	9.757	0.006	−0.2	1.9
2.00	−10.040	8.153	0.049	2.00	−26.696	6.718	0.009	−0.4	3.3
2.25	−7.983	7.972	0.063	2.25	−19.112	5.428	0.014	−0.8	8.7
2.50	−6.180	7.459	0.079	2.50	−13.794	4.945	0.023	−1.5	22.3
2.75	−4.739	7.155	0.097	2.75	−9.934	4.932	0.040	−1.0	46.1
3.00	−3.917	6.950	0.109	3.00	−7.103	5.268	0.067	1.8	71.2
3.25	−3.285	6.444	0.123	3.25	−5.121	5.898	0.097	4.8	88.4
3.50	−2.609	5.922	0.141	3.50	−3.996	6.705	0.110	5.3	97.8
3.75	−1.802	5.503	0.164	3.75	−3.742	7.351	0.108	3.8	101.4
4.00	−1.069	5.653	0.171	4.00	−4.026	7.393	0.104	2.0	102.2
4.25	−0.881	5.677	0.172	4.25	−4.207	6.838	0.106	0.8	101.9
4.50	−0.326	5.632	0.177	4.50	−3.982	6.206	0.114	0.3	101.6
4.75	−0.387	6.684	0.149	4.75	−3.825	6.013	0.118	0.3	101.3
5.0	−1.537	6.586	0.144	5.0	−4.101	5.185	0.119	0.7	101.0
5.5	−2.102	4.852	0.174	5.5	−3.056	3.918	0.159	2.4	101.1
6.0	−1.560	3.826	0.224	6.0	−2.248	3.429	0.204	4.3	106.4
6.5	−1.023	3.345	0.273	6.5	−1.687	3.128	0.248	5.8	118.3
7.0	−0.706	3.257	0.293	7.0	−1.281	2.902	0.288	7.0	128.1
7.5	−0.682	2.988	0.318	7.5	−0.971	2.714	0.327	7.5	126.2
8.0	−0.582	2.685	0.356	8.0	−0.726	2.553	0.362	7.6	115.8
8.5	−0.330	2.375	0.413	8.5	−0.525	2.414	0.396	8.9	103.8
9.0	−0.303	2.304	0.427	9.0	−0.356	2.296	0.425	10.7	94.0
9.5	−0.203	2.031	0.487	9.5	−0.214	2.198	0.451	11.7	86.9
10.0	−0.010	1.808	0.553	10.0	−0.097	2.118	0.471	11.7	80.5
10.5	0.227	1.783	0.552	10.5	−0.002	2.054	0.487	12.1	72.7
11.0	0.309	1.757	0.552	11.0	0.070	2.002	0.499	13.1	64.8
11.5	0.399	1.699	0.558	11.5	0.120	1.959	0.509	12.8	62.1
12.0	0.532	1.742	0.525	12.0	0.148	1.918	0.518	12.2	58.8
12.5	0.498	1.804	0.515	12.5	0.157	1.876	0.529	13.4	49.7
13.0	0.453	1.774	0.529	13.0	0.151	1.826	0.544	14.2	45.5
13.5	0.433	1.738	0.542	13.5	0.136	1.765	0.563	13.4	47.8
14.0	0.422	1.707	0.552	14.0	0.117	1.693	0.588	13.5	44.5
14.5	0.395	1.732	0.549	14.5	0.101	1.611	0.618	14.6	38.5
15.0	0.240	1.674	0.585	15.0	0.092	1.520	0.655	15.1	39.4
15.5	0.178	1.536	0.642	15.5	0.092	1.426	0.699	15.3	41.3
16.0	0.163	1.410	0.700	16.0	0.102	1.331	0.747	15.7	37.9
16.5	0.171	1.299	0.757	16.5	0.121	1.239	0.800	16.1	34.9
17.0	0.191	1.204	0.810	17.0	0.150	1.152	0.854	17.0	34.6
17.5	0.211	1.132	0.854	17.5	0.186	1.071	0.906	18.2	33.8
18.0	0.218	1.044	0.918	18.0	0.227	0.998	0.952	18.3	32.9
18.5	0.245	0.949	0.987	18.5	0.273	0.934	0.987	17.7	32.4
19.0	0.293	0.864	1.038	19.0	0.322	0.877	1.005	17.7	30.3
19.5	0.354	0.793	1.051	19.5	0.373	0.829	1.003	18.9	26.9
20.0	0.423	0.741	1.018	20.0	0.427	0.790	0.980	20.4	21.8
20.5	0.496	0.707	0.948	20.5	0.482	0.760	0.938	19.8	20.1
21.0	0.566	0.691	0.865	21.0	0.539	0.740	0.883	17.5	24.5
21.5	0.633	0.692	0.787	21.5	0.598	0.733	0.819	17.0	23.5

TABLE 16. Values of the real (ε_1) and imaginary (ε_2) parts of the complex dielectric constant and the ELF ($\mathrm{Im}\{-1/\varepsilon(\omega)\}$) of Cu calculated with DFT and derived from REELS data. The last two columns contain values for the volume and surface single-scattering loss distributions the DIIMFP (w_b) and the DSEP (w_s)—Continued

Cu									
DFT				REELS					
E (eV)	ε_1	ε_2	ELF	E (eV)	ε_1	ε_2	ELF	w_b (meV^{-1})	w_s (arb. un.)
22.0	0.695	0.706	0.719	22.0	0.656	0.743	0.756	17.9	15.8
22.5	0.757	0.741	0.660	22.5	0.708	0.777	0.703	17.1	15.6
23.0	0.818	0.813	0.611	23.0	0.742	0.841	0.669	14.9	22.6
23.5	0.812	0.983	0.605	23.5	0.727	0.933	0.666	14.1	23.4
24.0	0.650	1.040	0.692	24.0	0.632	1.013	0.711	15.0	19.0
24.5	0.545	1.011	0.766	24.5	0.481	1.004	0.810	15.2	18.4
25.0	0.429	0.980	0.856	25.0	0.370	0.897	0.952	15.0	19.5
25.5	0.342	0.869	0.997	25.5	0.340	0.766	1.090	15.2	18.8
26.0	0.322	0.752	1.123	26.0	0.360	0.660	1.168	16.0	16.9
26.5	0.328	0.659	1.216	26.5	0.400	0.583	1.167	17.1	12.8
27.0	0.356	0.582	1.250	27.0	0.444	0.528	1.110	17.7	9.8
27.5	0.363	0.515	1.297	27.5	0.486	0.489	1.029	17.1	11.8
28.0	0.416	0.410	1.201	28.0	0.525	0.460	0.944	16.3	14.8
28.5	0.511	0.359	0.920	28.5	0.560	0.438	0.866	16.9	9.8
29.0	0.608	0.367	0.727	29.0	0.592	0.420	0.797	17.9	2.0
29.5	0.664	0.412	0.675	29.5	0.621	0.406	0.738	16.4	5.7
30.0	0.635	0.456	0.747	30.0	0.647	0.395	0.687	13.3	15.7
30.5	0.627	0.438	0.748	30.5	0.671	0.386	0.644	11.5	19.9
31.0	0.626	0.420	0.740	31.0	0.693	0.378	0.607	12.3	14.7
31.5	0.640	0.387	0.692	31.5	0.713	0.372	0.575	13.9	5.9
32.0	0.669	0.373	0.636	32.0	0.732	0.367	0.547	13.3	5.3
32.5	0.700	0.379	0.599	32.5	0.749	0.362	0.523	11.7	10.8
33.0	0.709	0.388	0.594	33.0	0.765	0.359	0.503	11.4	11.6
33.5	0.707	0.387	0.596	33.5	0.780	0.356	0.485	11.7	8.5
34.0	0.712	0.394	0.595	34.0	0.793	0.354	0.469	11.5	7.8
34.5	0.704	0.384	0.597	34.5	0.806	0.352	0.455	11.2	8.7
35.0	0.707	0.372	0.584	35.0	0.817	0.351	0.443	11.3	6.7
35.5	0.712	0.358	0.564	35.5	0.828	0.350	0.433	10.7	7.1
36.0	0.723	0.348	0.540	36.0	0.838	0.349	0.423	9.2	12.8
36.5	0.732	0.346	0.527	36.5	0.848	0.349	0.415	8.8	14.3
37.0	0.734	0.340	0.520	37.0	0.856	0.349	0.408	9.0	10.6
37.5	0.741	0.330	0.502	37.5	0.864	0.349	0.402	9.0	9.3
38.0	0.749	0.323	0.485	38.0	0.871	0.350	0.397	9.1	10.9
38.5	0.761	0.317	0.466	38.5	0.878	0.351	0.392	9.0	11.5
39.0	0.770	0.317	0.458	39.0	0.884	0.352	0.389	8.6	9.4
39.5	0.775	0.320	0.455	39.5	0.889	0.353	0.385	8.7	6.9
40.0	0.774	0.320	0.456	40.0	0.894	0.354	0.383	9.1	6.8
40.5	0.773	0.313	0.450	40.5	0.899	0.355	0.380	9.1	8.2
41.0	0.776	0.306	0.440	41.0	0.903	0.357	0.379	8.5	8.7
41.5	0.785	0.297	0.422	41.5	0.906	0.358	0.377	7.9	7.7
42.0	0.794	0.299	0.415	42.0	0.909	0.359	0.376	7.9	6.6
42.5	0.796	0.297	0.412	42.5	0.911	0.361	0.376	7.9	8.8
43.0	0.800	0.295	0.407	43.0	0.914	0.362	0.375	7.5	11.3
43.5	0.805	0.295	0.402	43.5	0.915	0.364	0.375	7.8	7.9
44.0	0.810	0.291	0.393	44.0	0.916	0.366	0.376	7.8	6.0
44.5	0.818	0.297	0.393	44.5	0.917	0.367	0.376	7.3	7.8
45.0	0.815	0.304	0.402	45.0	0.918	0.368	0.377	7.7	6.7
45.5	0.810	0.303	0.405	45.5	0.918	0.370	0.378	7.4	7.5
46.0	0.812	0.306	0.406	46.0	0.918	0.371	0.379	6.3	10.8
46.5	0.798	0.314	0.427	46.5	0.917	0.372	0.380	6.0	10.4
47.0	0.786	0.301	0.424	47.0	0.916	0.373	0.381	6.1	10.0
47.5	0.786	0.291	0.414	47.5	0.915	0.374	0.383	6.2	9.7

TABLE 16. Values of the real (ε_1) and imaginary (ε_2) parts of the complex dielectric constant and the ELF ($\mathrm{Im}\{-1/\varepsilon(\omega)\}$) of Cu calculated with DFT and derived from REELS data. The last two columns contain values for the volume and surface single-scattering loss distributions the DIIMFP (w_b) and the DSEP (w_s)—Continued

Cu									
DFT				REELS					
E (eV)	ε_1	ε_2	ELF	E (eV)	ε_1	ε_2	ELF	w_b (meV^{-1})	w_s (arb. un.)
48.0	0.781	0.288	0.415	48.0	0.914	0.375	0.384	6.9	5.6
48.5	0.778	0.272	0.400	48.5	0.912	0.376	0.386	7.3	4.2
49.0	0.783	0.264	0.386	49.0	0.910	0.376	0.388	6.5	8.2
49.5	0.785	0.257	0.376	49.5	0.908	0.377	0.390	5.4	10.9
50.0	0.792	0.249	0.362	50.0	0.906	0.377	0.391	5.6	–
50.5	0.788	0.249	0.365	50.5	0.904	0.377	0.393	6.8	–
51.0	0.795	0.240	0.348	51.0	0.901	0.377	0.395	7.1	–
51.5	0.792	0.235	0.345	51.5	0.898	0.376	0.397	6.3	–
52.0	0.793	0.233	0.341	52.0	0.895	0.376	0.399	5.8	–
52.5	0.794	0.220	0.324	52.5	0.892	0.375	0.401	6.2	–
53.0	0.808	0.211	0.302	53.0	0.889	0.374	0.402	6.4	–
53.5	0.811	0.218	0.309	53.5	0.886	0.373	0.404	5.4	–
54.0	0.813	0.213	0.302	54.0	0.882	0.372	0.406	4.9	–
54.5	0.812	0.210	0.298	54.5	0.879	0.370	0.407	5.6	–
55.0	0.811	0.201	0.288	55.0	0.875	0.368	0.409	6.5	–
55.5	0.821	0.186	0.262	55.5	0.872	0.367	0.410	6.5	–
56.0	0.838	0.187	0.253	56.0	0.868	0.364	0.411	6.0	–
56.5	0.858	0.192	0.248	56.5	0.865	0.362	0.412	5.9	–
57.0	0.857	0.220	0.281	57.0	0.861	0.360	0.413	6.4	–
57.5	0.842	0.225	0.296	57.5	0.858	0.357	0.413	6.8	–
58.0	0.830	0.221	0.299	58.0	0.855	0.354	0.414	6.7	–
58.5	0.825	0.212	0.292	58.5	0.851	0.351	0.414	6.4	–
59.0	0.827	0.206	0.284	59.0	0.848	0.348	0.414	6.1	–
59.5	0.829	0.204	0.280	59.5	0.845	0.345	0.414	6.1	–
60.0	0.831	0.205	0.280	60.0	0.842	0.341	0.414	6.4	–
60.5	0.824	0.208	0.288	60.5	0.839	0.338	0.413	6.5	–
61.0	0.816	0.204	0.288	61.0	0.836	0.334	0.412	6.4	–
61.5	0.807	0.193	0.281	61.5	0.833	0.330	0.411	6.6	–
62.0	0.805	0.179	0.263	62.0	0.830	0.326	0.410	6.3	–
62.5	0.807	0.161	0.238	62.5	0.828	0.322	0.409	5.6	–
63.0	0.820	0.149	0.215	63.0	0.825	0.318	0.407	6.0	–
63.5	0.834	0.147	0.204	63.5	0.823	0.314	0.405	6.9	–
64.0	0.842	0.149	0.204	64.0	0.821	0.310	0.403	6.9	–
64.5	0.846	0.151	0.204	64.5	0.819	0.306	0.400	6.3	–
65.0	0.850	0.148	0.199	65.0	0.817	0.301	0.398	5.8	–
65.5	0.853	0.149	0.198	65.5	0.815	0.297	0.395	5.2	–
66.0	0.854	0.148	0.197	66.0	0.813	0.292	0.392	5.5	–
66.5	0.862	0.146	0.191	66.5	0.811	0.288	0.389	6.4	–
67.0	0.860	0.144	0.190	67.0	0.810	0.284	0.385	6.3	–
67.5	0.867	0.138	0.179	67.5	0.809	0.279	0.381	5.0	–
68.0	0.877	0.136	0.173	68.0	0.807	0.275	0.378	4.9	–
68.5	0.885	0.141	0.175	68.5	0.806	0.270	0.374	6.4	–
69.0	0.898	0.133	0.161	69.0	0.805	0.266	0.370	6.7	–
69.5	0.924	0.138	0.158	69.5	0.804	0.261	0.365	5.5	–
70.0	0.976	0.191	0.193	70.0	0.804	0.257	0.361	4.9	–
70.5	0.898	0.247	0.285	70.5	0.803	0.253	0.356	5.4	–

TABLE 17. Values of the real (ε_1) and imaginary (ε_2) parts of the complex dielectric constant and the ELF ($\mathrm{Im}\{-1/\varepsilon(\omega)\}$) of Zn calculated with DFT and derived from REELS data. The last two columns contain values for the volume and surface single-scattering loss distributions the DIIMFP (w_b) and the DSEP (w_s)

Zn									
DFT				REELS					
E (eV)	ε_1	ε_2	ELF	E (eV)	ε_1	ε_2	ELF	w_b (meV^{-1})	w_s (arb. un.)
0.50	−275.430	67.392	0.001	0.50	−179.123	276.550	0.003	0.0	0.2
0.75	−101.234	23.545	0.002	0.75	−129.337	133.940	0.004	0.0	0.3
1.00	−27.773	19.008	0.017	1.00	−92.759	72.687	0.005	0.1	0.4
1.25	8.567	49.900	0.019	1.25	−67.690	42.949	0.007	0.1	0.4
1.50	−13.915	69.615	0.014	1.50	−50.584	27.174	0.008	0.1	0.5
1.75	−30.897	59.184	0.013	1.75	−38.689	18.182	0.010	0.0	0.5
2.00	−40.810	42.263	0.012	2.00	−30.201	12.745	0.012	0.0	0.8
2.25	−37.319	24.856	0.012	2.25	−23.981	9.294	0.014	−0.1	1.8
2.50	−30.798	15.829	0.013	2.50	−19.306	7.015	0.017	−0.2	4.2
2.75	−25.283	10.759	0.014	2.75	−15.706	5.464	0.020	−0.6	9.1
3.00	−20.922	7.669	0.015	3.00	−12.869	4.386	0.024	−1.0	15.7
3.25	−17.484	5.664	0.017	3.25	−10.577	3.634	0.029	−1.2	22.0
3.50	−14.745	4.304	0.018	3.50	−8.670	3.134	0.037	−1.2	26.0
3.75	−12.536	3.353	0.020	3.75	−7.021	2.899	0.050	−0.8	27.4
4.00	−10.741	2.674	0.022	4.00	−5.647	3.156	0.075	−0.4	27.7
4.25	−9.286	2.154	0.024	4.25	−5.612	3.698	0.082	0.0	27.8
4.50	−8.035	1.734	0.026	4.50	−5.426	2.645	0.073	0.4	28.8
4.75	−6.967	1.422	0.028	4.75	−4.480	2.117	0.086	0.8	30.9
5.0	−6.049	1.184	0.031	5.0	−3.669	1.977	0.114	1.2	33.8
5.5	−4.572	0.867	0.040	5.5	−2.666	2.164	0.184	2.4	41.2
6.0	−3.458	0.703	0.057	6.0	−2.550	2.118	0.193	3.6	49.6
6.5	−2.568	0.550	0.080	6.5	−2.205	1.545	0.213	5.4	56.5
7.0	−1.706	0.538	0.168	7.0	−1.644	1.206	0.290	9.6	65.3
7.5	−1.177	0.766	0.388	7.5	−1.158	1.054	0.430	16.6	94.4
8.0	−0.884	0.876	0.565	8.0	−0.771	0.991	0.629	24.9	159.8
8.5	−0.617	0.960	0.737	8.5	−0.467	0.980	0.831	29.2	229.7
9.0	−0.484	1.046	0.787	9.0	−0.238	1.005	0.943	28.0	221.7
9.5	−0.411	1.044	0.830	9.5	−0.085	1.049	0.947	26.7	156.0
10.0	−0.312	1.016	0.899	10.0	−0.012	1.083	0.923	26.6	112.9
10.5	−0.289	1.014	0.912	10.5	0.010	1.068	0.936	27.7	102.1
11.0	−0.254	0.896	1.033	11.0	0.032	1.002	0.997	29.6	94.1
11.5	−0.160	0.798	1.205	11.5	0.081	0.918	1.081	29.5	86.9
12.0	−0.068	0.719	1.379	12.0	0.150	0.843	1.150	27.9	86.9
12.5	0.049	0.645	1.542	12.5	0.224	0.784	1.179	29.0	78.4
13.0	0.177	0.629	1.472	13.0	0.295	0.740	1.166	30.5	70.4
13.5	0.251	0.644	1.347	13.5	0.359	0.707	1.125	30.4	69.8
14.0	0.292	0.640	1.293	14.0	0.416	0.681	1.070	31.3	63.7
14.5	0.342	0.619	1.238	14.5	0.466	0.660	1.012	31.8	55.7
15.0	0.394	0.611	1.156	15.0	0.509	0.642	0.956	30.0	54.4
15.5	0.440	0.609	1.079	15.5	0.547	0.627	0.906	26.1	61.8
16.0	0.478	0.614	1.014	16.0	0.580	0.614	0.861	23.5	64.4
16.5	0.511	0.633	0.956	16.5	0.609	0.602	0.822	24.9	51.7
17.0	0.514	0.680	0.935	17.0	0.634	0.591	0.787	25.8	42.6
17.5	0.454	0.687	1.013	17.5	0.656	0.580	0.757	22.7	47.4
18.0	0.408	0.645	1.108	18.0	0.676	0.571	0.730	20.0	51.0
18.5	0.382	0.585	1.198	18.5	0.693	0.561	0.706	19.4	49.8
19.0	0.367	0.496	1.304	19.0	0.708	0.552	0.685	19.8	43.7
19.5	0.413	0.409	1.211	19.5	0.721	0.543	0.666	20.8	32.8
20.0	0.473	0.357	1.018	20.0	0.733	0.534	0.649	19.9	32.3
20.5	0.534	0.326	0.832	20.5	0.744	0.526	0.633	17.9	38.5
21.0	0.591	0.317	0.705	21.0	0.753	0.517	0.619	17.9	33.8
21.5	0.630	0.323	0.644	21.5	0.762	0.509	0.606	18.5	25.7

TABLE 17. Values of the real (ε_1) and imaginary (ε_2) parts of the complex dielectric constant and the ELF ($\mathrm{Im}\{-1/\varepsilon(\omega)\}$) of Zn calculated with DFT and derived from REELS data. The last two columns contain values for the volume and surface single-scattering loss distributions the DIIMFP (w_b) and the DSEP (w_s)—Continued

Zn									
DFT				REELS					
E (eV)	ε_1	ε_2	ELF	E (eV)	ε_1	ε_2	ELF	w_b (meV^{-1})	w_s (arb. un.)
22.0	0.663	0.315	0.584	22.0	0.770	0.501	0.594	18.1	25.4
22.5	0.690	0.306	0.537	22.5	0.777	0.493	0.583	16.9	29.4
23.0	0.740	0.310	0.482	23.0	0.783	0.485	0.572	15.1	31.0
23.5	0.775	0.335	0.470	23.5	0.788	0.477	0.562	13.5	29.5
24.0	0.797	0.377	0.485	24.0	0.794	0.469	0.552	13.0	27.5
24.5	0.783	0.417	0.529	24.5	0.798	0.462	0.543	12.3	28.1
25.0	0.749	0.437	0.582	25.0	0.803	0.454	0.534	12.0	25.1
25.5	0.718	0.428	0.613	25.5	0.806	0.447	0.526	12.7	21.2
26.0	0.689	0.409	0.637	26.0	0.810	0.440	0.517	11.6	27.4
26.5	0.676	0.371	0.624	26.5	0.814	0.432	0.509	10.0	32.7
27.0	0.676	0.341	0.594	27.0	0.817	0.425	0.502	11.1	24.8
27.5	0.676	0.310	0.561	27.5	0.820	0.418	0.494	12.6	16.5
28.0	0.692	0.267	0.486	28.0	0.822	0.412	0.487	12.3	15.6
28.5	0.738	0.238	0.395	28.5	0.825	0.405	0.479	12.0	14.3
29.0	0.784	0.241	0.358	29.0	0.827	0.398	0.472	11.6	15.1
29.5	0.804	0.273	0.378	29.5	0.830	0.392	0.465	9.5	23.5
30.0	0.790	0.295	0.415	30.0	0.832	0.386	0.459	8.5	25.9
30.5	0.778	0.276	0.405	30.5	0.834	0.379	0.452	10.0	16.6
31.0	0.784	0.264	0.385	31.0	0.836	0.373	0.445	10.8	11.6
31.5	0.793	0.252	0.364	31.5	0.838	0.367	0.439	9.8	15.6
32.0	0.804	0.248	0.350	32.0	0.840	0.362	0.433	9.6	15.7
32.5	0.811	0.244	0.340	32.5	0.841	0.356	0.426	9.4	14.8
33.0	0.821	0.244	0.333	33.0	0.843	0.350	0.420	8.0	19.5
33.5	0.826	0.239	0.323	33.5	0.845	0.345	0.414	8.5	17.9
34.0	0.830	0.242	0.323	34.0	0.846	0.339	0.408	9.0	15.2
34.5	0.841	0.231	0.304	34.5	0.848	0.334	0.403	6.9	21.4
35.0	0.849	0.238	0.306	35.0	0.849	0.329	0.397	6.3	20.6
35.5	0.856	0.240	0.304	35.5	0.851	0.324	0.391	8.5	10.6
36.0	0.856	0.245	0.309	36.0	0.852	0.319	0.386	9.5	7.4
36.5	0.857	0.244	0.307	36.5	0.853	0.314	0.380	8.1	16.0
37.0	0.859	0.240	0.302	37.0	0.854	0.310	0.375	6.1	24.9
37.5	0.863	0.242	0.302	37.5	0.856	0.305	0.370	5.7	22.0
38.0	0.868	0.243	0.299	38.0	0.857	0.301	0.365	7.2	13.1
38.5	0.870	0.250	0.306	38.5	0.858	0.296	0.360	8.3	11.6
39.0	0.864	0.255	0.314	39.0	0.859	0.292	0.355	7.8	16.7
39.5	0.857	0.256	0.320	39.5	0.860	0.288	0.350	6.7	17.5
40.0	0.855	0.251	0.316	40.0	0.861	0.283	0.345	6.3	14.3
40.5	0.852	0.250	0.317	40.5	0.862	0.279	0.340	7.2	11.7
41.0	0.849	0.246	0.316	41.0	0.863	0.275	0.335	8.0	11.3
41.5	0.849	0.245	0.313	41.5	0.864	0.271	0.331	7.0	13.0
42.0	0.841	0.243	0.317	42.0	0.865	0.268	0.326	6.1	11.2
42.5	0.839	0.237	0.311	42.5	0.866	0.264	0.322	6.4	9.3
43.0	0.833	0.231	0.310	43.0	0.867	0.260	0.318	6.8	10.9
43.5	0.833	0.222	0.298	43.5	0.868	0.257	0.313	6.9	11.8
44.0	0.833	0.213	0.288	44.0	0.869	0.253	0.309	6.7	12.2
44.5	0.839	0.208	0.279	44.5	0.870	0.249	0.305	5.9	14.1
45.0	0.840	0.205	0.275	45.0	0.870	0.246	0.301	6.3	11.6
45.5	0.845	0.199	0.264	45.5	0.871	0.243	0.297	7.7	6.7
46.0	0.847	0.200	0.264	46.0	0.872	0.239	0.293	7.6	6.4
46.5	0.847	0.197	0.261	46.5	0.873	0.236	0.289	6.4	9.9
47.0	0.847	0.198	0.262	47.0	0.874	0.233	0.285	6.6	9.4
47.5	0.844	0.198	0.263	47.5	0.874	0.230	0.281	7.9	4.0

TABLE 17. Values of the real (ε_1) and imaginary (ε_2) parts of the complex dielectric constant and the ELF ($\mathrm{Im}\{-1/\varepsilon(\omega)\}$) of Zn calculated with DFT and derived from REELS data. The last two columns contain values for the volume and surface single-scattering loss distributions the DIIMFP (w_b) and the DSEP (w_s)—Continued

Zn									
DFT				REELS					
E (eV)	ε_1	ε_2	ELF	E (eV)	ε_1	ε_2	ELF	w_b (meV^{-1})	w_s (arb. un.)
48.0	0.838	0.195	0.263	48.0	0.875	0.227	0.278	7.3	5.2
48.5	0.831	0.183	0.253	48.5	0.876	0.224	0.274	5.9	10.5
49.0	0.837	0.168	0.230	49.0	0.877	0.221	0.270	6.6	5.9
49.5	0.849	0.163	0.219	49.5	0.877	0.218	0.267	8.1	–0.5
50.0	0.856	0.164	0.216	50.0	0.878	0.215	0.263	7.6	–
50.5	0.861	0.167	0.217	50.5	0.879	0.212	0.260	6.1	–
51.0	0.858	0.169	0.221	51.0	0.879	0.210	0.256	6.1	–
51.5	0.858	0.168	0.220	51.5	0.880	0.207	0.253	7.1	–
52.0	0.856	0.165	0.216	52.0	0.881	0.204	0.250	7.8	–
52.5	0.859	0.162	0.212	52.5	0.882	0.202	0.246	6.9	–
53.0	0.860	0.164	0.214	53.0	0.882	0.199	0.243	5.0	–
53.5	0.856	0.164	0.215	53.5	0.883	0.196	0.240	4.6	–
54.0	0.854	0.159	0.211	54.0	0.883	0.194	0.237	5.8	–
54.5	0.854	0.153	0.204	54.5	0.884	0.192	0.234	6.4	–
55.0	0.856	0.147	0.196	55.0	0.885	0.189	0.231	5.7	–
55.5	0.860	0.145	0.190	55.5	0.885	0.187	0.228	5.3	–
56.0	0.863	0.147	0.191	56.0	0.886	0.184	0.225	5.1	–
56.5	0.861	0.145	0.190	56.5	0.887	0.182	0.222	5.7	–
57.0	0.862	0.144	0.188	57.0	0.887	0.180	0.219	7.5	–
57.5	0.863	0.144	0.188	57.5	0.888	0.178	0.217	7.5	–
58.0	0.862	0.144	0.188	58.0	0.888	0.175	0.214	5.4	–
58.5	0.859	0.146	0.192	58.5	0.889	0.173	0.211	4.8	–
59.0	0.853	0.143	0.191	59.0	0.890	0.171	0.209	5.4	–
59.5	0.849	0.136	0.184	59.5	0.890	0.169	0.206	5.5	–
60.0	0.847	0.131	0.178	60.0	0.891	0.167	0.203	5.8	–
60.5	0.847	0.122	0.166	60.5	0.891	0.165	0.201	5.8	–
61.0	0.847	0.114	0.156	61.0	0.892	0.163	0.198	5.3	–
61.5	0.851	0.103	0.141	61.5	0.893	0.161	0.196	5.2	–
62.0	0.863	0.101	0.133	62.0	0.893	0.159	0.193	5.2	–
62.5	0.868	0.104	0.136	62.5	0.894	0.157	0.191	5.3	–
63.0	0.870	0.104	0.136	63.0	0.894	0.155	0.189	5.3	–
63.5	0.871	0.107	0.138	63.5	0.895	0.154	0.186	4.8	–
64.0	0.869	0.107	0.139	64.0	0.895	0.152	0.184	5.0	–
64.5	0.866	0.103	0.136	64.5	0.896	0.150	0.182	5.8	–
65.0	0.867	0.099	0.130	65.0	0.896	0.148	0.180	5.2	–
65.5	0.871	0.095	0.124	65.5	0.897	0.146	0.177	3.9	–
66.0	0.873	0.096	0.124	66.0	0.898	0.145	0.175	3.9	–
66.5	0.873	0.095	0.124	66.5	0.898	0.143	0.173	5.0	–
67.0	0.872	0.093	0.121	67.0	0.899	0.141	0.171	5.4	–
67.5	0.872	0.089	0.115	67.5	0.899	0.140	0.169	4.7	–
68.0	0.875	0.086	0.111	68.0	0.900	0.138	0.167	4.1	–
68.5	0.877	0.084	0.108	68.5	0.900	0.137	0.165	4.9	–
69.0	0.879	0.083	0.107	69.0	0.901	0.135	0.163	5.1	–
69.5	0.880	0.082	0.106	69.5	0.901	0.134	0.161	4.6	–
70.0	0.880	0.080	0.103	70.0	0.902	0.132	0.159	4.7	–
70.5	0.881	0.079	0.101	70.5	0.902	0.131	0.157	5.2	–

TABLE 18. Values of the real (ε_1) and imaginary (ε_2) parts of the complex dielectric constant and the ELF ($\mathrm{Im}\{-1/\varepsilon(\omega)\}$) of Mo calculated with DFT and derived from REELS data. The last two columns contain values for the volume and surface single-scattering loss distributions the DIIMFP (w_b) and the DSEP (w_s)

Mo									
DFT				REELS					
E (eV)	ε_1	ε_2	ELF	E (eV)	ε_1	ε_2	ELF	w_b (meV^{-1})	w_s (arb. un.)
0.50	−245.480	66.346	0.001	0.50	−565.328	85.961	0.000	−0.1	0.7
0.75	−90.107	31.720	0.003	0.75	−164.779	141.347	0.003	−0.1	1.0
1.00	−38.529	25.541	0.012	1.00	−171.790	223.146	0.003	−0.1	1.3
1.25	−14.020	23.209	0.032	1.25	−194.298	103.268	0.002	−0.1	1.6
1.50	−0.141	25.336	0.039	1.50	−138.958	43.207	0.002	−0.2	2.0
1.75	4.460	30.154	0.032	1.75	−98.839	22.220	0.002	−0.2	1.7
2.00	4.258	32.189	0.031	2.00	−72.983	13.377	0.002	−0.3	2.6
2.25	1.759	34.183	0.029	2.25	−55.691	9.033	0.003	−0.6	5.6
2.50	−2.094	29.695	0.034	2.50	−43.596	6.679	0.003	−1.2	11.8
2.75	−2.053	26.661	0.037	2.75	−34.810	5.327	0.004	−1.9	21.3
3.00	−1.119	24.459	0.041	3.00	−28.233	4.534	0.006	−2.1	30.1
3.25	0.053	23.949	0.042	3.25	−23.191	4.079	0.007	−1.6	33.7
3.50	−0.124	24.665	0.041	3.50	−19.258	3.839	0.010	−1.0	32.8
3.75	−0.536	25.181	0.040	3.75	−16.151	3.742	0.014	−0.5	30.2
4.00	−1.829	27.525	0.036	4.00	−13.680	3.739	0.019	−0.3	28.1
4.25	−9.162	28.691	0.032	4.25	−11.712	3.793	0.025	−0.1	27.3
4.50	−12.729	23.656	0.033	4.50	−10.150	3.873	0.033	−0.1	28.0
4.75	−14.486	18.351	0.034	4.75	−8.918	3.952	0.042	−0.1	30.1
5.0	−13.564	14.703	0.037	5.0	−7.951	4.003	0.051	−0.2	33.1
5.5	−12.066	10.204	0.041	5.5	−6.587	3.958	0.067	−0.2	40.0
6.0	−10.568	6.528	0.042	6.0	−5.657	3.691	0.081	0.4	45.2
6.5	−8.084	4.427	0.052	6.5	−4.892	3.282	0.095	1.3	48.7
7.0	−5.450	3.450	0.083	7.0	−4.173	2.848	0.112	1.7	52.4
7.5	−6.134	3.860	0.073	7.5	−3.479	2.470	0.136	2.1	56.9
8.0	−4.952	2.241	0.076	8.0	−2.822	2.179	0.171	3.1	62.2
8.5	−3.765	1.555	0.094	8.5	−2.215	1.978	0.224	4.6	68.4
9.0	−2.754	1.192	0.132	9.0	−1.661	1.860	0.299	6.4	74.0
9.5	−1.894	0.995	0.217	9.5	−1.160	1.817	0.391	8.8	77.8
10.0	−1.126	0.891	0.432	10.0	−0.702	1.849	0.473	11.5	78.1
10.5	−0.341	0.848	1.014	10.5	−0.274	1.973	0.497	13.0	75.9
11.0	0.749	1.118	0.618	11.0	0.135	2.272	0.439	12.8	73.5
11.5	1.165	2.416	0.336	11.5	0.269	3.035	0.327	11.8	71.3
12.0	0.348	3.003	0.329	12.0	−0.730	3.219	0.295	10.4	68.3
12.5	−0.051	2.765	0.362	12.5	−0.810	2.652	0.345	9.7	64.2
13.0	−0.138	2.652	0.376	13.0	−0.709	2.501	0.370	10.2	59.9
13.5	−0.254	2.412	0.410	13.5	−0.710	2.439	0.378	10.8	57.8
14.0	−0.156	2.151	0.462	14.0	−0.770	2.352	0.384	10.5	57.8
14.5	0.069	2.015	0.496	14.5	−0.840	2.218	0.394	10.8	55.1
15.0	0.329	1.995	0.488	15.0	−0.890	2.048	0.411	11.6	51.1
15.5	0.729	2.357	0.387	15.5	−0.904	1.859	0.435	11.7	50.6
16.0	0.725	2.994	0.316	16.0	−0.882	1.672	0.468	11.5	52.1
16.5	−0.156	3.530	0.283	16.5	−0.832	1.497	0.510	11.7	52.0
17.0	−0.803	3.031	0.308	17.0	−0.760	1.344	0.564	12.5	50.5
17.5	−1.139	2.828	0.304	17.5	−0.678	1.212	0.629	13.8	48.7
18.0	−1.369	2.371	0.316	18.0	−0.590	1.102	0.705	14.8	47.3
18.5	−1.926	1.572	0.254	18.5	−0.504	1.011	0.792	15.4	47.2
19.0	−1.256	0.899	0.377	19.0	−0.421	0.937	0.888	16.4	47.5
19.5	−0.869	0.818	0.574	19.5	−0.346	0.875	0.989	18.6	45.0
20.0	−0.631	0.748	0.781	20.0	−0.278	0.821	1.092	21.0	40.9
20.5	−0.440	0.731	1.004	20.5	−0.217	0.774	1.197	22.1	39.5
21.0	−0.333	0.785	1.080	21.0	−0.163	0.730	1.305	23.2	38.3
21.5	−0.317	0.758	1.123	21.5	−0.115	0.686	1.417	25.0	34.8

TABLE 18. Values of the real (ε_1) and imaginary (ε_2) parts of the complex dielectric constant and the ELF ($\mathrm{Im}\{-1/\varepsilon(\omega)\}$) of Mo calculated with DFT and derived from REELS data. The last two columns contain values for the volume and surface single-scattering loss distributions the DIIMFP (w_b) and the DSEP (w_s)—Continued

Mo									
DFT				REELS					
E (eV)	ε_1	ε_2	ELF	E (eV)	ε_1	ε_2	ELF	w_b (meV^{-1})	w_s (arb. un.)
22.0	−0.226	0.730	1.249	22.0	−0.069	0.643	1.537	26.4	31.8
22.5	−0.294	0.685	1.234	22.5	−0.024	0.600	1.664	27.8	29.5
23.0	−0.245	0.441	1.731	23.0	0.021	0.558	1.791	30.0	26.1
23.5	−0.059	0.358	2.722	23.5	0.067	0.516	1.905	31.1	22.3
24.0	0.072	0.339	2.825	24.0	0.114	0.477	1.982	31.3	18.6
24.5	0.174	0.337	2.341	24.5	0.162	0.441	1.998	32.6	14.4
25.0	0.262	0.333	1.855	25.0	0.211	0.408	1.936	33.7	10.8
25.5	0.338	0.358	1.476	25.5	0.260	0.378	1.797	32.6	10.4
26.0	0.358	0.371	1.396	26.0	0.309	0.352	1.606	30.5	11.3
26.5	0.399	0.337	1.234	26.5	0.358	0.328	1.393	28.6	10.6
27.0	0.430	0.325	1.118	27.0	0.406	0.308	1.185	26.7	10.6
27.5	0.482	0.282	0.904	27.5	0.455	0.291	0.998	24.5	11.7
28.0	0.550	0.252	0.689	28.0	0.503	0.276	0.839	22.5	12.0
28.5	0.614	0.222	0.522	28.5	0.550	0.263	0.707	20.4	12.2
29.0	0.714	0.189	0.347	29.0	0.598	0.253	0.600	18.3	13.3
29.5	0.817	0.202	0.285	29.5	0.647	0.246	0.514	16.9	13.5
30.0	0.915	0.242	0.271	30.0	0.695	0.240	0.444	16.2	12.3
30.5	0.960	0.340	0.328	30.5	0.745	0.237	0.388	14.7	12.8
31.0	0.971	0.308	0.297	31.0	0.797	0.237	0.343	13.2	12.8
31.5	1.028	0.328	0.282	31.5	0.852	0.240	0.306	12.6	10.7
32.0	1.084	0.289	0.229	32.0	0.911	0.246	0.277	11.4	10.6
32.5	1.201	0.283	0.186	32.5	0.975	0.258	0.253	9.9	12.2
33.0	1.310	0.307	0.170	33.0	1.049	0.277	0.235	9.0	11.6
33.5	1.480	0.296	0.130	33.5	1.139	0.309	0.222	8.5	9.5
34.0	1.709	0.317	0.105	34.0	1.264	0.375	0.216	7.7	9.5
34.5	2.175	0.405	0.083	34.5	1.406	0.652	0.272	7.2	10.0
35.0	2.817	1.185	0.127	35.0	1.124	0.621	0.377	7.5	8.5
35.5	2.377	2.272	0.210	35.5	1.299	0.665	0.312	8.0	6.4
36.0	1.597	2.700	0.274	36.0	1.359	0.908	0.340	8.3	6.8
36.5	0.861	2.795	0.327	36.5	1.168	1.179	0.428	8.1	9.0
37.0	0.356	2.889	0.341	37.0	0.858	1.160	0.557	7.8	9.8
37.5	−0.574	2.022	0.458	37.5	0.776	1.012	0.622	8.2	8.6
38.0	−0.324	1.972	0.494	38.0	0.801	0.980	0.612	9.0	6.3
38.5	−0.692	1.384	0.578	38.5	0.782	1.041	0.614	9.6	5.7
39.0	−0.537	1.092	0.737	39.0	0.671	1.099	0.663	9.6	8.0
39.5	−0.578	0.916	0.780	39.5	0.517	1.071	0.757	9.9	8.6
40.0	−0.434	0.610	1.089	40.0	0.410	0.965	0.878	10.9	5.7
40.5	−0.253	0.483	1.625	40.5	0.376	0.848	0.986	11.6	4.5
41.0	−0.148	0.429	2.084	41.0	0.386	0.760	1.046	11.7	4.5
41.5	−0.058	0.379	2.575	41.5	0.408	0.707	1.061	12.6	3.3
42.0	0.021	0.341	2.924	42.0	0.423	0.677	1.062	13.9	2.3
42.5	0.081	0.319	2.949	42.5	0.425	0.656	1.073	14.4	2.2
43.0	0.130	0.286	2.895	43.0	0.417	0.633	1.102	14.5	2.6
43.5	0.186	0.258	2.552	43.5	0.408	0.600	1.140	14.9	2.1
44.0	0.237	0.241	2.107	44.0	0.405	0.560	1.172	15.4	1.3
44.5	0.286	0.215	1.680	44.5	0.414	0.519	1.178	15.5	0.8
45.0	0.365	0.202	1.162	45.0	0.435	0.483	1.143	15.7	0.5
45.5	0.458	0.228	0.872	45.5	0.470	0.458	1.064	16.4	−0.1
46.0	0.477	0.313	0.960	46.0	0.524	0.458	0.946	16.7	−1.1
46.5	0.461	0.347	1.041	46.5	0.554	0.596	0.900	16.1	−0.8
47.0	0.443	0.376	1.112	47.0	0.373	0.483	1.296	15.5	0.7
47.5	0.387	0.400	1.292	47.5	0.431	0.425	1.159	15.6	0.7

TABLE 18. Values of the real (ε_1) and imaginary (ε_2) parts of the complex dielectric constant and the ELF ($\mathrm{Im}\{-1/\varepsilon(\omega)\}$) of Mo calculated with DFT and derived from REELS data. The last two columns contain values for the volume and surface single-scattering loss distributions the DIIMFP (w_b) and the DSEP (w_s)—Continued

Mo									
DFT				REELS					
E (eV)	ε_1	ε_2	ELF	E (eV)	ε_1	ε_2	ELF	w_b (meV^{-1})	w_s (arb. un.)
48.0	0.355	0.339	1.406	48.0	0.458	0.417	1.086	16.1	−0.5
48.5	0.359	0.303	1.373	48.5	0.466	0.417	1.066	16.6	−1.6
49.0	0.367	0.279	1.313	49.0	0.462	0.413	1.075	16.8	−2.5
49.5	0.374	0.266	1.262	49.5	0.452	0.404	1.099	16.2	−1.6
50.0	0.378	0.238	1.192	50.0	0.441	0.386	1.123	15.5	–
50.5	0.397	0.214	1.054	50.5	0.434	0.363	1.134	15.8	–
51.0	0.408	0.211	0.998	51.0	0.432	0.337	1.122	16.6	–
51.5	0.407	0.204	0.983	51.5	0.435	0.310	1.085	16.9	–
52.0	0.416	0.170	0.843	52.0	0.443	0.286	1.028	16.6	–
52.5	0.426	0.140	0.699	52.5	0.453	0.264	0.959	15.6	–
53.0	0.455	0.125	0.559	53.0	0.465	0.245	0.887	14.9	–
53.5	0.485	0.115	0.463	53.5	0.478	0.229	0.816	15.4	–
54.0	0.510	0.126	0.458	54.0	0.490	0.215	0.750	15.7	–
54.5	0.509	0.137	0.492	54.5	0.502	0.203	0.691	14.3	–
55.0	0.504	0.124	0.458	55.0	0.514	0.192	0.639	13.3	–
55.5	0.506	0.110	0.408	55.5	0.525	0.183	0.592	13.9	–
56.0	0.519	0.086	0.310	56.0	0.535	0.174	0.551	14.4	–
56.5	0.538	0.076	0.258	56.5	0.545	0.167	0.514	13.1	–
57.0	0.556	0.067	0.215	57.0	0.554	0.159	0.480	11.4	–
57.5	0.575	0.065	0.194	57.5	0.562	0.153	0.449	11.1	–
58.0	0.592	0.067	0.189	58.0	0.571	0.146	0.421	11.3	–
58.5	0.600	0.073	0.200	58.5	0.579	0.140	0.395	10.8	–
59.0	0.605	0.068	0.183	59.0	0.586	0.134	0.370	10.0	–
59.5	0.616	0.066	0.171	59.5	0.594	0.128	0.347	9.6	–
60.0	0.623	0.067	0.170	60.0	0.601	0.122	0.325	9.8	–
60.5	0.628	0.062	0.155	60.5	0.608	0.117	0.305	9.6	–
61.0	0.639	0.057	0.138	61.0	0.615	0.111	0.286	8.6	–
61.5	0.650	0.055	0.129	61.5	0.621	0.106	0.268	8.1	–
62.0	0.664	0.064	0.145	62.0	0.628	0.102	0.251	8.6	–
62.5	0.652	0.064	0.150	62.5	0.635	0.097	0.235	8.7	–
63.0	0.659	0.057	0.130	63.0	0.641	0.092	0.220	7.5	–
63.5	0.665	0.050	0.113	63.5	0.648	0.088	0.206	6.9	–
64.0	0.677	0.047	0.101	64.0	0.654	0.084	0.193	7.2	–
64.5	0.686	0.048	0.101	64.5	0.660	0.080	0.181	7.4	–
65.0	0.692	0.053	0.110	65.0	0.666	0.077	0.170	7.2	–
65.5	0.689	0.051	0.108	65.5	0.672	0.073	0.160	7.1	–
66.0	0.694	0.046	0.095	66.0	0.678	0.070	0.150	6.8	–
66.5	0.698	0.043	0.088	66.5	0.684	0.067	0.141	5.9	–
67.0	0.702	0.040	0.081	67.0	0.690	0.064	0.133	5.3	–
67.5	0.707	0.035	0.070	67.5	0.695	0.061	0.125	5.3	–
68.0	0.714	0.030	0.058	68.0	0.701	0.058	0.118	6.0	–
68.5	0.723	0.027	0.052	68.5	0.706	0.056	0.111	6.1	–
69.0	0.731	0.027	0.050	69.0	0.711	0.054	0.105	5.3	–
69.5	0.739	0.027	0.048	69.5	0.716	0.051	0.100	4.7	–
70.0	0.746	0.029	0.052	70.0	0.721	0.049	0.094	4.8	–
70.5	0.752	0.032	0.056	70.5	0.726	0.047	0.089	5.1	–

TABLE 19. Values of the real (ε_1) and imaginary (ε_2) parts of the complex dielectric constant and the ELF ($\mathrm{Im}\{-1/\varepsilon(\omega)\}$) of Pd calculated with DFT and derived from REELS data. The last two columns contain values for the volume and surface single-scattering loss distributions the DIIMFP (w_b) and the DSEP (w_s)

Pd									
DFT				REELS					
E (eV)	ε_1	ε_2	ELF	E (eV)	ε_1	ε_2	ELF	w_b (meV^{-1})	w_s (arb. un.)
0.50	−142.506	109.816	0.003	0.50	−545.897	30.623	0.000	0.0	0.6
0.75	−68.572	73.262	0.007	0.75	−238.405	9.671	0.000	0.0	0.9
1.00	−44.612	53.255	0.011	1.00	−130.490	4.781	0.000	0.0	1.3
1.25	−33.219	40.430	0.015	1.25	−80.442	3.262	0.001	0.0	1.6
1.50	−27.262	31.145	0.018	1.50	−53.195	2.826	0.001	0.0	1.9
1.75	−22.162	23.870	0.022	1.75	−36.727	2.866	0.002	−0.1	2.3
2.00	−18.074	18.900	0.028	2.00	−26.030	3.183	0.005	−0.4	4.6
2.25	−14.881	15.321	0.034	2.25	−18.742	3.708	0.010	−1.0	11.9
2.50	−12.544	12.957	0.040	2.50	−13.660	4.406	0.021	−2.2	27.6
2.75	−10.462	10.558	0.048	2.75	−10.153	5.229	0.040	−2.9	49.4
3.00	−8.655	9.171	0.058	3.00	−7.884	6.070	0.061	−1.9	65.6
3.25	−7.296	8.093	0.068	3.25	−6.616	6.745	0.076	0.4	68.8
3.50	−6.170	7.163	0.080	3.50	−6.063	7.042	0.082	2.1	65.1
3.75	−5.219	6.605	0.093	3.75	−5.859	6.861	0.084	2.6	61.3
4.00	−4.601	5.948	0.105	4.00	−5.670	6.295	0.088	2.5	60.5
4.25	−3.939	5.352	0.121	4.25	−5.326	5.555	0.094	2.3	63.2
4.50	−3.234	4.865	0.143	4.50	−4.816	4.825	0.104	2.1	68.4
4.75	−2.537	4.849	0.162	4.75	−4.203	4.209	0.119	2.1	75.0
5.0	−2.579	4.860	0.161	5.0	−3.560	3.741	0.140	2.4	81.6
5.5	−2.392	3.892	0.187	5.5	−2.411	3.223	0.199	3.9	89.0
6.0	−1.845	3.100	0.238	6.0	−1.676	2.966	0.256	6.6	88.4
6.5	−1.299	2.519	0.314	6.5	−1.115	2.596	0.325	9.4	86.2
7.0	−0.761	2.004	0.436	7.0	−0.471	2.309	0.416	11.9	83.3
7.5	−0.061	1.633	0.612	7.5	0.132	2.213	0.450	13.5	76.6
8.0	0.564	1.735	0.521	8.0	0.625	2.256	0.412	13.6	68.4
8.5	0.885	1.682	0.465	8.5	1.002	2.392	0.356	11.9	63.2
9.0	1.402	1.866	0.343	9.0	1.262	2.590	0.312	10.0	59.7
9.5	1.220	2.129	0.354	9.5	1.403	2.827	0.284	9.7	54.2
10.0	1.386	2.232	0.323	10.0	1.423	3.072	0.268	9.9	48.3
10.5	1.259	2.119	0.349	10.5	1.326	3.293	0.261	9.3	45.5
11.0	1.453	2.075	0.323	11.0	1.127	3.450	0.262	8.9	43.5
11.5	1.518	2.224	0.307	11.5	0.863	3.512	0.269	8.7	41.4
12.0	1.424	2.283	0.315	12.0	0.581	3.465	0.281	8.4	39.8
12.5	1.435	2.219	0.318	12.5	0.327	3.322	0.298	8.7	36.8
13.0	1.510	2.292	0.304	13.0	0.135	3.110	0.321	9.2	34.3
13.5	1.460	2.390	0.305	13.5	0.019	2.867	0.349	9.3	33.5
14.0	1.291	2.380	0.325	14.0	−0.026	2.626	0.381	9.5	32.5
14.5	1.260	2.326	0.332	14.5	−0.012	2.410	0.415	9.7	31.8
15.0	1.175	2.384	0.338	15.0	0.044	2.234	0.448	9.9	32.1
15.5	1.045	2.323	0.358	15.5	0.123	2.105	0.473	10.5	30.7
16.0	0.981	2.181	0.381	16.0	0.209	2.027	0.488	11.2	27.7
16.5	1.012	2.077	0.389	16.5	0.282	1.998	0.491	11.6	25.8
17.0	1.034	1.971	0.398	17.0	0.321	2.012	0.485	11.5	26.2
17.5	1.150	1.916	0.384	17.5	0.306	2.049	0.477	11.3	26.9
18.0	1.270	1.948	0.360	18.0	0.229	2.077	0.476	11.7	25.6
18.5	1.435	1.989	0.331	18.5	0.103	2.057	0.485	11.9	24.8
19.0	1.714	2.215	0.282	19.0	−0.033	1.967	0.508	11.4	25.5
19.5	1.541	2.760	0.276	19.5	−0.137	1.817	0.547	11.4	24.9
20.0	0.863	3.244	0.288	20.0	−0.185	1.640	0.602	12.2	23.6
20.5	0.310	3.203	0.309	20.5	−0.178	1.467	0.672	12.7	23.5
21.0	−0.231	2.737	0.363	21.0	−0.134	1.320	0.750	13.3	23.0
21.5	−0.145	2.228	0.447	21.5	−0.069	1.205	0.827	14.4	20.6

TABLE 19. Values of the real (ε_1) and imaginary (ε_2) parts of the complex dielectric constant and the ELF ($\mathrm{Im}\{-1/\varepsilon(\omega)\}$) of Pd calculated with DFT and derived from REELS data. The last two columns contain values for the volume and surface single-scattering loss distributions the DIIMFP (w_b) and the DSEP (w_s)—Continued

Pd									
DFT				REELS					
E (eV)	ε_1	ε_2	ELF	E (eV)	ε_1	ε_2	ELF	w_b (meV^{-1})	w_s (arb. un.)
22.0	−0.245	2.044	0.482	22.0	0.000	1.121	0.892	15.7	18.3
22.5	−0.220	1.831	0.538	22.5	0.062	1.062	0.939	16.4	17.7
23.0	−0.207	1.739	0.567	23.0	0.112	1.017	0.972	16.7	17.7
23.5	−0.260	1.507	0.644	23.5	0.148	0.975	1.003	17.5	16.1
24.0	−0.199	1.338	0.731	24.0	0.178	0.929	1.038	18.8	13.2
24.5	−0.136	1.158	0.852	24.5	0.213	0.879	1.074	19.3	11.6
25.0	−0.047	1.017	0.982	25.0	0.255	0.832	1.098	18.7	12.7
25.5	0.131	0.948	1.035	25.5	0.304	0.794	1.098	19.1	11.9
26.0	0.221	0.922	1.026	26.0	0.357	0.769	1.070	20.5	8.4
26.5	0.312	0.936	0.961	26.5	0.406	0.757	1.025	20.6	6.9
27.0	0.368	0.992	0.887	27.0	0.449	0.758	0.976	19.6	7.4
27.5	0.321	0.955	0.941	27.5	0.481	0.768	0.935	19.0	7.0
28.0	0.388	0.871	0.958	28.0	0.499	0.784	0.907	18.7	6.9
28.5	0.527	0.870	0.841	28.5	0.502	0.801	0.897	18.4	6.7
29.0	0.630	1.018	0.710	29.0	0.490	0.811	0.904	18.5	5.4
29.5	0.541	1.185	0.698	29.5	0.467	0.809	0.927	18.4	4.4
30.0	0.371	1.157	0.783	30.0	0.440	0.792	0.965	17.7	5.2
30.5	0.349	1.160	0.790	30.5	0.416	0.760	1.012	17.4	6.0
31.0	0.199	1.119	0.866	31.0	0.401	0.718	1.062	17.8	4.9
31.5	0.123	1.129	0.875	31.5	0.397	0.669	1.105	18.2	3.4
32.0	−0.099	0.868	1.137	32.0	0.406	0.619	1.129	18.4	2.9
32.5	0.016	0.669	1.494	32.5	0.425	0.573	1.126	18.6	2.6
33.0	0.089	0.565	1.727	33.0	0.452	0.533	1.091	18.4	2.1
33.5	0.185	0.476	1.824	33.5	0.485	0.500	1.031	18.0	1.1
34.0	0.285	0.433	1.612	34.0	0.521	0.474	0.956	17.8	0.7
34.5	0.367	0.414	1.352	34.5	0.559	0.456	0.876	17.5	0.8
35.0	0.457	0.412	1.090	35.0	0.597	0.446	0.802	17.0	0.9
35.5	0.518	0.461	0.958	35.5	0.635	0.444	0.740	16.5	1.0
36.0	0.509	0.478	0.981	36.0	0.669	0.450	0.692	15.9	1.4
36.5	0.540	0.495	0.923	36.5	0.698	0.464	0.660	15.1	2.0
37.0	0.535	0.471	0.927	37.0	0.719	0.485	0.644	14.5	1.8
37.5	0.581	0.472	0.843	37.5	0.729	0.509	0.644	14.5	0.8
38.0	0.607	0.507	0.810	38.0	0.725	0.533	0.659	14.2	0.9
38.5	0.598	0.534	0.830	38.5	0.709	0.547	0.683	13.1	2.7
39.0	0.578	0.574	0.865	39.0	0.687	0.548	0.710	12.7	3.1
39.5	0.539	0.510	0.927	39.5	0.668	0.534	0.730	13.0	1.4
40.0	0.549	0.493	0.905	40.0	0.660	0.510	0.733	12.6	1.0
40.5	0.560	0.446	0.871	40.5	0.666	0.485	0.715	12.1	1.8
41.0	0.582	0.476	0.842	41.0	0.683	0.464	0.681	12.3	1.2
41.5	0.564	0.447	0.864	41.5	0.707	0.454	0.643	12.6	0.1
42.0	0.579	0.414	0.817	42.0	0.734	0.456	0.611	12.0	0.8
42.5	0.619	0.403	0.739	42.5	0.756	0.474	0.595	11.3	1.9
43.0	0.634	0.388	0.703	43.0	0.765	0.504	0.601	11.6	1.0
43.5	0.690	0.434	0.653	43.5	0.748	0.537	0.633	11.8	−0.1
44.0	0.672	0.418	0.667	44.0	0.709	0.551	0.683	11.1	0.8
44.5	0.667	0.438	0.689	44.5	0.669	0.533	0.729	10.5	1.8
45.0	0.672	0.424	0.671	45.0	0.649	0.496	0.744	10.9	0.5
45.5	0.687	0.423	0.650	45.5	0.652	0.458	0.722	11.5	−0.9
46.0	0.672	0.439	0.681	46.0	0.669	0.431	0.681	10.9	0.2
46.5	0.671	0.407	0.660	46.5	0.692	0.416	0.639	10.4	0.9
47.0	0.725	0.375	0.562	47.0	0.714	0.411	0.605	10.9	−0.9
47.5	0.788	0.403	0.515	47.5	0.734	0.414	0.583	11.2	−2.1

TABLE 19. Values of the real (ε_1) and imaginary (ε_2) parts of the complex dielectric constant and the ELF ($\mathrm{Im}\{-1/\varepsilon(\omega)\}$) of Pd calculated with DFT and derived from REELS data. The last two columns contain values for the volume and surface single-scattering loss distributions the DIIMFP (w_b) and the DSEP (w_s)—Continued

Pd									
DFT				REELS					
E (eV)	ε_1	ε_2	ELF	E (eV)	ε_1	ε_2	ELF	w_b (meV^{-1})	w_s (arb. un.)
48.0	0.912	0.415	0.413	48.0	0.750	0.423	0.570	10.7	−1.2
48.5	1.041	1.098	0.480	48.5	0.761	0.436	0.567	10.4	−1.1
49.0	0.318	0.603	1.296	49.0	0.766	0.452	0.571	10.5	−2.0
49.5	0.463	0.453	1.080	49.5	0.765	0.469	0.583	10.2	−1.8
50.0	0.525	0.420	0.929	50.0	0.758	0.485	0.599	9.8	–
50.5	0.552	0.417	0.871	50.5	0.745	0.499	0.621	10.0	–
51.0	0.537	0.387	0.883	51.0	0.727	0.509	0.647	10.6	–
51.5	0.562	0.327	0.774	51.5	0.706	0.513	0.674	10.9	–
52.0	0.642	0.303	0.602	52.0	0.684	0.511	0.702	10.2	–
52.5	0.771	0.348	0.487	52.5	0.663	0.503	0.727	9.7	–
53.0	0.465	0.588	1.046	53.0	0.645	0.490	0.747	10.5	–
53.5	0.541	0.359	0.851	53.5	0.634	0.474	0.757	11.5	–
54.0	0.569	0.358	0.792	54.0	0.632	0.460	0.752	11.5	–
54.5	0.567	0.332	0.768	54.5	0.649	0.472	0.732	11.1	–
55.0	0.603	0.302	0.665	55.0	0.528	0.491	0.944	11.2	–
55.5	0.653	0.308	0.592	55.5	0.544	0.399	0.876	11.4	–
56.0	0.624	0.412	0.737	56.0	0.562	0.370	0.817	11.6	–
56.5	0.575	0.353	0.776	56.5	0.574	0.350	0.775	11.8	–
57.0	0.588	0.330	0.725	57.0	0.584	0.334	0.737	12.3	–
57.5	0.574	0.315	0.735	57.5	0.594	0.320	0.703	12.3	–
58.0	0.599	0.305	0.676	58.0	0.604	0.309	0.672	11.4	–
58.5	0.595	0.292	0.665	58.5	0.613	0.300	0.645	11.2	–
59.0	0.620	0.294	0.625	59.0	0.621	0.294	0.622	11.8	–
59.5	0.603	0.327	0.695	59.5	0.629	0.288	0.603	11.7	–
60.0	0.613	0.324	0.673	60.0	0.635	0.284	0.587	10.9	–
60.5	0.546	0.325	0.804	60.5	0.640	0.281	0.575	10.7	–
61.0	0.511	0.277	0.819	61.0	0.644	0.279	0.566	11.1	–
61.5	0.525	0.223	0.686	61.5	0.647	0.278	0.560	11.1	–
62.0	0.546	0.195	0.581	62.0	0.648	0.276	0.556	10.7	–
62.5	0.571	0.183	0.510	62.5	0.648	0.274	0.554	10.4	–
63.0	0.585	0.175	0.469	63.0	0.646	0.272	0.553	10.4	–
63.5	0.605	0.179	0.450	63.5	0.644	0.269	0.552	10.1	–
64.0	0.594	0.176	0.459	64.0	0.641	0.265	0.550	9.7	–
64.5	0.601	0.165	0.424	64.5	0.638	0.259	0.547	9.3	–
65.0	0.602	0.157	0.407	65.0	0.635	0.253	0.542	9.2	–
65.5	0.607	0.142	0.366	65.5	0.631	0.246	0.535	9.7	–
66.0	0.616	0.131	0.330	66.0	0.629	0.237	0.526	10.0	–
66.5	0.626	0.123	0.302	66.5	0.627	0.228	0.513	9.6	–
67.0	0.637	0.114	0.273	67.0	0.625	0.219	0.498	9.4	–
67.5	0.650	0.110	0.253	67.5	0.625	0.209	0.481	9.2	–
68.0	0.660	0.110	0.246	68.0	0.625	0.199	0.461	8.8	–
68.5	0.663	0.110	0.244	68.5	0.627	0.188	0.440	8.7	–
69.0	0.667	0.110	0.240	69.0	0.629	0.178	0.418	8.9	–
69.5	0.668	0.104	0.227	69.5	0.632	0.169	0.395	8.7	–
70.0	0.672	0.098	0.212	70.0	0.635	0.159	0.372	8.3	–
70.5	0.676	0.090	0.193	70.5	0.639	0.151	0.349	8.1	–

TABLE 20. Values of the real (ε_1) and imaginary (ε_2) parts of the complex dielectric constant and the ELF ($\mathrm{Im}\{-1/\varepsilon(\omega)\}$) of Ag calculated with DFT and derived from REELS data. The last two columns contain values for the volume and surface single-scattering loss distributions the DIIMFP (w_b) and the DSEP (w_s)

Ag									
DFT				REELS					
E (eV)	ε_1	ε_2	ELF	E (eV)	ε_1	ε_2	ELF	w_b (meV^{-1})	w_s (arb. un.)
0.50	−315.856	64.244	0.001	0.50	−381.046	52.998	0.000	0.0	0.1
0.75	−140.655	19.452	0.001	0.75	−167.668	17.070	0.001	0.0	0.2
1.00	−77.567	8.304	0.001	1.00	−92.057	8.164	0.001	0.0	0.2
1.25	−47.965	4.299	0.002	1.25	−56.909	4.990	0.002	0.0	0.3
1.50	−31.729	2.528	0.002	1.50	−37.787	3.618	0.003	0.1	0.4
1.75	−21.829	1.634	0.003	1.75	−26.256	2.959	0.004	0.0	0.3
2.00	−15.290	1.147	0.005	2.00	−18.776	2.629	0.007	0.0	0.5
2.25	−10.668	0.875	0.008	2.25	−13.650	2.467	0.013	−0.1	1.2
2.50	−7.155	0.747	0.014	2.50	−9.980	2.399	0.023	−0.2	4.0
2.75	−4.194	0.794	0.044	2.75	−7.253	2.390	0.041	−0.3	13.1
3.00	−1.376	1.655	0.357	3.00	−5.158	2.422	0.075	0.8	34.9
3.25	−0.239	3.255	0.306	3.25	−3.488	2.489	0.136	6.1	73.6
3.50	0.183	4.126	0.242	3.50	−2.104	2.598	0.232	15.6	120.2
3.75	0.294	5.126	0.194	3.75	−0.893	2.773	0.327	22.0	158.5
4.00	−0.472	5.480	0.181	4.00	0.242	3.074	0.323	19.3	175.1
4.25	−0.778	5.124	0.191	4.25	1.387	3.658	0.239	11.4	165.3
4.50	−1.011	4.824	0.199	4.50	2.507	4.957	0.161	4.9	142.2
4.75	−1.089	4.404	0.214	4.75	2.474	7.803	0.116	2.0	119.3
5.0	−1.076	4.008	0.233	5.0	−1.599	9.249	0.105	1.4	103.7
5.5	−0.883	3.292	0.283	5.5	−2.937	4.175	0.160	3.8	96.5
6.0	−0.578	2.739	0.349	6.0	−1.497	2.939	0.270	7.4	105.4
6.5	−0.252	2.287	0.432	6.5	−0.666	2.589	0.362	9.4	110.9
7.0	0.173	1.980	0.501	7.0	−0.153	2.435	0.409	11.0	106.4
7.5	0.536	1.852	0.498	7.5	0.193	2.347	0.423	13.1	97.5
8.0	0.881	1.850	0.441	8.0	0.441	2.289	0.421	13.9	87.8
8.5	0.890	1.941	0.426	8.5	0.627	2.250	0.412	12.7	77.9
9.0	0.978	1.857	0.422	9.0	0.769	2.227	0.401	11.5	67.2
9.5	1.120	1.796	0.401	9.5	0.878	2.221	0.389	11.8	55.5
10.0	1.161	1.876	0.385	10.0	0.956	2.232	0.379	12.2	46.3
10.5	1.129	1.830	0.396	10.5	1.002	2.259	0.370	11.7	41.9
11.0	1.187	1.745	0.392	11.0	1.012	2.298	0.365	11.4	38.9
11.5	1.299	1.702	0.371	11.5	0.980	2.339	0.364	11.3	35.6
12.0	1.438	1.767	0.340	12.0	0.905	2.368	0.368	11.4	32.9
12.5	1.497	1.917	0.324	12.5	0.793	2.366	0.380	11.9	30.1
13.0	1.360	2.113	0.335	13.0	0.664	2.317	0.399	11.9	27.8
13.5	1.165	2.209	0.354	13.5	0.542	2.219	0.425	11.3	26.8
14.0	0.908	2.107	0.400	14.0	0.449	2.084	0.459	11.2	26.1
14.5	0.803	1.940	0.440	14.5	0.394	1.932	0.497	11.6	25.4
15.0	0.762	1.793	0.472	15.0	0.378	1.780	0.538	12.2	24.2
15.5	0.760	1.668	0.496	15.5	0.392	1.639	0.577	13.3	21.9
16.0	0.780	1.567	0.512	16.0	0.430	1.516	0.610	14.3	19.9
16.5	0.814	1.491	0.517	16.5	0.483	1.414	0.633	14.5	19.4
17.0	0.839	1.440	0.518	17.0	0.548	1.332	0.642	14.2	19.0
17.5	0.864	1.367	0.523	17.5	0.620	1.272	0.635	14.4	18.0
18.0	0.925	1.302	0.511	18.0	0.697	1.236	0.614	15.1	17.2
18.5	1.027	1.245	0.478	18.5	0.775	1.227	0.582	15.2	16.1
19.0	1.199	1.259	0.416	19.0	0.850	1.252	0.547	14.4	15.5
19.5	1.425	1.444	0.351	19.5	0.906	1.320	0.515	13.3	16.9
20.0	1.267	1.951	0.361	20.0	0.915	1.432	0.496	13.0	18.1
20.5	1.063	2.234	0.365	20.5	0.831	1.564	0.499	13.2	16.6
21.0	0.347	2.008	0.484	21.0	0.637	1.633	0.531	13.4	14.6
21.5	0.260	1.612	0.604	21.5	0.413	1.559	0.599	13.3	14.2

TABLE 20. Values of the real (ε_1) and imaginary (ε_2) parts of the complex dielectric constant and the ELF ($\mathrm{Im}\{-1/\varepsilon(\omega)\}$) of Ag calculated with DFT and derived from REELS data. The last two columns contain values for the volume and surface single-scattering loss distributions the DIIMFP (w_b) and the DSEP (w_s)—Continued

Ag									
DFT				REELS					
E (eV)	ε_1	ε_2	ELF	E (eV)	ε_1	ε_2	ELF	w_b (meV^{-1})	w_s (arb. un.)
22.0	0.356	1.423	0.661	22.0	0.272	1.376	0.699	13.4	14.8
22.5	0.328	1.410	0.673	22.5	0.238	1.179	0.815	13.7	15.1
23.0	0.251	1.314	0.734	23.0	0.270	1.019	0.917	14.4	13.7
23.5	0.150	1.113	0.883	23.5	0.329	0.900	0.981	16.0	10.8
24.0	0.213	0.904	1.048	24.0	0.396	0.813	0.994	17.7	8.6
24.5	0.319	0.729	1.151	24.5	0.463	0.751	0.964	17.9	9.1
25.0	0.513	0.630	0.955	25.0	0.528	0.706	0.909	17.2	9.7
25.5	0.680	0.656	0.735	25.5	0.589	0.674	0.841	17.4	7.2
26.0	0.800	0.739	0.623	26.0	0.647	0.653	0.773	17.8	4.5
26.5	0.764	0.821	0.653	26.5	0.702	0.641	0.709	17.1	5.0
27.0	0.789	0.807	0.634	27.0	0.754	0.640	0.654	15.6	6.6
27.5	0.807	0.858	0.618	27.5	0.803	0.650	0.609	15.0	6.0
28.0	0.803	0.829	0.623	28.0	0.847	0.673	0.575	14.7	5.1
28.5	0.867	0.890	0.577	28.5	0.879	0.711	0.557	13.9	6.0
29.0	0.805	0.953	0.613	29.0	0.889	0.764	0.556	13.3	6.5
29.5	0.804	0.980	0.610	29.5	0.865	0.821	0.577	13.1	5.7
30.0	0.715	1.087	0.642	30.0	0.803	0.854	0.622	13.0	5.5
30.5	0.556	1.022	0.755	30.5	0.727	0.839	0.680	13.4	5.1
31.0	0.504	0.934	0.829	31.0	0.675	0.784	0.732	13.7	4.7
31.5	0.481	0.868	0.881	31.5	0.659	0.718	0.756	13.3	5.2
32.0	0.404	0.776	1.013	32.0	0.670	0.661	0.746	13.3	4.7
32.5	0.457	0.625	1.042	32.5	0.694	0.618	0.716	13.7	3.4
33.0	0.552	0.559	0.905	33.0	0.722	0.588	0.678	13.6	3.6
33.5	0.642	0.549	0.769	33.5	0.751	0.569	0.641	13.2	4.3
34.0	0.708	0.575	0.691	34.0	0.779	0.557	0.608	13.4	3.0
34.5	0.753	0.616	0.650	34.5	0.803	0.552	0.581	13.8	1.3
35.0	0.738	0.698	0.676	35.0	0.826	0.551	0.559	12.8	2.7
35.5	0.675	0.677	0.741	35.5	0.845	0.553	0.542	11.6	4.2
36.0	0.680	0.646	0.734	36.0	0.861	0.558	0.530	11.9	2.8
36.5	0.697	0.686	0.717	36.5	0.874	0.566	0.522	12.3	1.5
37.0	0.679	0.666	0.736	37.0	0.884	0.575	0.517	12.0	1.6
37.5	0.649	0.679	0.769	37.5	0.891	0.585	0.515	11.5	1.6
38.0	0.629	0.648	0.795	38.0	0.895	0.596	0.515	11.1	1.5
38.5	0.606	0.617	0.825	38.5	0.896	0.608	0.519	10.8	1.8
39.0	0.621	0.580	0.803	39.0	0.894	0.620	0.524	11.1	1.2
39.5	0.620	0.554	0.801	39.5	0.888	0.631	0.532	11.3	0.9
40.0	0.652	0.552	0.756	40.0	0.880	0.641	0.541	10.8	1.7
40.5	0.647	0.565	0.765	40.5	0.868	0.649	0.552	10.3	1.9
41.0	0.661	0.560	0.747	41.0	0.855	0.655	0.565	10.2	1.6
41.5	0.639	0.561	0.776	41.5	0.839	0.659	0.579	10.5	1.3
42.0	0.627	0.524	0.785	42.0	0.823	0.660	0.593	10.6	0.9
42.5	0.633	0.540	0.779	42.5	0.805	0.658	0.609	10.6	0.4
43.0	0.632	0.551	0.783	43.0	0.788	0.654	0.624	10.3	0.5
43.5	0.584	0.523	0.852	43.5	0.770	0.646	0.639	10.2	1.0
44.0	0.614	0.480	0.790	44.0	0.754	0.637	0.654	10.5	0.9
44.5	0.665	0.525	0.731	44.5	0.739	0.625	0.667	10.7	0.3
45.0	0.590	0.539	0.844	45.0	0.726	0.611	0.679	10.5	−0.9
45.5	0.554	0.500	0.898	45.5	0.714	0.596	0.689	10.4	−1.7
46.0	0.569	0.529	0.876	46.0	0.705	0.580	0.696	10.3	−1.1
46.5	0.454	0.459	1.101	46.5	0.697	0.563	0.701	10.1	−0.2
47.0	0.485	0.354	0.981	47.0	0.692	0.546	0.703	10.0	−0.4
47.5	0.519	0.339	0.883	47.5	0.688	0.530	0.703	10.4	−2.1

TABLE 20. Values of the real (ε_1) and imaginary (ε_2) parts of the complex dielectric constant and the ELF ($\mathrm{Im}\{-1/\varepsilon(\omega)\}$) of Ag calculated with DFT and derived from REELS data. The last two columns contain values for the volume and surface single-scattering loss distributions the DIIMFP (w_b) and the DSEP (w_s)—Continued

Ag									
DFT				REELS					
E (eV)	ε_1	ε_2	ELF	E (eV)	ε_1	ε_2	ELF	w_b (meV^{-1})	w_s (arb. un.)
48.0	0.549	0.287	0.748	48.0	0.685	0.514	0.700	11.2	−3.8
48.5	0.596	0.280	0.645	48.5	0.684	0.498	0.695	11.0	−3.1
49.0	0.623	0.265	0.579	49.0	0.685	0.483	0.688	9.9	−0.6
49.5	0.667	0.288	0.545	49.5	0.686	0.469	0.679	9.7	−0.7
50.0	0.659	0.299	0.570	50.0	0.688	0.456	0.669	10.5	–
50.5	0.667	0.308	0.571	50.5	0.691	0.444	0.658	10.7	–
51.0	0.652	0.305	0.589	51.0	0.694	0.432	0.647	10.5	–
51.5	0.654	0.283	0.557	51.5	0.697	0.422	0.635	10.5	–
52.0	0.672	0.273	0.518	52.0	0.701	0.412	0.623	10.5	–
52.5	0.691	0.265	0.484	52.5	0.705	0.403	0.611	10.4	–
53.0	0.705	0.283	0.491	53.0	0.709	0.395	0.600	10.1	–
53.5	0.728	0.263	0.439	53.5	0.713	0.388	0.589	10.2	–
54.0	0.748	0.310	0.473	54.0	0.717	0.381	0.578	11.1	–
54.5	0.717	0.334	0.534	54.5	0.720	0.375	0.568	11.3	–
55.0	0.703	0.334	0.551	55.0	0.724	0.369	0.559	10.3	–
55.5	0.739	0.334	0.509	55.5	0.727	0.364	0.551	9.8	–
56.0	0.666	0.428	0.683	56.0	0.730	0.359	0.543	10.2	–
56.5	0.542	0.325	0.815	56.5	0.733	0.355	0.535	10.0	–
57.0	0.582	0.240	0.606	57.0	0.735	0.351	0.529	9.3	–
57.5	0.609	0.219	0.522	57.5	0.737	0.347	0.522	9.4	–
58.0	0.635	0.194	0.439	58.0	0.739	0.343	0.517	10.2	–
58.5	0.667	0.180	0.377	58.5	0.741	0.340	0.512	9.6	–
59.0	0.722	0.185	0.333	59.0	0.742	0.336	0.507	8.0	–
59.5	0.696	0.247	0.453	59.5	0.743	0.333	0.503	8.1	–
60.0	0.669	0.228	0.457	60.0	0.744	0.330	0.498	9.6	–
60.5	0.669	0.204	0.417	60.5	0.744	0.327	0.495	9.4	–
61.0	0.684	0.186	0.370	61.0	0.744	0.323	0.491	7.7	–
61.5	0.702	0.180	0.343	61.5	0.744	0.320	0.488	7.6	–
62.0	0.734	0.185	0.323	62.0	0.744	0.317	0.484	9.1	–
62.5	0.718	0.224	0.396	62.5	0.744	0.314	0.481	9.3	–
63.0	0.691	0.229	0.432	63.0	0.743	0.310	0.478	8.1	–
63.5	0.674	0.209	0.420	63.5	0.743	0.307	0.475	7.4	–
64.0	0.672	0.189	0.387	64.0	0.742	0.303	0.471	8.3	–
64.5	0.677	0.173	0.354	64.5	0.741	0.299	0.468	9.3	–
65.0	0.686	0.162	0.327	65.0	0.741	0.295	0.464	8.6	–
65.5	0.694	0.155	0.306	65.5	0.740	0.291	0.461	7.7	–
66.0	0.705	0.151	0.290	66.0	0.739	0.287	0.457	8.1	–
66.5	0.710	0.153	0.290	66.5	0.738	0.283	0.452	8.7	–
67.0	0.713	0.155	0.290	67.0	0.737	0.278	0.448	8.6	–
67.5	0.709	0.159	0.302	67.5	0.737	0.274	0.443	7.9	–
68.0	0.701	0.159	0.308	68.0	0.736	0.269	0.438	7.5	–
68.5	0.688	0.145	0.292	68.5	0.736	0.264	0.433	7.6	–
69.0	0.688	0.130	0.266	69.0	0.735	0.260	0.427	7.9	–
69.5	0.690	0.114	0.234	69.5	0.735	0.255	0.421	8.4	–
70.0	0.696	0.099	0.200	70.0	0.735	0.250	0.415	8.7	–
70.5	0.705	0.090	0.179	70.5	0.734	0.245	0.409	8.0	–

TABLE 21. Values of the real (ε_1) and imaginary (ε_2) parts of the complex dielectric constant and the ELF ($\mathrm{Im}\{-1/\varepsilon(\omega)\}$) of Ta calculated with DFT and derived from REELS data. The last two columns contain values for the volume and surface single-scattering loss distributions the DIIMFP (w_b) and the DSEP (w_s)

Ta									
DFT				REELS					
E (eV)	ε_1	ε_2	ELF	E (eV)	ε_1	ε_2	ELF	w_b (meV^{-1})	w_s (arb. un.)
0.50	−288.473	64.569	0.001	0.50	−541.808	64.899	0.000	−0.1	0.7
0.75	−121.442	21.888	0.001	0.75	−238.276	33.368	0.001	−0.1	1.0
1.00	−60.953	12.115	0.003	1.00	−131.924	22.804	0.001	−0.1	1.4
1.25	−33.328	9.805	0.008	1.25	−82.720	17.751	0.002	−0.1	1.7
1.50	−19.051	8.694	0.020	1.50	−56.042	14.864	0.004	−0.2	2.0
1.75	−10.073	7.549	0.048	1.75	−40.018	13.041	0.007	−0.2	2.1
2.00	−3.000	7.375	0.116	2.00	−29.690	11.818	0.012	−0.2	3.0
2.25	2.022	9.025	0.106	2.25	−22.689	10.962	0.017	−0.2	6.0
2.50	4.715	11.395	0.075	2.50	−17.770	10.343	0.024	0.1	12.3
2.75	5.365	13.703	0.063	2.75	−14.223	9.880	0.033	1.0	22.7
3.00	4.746	15.239	0.060	3.00	−11.623	9.518	0.042	2.0	33.7
3.25	3.321	15.867	0.060	3.25	−9.695	9.217	0.052	2.3	40.1
3.50	1.950	15.133	0.065	3.50	−8.259	8.947	0.060	2.2	40.6
3.75	1.509	13.908	0.071	3.75	−7.187	8.687	0.068	2.0	37.6
4.00	1.898	12.912	0.076	4.00	−6.385	8.422	0.075	2.0	34.6
4.25	2.753	12.549	0.076	4.25	−5.782	8.141	0.082	2.0	33.1
4.50	3.887	13.000	0.071	4.50	−5.325	7.839	0.087	2.1	33.1
4.75	5.040	14.948	0.060	4.75	−4.970	7.517	0.093	2.3	34.1
5.0	4.191	18.390	0.052	5.0	−4.686	7.177	0.098	2.6	35.6
5.5	−8.114	19.484	0.044	5.5	−4.237	6.462	0.108	3.2	39.1
6.0	−9.550	10.263	0.052	6.0	−3.855	5.745	0.120	3.7	41.8
6.5	−7.493	6.282	0.066	6.5	−3.482	5.070	0.134	4.0	43.2
7.0	−5.120	4.382	0.096	7.0	−3.101	4.464	0.151	4.3	44.5
7.5	−3.453	3.647	0.145	7.5	−2.707	3.943	0.172	5.0	45.9
8.0	−2.236	3.355	0.206	8.0	−2.292	3.516	0.200	6.1	46.8
8.5	−1.292	3.977	0.227	8.5	−1.829	3.205	0.235	6.4	49.6
9.0	−1.679	4.366	0.200	9.0	−1.213	3.182	0.274	6.5	52.3
9.5	−2.052	3.972	0.199	9.5	−1.837	4.357	0.195	7.4	52.0
10.0	−2.040	3.294	0.219	10.0	−2.140	2.705	0.227	7.8	53.5
10.5	−1.814	2.807	0.251	10.5	−1.634	2.328	0.288	8.0	56.2
11.0	−1.631	2.536	0.279	11.0	−1.325	2.169	0.336	9.3	55.5
11.5	−1.191	2.317	0.341	11.5	−1.115	2.072	0.374	10.0	56.3
12.0	−1.126	2.223	0.358	12.0	−0.971	1.999	0.405	9.6	61.4
12.5	−1.015	1.965	0.402	12.5	−0.879	1.932	0.429	9.7	64.5
13.0	−0.682	1.834	0.479	13.0	−0.824	1.856	0.450	11.2	62.6
13.5	−0.442	2.011	0.474	13.5	−0.791	1.763	0.472	13.0	60.7
14.0	−0.473	2.057	0.462	14.0	−0.764	1.651	0.499	13.8	62.6
14.5	−0.459	2.147	0.445	14.5	−0.730	1.526	0.533	14.1	65.0
15.0	−0.830	2.285	0.387	15.0	−0.683	1.395	0.578	14.5	65.9
15.5	−1.062	1.921	0.399	15.5	−0.621	1.268	0.636	14.9	67.0
16.0	−1.199	1.441	0.410	16.0	−0.545	1.152	0.709	15.8	66.9
16.5	−0.926	1.080	0.534	16.5	−0.459	1.052	0.798	17.6	64.6
17.0	−0.775	1.185	0.591	17.0	−0.367	0.976	0.898	19.3	62.2
17.5	−0.863	0.741	0.573	17.5	−0.280	0.932	0.984	20.5	59.9
18.0	−0.548	0.519	0.910	18.0	−0.236	0.920	1.020	21.7	57.8
18.5	−0.275	0.429	1.652	18.5	−0.252	0.866	1.064	23.1	56.6
19.0	−0.061	0.564	1.752	19.0	−0.230	0.748	1.221	24.4	55.5
19.5	−0.058	0.500	1.973	19.5	−0.156	0.647	1.459	26.0	50.7
20.0	0.113	0.462	2.040	20.0	−0.073	0.577	1.707	29.0	42.4
20.5	0.221	0.497	1.681	20.5	0.008	0.525	1.904	32.1	36.0
21.0	0.264	0.561	1.460	21.0	0.083	0.485	2.001	34.0	32.2
21.5	0.273	0.506	1.529	21.5	0.154	0.455	1.974	35.1	25.8

TABLE 21. Values of the real (ε_1) and imaginary (ε_2) parts of the complex dielectric constant and the ELF ($\mathrm{Im}\{-1/\varepsilon(\omega)\}$) of Ta calculated with DFT and derived from REELS data. The last two columns contain values for the volume and surface single-scattering loss distributions the DIIMFP (w_b) and the DSEP (w_s)—Continued

Ta									
DFT				REELS					
E (eV)	ε_1	ε_2	ELF	E (eV)	ε_1	ε_2	ELF	w_b (meV^{-1})	w_s (arb. un.)
22.0	0.366	0.510	1.295	22.0	0.220	0.431	1.842	35.2	18.6
22.5	0.416	0.516	1.175	22.5	0.282	0.413	1.650	34.1	15.4
23.0	0.462	0.536	1.070	23.0	0.341	0.402	1.446	31.7	17.2
23.5	0.592	0.688	0.835	23.5	0.395	0.398	1.265	28.7	18.7
24.0	0.098	0.643	1.521	24.0	0.443	0.401	1.124	27.2	14.0
24.5	0.273	0.379	1.739	24.5	0.479	0.411	1.032	26.3	9.9
25.0	0.384	0.311	1.273	25.0	0.499	0.421	0.988	24.5	12.2
25.5	0.468	0.276	0.937	25.5	0.505	0.418	0.973	22.6	14.7
26.0	0.544	0.243	0.685	26.0	0.511	0.398	0.949	21.7	13.6
26.5	0.612	0.231	0.540	26.5	0.529	0.368	0.887	20.8	13.0
27.0	0.668	0.201	0.413	27.0	0.558	0.339	0.795	19.5	12.8
27.5	0.750	0.182	0.305	27.5	0.595	0.316	0.696	18.9	10.0
28.0	0.830	0.188	0.259	28.0	0.635	0.300	0.608	18.4	7.7
28.5	0.887	0.200	0.242	28.5	0.675	0.289	0.536	16.9	9.0
29.0	0.929	0.210	0.231	29.0	0.714	0.282	0.478	15.0	11.3
29.5	0.987	0.195	0.193	29.5	0.754	0.279	0.432	13.7	11.3
30.0	1.054	0.191	0.167	30.0	0.792	0.280	0.396	12.9	9.2
30.5	1.112	0.196	0.153	30.5	0.831	0.284	0.368	11.9	8.2
31.0	1.200	0.168	0.114	31.0	0.869	0.291	0.347	10.8	8.3
31.5	1.324	0.160	0.090	31.5	0.907	0.303	0.331	9.9	8.4
32.0	1.488	0.188	0.084	32.0	0.946	0.319	0.320	8.9	8.9
32.5	1.664	0.245	0.087	32.5	0.984	0.341	0.314	8.8	7.0
33.0	2.073	0.395	0.089	33.0	1.021	0.370	0.314	9.4	3.6
33.5	1.963	1.311	0.235	33.5	1.056	0.408	0.318	9.0	5.3
34.0	1.311	0.874	0.352	34.0	1.086	0.457	0.329	7.8	10.1
34.5	1.550	0.787	0.260	34.5	1.107	0.520	0.347	7.8	9.8
35.0	1.849	0.894	0.212	35.0	1.112	0.594	0.374	9.3	5.8
35.5	1.897	1.376	0.251	35.5	1.090	0.677	0.411	9.8	5.8
36.0	1.766	1.663	0.283	36.0	1.033	0.754	0.461	9.1	9.0
36.5	1.486	2.003	0.322	36.5	0.945	0.804	0.523	8.8	9.1
37.0	1.160	2.114	0.364	37.0	0.842	0.810	0.593	9.4	7.2
37.5	0.969	2.036	0.401	37.5	0.754	0.773	0.663	10.4	6.9
38.0	0.624	2.895	0.330	38.0	0.699	0.711	0.715	10.6	8.3
38.5	−0.122	1.957	0.509	38.5	0.677	0.645	0.738	10.5	7.9
39.0	−0.776	1.999	0.435	39.0	0.680	0.589	0.728	11.3	5.0
39.5	−0.595	1.042	0.724	39.5	0.698	0.547	0.695	11.7	4.7
40.0	−0.309	0.791	1.097	40.0	0.724	0.521	0.655	11.0	7.7
40.5	−0.140	0.702	1.370	40.5	0.751	0.509	0.618	10.9	7.2
41.0	−0.024	0.609	1.639	41.0	0.777	0.509	0.590	11.4	2.9
41.5	0.052	0.566	1.752	41.5	0.799	0.520	0.573	11.4	1.0
42.0	0.103	0.555	1.740	42.0	0.813	0.540	0.567	11.6	1.1
42.5	0.152	0.490	1.862	42.5	0.819	0.568	0.572	11.8	0.8
43.0	0.213	0.468	1.769	43.0	0.812	0.599	0.588	11.1	1.7
43.5	0.273	0.468	1.595	43.5	0.792	0.631	0.616	10.1	3.7
44.0	0.295	0.446	1.559	44.0	0.757	0.659	0.654	9.9	4.7
44.5	0.326	0.468	1.440	44.5	0.711	0.675	0.702	11.0	3.4
45.0	0.327	0.451	1.452	45.0	0.657	0.677	0.760	12.1	1.3
45.5	0.339	0.451	1.417	45.5	0.603	0.662	0.825	11.3	2.5
46.0	0.308	0.442	1.524	46.0	0.555	0.632	0.894	10.6	4.1
46.5	0.328	0.401	1.493	46.5	0.517	0.591	0.959	12.1	2.2
47.0	0.326	0.398	1.503	47.0	0.491	0.545	1.013	13.1	2.3
47.5	0.315	0.365	1.569	47.5	0.477	0.497	1.047	12.4	4.2

TABLE 21. Values of the real (ε_1) and imaginary (ε_2) parts of the complex dielectric constant and the ELF ($\mathrm{Im}\{-1/\varepsilon(\omega)\}$) of Ta calculated with DFT and derived from REELS data. The last two columns contain values for the volume and surface single-scattering loss distributions the DIIMFP (w_b) and the DSEP (w_s)—Continued

Ta									
DFT				REELS					
E (eV)	ε_1	ε_2	ELF	E (eV)	ε_1	ε_2	ELF	w_b (meV^{-1})	w_s (arb. un.)
48.0	0.314	0.322	1.591	48.0	0.472	0.452	1.058	12.9	1.6
48.5	0.339	0.279	1.445	48.5	0.475	0.411	1.042	14.5	−2.1
49.0	0.368	0.252	1.267	49.0	0.483	0.374	1.003	15.0	−2.3
49.5	0.400	0.235	1.094	49.5	0.494	0.342	0.948	14.3	0.1
50.0	0.425	0.235	0.994	50.0	0.507	0.315	0.884	13.8	–
50.5	0.422	0.233	1.002	50.5	0.521	0.291	0.817	14.8	–
51.0	0.432	0.202	0.887	51.0	0.536	0.270	0.751	14.8	–
51.5	0.450	0.192	0.802	51.5	0.550	0.253	0.689	12.8	–
52.0	0.466	0.167	0.683	52.0	0.564	0.237	0.633	12.2	–
52.5	0.490	0.154	0.583	52.5	0.578	0.224	0.583	13.4	–
53.0	0.518	0.143	0.493	53.0	0.592	0.213	0.539	13.3	–
53.5	0.553	0.150	0.458	53.5	0.604	0.203	0.500	11.7	–
54.0	0.545	0.184	0.556	54.0	0.616	0.194	0.466	10.6	–
54.5	0.540	0.159	0.500	54.5	0.628	0.187	0.435	10.3	–
55.0	0.541	0.138	0.441	55.0	0.638	0.180	0.409	10.5	–
55.5	0.568	0.126	0.372	55.5	0.649	0.174	0.386	10.0	–
56.0	0.587	0.126	0.349	56.0	0.658	0.169	0.365	9.4	–
56.5	0.593	0.134	0.362	56.5	0.667	0.164	0.347	9.5	–
57.0	0.598	0.125	0.336	57.0	0.676	0.159	0.331	9.7	–
57.5	0.603	0.120	0.318	57.5	0.684	0.156	0.316	8.9	–
58.0	0.615	0.114	0.290	58.0	0.692	0.152	0.303	7.9	–
58.5	0.622	0.105	0.263	58.5	0.699	0.149	0.291	8.5	–
59.0	0.640	0.098	0.233	59.0	0.706	0.146	0.280	9.6	–
59.5	0.661	0.097	0.218	59.5	0.712	0.143	0.271	9.0	–
60.0	0.681	0.114	0.239	60.0	0.718	0.140	0.262	7.5	–
60.5	0.674	0.132	0.280	60.5	0.724	0.138	0.254	6.8	–
61.0	0.659	0.137	0.301	61.0	0.730	0.136	0.246	7.5	–
61.5	0.645	0.123	0.285	61.5	0.735	0.134	0.239	7.9	–
62.0	0.647	0.101	0.235	62.0	0.740	0.132	0.233	7.0	–
62.5	0.659	0.099	0.224	62.5	0.745	0.130	0.227	6.2	–
63.0	0.662	0.088	0.196	63.0	0.749	0.128	0.221	6.4	–
63.5	0.674	0.076	0.165	63.5	0.754	0.126	0.216	6.5	–
64.0	0.692	0.074	0.152	64.0	0.758	0.124	0.211	5.5	–
64.5	0.698	0.078	0.159	64.5	0.762	0.123	0.206	5.0	–
65.0	0.702	0.077	0.155	65.0	0.765	0.121	0.202	5.6	–
65.5	0.707	0.073	0.144	65.5	0.769	0.120	0.198	6.0	–
66.0	0.715	0.073	0.141	66.0	0.772	0.118	0.194	5.5	–
66.5	0.721	0.072	0.137	66.5	0.776	0.117	0.190	4.7	–
67.0	0.727	0.072	0.135	67.0	0.779	0.115	0.186	4.9	–
67.5	0.729	0.070	0.130	67.5	0.782	0.114	0.183	5.6	–
68.0	0.736	0.069	0.126	68.0	0.785	0.113	0.179	5.3	–
68.5	0.740	0.071	0.129	68.5	0.787	0.111	0.176	4.3	–
69.0	0.741	0.071	0.128	69.0	0.790	0.110	0.173	4.1	–
69.5	0.742	0.068	0.123	69.5	0.793	0.108	0.169	4.9	–
70.0	0.746	0.064	0.115	70.0	0.795	0.107	0.166	5.0	–
70.5	0.751	0.062	0.110	70.5	0.798	0.106	0.164	4.1	–

TABLE 22. Values of the real (ε_1) and imaginary (ε_2) parts of the complex dielectric constant and the ELF ($\mathrm{Im}\{-1/\varepsilon(\omega)\}$) of W calculated with DFT and derived from REELS data. The last two columns contain values for the volume and surface single-scattering loss distributions the DIIMFP (w_b) and the DSEP (w_s)

W									
DFT				REELS					
E (eV)	ε_1	ε_2	ELF	E (eV)	ε_1	ε_2	ELF	w_b (meV^{-1})	w_s (arb. un.)
0.50	−156.936	54.751	0.002	0.50	−591.677	58.689	0.000	−0.1	0.8
0.75	−50.462	30.936	0.009	0.75	−213.138	72.950	0.001	−0.1	1.1
1.00	−21.027	29.63	0.022	1.00	−153.784	114.349	0.003	−0.1	1.5
1.25	−8.119	23.739	0.038	1.25	−135.890	52.032	0.002	−0.2	1.9
1.50	1.527	21.326	0.047	1.50	−90.863	22.973	0.003	−0.2	2.3
1.75	6.747	23.220	0.040	1.75	−60.175	14.008	0.004	−0.2	2.2
2.00	6.848	24.892	0.037	2.00	−39.721	11.889	0.007	−0.3	2.9
2.25	5.737	24.423	0.039	2.25	−25.668	13.929	0.016	−0.4	5.5
2.50	5.081	22.972	0.042	2.50	−18.551	19.871	0.027	−0.6	10.5
2.75	5.268	21.961	0.043	2.75	−21.449	23.118	0.023	−0.2	17.5
3.00	5.303	21.915	0.043	3.00	−23.295	16.895	0.020	0.7	23.7
3.25	3.868	22.053	0.044	3.25	−18.804	11.390	0.024	1.4	26.8
3.50	2.568	20.794	0.047	3.50	−12.725	10.101	0.038	1.6	27.0
3.75	2.255	19.453	0.051	3.75	−8.725	14.450	0.051	1.4	25.6
4.00	2.454	18.511	0.053	4.00	−15.518	15.600	0.032	1.2	24.1
4.25	2.866	18.417	0.053	4.25	−14.260	8.807	0.031	1.0	23.3
4.50	3.041	18.631	0.052	4.50	−10.131	7.253	0.047	0.9	23.4
4.75	3.621	19.774	0.049	4.75	−7.494	8.646	0.066	1.0	24.4
5.0	3.042	23.437	0.042	5.0	−8.485	10.712	0.057	1.1	26.0
5.5	−10.483	22.284	0.037	5.5	−10.067	6.051	0.044	1.4	30.2
6.0	−11.305	12.727	0.044	6.0	−6.983	4.077	0.062	1.5	34.9
6.5	−9.064	8.316	0.055	6.5	−5.094	3.967	0.095	1.9	38.6
7.0	−7.398	6.286	0.067	7.0	−4.315	3.963	0.115	2.6	42.4
7.5	−5.512	4.547	0.089	7.5	−3.808	3.547	0.131	2.9	50.0
8.0	−4.155	3.564	0.119	8.0	−3.130	3.110	0.160	3.2	58.1
8.5	−2.766	3.571	0.175	8.5	−2.433	2.903	0.202	4.3	61.3
9.0	−2.084	3.408	0.214	9.0	−1.874	2.896	0.243	5.7	62.3
9.5	−0.783	3.754	0.255	9.5	−1.506	2.995	0.266	6.7	64.1
10.0	−1.313	3.995	0.226	10.0	−1.331	3.111	0.272	7.2	66.0
10.5	−1.402	4.281	0.211	10.5	−1.310	3.167	0.270	7.5	66.2
11.0	−1.747	3.927	0.213	11.0	−1.374	3.115	0.269	7.4	66.1
11.5	−1.720	3.580	0.227	11.5	−1.444	2.959	0.273	7.2	67.3
12.0	−1.805	3.225	0.236	12.0	−1.467	2.735	0.284	7.5	67.7
12.5	−1.384	2.803	0.287	12.5	−1.429	2.495	0.302	8.0	67.2
13.0	−1.591	2.708	0.275	13.0	−1.340	2.275	0.326	8.0	67.3
13.5	−1.567	2.165	0.303	13.5	−1.224	2.095	0.356	8.1	67.6
14.0	−1.046	1.833	0.412	14.0	−1.104	1.958	0.388	8.7	67.9
14.5	−0.671	1.761	0.496	14.5	−0.997	1.859	0.418	9.2	69.2
15.0	−0.316	1.859	0.523	15.0	−0.914	1.785	0.444	9.7	68.6
15.5	−0.112	2.031	0.491	15.5	−0.861	1.720	0.465	10.7	64.3
16.0	0.086	2.365	0.422	16.0	−0.833	1.652	0.483	11.2	61.2
16.5	−0.450	2.960	0.330	16.5	−0.822	1.568	0.500	10.8	62.3
17.0	−1.021	2.548	0.338	17.0	−0.814	1.467	0.521	10.7	63.6
17.5	−1.133	2.290	0.351	17.5	−0.799	1.351	0.548	11.7	61.6
18.0	−1.265	1.819	0.371	18.0	−0.770	1.226	0.585	12.9	60.9
18.5	−0.985	1.647	0.447	18.5	−0.725	1.102	0.633	13.3	63.2
19.0	−1.429	1.607	0.348	19.0	−0.666	0.985	0.697	14.1	63.0
19.5	−1.229	0.981	0.397	19.5	−0.596	0.877	0.780	15.4	61.0
20.0	−0.980	0.743	0.491	20.0	−0.518	0.782	0.889	16.8	60.6
20.5	−0.721	0.584	0.678	20.5	−0.436	0.699	1.030	18.6	60.2
21.0	−0.448	0.536	1.098	21.0	−0.351	0.628	1.213	20.2	57.5
21.5	−0.298	0.611	1.321	21.5	−0.262	0.570	1.448	21.7	52.7

TABLE 22. Values of the real (ε_1) and imaginary (ε_2) parts of the complex dielectric constant and the ELF ($\mathrm{Im}\{-1/\varepsilon(\omega)\}$) of W calculated with DFT and derived from REELS data. The last two columns contain values for the volume and surface single-scattering loss distributions the DIIMFP (w_b) and the DSEP (w_s)—Continued

W									
DFT				REELS					
E (eV)	ε_1	ε_2	ELF	E (eV)	ε_1	ε_2	ELF	w_b (meV^{-1})	w_s (arb. un.)
22.0	−0.249	0.624	1.382	22.0	−0.166	0.529	1.721	24.4	46.2
22.5	−0.256	0.586	1.433	22.5	−0.059	0.547	1.807	27.5	39.5
23.0	−0.203	0.522	1.664	23.0	−0.165	0.582	1.590	28.9	35.3
23.5	−0.120	0.394	2.322	23.5	−0.100	0.422	2.244	29.9	31.7
24.0	−0.039	0.335	2.944	24.0	−0.009	0.368	2.715	32.8	23.7
24.5	0.121	0.254	3.204	24.5	0.066	0.335	2.871	37.1	11.1
25.0	0.249	0.280	1.997	25.0	0.131	0.310	2.734	39.7	0.7
25.5	0.321	0.309	1.554	25.5	0.191	0.290	2.406	39.2	−1.7
26.0	0.374	0.306	1.310	26.0	0.247	0.272	2.016	36.4	2.4
26.5	0.438	0.288	1.049	26.5	0.299	0.257	1.651	33.0	5.6
27.0	0.523	0.260	0.761	27.0	0.349	0.244	1.345	31.2	1.6
27.5	0.645	0.316	0.612	27.5	0.397	0.234	1.102	29.0	−0.7
28.0	0.654	0.359	0.646	28.0	0.442	0.224	0.913	25.7	2.9
28.5	0.688	0.374	0.610	28.5	0.486	0.217	0.766	22.8	5.1
29.0	0.710	0.379	0.585	29.0	0.529	0.211	0.651	20.4	5.3
29.5	0.772	0.366	0.501	29.5	0.570	0.206	0.561	18.4	5.3
30.0	0.851	0.408	0.458	30.0	0.610	0.203	0.490	16.8	5.1
30.5	0.835	0.606	0.569	30.5	0.650	0.201	0.434	14.5	5.9
31.0	0.763	0.431	0.561	31.0	0.690	0.201	0.388	12.5	6.9
31.5	0.827	0.428	0.494	31.5	0.730	0.202	0.352	12.0	6.2
32.0	0.851	0.391	0.446	32.0	0.770	0.205	0.322	12.3	5.0
32.5	0.950	0.402	0.378	32.5	0.811	0.210	0.299	11.6	5.6
33.0	0.874	0.379	0.418	33.0	0.853	0.217	0.281	10.3	6.5
33.5	1.008	0.289	0.262	33.5	0.896	0.229	0.267	9.7	6.8
34.0	1.161	0.266	0.187	34.0	0.942	0.244	0.258	9.2	6.9
34.5	1.362	0.262	0.136	34.5	0.991	0.265	0.252	8.9	5.2
35.0	1.688	0.336	0.113	35.0	1.042	0.295	0.252	8.9	3.2
35.5	2.033	0.810	0.169	35.5	1.097	0.338	0.256	8.4	3.9
36.0	1.819	1.374	0.264	36.0	1.153	0.399	0.268	7.5	5.2
36.5	1.496	1.661	0.332	36.5	1.204	0.488	0.289	7.3	4.4
37.0	1.216	1.728	0.387	37.0	1.233	0.614	0.324	7.7	3.6
37.5	0.903	1.703	0.458	37.5	1.207	0.779	0.378	8.1	4.9
38.0	0.882	1.800	0.448	38.0	1.078	0.941	0.460	8.4	5.9
38.5	0.267	2.138	0.461	38.5	0.857	1.000	0.577	8.7	5.9
39.0	0.008	1.804	0.554	39.0	0.662	0.913	0.718	8.5	6.8
39.5	−0.420	1.028	0.833	39.5	0.583	0.764	0.827	9.0	5.5
40.0	−0.127	0.747	1.302	40.0	0.603	0.648	0.827	10.7	2.2
40.5	0.033	0.650	1.533	40.5	0.672	0.620	0.741	11.4	3.3
41.0	0.114	0.587	1.643	41.0	0.618	0.720	0.800	11.1	6.3
41.5	0.191	0.465	1.841	41.5	0.486	0.556	1.019	11.1	6.1
42.0	0.333	0.438	1.447	42.0	0.560	0.439	0.867	11.8	4.2
42.5	0.392	0.414	1.275	42.5	0.632	0.401	0.715	12.9	2.1
43.0	0.483	0.389	1.012	43.0	0.689	0.391	0.624	13.0	1.7
43.5	0.582	0.384	0.790	43.5	0.733	0.396	0.570	11.5	3.9
44.0	0.710	0.415	0.614	44.0	0.768	0.409	0.540	10.2	5.2
44.5	0.797	0.602	0.604	44.5	0.795	0.430	0.526	10.3	3.6
45.0	0.770	0.634	0.637	45.0	0.813	0.456	0.524	10.9	1.3
45.5	0.788	0.770	0.635	45.5	0.822	0.486	0.533	10.9	1.1
46.0	0.715	0.872	0.685	46.0	0.821	0.519	0.550	10.3	1.3
46.5	0.512	0.955	0.813	46.5	0.809	0.552	0.575	9.9	0.0
47.0	0.502	0.942	0.826	47.0	0.786	0.581	0.608	9.6	−0.4
47.5	0.082	1.209	0.824	47.5	0.753	0.604	0.648	9.6	0.8

TABLE 22. Values of the real (ε_1) and imaginary (ε_2) parts of the complex dielectric constant and the ELF ($\mathrm{Im}\{-1/\varepsilon(\omega)\}$) of W calculated with DFT and derived from REELS data. The last two columns contain values for the volume and surface single-scattering loss distributions the DIIMFP (w_b) and the DSEP (w_s)—Continued

W									
DFT				REELS					
E (eV)	ε_1	ε_2	ELF	E (eV)	ε_1	ε_2	ELF	w_b (meV^{-1})	w_s (arb. un.)
48.0	0.011	0.643	1.555	48.0	0.712	0.616	0.695	9.5	2.1
48.5	0.124	0.516	1.831	48.5	0.667	0.617	0.748	9.4	2.2
49.0	0.186	0.459	1.869	49.0	0.622	0.605	0.804	9.7	1.1
49.5	0.225	0.412	1.869	49.5	0.582	0.582	0.859	10.9	−1.0
50.0	0.262	0.369	1.802	50.0	0.549	0.550	0.911	11.8	–
50.5	0.274	0.348	1.772	50.5	0.525	0.514	0.952	11.6	–
51.0	0.320	0.300	1.560	51.0	0.510	0.475	0.978	11.4	–
51.5	0.360	0.286	1.354	51.5	0.502	0.437	0.986	11.7	–
52.0	0.381	0.282	1.253	52.0	0.501	0.401	0.974	12.5	–
52.5	0.405	0.267	1.136	52.5	0.505	0.369	0.943	13.0	–
53.0	0.403	0.259	1.130	53.0	0.512	0.339	0.899	12.6	–
53.5	0.457	0.235	0.888	53.5	0.522	0.313	0.845	12.3	–
54.0	0.490	0.243	0.812	54.0	0.533	0.290	0.787	12.4	–
54.5	0.493	0.261	0.837	54.5	0.545	0.270	0.729	12.1	–
55.0	0.498	0.270	0.842	55.0	0.558	0.252	0.673	11.4	–
55.5	0.481	0.263	0.874	55.5	0.571	0.237	0.620	11.0	–
56.0	0.489	0.265	0.856	56.0	0.584	0.224	0.573	10.9	–
56.5	0.483	0.248	0.842	56.5	0.596	0.212	0.530	11.3	–
57.0	0.476	0.223	0.806	57.0	0.608	0.202	0.492	11.5	–
57.5	0.489	0.206	0.730	57.5	0.620	0.193	0.458	10.7	–
58.0	0.500	0.191	0.668	58.0	0.631	0.185	0.429	9.9	–
58.5	0.509	0.184	0.628	58.5	0.642	0.179	0.402	9.5	–
59.0	0.520	0.168	0.561	59.0	0.652	0.173	0.379	9.5	–
59.5	0.535	0.158	0.508	59.5	0.662	0.167	0.359	9.6	–
60.0	0.546	0.151	0.472	60.0	0.671	0.163	0.341	9.4	–
60.5	0.561	0.153	0.452	60.5	0.680	0.159	0.325	8.4	–
61.0	0.560	0.150	0.446	61.0	0.688	0.155	0.311	7.7	–
61.5	0.571	0.132	0.386	61.5	0.696	0.152	0.299	7.7	–
62.0	0.586	0.127	0.354	62.0	0.703	0.149	0.288	7.2	–
62.5	0.597	0.129	0.347	62.5	0.711	0.146	0.278	7.0	–
63.0	0.604	0.123	0.324	63.0	0.717	0.144	0.269	7.9	–
63.5	0.610	0.126	0.326	63.5	0.724	0.142	0.260	7.8	–
64.0	0.614	0.118	0.301	64.0	0.730	0.140	0.253	6.3	–
64.5	0.632	0.128	0.308	64.5	0.736	0.138	0.246	6.0	–
65.0	0.618	0.144	0.357	65.0	0.741	0.137	0.240	7.0	–
65.5	0.604	0.115	0.303	65.5	0.746	0.135	0.235	7.0	–
66.0	0.617	0.090	0.231	66.0	0.751	0.134	0.230	6.4	–
66.5	0.640	0.083	0.199	66.5	0.756	0.133	0.225	6.7	–
67.0	0.650	0.087	0.203	67.0	0.760	0.132	0.221	6.9	–
67.5	0.656	0.082	0.189	67.5	0.764	0.131	0.217	6.5	–
68.0	0.668	0.081	0.179	68.0	0.768	0.130	0.214	5.7	–
68.5	0.674	0.083	0.179	68.5	0.772	0.129	0.210	4.6	–
69.0	0.676	0.081	0.174	69.0	0.776	0.128	0.207	4.7	–
69.5	0.683	0.076	0.161	69.5	0.779	0.127	0.204	5.5	–
70.0	0.693	0.072	0.149	70.0	0.782	0.126	0.201	4.9	–
70.5	0.703	0.076	0.152	70.5	0.785	0.125	0.198	4.2	–

TABLE 23. Values of the real (ε_1) and imaginary (ε_2) parts of the complex dielectric constant and the ELF ($\mathrm{Im}\{-1/\varepsilon(\omega)\}$) of Pt calculated with DFT and derived from REELS data. The last two columns contain values for the volume and surface single-scattering loss distributions the DIIMFP (w_b) and the DSEP (w_s)

Pt									
DFT				REELS					
E (eV)	ε_1	ε_2	ELF	E (eV)	ε_1	ε_2	ELF	w_b (meV^{-1})	w_s (arb. un.)
0.50	−123.344	72.533	0.004	0.50	−635.547	216.023	0.000	0.0	0.4
0.75	−32.952	101.354	0.009	0.75	−294.704	68.276	0.001	0.0	0.6
1.00	−44.891	81.698	0.009	1.00	−165.622	29.962	0.001	−0.1	0.8
1.25	−40.081	57.069	0.012	1.25	−103.964	16.097	0.001	−0.1	1.0
1.50	−33.179	40.443	0.015	1.50	−69.907	10.023	0.002	−0.1	1.3
1.75	−26.710	29.831	0.019	1.75	−49.132	7.046	0.003	−0.1	1.3
2.00	−21.394	23.502	0.023	2.00	−35.496	5.511	0.004	−0.2	1.9
2.25	−17.271	18.644	0.029	2.25	−26.009	4.755	0.007	−0.3	4.2
2.50	−13.732	15.691	0.036	2.50	−19.067	4.506	0.012	−0.5	9.9
2.75	−11.458	13.892	0.043	2.75	−13.748	4.718	0.022	−0.4	20.3
3.00	−9.901	11.956	0.050	3.00	−9.570	5.574	0.045	0.4	32.0
3.25	−8.355	10.503	0.058	3.25	−6.797	7.492	0.073	1.6	39.7
3.50	−7.181	9.459	0.067	3.50	−7.017	9.412	0.068	2.3	42.6
3.75	−6.385	8.469	0.075	3.75	−7.938	8.097	0.063	2.3	42.8
4.00	−5.611	7.295	0.086	4.00	−6.730	6.530	0.074	2.3	42.8
4.25	−4.607	6.473	0.103	4.25	−5.354	6.182	0.092	2.5	43.8
4.50	−3.868	5.880	0.119	4.50	−4.825	6.126	0.101	3.0	46.3
4.75	−3.223	5.274	0.138	4.75	−4.448	5.495	0.110	3.7	50.4
5.0	−2.493	4.740	0.165	5.0	−3.694	4.904	0.130	4.3	56.2
5.5	−1.352	4.070	0.221	5.5	−2.255	4.480	0.178	4.9	69.7
6.0	−0.141	3.883	0.257	6.0	−1.320	4.444	0.207	5.7	74.6
6.5	0.686	3.817	0.254	6.5	−0.756	4.487	0.217	6.9	67.6
7.0	1.560	4.288	0.206	7.0	−0.433	4.519	0.219	6.8	61.5
7.5	1.086	4.800	0.198	7.5	−0.261	4.511	0.221	6.0	61.2
8.0	1.316	4.863	0.192	8.0	−0.168	4.462	0.224	5.9	61.5
8.5	0.686	5.058	0.194	8.5	−0.077	4.425	0.226	6.4	58.7
9.0	0.775	4.839	0.201	9.0	−0.353	4.617	0.215	6.3	55.9
9.5	−0.128	5.073	0.197	9.5	−0.442	4.178	0.237	5.8	56.0
10.0	−0.506	4.098	0.240	10.0	−0.583	3.845	0.254	5.9	56.5
10.5	−0.289	3.496	0.284	10.5	−0.505	3.558	0.276	6.6	54.3
11.0	−0.071	3.088	0.324	11.0	−0.445	3.330	0.295	7.4	50.8
11.5	0.132	3.176	0.314	11.5	−0.382	3.122	0.316	8.2	48.1
12.0	0.126	2.571	0.388	12.0	−0.309	2.933	0.337	9.2	45.4
12.5	0.508	2.513	0.382	12.5	−0.227	2.766	0.359	9.5	44.1
13.0	0.649	2.448	0.382	13.0	−0.136	2.622	0.380	8.8	44.7
13.5	0.830	2.479	0.363	13.5	−0.039	2.503	0.399	8.5	44.4
14.0	0.860	2.539	0.353	14.0	0.062	2.412	0.414	9.1	42.5
14.5	0.830	2.523	0.358	14.5	0.162	2.352	0.423	9.8	39.4
15.0	0.830	2.479	0.363	15.0	0.257	2.327	0.425	10.1	36.7
15.5	0.799	2.313	0.386	15.5	0.337	2.339	0.419	10.3	35.3
16.0	0.964	2.160	0.386	16.0	0.387	2.391	0.408	10.2	35.2
16.5	1.196	2.130	0.357	16.5	0.387	2.476	0.394	9.8	34.8
17.0	1.456	2.187	0.317	17.0	0.313	2.573	0.383	9.5	33.5
17.5	1.805	2.402	0.266	17.5	0.156	2.639	0.378	9.5	32.3
18.0	1.928	3.003	0.236	18.0	−0.061	2.623	0.381	9.6	30.9
18.5	1.358	3.406	0.253	18.5	−0.279	2.503	0.395	9.5	29.3
19.0	1.423	3.868	0.228	19.0	−0.439	2.301	0.419	9.4	29.5
19.5	0.385	4.657	0.213	19.5	−0.520	2.069	0.455	9.3	31.3
20.0	−0.684	3.630	0.266	20.0	−0.533	1.846	0.500	9.6	32.1
20.5	−0.553	3.095	0.313	20.5	−0.500	1.652	0.554	10.4	30.6
21.0	−0.500	2.768	0.350	21.0	−0.442	1.490	0.617	11.4	28.5
21.5	−0.715	2.752	0.340	21.5	−0.372	1.358	0.685	12.0	28.6

TABLE 23. Values of the real (ε_1) and imaginary (ε_2) parts of the complex dielectric constant and the ELF ($\mathrm{Im}\{-1/\varepsilon(\omega)\}$) of Pt calculated with DFT and derived from REELS data. The last two columns contain values for the volume and surface single-scattering loss distributions the DIIMFP (w_b) and the DSEP (w_s)—Continued

Pt									
DFT				REELS					
E (eV)	ε_1	ε_2	ELF	E (eV)	ε_1	ε_2	ELF	w_b (meV^{-1})	w_s (arb. un.)
22.0	−0.983	2.315	0.366	22.0	−0.298	1.250	0.757	12.3	30.2
22.5	−0.890	1.867	0.436	22.5	−0.223	1.161	0.831	13.1	29.1
23.0	−0.733	1.628	0.511	23.0	−0.150	1.089	0.901	14.3	25.7
23.5	−0.651	1.430	0.579	23.5	−0.080	1.030	0.965	15.3	23.9
24.0	−0.384	1.163	0.775	24.0	−0.013	0.983	1.017	15.9	23.6
24.5	−0.139	1.145	0.861	24.5	0.051	0.947	1.053	16.9	21.7
25.0	0.023	1.251	0.799	25.0	0.111	0.921	1.070	17.9	18.3
25.5	−0.039	1.301	0.768	25.5	0.167	0.907	1.066	18.4	15.8
26.0	0.023	1.277	0.783	26.0	0.216	0.905	1.045	18.2	15.4
26.5	−0.051	1.269	0.787	26.5	0.254	0.917	1.013	18.2	16.1
27.0	−0.025	1.088	0.918	27.0	0.271	0.940	0.982	18.4	15.6
27.5	0.128	0.986	0.997	27.5	0.258	0.963	0.969	18.2	14.0
28.0	0.426	1.114	0.783	28.0	0.218	0.965	0.986	18.2	11.5
28.5	0.386	1.383	0.671	28.5	0.170	0.930	1.040	18.8	8.7
29.0	0.131	1.628	0.611	29.0	0.140	0.867	1.125	19.0	8.0
29.5	−0.204	1.513	0.649	29.5	0.137	0.794	1.222	18.1	10.5
30.0	−0.372	1.211	0.755	30.0	0.155	0.728	1.313	18.1	10.3
30.5	−0.341	0.979	0.911	30.5	0.184	0.673	1.382	20.0	4.8
31.0	−0.305	0.809	1.082	31.0	0.217	0.629	1.421	21.4	1.2
31.5	−0.194	0.673	1.373	31.5	0.251	0.593	1.430	20.6	3.1
32.0	−0.084	0.563	1.737	32.0	0.284	0.564	1.415	20.2	3.9
32.5	0.078	0.537	1.825	32.5	0.315	0.539	1.382	21.3	0.6
33.0	0.147	0.552	1.693	33.0	0.345	0.519	1.336	22.3	−3.4
33.5	0.184	0.573	1.582	33.5	0.374	0.501	1.283	21.9	−4.1
34.0	0.196	0.517	1.691	34.0	0.400	0.486	1.226	20.5	−1.1
34.5	0.283	0.511	1.497	34.5	0.425	0.473	1.169	19.3	2.2
35.0	0.324	0.550	1.350	35.0	0.449	0.462	1.112	19.0	1.5
35.5	0.324	0.533	1.370	35.5	0.472	0.453	1.059	19.3	−2.2
36.0	0.371	0.511	1.281	36.0	0.492	0.446	1.011	19.7	−4.7
36.5	0.401	0.545	1.191	36.5	0.511	0.440	0.968	19.2	−4.2
37.0	0.375	0.577	1.219	37.0	0.528	0.436	0.931	17.9	−1.6
37.5	0.372	0.515	1.276	37.5	0.542	0.432	0.900	17.0	0.0
38.0	0.405	0.507	1.203	38.0	0.553	0.428	0.876	16.8	−2.0
38.5	0.409	0.499	1.199	38.5	0.562	0.423	0.855	16.0	−2.4
39.0	0.419	0.484	1.182	39.0	0.569	0.415	0.836	15.0	0.5
39.5	0.442	0.469	1.129	39.5	0.577	0.405	0.815	15.1	0.1
40.0	0.480	0.439	1.037	40.0	0.587	0.394	0.789	15.5	−2.9
40.5	0.479	0.471	1.043	40.5	0.598	0.382	0.760	15.0	−3.2
41.0	0.480	0.447	1.039	41.0	0.610	0.371	0.728	14.4	−1.9
41.5	0.497	0.426	0.994	41.5	0.624	0.361	0.695	13.7	−0.3
42.0	0.523	0.399	0.923	42.0	0.639	0.352	0.662	12.9	1.6
42.5	0.567	0.395	0.827	42.5	0.654	0.344	0.630	12.6	1.9
43.0	0.609	0.439	0.778	43.0	0.670	0.338	0.601	12.7	0.5
43.5	0.555	0.441	0.878	43.5	0.685	0.332	0.573	12.6	−0.4
44.0	0.579	0.415	0.818	44.0	0.701	0.328	0.547	12.1	0.3
44.5	0.610	0.439	0.777	44.5	0.718	0.324	0.523	11.8	1.1
45.0	0.554	0.444	0.881	45.0	0.734	0.322	0.500	11.4	0.9
45.5	0.558	0.376	0.830	45.5	0.752	0.320	0.479	10.8	1.1
46.0	0.612	0.333	0.686	46.0	0.771	0.320	0.459	10.3	2.0
46.5	0.677	0.348	0.600	46.5	0.791	0.321	0.441	10.1	2.3
47.0	0.701	0.346	0.567	47.0	0.813	0.324	0.423	10.2	1.1
47.5	0.764	0.339	0.485	47.5	0.840	0.329	0.405	10.2	0.2

TABLE 23. Values of the real (ε_1) and imaginary (ε_2) parts of the complex dielectric constant and the ELF ($\mathrm{Im}\{-1/\varepsilon(\omega)\}$) of Pt calculated with DFT and derived from REELS data. The last two columns contain values for the volume and surface single-scattering loss distributions the DIIMFP (w_b) and the DSEP (w_s)—Continued

Pt									
DFT				REELS					
E (eV)	ε_1	ε_2	ELF	E (eV)	ε_1	ε_2	ELF	w_b (meV^{-1})	w_s (arb. un.)
48.0	0.903	0.329	0.356	48.0	0.874	0.339	0.386	9.5	1.3
48.5	1.276	0.656	0.318	48.5	0.923	0.360	0.366	8.8	1.6
49.0	0.477	1.148	0.743	49.0	1.015	0.423	0.349	8.9	–0.4
49.5	0.326	0.631	1.251	49.5	1.052	0.828	0.462	8.8	–0.9
50.0	0.420	0.510	1.168	50.0	0.569	0.543	0.877	8.0	–
50.5	0.465	0.474	1.076	50.5	0.692	0.431	0.648	7.8	–
51.0	0.487	0.457	1.024	51.0	0.748	0.430	0.577	8.3	–
51.5	0.491	0.431	1.010	51.5	0.772	0.449	0.563	8.6	–
52.0	0.498	0.412	0.987	52.0	0.776	0.476	0.575	8.7	–
52.5	0.508	0.376	0.942	52.5	0.762	0.502	0.603	8.9	–
53.0	0.526	0.356	0.883	53.0	0.733	0.521	0.644	9.3	–
53.5	0.561	0.342	0.793	53.5	0.694	0.525	0.693	9.3	–
54.0	0.605	0.350	0.717	54.0	0.655	0.513	0.741	8.9	–
54.5	0.571	0.439	0.847	54.5	0.623	0.487	0.779	9.0	–
55.0	0.537	0.362	0.863	55.0	0.603	0.455	0.797	9.6	–
55.5	0.566	0.355	0.796	55.5	0.594	0.421	0.795	10.3	–
56.0	0.555	0.349	0.812	56.0	0.593	0.390	0.775	10.5	–
56.5	0.554	0.351	0.816	56.5	0.597	0.363	0.743	9.9	–
57.0	0.534	0.319	0.824	57.0	0.605	0.341	0.706	9.6	–
57.5	0.553	0.304	0.762	57.5	0.615	0.322	0.669	10.4	–
58.0	0.558	0.286	0.728	58.0	0.625	0.307	0.634	10.9	–
58.5	0.571	0.277	0.687	58.5	0.635	0.295	0.601	10.0	–
59.0	0.580	0.267	0.655	59.0	0.645	0.284	0.573	9.0	–
59.5	0.588	0.264	0.635	59.5	0.654	0.276	0.547	9.5	–
60.0	0.600	0.237	0.571	60.0	0.663	0.269	0.525	10.5	–
60.5	0.631	0.224	0.499	60.5	0.671	0.262	0.506	10.2	–
61.0	0.674	0.223	0.442	61.0	0.678	0.257	0.489	9.1	–
61.5	0.799	0.265	0.373	61.5	0.685	0.252	0.473	8.4	–
62.0	0.572	0.455	0.852	62.0	0.691	0.248	0.460	8.3	–
62.5	0.543	0.290	0.765	62.5	0.697	0.245	0.448	8.4	–
63.0	0.576	0.265	0.660	63.0	0.703	0.241	0.437	8.7	–
63.5	0.583	0.264	0.646	63.5	0.707	0.238	0.428	8.6	–
64.0	0.581	0.246	0.618	64.0	0.712	0.236	0.419	7.8	–
64.5	0.589	0.227	0.570	64.5	0.716	0.233	0.411	7.6	–
65.0	0.603	0.220	0.534	65.0	0.720	0.231	0.404	8.0	–
65.5	0.637	0.226	0.494	65.5	0.723	0.228	0.397	8.1	–
66.0	0.571	0.228	0.604	66.0	0.726	0.226	0.390	7.4	–
66.5	0.592	0.178	0.466	66.5	0.729	0.224	0.385	6.7	–
67.0	0.635	0.166	0.385	67.0	0.732	0.222	0.379	7.2	–
67.5	0.625	0.207	0.477	67.5	0.734	0.220	0.374	7.6	–
68.0	0.631	0.178	0.413	68.0	0.737	0.217	0.368	7.2	–
68.5	0.643	0.177	0.398	68.5	0.739	0.215	0.364	6.8	–
69.0	0.669	0.199	0.409	69.0	0.741	0.213	0.359	6.5	–
69.5	0.618	0.194	0.463	69.5	0.742	0.211	0.354	6.5	–
70.0	0.624	0.168	0.403	70.0	0.744	0.209	0.349	6.9	–
70.5	0.634	0.155	0.363	70.5	0.746	0.206	0.345	6.3	–

TABLE 24. Values of the real (ε_1) and imaginary (ε_2) parts of the complex dielectric constant and the ELF ($\mathrm{Im}\{-1/\varepsilon(\omega)\}$) of Au calculated with DFT and derived from REELS data. The last two columns contain values for the volume and surface single-scattering loss distributions the DIIMFP (w_b) and the DSEP (w_s)

Au									
DFT				REELS					
E (eV)	ε_1	ε_2	ELF	E (eV)	ε_1	ε_2	ELF	w_b (meV^{-1})	w_s (arb. un.)
0.50	−289.567	59.936	0.001	0.50	−404.801	127.357	0.001	0.0	0.7
0.75	−126.211	18.250	0.001	0.75	−184.411	40.136	0.001	−0.1	1.0
1.00	−67.156	7.925	0.002	1.00	−101.906	17.819	0.002	−0.1	1.3
1.25	−39.078	4.353	0.003	1.25	−62.665	9.848	0.002	−0.1	1.7
1.50	−23.319	3.240	0.006	1.50	−41.020	6.436	0.004	−0.1	2.0
1.75	−13.471	3.246	0.017	1.75	−27.810	4.844	0.006	−0.2	2.2
2.00	−6.685	4.448	0.069	2.00	−19.125	4.117	0.011	−0.2	3.7
2.25	−3.447	6.621	0.119	2.25	−13.069	3.878	0.021	−0.3	9.4
2.50	−2.222	7.642	0.121	2.50	−8.644	3.982	0.044	0.5	23.3
2.75	−1.594	7.866	0.122	2.75	−5.295	4.395	0.093	3.6	47.0
3.00	−0.992	7.826	0.126	3.00	−2.745	5.158	0.151	7.8	70.0
3.25	−0.804	7.923	0.125	3.25	−0.957	6.339	0.154	8.9	79.1
3.50	−0.873	7.627	0.129	3.50	−0.164	7.883	0.127	7.2	74.3
3.75	−0.860	7.164	0.138	3.75	−0.693	9.258	0.107	5.1	64.3
4.00	−0.875	6.684	0.147	4.00	−2.154	9.472	0.100	3.7	56.8
4.25	−0.788	5.930	0.166	4.25	−3.269	8.378	0.104	3.3	54.4
4.50	−0.353	5.329	0.187	4.50	−3.440	6.919	0.116	3.4	56.3
4.75	0.150	4.966	0.201	4.75	−2.997	5.754	0.137	4.1	61.6
5.0	0.608	4.916	0.200	5.0	−2.340	4.989	0.164	5.0	68.3
5.5	0.829	4.688	0.207	5.5	−1.087	4.311	0.218	6.7	78.4
6.0	1.382	4.384	0.207	6.0	−0.233	4.272	0.233	7.0	79.5
6.5	1.892	5.251	0.169	6.5	0.118	4.495	0.222	6.2	75.4
7.0	0.873	5.129	0.189	7.0	0.001	4.630	0.216	6.0	69.4
7.5	0.862	5.182	0.188	7.5	−0.297	4.429	0.225	6.6	64.1
8.0	0.075	4.448	0.225	8.0	−0.447	3.991	0.247	6.8	62.8
8.5	0.197	4.113	0.243	8.5	−0.400	3.552	0.278	6.7	63.6
9.0	−0.027	3.736	0.268	9.0	−0.257	3.219	0.309	7.5	61.0
9.5	−0.045	3.166	0.316	9.5	−0.100	2.988	0.334	8.7	54.8
10.0	0.218	2.715	0.366	10.0	0.033	2.828	0.354	9.3	49.8
10.5	0.586	2.532	0.375	10.5	0.132	2.711	0.368	9.4	48.5
11.0	0.710	2.411	0.382	11.0	0.198	2.615	0.380	9.8	46.2
11.5	1.026	2.460	0.346	11.5	0.238	2.526	0.392	10.4	41.6
12.0	0.868	2.629	0.343	12.0	0.260	2.437	0.406	10.2	39.5
12.5	0.976	2.418	0.356	12.5	0.273	2.344	0.421	9.7	38.7
13.0	0.936	2.663	0.334	13.0	0.284	2.246	0.438	10.2	36.0
13.5	0.719	2.480	0.372	13.5	0.297	2.145	0.457	11.0	32.5
14.0	0.710	2.302	0.397	14.0	0.318	2.045	0.478	11.2	30.7
14.5	0.749	2.157	0.414	14.5	0.347	1.947	0.498	11.3	29.6
15.0	0.822	2.050	0.420	15.0	0.385	1.856	0.517	11.8	28.3
15.5	0.918	2.002	0.413	15.5	0.435	1.774	0.532	12.2	26.0
16.0	0.957	2.013	0.405	16.0	0.494	1.705	0.541	12.9	22.6
16.5	0.979	1.915	0.414	16.5	0.563	1.654	0.542	12.6	21.8
17.0	1.123	1.856	0.394	17.0	0.642	1.626	0.532	11.7	23.1
17.5	1.265	1.878	0.366	17.5	0.726	1.633	0.511	11.7	21.6
18.0	1.549	1.981	0.313	18.0	0.806	1.687	0.483	12.2	19.0
18.5	1.333	2.627	0.303	18.5	0.854	1.807	0.452	12.2	17.9
19.0	1.224	2.851	0.296	19.0	0.808	1.994	0.431	11.6	18.0
19.5	0.924	3.245	0.285	19.5	0.588	2.164	0.430	11.0	19.1
20.0	0.410	2.595	0.376	20.0	0.240	2.144	0.461	10.9	20.1
20.5	0.206	2.691	0.369	20.5	−0.020	1.904	0.525	11.2	20.1
21.0	−0.246	2.502	0.396	21.0	−0.098	1.614	0.617	11.4	19.7
21.5	−0.328	2.084	0.468	21.5	−0.064	1.381	0.723	11.9	18.7

TABLE 24. Values of the real (ε_1) and imaginary (ε_2) parts of the complex dielectric constant and the ELF ($\mathrm{Im}\{-1/\varepsilon(\omega)\}$) of Au calculated with DFT and derived from REELS data. The last two columns contain values for the volume and surface single-scattering loss distributions the DIIMFP (w_b) and the DSEP (w_s)—Continued

Au									
DFT				REELS					
E (eV)	ε_1	ε_2	ELF	E (eV)	ε_1	ε_2	ELF	w_b (meV^{-1})	w_s (arb. un.)
22.0	−0.293	1.690	0.574	22.0	0.012	1.214	0.823	13.4	16.7
22.5	−0.164	1.513	0.653	22.5	0.097	1.097	0.905	14.8	15.9
23.0	−0.069	1.333	0.748	23.0	0.179	1.013	0.957	15.0	17.9
23.5	0.052	1.111	0.898	23.5	0.256	0.951	0.980	15.0	19.0
24.0	0.291	1.093	0.854	24.0	0.327	0.906	0.976	15.9	15.0
24.5	0.373	1.152	0.786	24.5	0.394	0.874	0.951	17.2	10.0
25.0	0.396	1.105	0.802	25.0	0.455	0.854	0.912	17.5	9.5
25.5	0.485	1.084	0.769	25.5	0.514	0.844	0.865	17.1	10.5
26.0	0.522	1.161	0.717	26.0	0.567	0.847	0.815	16.6	9.8
26.5	0.590	1.032	0.730	26.5	0.614	0.864	0.769	15.9	9.2
27.0	0.783	1.113	0.601	27.0	0.650	0.897	0.731	15.7	8.8
27.5	0.895	1.384	0.509	27.5	0.665	0.945	0.708	15.8	8.3
28.0	0.590	1.614	0.547	28.0	0.645	1.001	0.706	15.4	7.7
28.5	0.363	1.543	0.614	28.5	0.583	1.039	0.732	14.7	7.7
29.0	0.331	1.436	0.661	29.0	0.497	1.032	0.786	14.5	8.4
29.5	0.189	1.446	0.680	29.5	0.426	0.976	0.861	15.0	7.2
30.0	0.015	1.265	0.791	30.0	0.390	0.896	0.938	15.3	6.0
30.5	−0.022	1.014	0.985	30.5	0.389	0.818	0.997	15.2	5.5
31.0	0.115	0.865	1.136	31.0	0.407	0.755	1.026	15.8	4.5
31.5	0.212	0.819	1.144	31.5	0.434	0.706	1.028	16.2	4.6
32.0	0.279	0.792	1.123	32.0	0.463	0.670	1.010	16.0	5.5
32.5	0.357	0.763	1.075	32.5	0.492	0.643	0.981	16.2	4.2
33.0	0.404	0.828	0.976	33.0	0.518	0.622	0.949	16.6	2.1
33.5	0.329	0.800	1.069	33.5	0.542	0.607	0.916	16.5	1.5
34.0	0.407	0.739	1.038	34.0	0.564	0.596	0.886	16.2	1.5
34.5	0.427	0.759	1.001	34.5	0.582	0.588	0.859	15.9	0.7
35.0	0.454	0.753	0.974	35.0	0.597	0.582	0.837	15.3	0.8
35.5	0.428	0.792	0.977	35.5	0.609	0.577	0.819	14.9	1.9
36.0	0.430	0.762	0.996	36.0	0.619	0.573	0.805	15.0	1.4
36.5	0.396	0.769	1.028	36.5	0.627	0.569	0.794	14.9	−0.1
37.0	0.381	0.740	1.068	37.0	0.632	0.565	0.787	14.7	−1.1
37.5	0.340	0.708	1.148	37.5	0.635	0.560	0.781	14.6	−1.0
38.0	0.384	0.607	1.176	38.0	0.637	0.554	0.778	14.2	−1.2
38.5	0.434	0.626	1.078	38.5	0.638	0.547	0.775	13.8	−1.5
39.0	0.422	0.597	1.116	39.0	0.638	0.539	0.773	13.4	−0.5
39.5	0.444	0.581	1.087	39.5	0.638	0.530	0.770	12.9	0.8
40.0	0.469	0.563	1.049	40.0	0.639	0.519	0.766	13.2	−0.8
40.5	0.522	0.557	0.955	40.5	0.640	0.508	0.760	13.6	−3.2
41.0	0.502	0.610	0.977	41.0	0.643	0.497	0.753	13.3	−3.8
41.5	0.482	0.618	1.006	41.5	0.645	0.485	0.744	12.8	−2.6
42.0	0.465	0.585	1.047	42.0	0.649	0.474	0.734	12.5	−0.9
42.5	0.460	0.609	1.046	42.5	0.653	0.463	0.723	12.5	−0.8
43.0	0.413	0.560	1.158	43.0	0.658	0.453	0.710	12.3	−1.6
43.5	0.441	0.523	1.118	43.5	0.663	0.443	0.697	12.2	−2.4
44.0	0.440	0.542	1.113	44.0	0.668	0.433	0.683	12.5	−3.2
44.5	0.421	0.492	1.174	44.5	0.674	0.424	0.669	12.5	−3.2
45.0	0.414	0.470	1.199	45.0	0.680	0.416	0.655	11.9	−1.9
45.5	0.408	0.429	1.224	45.5	0.686	0.408	0.641	11.4	−0.7
46.0	0.442	0.386	1.121	46.0	0.691	0.401	0.628	11.4	−0.4
46.5	0.470	0.379	1.040	46.5	0.697	0.395	0.615	11.3	−1.1
47.0	0.475	0.352	1.008	47.0	0.702	0.389	0.603	11.2	−1.9
47.5	0.486	0.349	0.976	47.5	0.708	0.383	0.592	11.0	−2.0

TABLE 24. Values of the real (ε_1) and imaginary (ε_2) parts of the complex dielectric constant and the ELF ($\mathrm{Im}\{-1/\varepsilon(\omega)\}$) of Au calculated with DFT and derived from REELS data. The last two columns contain values for the volume and surface single-scattering loss distributions the DIIMFP (w_b) and the DSEP (w_s)—Continued

Au									
DFT				REELS					
E (eV)	ε_1	ε_2	ELF	E (eV)	ε_1	ε_2	ELF	w_b (meV^{-1})	w_s (arb. un.)
48.0	0.488	0.305	0.921	48.0	0.713	0.378	0.581	11.0	−1.8
48.5	0.547	0.282	0.744	48.5	0.718	0.373	0.571	11.1	−2.1
49.0	0.576	0.294	0.703	49.0	0.722	0.369	0.561	10.7	−2.1
49.5	0.602	0.298	0.661	49.5	0.726	0.365	0.552	10.3	−1.9
50.0	0.608	0.299	0.652	50.0	0.730	0.361	0.544	10.2	–
50.5	0.632	0.287	0.595	50.5	0.734	0.357	0.536	10.0	–
51.0	0.651	0.313	0.600	51.0	0.738	0.354	0.528	9.9	–
51.5	0.662	0.305	0.574	51.5	0.741	0.351	0.522	9.8	–
52.0	0.700	0.319	0.539	52.0	0.744	0.347	0.515	9.4	–
52.5	0.756	0.347	0.501	52.5	0.747	0.344	0.509	9.1	–
53.0	0.700	0.435	0.640	53.0	0.749	0.342	0.504	9.5	–
53.5	0.637	0.446	0.738	53.5	0.752	0.339	0.498	9.8	–
54.0	0.600	0.422	0.784	54.0	0.754	0.336	0.493	9.0	–
54.5	0.597	0.390	0.768	54.5	0.756	0.333	0.489	8.0	–
55.0	0.612	0.371	0.725	55.0	0.757	0.331	0.484	8.2	–
55.5	0.640	0.441	0.729	55.5	0.759	0.328	0.480	9.2	–
56.0	0.511	0.404	0.953	56.0	0.760	0.325	0.476	9.1	–
56.5	0.500	0.328	0.919	56.5	0.761	0.323	0.472	8.3	–
57.0	0.543	0.290	0.765	57.0	0.762	0.320	0.468	8.3	–
57.5	0.557	0.296	0.745	57.5	0.763	0.318	0.465	8.4	–
58.0	0.548	0.290	0.753	58.0	0.764	0.315	0.461	8.0	–
58.5	0.540	0.262	0.727	58.5	0.765	0.312	0.458	7.9	–
59.0	0.556	0.238	0.649	59.0	0.765	0.310	0.454	8.2	–
59.5	0.576	0.228	0.595	59.5	0.766	0.307	0.451	8.5	–
60.0	0.575	0.229	0.598	60.0	0.766	0.304	0.448	8.6	–
60.5	0.576	0.211	0.561	60.5	0.766	0.301	0.444	8.2	–
61.0	0.589	0.196	0.508	61.0	0.766	0.298	0.441	7.7	–
61.5	0.599	0.187	0.474	61.5	0.766	0.295	0.437	7.8	–
62.0	0.613	0.177	0.435	62.0	0.766	0.292	0.434	8.2	–
62.5	0.622	0.177	0.423	62.5	0.767	0.289	0.431	8.3	–
63.0	0.624	0.165	0.397	63.0	0.767	0.286	0.427	7.9	–
63.5	0.636	0.155	0.361	63.5	0.767	0.282	0.423	7.4	–
64.0	0.652	0.148	0.331	64.0	0.767	0.279	0.420	7.6	–
64.5	0.670	0.151	0.320	64.5	0.767	0.276	0.416	8.0	–
65.0	0.674	0.154	0.323	65.0	0.767	0.273	0.412	7.7	–
65.5	0.682	0.157	0.320	65.5	0.767	0.269	0.408	7.2	–
66.0	0.686	0.158	0.318	66.0	0.767	0.266	0.404	7.5	–
66.5	0.695	0.159	0.313	66.5	0.767	0.262	0.399	7.6	–
67.0	0.705	0.180	0.341	67.0	0.767	0.259	0.395	7.1	–
67.5	0.681	0.180	0.363	67.5	0.767	0.255	0.391	7.1	–
68.0	0.674	0.165	0.343	68.0	0.767	0.252	0.386	7.4	–
68.5	0.676	0.152	0.317	68.5	0.767	0.248	0.382	7.2	–
69.0	0.692	0.136	0.274	69.0	0.767	0.244	0.377	6.5	–
69.5	0.717	0.148	0.275	69.5	0.768	0.241	0.372	6.3	–
70.0	0.690	0.186	0.365	70.0	0.768	0.237	0.367	6.8	–
70.5	0.667	0.158	0.337	70.5	0.768	0.234	0.362	6.9	–

TABLE 25. Values of the real (ε_1) and imaginary (ε_2) parts of the complex dielectric constant and the ELF ($\mathrm{Im}\{-1/\varepsilon(\omega)\}$) of Pb calculated with DFT and derived from REELS data. The last two columns contain values for the volume and surface single-scattering loss distributions the DIIMFP (w_b) and the DSEP (w_s)

Pb									
DFT				REELS					
E (eV)	ε_1	ε_2	ELF	E (eV)	ε_1	ε_2	ELF	w_b (meV^{-1})	w_s (arb. un.)
0.50	−296.591	63.202	0.001	0.50	−415.274	308.901	0.001	0.1	0.3
0.75	−124.313	20.144	0.001	0.75	−227.300	113.945	0.002	0.2	0.5
1.00	−60.575	12.326	0.003	1.00	−137.764	52.871	0.002	0.2	0.6
1.25	−32.451	11.877	0.010	1.25	−90.129	28.889	0.003	0.3	0.8
1.50	−17.019	12.106	0.028	1.50	−61.967	18.467	0.004	0.4	1.0
1.75	−5.973	16.910	0.053	1.75	−44.707	15.392	0.007	0.3	0.9
2.00	−6.995	23.855	0.039	2.00	−38.383	13.143	0.008	0.1	2.2
2.25	−9.950	21.094	0.039	2.25	−31.461	7.515	0.007	−0.2	6.4
2.50	−8.887	20.849	0.041	2.50	−24.905	4.858	0.008	−1.0	16.6
2.75	−13.705	21.232	0.033	2.75	−20.026	3.493	0.008	−2.3	34.8
3.00	−15.826	13.909	0.031	3.00	−16.357	2.668	0.010	−3.0	52.6
3.25	−13.482	9.569	0.035	3.25	−13.523	2.125	0.011	−1.9	59.0
3.50	−10.804	7.496	0.043	3.50	−11.284	1.749	0.013	0.3	54.7
3.75	−9.180	7.491	0.053	3.75	−9.479	1.484	0.016	2.3	47.4
4.00	−9.354	6.516	0.050	4.00	−8.001	1.293	0.020	3.4	43.0
4.25	−8.770	5.055	0.049	4.25	−6.774	1.158	0.025	3.5	43.1
4.50	−7.919	3.889	0.050	4.50	−5.742	1.063	0.031	3.2	46.8
4.75	−7.022	2.997	0.051	4.75	−4.865	1.001	0.041	2.8	52.7
5.0	−6.157	2.323	0.054	5.0	−4.113	0.966	0.054	2.5	59.5
5.5	−4.614	1.439	0.062	5.5	−2.898	0.961	0.103	3.6	72.8
6.0	−3.316	0.983	0.082	6.0	−1.972	1.034	0.208	7.4	84.5
6.5	−2.261	0.809	0.140	6.5	−1.273	1.179	0.392	12.8	96.4
7.0	−1.418	0.909	0.320	7.0	−0.777	1.391	0.548	18.2	103.8
7.5	−1.028	1.259	0.477	7.5	−0.495	1.641	0.559	22.6	98.7
8.0	−0.942	1.294	0.505	8.0	−0.435	1.856	0.511	24.3	92.2
8.5	−0.816	1.188	0.572	8.5	−0.549	1.931	0.479	25.2	92.1
9.0	−0.645	1.185	0.651	9.0	−0.704	1.813	0.479	27.2	96.6
9.5	−0.649	1.060	0.686	9.5	−0.779	1.562	0.513	30.0	98.6
10.0	−0.542	0.909	0.812	10.0	−0.740	1.277	0.586	32.9	93.9
10.5	−0.428	0.772	0.990	10.5	−0.622	1.024	0.713	32.9	94.0
11.0	−0.298	0.649	1.272	11.0	−0.463	0.824	0.922	30.3	99.3
11.5	−0.164	0.549	1.672	11.5	−0.292	0.672	1.251	33.2	88.0
12.0	−0.031	0.468	2.128	12.0	−0.124	0.559	1.704	45.7	56.2
12.5	0.097	0.408	2.317	12.5	0.036	0.476	2.089	61.6	18.8
13.0	0.211	0.364	2.058	13.0	0.185	0.415	2.009	66.7	4.6
13.5	0.323	0.328	1.548	13.5	0.325	0.371	1.524	59.0	15.6
14.0	0.416	0.306	1.148	14.0	0.457	0.341	1.049	48.3	24.6
14.5	0.505	0.271	0.825	14.5	0.583	0.322	0.727	38.3	28.8
15.0	0.617	0.232	0.535	15.0	0.704	0.314	0.528	29.9	31.9
15.5	0.754	0.219	0.355	15.5	0.825	0.317	0.406	25.2	28.3
16.0	0.955	0.314	0.311	16.0	0.947	0.334	0.331	22.7	22.2
16.5	0.907	0.460	0.445	16.5	1.075	0.368	0.285	19.7	19.1
17.0	0.888	0.475	0.468	17.0	1.211	0.428	0.260	16.1	20.9
17.5	0.896	0.470	0.459	17.5	1.357	0.534	0.251	14.0	26.2
18.0	0.946	0.478	0.426	18.0	1.503	0.718	0.259	15.7	26.7
18.5	0.984	0.560	0.437	18.5	1.594	1.039	0.287	19.5	20.6
19.0	0.896	0.616	0.521	19.0	1.448	1.504	0.345	21.0	19.1
19.5	0.851	0.592	0.551	19.5	0.870	1.782	0.453	19.7	23.4
20.0	0.833	0.570	0.560	20.0	0.317	1.489	0.642	18.5	23.4
20.5	0.817	0.547	0.565	20.5	0.190	1.050	0.922	18.9	19.7
21.0	0.796	0.527	0.579	21.0	0.277	0.765	1.155	20.8	17.8
21.5	0.781	0.465	0.563	21.5	0.404	0.616	1.134	24.3	11.6

TABLE 25. Values of the real (ε_1) and imaginary (ε_2) parts of the complex dielectric constant and the ELF ($\mathrm{Im}\{-1/\varepsilon(\omega)\}$) of Pb calculated with DFT and derived from REELS data. The last two columns contain values for the volume and surface single-scattering loss distributions the DIIMFP (w_b) and the DSEP (w_s)—Continued

Pb									
DFT				REELS					
E (eV)	ε_1	ε_2	ELF	E (eV)	ε_1	ε_2	ELF	w_b (meV^{-1})	w_s (arb. un.)
22.0	0.803	0.422	0.513	22.0	0.520	0.548	0.961	26.0	4.7
22.5	0.827	0.377	0.456	22.5	0.609	0.528	0.812	23.4	8.8
23.0	0.873	0.355	0.400	23.0	0.669	0.536	0.730	20.7	14.4
23.5	0.905	0.346	0.369	23.5	0.695	0.555	0.702	21.3	12.1
24.0	0.954	0.336	0.328	24.0	0.690	0.567	0.711	22.6	7.1
24.5	0.999	0.390	0.339	24.5	0.669	0.556	0.735	20.9	6.7
25.0	0.951	0.412	0.384	25.0	0.651	0.521	0.750	17.7	9.6
25.5	0.906	0.373	0.389	25.5	0.648	0.473	0.735	17.7	5.9
26.0	0.958	0.274	0.275	26.0	0.662	0.424	0.685	20.4	−1.8
26.5	1.062	0.284	0.235	26.5	0.689	0.381	0.614	19.8	0.5
27.0	1.083	0.373	0.284	27.0	0.724	0.348	0.540	16.1	10.0
27.5	1.050	0.379	0.304	27.5	0.760	0.324	0.475	14.5	10.8
28.0	1.051	0.363	0.294	28.0	0.798	0.309	0.422	15.4	5.2
28.5	1.069	0.324	0.260	28.5	0.833	0.300	0.383	15.9	3.9
29.0	1.135	0.333	0.238	29.0	0.867	0.297	0.354	15.2	5.2
29.5	1.157	0.389	0.261	29.5	0.898	0.298	0.333	13.2	8.8
30.0	1.160	0.403	0.267	30.0	0.926	0.304	0.320	11.5	12.3
30.5	1.189	0.431	0.269	30.5	0.952	0.313	0.312	11.7	10.4
31.0	1.180	0.484	0.297	31.0	0.974	0.325	0.309	12.7	5.3
31.5	1.165	0.499	0.311	31.5	0.992	0.340	0.309	12.2	3.8
32.0	1.161	0.527	0.324	32.0	1.006	0.357	0.313	10.7	5.4
32.5	1.146	0.546	0.338	32.5	1.016	0.376	0.320	10.9	6.1
33.0	1.133	0.573	0.356	33.0	1.021	0.395	0.330	12.2	6.9
33.5	1.112	0.597	0.375	33.5	1.021	0.414	0.341	11.7	8.8
34.0	1.063	0.613	0.407	34.0	1.016	0.431	0.353	10.1	7.9
34.5	1.067	0.571	0.390	34.5	1.008	0.445	0.367	10.0	4.4
35.0	1.086	0.634	0.401	35.0	0.996	0.456	0.380	11.7	0.7
35.5	0.989	0.675	0.471	35.5	0.982	0.462	0.392	12.1	2.3
36.0	0.937	0.584	0.479	36.0	0.968	0.464	0.403	9.7	8.8
36.5	0.978	0.592	0.453	36.5	0.955	0.461	0.410	8.7	8.6
37.0	0.923	0.549	0.476	37.0	0.944	0.455	0.414	10.9	2.1
37.5	0.996	0.532	0.417	37.5	0.936	0.447	0.415	13.1	−2.1
38.0	0.983	0.589	0.449	38.0	0.932	0.437	0.413	12.6	−2.2
38.5	0.952	0.575	0.465	38.5	0.931	0.428	0.408	10.7	−0.6
39.0	0.966	0.591	0.461	39.0	0.933	0.420	0.401	9.5	2.4
39.5	0.906	0.593	0.506	39.5	0.937	0.414	0.395	11.0	0.7
40.0	0.935	0.559	0.471	40.0	0.942	0.411	0.389	13.5	−6.1
40.5	0.952	0.568	0.462	40.5	0.949	0.410	0.384	12.7	−4.6
41.0	1.053	0.691	0.436	41.0	0.955	0.413	0.381	10.5	0.9
41.5	0.850	0.669	0.572	41.5	0.960	0.418	0.381	10.2	0.3
42.0	0.756	0.725	0.661	42.0	0.963	0.426	0.385	10.5	0.0
42.5	0.704	0.562	0.693	42.5	0.963	0.436	0.391	10.4	1.3
43.0	0.778	0.522	0.594	43.0	0.959	0.448	0.400	10.6	−0.2
43.5	0.816	0.551	0.568	43.5	0.951	0.459	0.412	10.9	−2.0
44.0	0.748	0.518	0.626	44.0	0.939	0.469	0.426	11.2	−2.6
44.5	0.762	0.558	0.625	44.5	0.923	0.476	0.441	10.9	−1.8
45.0	0.772	0.490	0.586	45.0	0.905	0.479	0.457	10.5	−1.1
45.5	0.876	0.625	0.540	45.5	0.886	0.477	0.471	11.8	−4.7
46.0	0.611	0.695	0.812	46.0	0.867	0.470	0.483	12.8	−5.7
46.5	0.432	0.520	1.137	46.5	0.851	0.459	0.491	11.6	−1.6
47.0	0.576	0.315	0.731	47.0	0.839	0.446	0.494	10.4	1.7
47.5	0.701	0.338	0.559	47.5	0.830	0.431	0.493	11.5	−1.5

TABLE 25. Values of the real (ε_1) and imaginary (ε_2) parts of the complex dielectric constant and the ELF ($\mathrm{Im}\{-1/\varepsilon(\omega)\}$) of Pb calculated with DFT and derived from REELS data. The last two columns contain values for the volume and surface single-scattering loss distributions the DIIMFP (w_b) and the DSEP (w_s)—Continued

Pb									
DFT				REELS					
E (eV)	ε_1	ε_2	ELF	E (eV)	ε_1	ε_2	ELF	w_b (meV^{-1})	w_s (arb. un.)
48.0	0.732	0.424	0.592	48.0	0.824	0.416	0.488	13.3	−8.8
48.5	0.600	0.462	0.806	48.5	0.822	0.401	0.480	12.9	−7.8
49.0	0.486	0.358	0.983	49.0	0.822	0.388	0.469	10.5	2.5
49.5	0.599	0.205	0.510	49.5	0.825	0.377	0.458	9.9	4.7
50.0	0.687	0.217	0.419	50.0	0.828	0.368	0.448	11.9	–
50.5	0.715	0.228	0.404	50.5	0.833	0.360	0.438	13.6	–
51.0	0.755	0.255	0.402	51.0	0.837	0.355	0.429	12.6	–
51.5	0.722	0.280	0.467	51.5	0.841	0.351	0.422	10.3	–
52.0	0.740	0.244	0.401	52.0	0.845	0.349	0.417	9.7	–
52.5	0.776	0.246	0.372	52.5	0.849	0.348	0.414	11.6	–
53.0	0.796	0.271	0.383	53.0	0.851	0.348	0.412	13.0	–
53.5	0.820	0.313	0.406	53.5	0.853	0.350	0.412	11.3	–
54.0	0.759	0.399	0.543	54.0	0.853	0.352	0.413	9.6	–
54.5	0.652	0.326	0.613	54.5	0.852	0.354	0.416	10.7	–
55.0	0.682	0.262	0.490	55.0	0.850	0.356	0.420	11.3	–
55.5	0.708	0.276	0.478	55.5	0.847	0.359	0.425	10.5	–
56.0	0.696	0.257	0.467	56.0	0.842	0.362	0.430	10.4	–
56.5	0.704	0.268	0.473	56.5	0.837	0.364	0.437	11.2	–
57.0	0.639	0.248	0.527	57.0	0.830	0.365	0.444	11.2	–
57.5	0.669	0.193	0.399	57.5	0.823	0.366	0.451	10.8	–
58.0	0.699	0.196	0.373	58.0	0.814	0.365	0.458	11.4	–
58.5	0.683	0.186	0.373	58.5	0.806	0.364	0.466	11.2	–
59.0	0.693	0.165	0.326	59.0	0.797	0.362	0.473	10.0	–
59.5	0.718	0.158	0.293	59.5	0.787	0.358	0.479	10.0	–
60.0	0.721	0.159	0.292	60.0	0.778	0.354	0.484	11.3	–
60.5	0.721	0.168	0.306	60.5	0.769	0.348	0.488	12.0	–
61.0	0.708	0.145	0.277	61.0	0.760	0.341	0.491	12.2	–
61.5	0.723	0.128	0.237	61.5	0.752	0.333	0.493	11.8	–
62.0	0.739	0.120	0.215	62.0	0.745	0.325	0.492	10.7	–
62.5	0.749	0.117	0.203	62.5	0.738	0.316	0.490	10.2	–
63.0	0.761	0.123	0.207	63.0	0.732	0.306	0.487	11.3	–
63.5	0.759	0.122	0.207	63.5	0.727	0.296	0.481	12.4	–
64.0	0.764	0.122	0.203	64.0	0.722	0.286	0.474	10.9	–
64.5	0.752	0.120	0.206	64.5	0.719	0.275	0.464	9.6	–
65.0	0.765	0.093	0.157	65.0	0.716	0.264	0.454	10.9	–
65.5	0.788	0.094	0.148	65.5	0.714	0.254	0.442	12.9	–
66.0	0.803	0.110	0.168	66.0	0.713	0.243	0.429	12.4	–
66.5	0.801	0.123	0.188	66.5	0.712	0.233	0.415	10.8	–
67.0	0.777	0.135	0.217	67.0	0.713	0.223	0.400	10.0	–
67.5	0.777	0.110	0.179	67.5	0.713	0.213	0.385	9.3	–
68.0	0.780	0.105	0.169	68.0	0.714	0.204	0.370	9.5	–
68.5	0.790	0.105	0.165	68.5	0.716	0.195	0.354	10.2	–
69.0	0.784	0.109	0.174	69.0	0.718	0.186	0.339	9.5	–
69.5	0.778	0.104	0.169	69.5	0.720	0.178	0.323	9.0	–
70.0	0.780	0.089	0.145	70.0	0.723	0.170	0.309	10.1	–
70.5	0.780	0.084	0.137	70.5	0.726	0.163	0.294	11.4	–

TABLE 26. Values of the real (ε_1) and imaginary (ε_2) parts of the complex dielectric constant and the ELF ($\mathrm{Im}\{-1/\varepsilon(\omega)\}$) of Bi calculated with DFT and derived from REELS data. The last two columns contain values for the volume and surface single-scattering loss distributions the DIIMFP (w_b) and the DSEP (w_s)

Bi									
DFT				REELS					
E (eV)	ε_1	ε_2	ELF	E (eV)	ε_1	ε_2	ELF	w_b (meV^{-1})	w_s (arb. un.)
0.50	−178.373	36.667	0.001	0.50	−416.687	73.052	0.000	0.0	0.4
0.75	−78.799	11.133	0.002	0.75	−185.820	22.209	0.001	0.0	0.7
1.00	−42.858	4.797	0.003	1.00	−103.181	9.673	0.001	0.0	0.9
1.25	−25.888	2.546	0.004	1.25	−64.569	5.253	0.001	0.0	1.1
1.50	−16.419	1.589	0.006	1.50	−43.467	3.374	0.002	0.0	1.3
1.75	−10.360	1.200	0.011	1.75	−30.669	2.507	0.003	0.0	1.5
2.00	−5.745	1.340	0.039	2.00	−22.307	2.126	0.004	0.0	2.3
2.25	−1.787	3.737	0.218	2.25	−16.528	2.025	0.007	0.0	5.2
2.50	−4.159	5.981	0.113	2.50	−12.362	2.125	0.014	0.2	11.7
2.75	−3.687	4.322	0.134	2.75	−9.282	2.401	0.026	1.2	22.6
3.00	−3.447	4.687	0.138	3.00	−7.013	2.851	0.050	2.7	34.3
3.25	−3.770	3.356	0.132	3.25	−5.452	3.442	0.083	4.1	42.4
3.50	−3.191	2.453	0.151	3.50	−4.584	4.040	0.108	4.7	46.6
3.75	−2.519	1.870	0.190	3.75	−4.306	4.372	0.116	4.6	48.5
4.00	−1.834	1.423	0.264	4.00	−4.270	4.250	0.117	4.5	50.5
4.25	−1.117	1.181	0.447	4.25	−4.120	3.815	0.121	4.7	53.7
4.50	−0.279	1.120	0.841	4.50	−3.772	3.340	0.132	5.3	58.1
4.75	0.784	1.733	0.479	4.75	−3.324	2.971	0.149	6.4	63.8
5.0	0.003	3.492	0.286	5.0	−2.875	2.731	0.174	7.7	70.0
5.5	−1.268	1.975	0.359	5.5	−2.165	2.514	0.228	9.8	82.2
6.0	−0.822	1.206	0.566	6.0	−1.758	2.421	0.270	10.4	90.3
6.5	−0.332	0.807	1.060	6.5	−1.555	2.279	0.299	11.3	91.8
7.0	0.168	0.654	1.434	7.0	−1.414	2.049	0.331	13.1	93.7
7.5	0.690	0.646	0.723	7.5	−1.247	1.785	0.376	14.9	100.8
8.0	1.340	1.215	0.371	8.0	−1.046	1.548	0.444	17.1	106.1
8.5	0.715	1.983	0.446	8.5	−0.834	1.367	0.533	20.1	104.9
9.0	−0.326	1.988	0.490	9.0	−0.637	1.244	0.637	22.7	102.0
9.5	0.120	0.753	1.296	9.5	−0.476	1.167	0.735	24.5	101.1
10.0	1.349	1.637	0.364	10.0	−0.359	1.116	0.812	26.5	99.0
10.5	−0.972	0.961	0.515	10.5	−0.284	1.070	0.873	29.6	90.6
11.0	−0.213	0.526	1.634	11.0	−0.240	1.012	0.935	32.6	80.1
11.5	0.040	0.499	1.990	11.5	−0.210	0.935	1.018	34.6	73.2
12.0	0.099	0.434	2.193	12.0	−0.177	0.842	1.138	36.6	67.6
12.5	0.200	0.355	2.139	12.5	−0.132	0.742	1.306	40.1	57.2
13.0	0.291	0.310	1.717	13.0	−0.076	0.645	1.528	44.2	45.7
13.5	0.346	0.277	1.410	13.5	−0.010	0.558	1.791	47.4	39.4
14.0	0.415	0.224	1.008	14.0	0.060	0.482	2.041	50.5	32.3
14.5	0.490	0.198	0.708	14.5	0.132	0.418	2.173	53.6	21.4
15.0	0.536	0.210	0.634	15.0	0.202	0.365	2.094	54.0	14.8
15.5	0.562	0.184	0.525	15.5	0.270	0.321	1.824	51.0	14.2
16.0	0.598	0.157	0.411	16.0	0.334	0.285	1.478	46.6	14.2
16.5	0.631	0.144	0.344	16.5	0.394	0.255	1.157	40.8	15.8
17.0	0.663	0.124	0.274	17.0	0.450	0.230	0.899	34.3	18.4
17.5	0.696	0.101	0.205	17.5	0.503	0.209	0.705	29.5	18.2
18.0	0.736	0.093	0.169	18.0	0.552	0.192	0.561	26.1	15.8
18.5	0.768	0.082	0.138	18.5	0.599	0.178	0.455	22.5	15.2
19.0	0.799	0.075	0.116	19.0	0.642	0.166	0.376	18.7	15.8
19.5	0.833	0.076	0.109	19.5	0.684	0.156	0.317	15.7	14.6
20.0	0.853	0.075	0.102	20.0	0.724	0.148	0.271	13.4	14.6
20.5	0.876	0.066	0.085	20.5	0.762	0.142	0.235	11.5	15.9
21.0	0.911	0.056	0.068	21.0	0.801	0.137	0.208	10.6	13.1
21.5	0.952	0.053	0.059	21.5	0.840	0.134	0.186	9.5	9.7

TABLE 26. Values of the real (ε_1) and imaginary (ε_2) parts of the complex dielectric constant and the ELF ($\mathrm{Im}\{-1/\varepsilon(\omega)\}$) of Bi calculated with DFT and derived from REELS data. The last two columns contain values for the volume and surface single-scattering loss distributions the DIIMFP (w_b) and the DSEP (w_s)—Continued

Bi									
DFT				REELS					
E (eV)	ε_1	ε_2	ELF	E (eV)	ε_1	ε_2	ELF	w_b (meV^{-1})	w_s (arb. un.)
22.0	1.003	0.053	0.052	22.0	0.881	0.134	0.169	8.0	11.2
22.5	1.110	0.071	0.058	22.5	0.927	0.138	0.157	7.4	10.8
23.0	1.123	0.329	0.240	23.0	0.987	0.153	0.153	7.5	6.3
23.5	0.902	0.364	0.385	23.5	1.075	0.208	0.173	7.5	4.9
24.0	0.862	0.193	0.247	24.0	1.089	0.487	0.342	8.3	7.9
24.5	0.922	0.187	0.211	24.5	0.745	0.316	0.482	9.7	10.2
25.0	0.892	0.207	0.247	25.0	0.850	0.188	0.248	10.4	9.4
25.5	0.894	0.166	0.200	25.5	0.926	0.173	0.194	9.6	9.0
26.0	0.913	0.159	0.185	26.0	0.984	0.188	0.187	8.4	8.7
26.5	0.906	0.142	0.169	26.5	1.029	0.230	0.207	8.2	7.0
27.0	0.916	0.129	0.151	27.0	1.037	0.307	0.262	8.2	7.5
27.5	0.921	0.121	0.141	27.5	0.958	0.369	0.350	8.3	9.7
28.0	0.932	0.101	0.114	28.0	0.867	0.319	0.374	8.6	9.0
28.5	0.934	0.095	0.108	28.5	0.860	0.240	0.301	9.0	4.6
29.0	0.954	0.053	0.058	29.0	0.889	0.193	0.234	8.9	2.3
29.5	1.002	0.052	0.052	29.5	0.922	0.170	0.193	7.8	4.7
30.0	1.029	0.071	0.067	30.0	0.952	0.159	0.171	7.2	5.7
30.5	1.043	0.082	0.075	30.5	0.979	0.155	0.158	7.3	3.5
31.0	1.059	0.097	0.086	31.0	1.002	0.154	0.150	6.8	4.0
31.5	1.069	0.116	0.100	31.5	1.023	0.157	0.146	5.9	6.8
32.0	1.068	0.129	0.112	32.0	1.042	0.161	0.145	5.6	7.3
32.5	1.073	0.145	0.124	32.5	1.060	0.167	0.145	5.7	6.3
33.0	1.051	0.147	0.131	33.0	1.076	0.175	0.147	5.7	5.7
33.5	1.055	0.141	0.124	33.5	1.091	0.184	0.151	4.9	7.5
34.0	1.068	0.144	0.124	34.0	1.104	0.195	0.155	4.4	9.5
34.5	1.067	0.145	0.125	34.5	1.117	0.208	0.161	5.4	6.6
35.0	1.076	0.145	0.123	35.0	1.127	0.222	0.168	6.5	3.1
35.5	1.093	0.152	0.125	35.5	1.136	0.238	0.176	6.0	4.4
36.0	1.104	0.166	0.133	36.0	1.143	0.255	0.186	4.9	6.9
36.5	1.104	0.177	0.142	36.5	1.147	0.274	0.197	5.0	5.8
37.0	1.117	0.196	0.153	37.0	1.147	0.294	0.210	6.3	1.5
37.5	1.108	0.216	0.169	37.5	1.143	0.314	0.224	6.9	0.6
38.0	1.109	0.230	0.180	38.0	1.136	0.334	0.239	5.8	5.0
38.5	1.087	0.254	0.203	38.5	1.124	0.353	0.254	5.2	5.9
39.0	1.082	0.242	0.197	39.0	1.107	0.368	0.270	5.7	3.2
39.5	1.082	0.251	0.204	39.5	1.088	0.379	0.285	5.4	4.4
40.0	1.087	0.267	0.213	40.0	1.067	0.385	0.299	5.1	5.8
40.5	1.065	0.279	0.230	40.5	1.046	0.385	0.310	6.2	2.1
41.0	1.053	0.287	0.241	41.0	1.027	0.381	0.317	7.4	−1.7
41.5	1.052	0.306	0.255	41.5	1.011	0.373	0.321	7.3	−0.9
42.0	1.016	0.306	0.272	42.0	0.998	0.362	0.321	6.4	2.0
42.5	1.005	0.295	0.269	42.5	0.989	0.351	0.318	6.4	1.4
43.0	1.003	0.280	0.258	43.0	0.984	0.339	0.313	7.1	−1.0
43.5	1.015	0.295	0.264	43.5	0.981	0.328	0.306	6.9	−0.3
44.0	0.992	0.299	0.279	44.0	0.981	0.319	0.299	6.3	1.4
44.5	0.993	0.294	0.274	44.5	0.983	0.311	0.293	6.9	0.2
45.0	0.999	0.315	0.287	45.0	0.985	0.305	0.286	7.7	−2.3
45.5	0.970	0.349	0.329	45.5	0.988	0.300	0.281	7.3	−1.6
46.0	0.948	0.338	0.334	46.0	0.992	0.297	0.277	6.1	1.7
46.5	0.916	0.351	0.364	46.5	0.996	0.296	0.274	5.8	3.5
47.0	0.876	0.336	0.382	47.0	0.999	0.296	0.273	6.3	2.8
47.5	0.825	0.302	0.391	47.5	1.001	0.297	0.272	6.2	2.1

TABLE 26. Values of the real (ε_1) and imaginary (ε_2) parts of the complex dielectric constant and the ELF ($\mathrm{Im}\{-1/\varepsilon(\omega)\}$) of Bi calculated with DFT and derived from REELS data. The last two columns contain values for the volume and surface single-scattering loss distributions the DIIMFP (w_b) and the DSEP (w_s)—Continued

Bi									
DFT				REELS					
E (eV)	ε_1	ε_2	ELF	E (eV)	ε_1	ε_2	ELF	w_b (meV^{-1})	w_s (arb. un.)
48.0	0.845	0.248	0.319	48.0	1.004	0.299	0.273	6.3	0.9
48.5	0.870	0.243	0.298	48.5	1.005	0.302	0.274	6.9	–0.6
49.0	0.859	0.227	0.287	49.0	1.005	0.306	0.277	6.7	1.0
49.5	0.882	0.228	0.275	49.5	1.005	0.310	0.280	6.1	2.9
50.0	0.872	0.223	0.276	50.0	1.003	0.314	0.285	6.4	–
50.5	0.888	0.230	0.273	50.5	1.001	0.319	0.289	6.9	–
51.0	0.865	0.234	0.292	51.0	0.997	0.324	0.295	7.0	–
51.5	0.863	0.256	0.315	51.5	0.992	0.328	0.300	7.3	–
52.0	0.815	0.216	0.304	52.0	0.987	0.332	0.307	7.3	–
52.5	0.837	0.191	0.259	52.5	0.980	0.336	0.313	7.0	–
53.0	0.838	0.186	0.253	53.0	0.973	0.339	0.319	7.0	–
53.5	0.840	0.176	0.239	53.5	0.965	0.341	0.326	7.0	–
54.0	0.845	0.164	0.221	54.0	0.956	0.342	0.332	6.7	–
54.5	0.845	0.171	0.230	54.5	0.947	0.342	0.337	6.8	–
55.0	0.843	0.157	0.214	55.0	0.938	0.342	0.343	7.3	–
55.5	0.846	0.153	0.207	55.5	0.929	0.340	0.347	7.1	–
56.0	0.840	0.136	0.188	56.0	0.920	0.337	0.351	6.4	–
56.5	0.862	0.136	0.179	56.5	0.911	0.333	0.355	6.3	–
57.0	0.875	0.133	0.170	57.0	0.902	0.329	0.357	6.4	–
57.5	0.856	0.170	0.223	57.5	0.894	0.324	0.358	6.7	–
58.0	0.838	0.129	0.179	58.0	0.887	0.317	0.358	7.1	–
58.5	0.855	0.123	0.165	58.5	0.880	0.311	0.357	6.9	–
59.0	0.850	0.129	0.175	59.0	0.874	0.304	0.355	6.8	–
59.5	0.849	0.115	0.157	59.5	0.869	0.297	0.352	6.7	–
60.0	0.856	0.113	0.151	60.0	0.864	0.289	0.348	6.5	–
60.5	0.852	0.115	0.155	60.5	0.860	0.281	0.343	7.0	–
61.0	0.856	0.101	0.136	61.0	0.857	0.274	0.338	7.6	–
61.5	0.864	0.105	0.138	61.5	0.854	0.266	0.332	7.0	–
62.0	0.859	0.105	0.140	62.0	0.853	0.258	0.326	6.0	–
62.5	0.853	0.102	0.138	62.5	0.851	0.251	0.319	6.2	–
63.0	0.847	0.090	0.124	63.0	0.850	0.244	0.312	7.5	–
63.5	0.857	0.084	0.113	63.5	0.850	0.237	0.305	7.7	–
64.0	0.862	0.084	0.112	64.0	0.850	0.231	0.297	6.8	–
64.5	0.860	0.083	0.112	64.5	0.850	0.224	0.290	6.2	–
65.0	0.857	0.073	0.099	65.0	0.851	0.218	0.283	6.4	–
65.5	0.862	0.069	0.093	65.5	0.851	0.213	0.276	6.8	–
66.0	0.865	0.065	0.087	66.0	0.852	0.208	0.270	6.8	–
66.5	0.867	0.059	0.079	66.5	0.854	0.203	0.263	6.4	–
67.0	0.875	0.055	0.072	67.0	0.855	0.198	0.257	6.3	–
67.5	0.880	0.057	0.073	67.5	0.856	0.194	0.251	6.5	–
68.0	0.881	0.058	0.074	68.0	0.858	0.189	0.245	6.0	–
68.5	0.883	0.058	0.074	68.5	0.859	0.186	0.240	5.7	–
69.0	0.883	0.058	0.074	69.0	0.861	0.182	0.235	6.3	–
69.5	0.881	0.055	0.071	69.5	0.862	0.179	0.230	6.4	–
70.0	0.883	0.052	0.066	70.0	0.864	0.176	0.226	5.6	–
70.5	0.885	0.050	0.063	70.5	0.865	0.173	0.222	5.2	–

10. Appendix C: Values of Optical Constants Derived from DFT and REELS

This appendix contains values of optical constants calculated by means of DFT and derived from REELS data as given in Tables 11–26.

11. References

[1] E. D. Palik, *Handbook of Optical Constants of Solids I* (Academic, New York, 1985); *Handbook of Optical Constants of Solids II* (Academic, New York, 1991).
[2] B. L. Henke, E. M. Gullikson, and J. C. Davis, At. Data Nucl. Data Tables **54**, 181 (1993).
[3] C. T. Chantler, J. Phys. Chem. Ref. Data **24**, 71 (1995).
[4] C. T. Chantler, J. Phys. Chem. Ref. Data **29**, 597 (2000).
[5] R. F. Egerton, *Electron Energy Loss Spectroscopy in the Electron Microscope* (Plenum, New York, 1985).
[6] W. S. M. Werner and P. Schattschneider, J. Electron Spectrosc. Relat. Phenom. **143**, 65 (2005).
[7] D. Y. Smith, in *Handbook of Optical Constants of Solids I* (Academic, New York, 1985), Vol. 1, Chap. 3; *Handbook of Optical Constants of Solids II* (Academic, New York, 1991), Vol. 1, Chap. 3.
[8] W. S. M. Werner, Phys. Rev. B **74**, 075421 (2006).
[9] W. S. M. Werner, Surf. Sci. **600**, L250 (2006).
[10] A. Jablonski, F. Salvat, and C. J. Powell, J. Phys. Chem. Ref. Data **33**, 409 (2004).
[11] L. D. Landau, E. M. Lifshitz, and L. P. Pitaevski, *Electrodynamics of Continuous Media*, 2nd ed. (Pergamom, Oxford, New York, 1984), translated by J. B. Sykes, J. S. Bell, and M. J. Kearsley.
[12] R. H. Ritchie, Phys. Rev. **106**, 874 (1957).
[13] H. Starke, Ann. Phys. **302**, 49 (1898).
[14] A. A. Campbell-Swinton, Proc. R. Soc. London **64**, 377 (1899).
[15] J. J. Rehr and R. C. Albers, Rev. Mod. Phys. **72**, 621 (2000).
[16] G. Onida, L. Reining, and A. Rubio, Rev. Mod. Phys. **74**, 601 (2002).
[17] C. Ambrosch-Draxl and J. O. Sofo, Comput. Phys. Commun. **175**, 1 (2006).
[18] W. Olovsson, I. Tanaka, T. Mizoguchi, P. Puschnig, and C. Ambrosch-Draxl, Phys. Rev. B **79**, 041101(R) (2009).
[19] W. Kohn, Rev. Mod. Phys. **71**, 1253 (1999).
[20] P. Blaha, K. Schwarz, G. K. H. Madsen, D. Kvasnicka, and J. Luitz, WIEN2K, an augmented plane wave and local orbitals program for calculating crystal properties, Karlheinz Schwarz, Techn. Universität Wien, (TU Vienna, 2001).
[21] O. K. Andersen, Phys. Rev. B **12**, 3060 (1975).
[22] D. J. Singh, *Planewaves, Pseudopotentials and the LAPW Method* (Kluwer Academic, Boston, 1994).
[23] C. Ambrosch-Draxl, Phys. Scr., T **T109**, 48 (2004).
[24] J. P. Perdew, K. Burke, and M. Ernzerhof, Phys. Rev. Lett. **77**, 3865 (1996).
[25] A. H. MacDonald, W. E. Pickett, and D. D. Koelling, J. Phys. C **13**, 2675 (1980).
[26] P. E. Böchl, O. Jepsen, and O. K. Andersen, Phys. Rev. B **49**, 16223 (1994).
[27] P. B. Johnson and R. W. Christy, Phys. Rev. B **6**, 4370 (1972).
[28] S. Hummel, A. Gross, and W. S. M. Werner, Surf. Interface Anal. **41**, 357 (2009).
[29] M. R. Went and M. Vos, Phys. Rev. B **74**, 205407 (2006).
[30] F. Salvat and R. Mayol, Comput. Phys. Commun. **74**, 358 (1993).
[31] W. S. M. Werner, Surf. Interface Anal. **31**, 141 (2001).
[32] C. J. Tung, Y. F. Chen, C. M. Kwei, and T. L. Chou, Phys. Rev. B **49**, 16684 (1994).
[33] W. Smekal, W. S. M. Werner, C. S. Fadley, and M. A. van Hove, J. Electron Spectrosc. Relat. Phenom. **137**, 183 (2004).
[34] W. S. M. Werner, Phys. Rev. B **71**, 115415 (2005).
[35] W. S. M. Werner, Surf. Sci. **526**, L159 (2003).
[36] W. S. M. Werner, C. Eisenmenger-Sittner, J. Zemek, and P. Jiricek, Phys. Rev. B **67**, 155412 (2003).
[37] W. S. M. Werner, Surf. Interface Anal. **35**, 347 (2003).
[38] W. S. M. Werner, H. Störi, and H. Winter, Surf. Sci. **518**, L569 (2002).
[39] W. S. M. Werner, Phys. Rev. B **55**, 14925 (1997).
[40] W. S. M. Werner, Surf. Sci. **588**, 26 (2005).
[41] W. H. Press, S. A. Teukolsky, W. T. Vetterling, and B. P. Flannery, *Numerical Recipes* (Cambridge University Press, Cambridge, 1986).
[42] S. Tanuma, C. J. Powell, and D. R. Penn, Surf. Interface Anal. **21**, 165 (1994).
[43] W. S. M. Werner, W. Smekal, C. Tomastik, and H. Störi, Surf. Sci. **486**, L461 (2001).
[44] W. S. M. Werner, Surf. Sci. **601**, 2125 (2007).
[45] W. S. M. Werner, Surf. Sci. (accepted for publication).
[46] Y. F. Chen, C. M. Kwei, and C. J. Tung, Phys. Rev. B **48**, 4373 (1993).
[47] W. S. M. Werner and M. Hayek, Surf. Interface Anal. **22**, 79 (1994).
[48] C. J. Powell and A. Jablonski, J. Phys. Chem. Ref. Data **28**, 19 (1999).
[49] R. Oswald, Ph.D. thesis, Eberhard-Karls-Universitäat Tübingen, 1992.
[50] R. Schmid, Ph.D. thesis, University of Tübingen, 1982.
[51] W. S. M. Werner, C. Tomastik, T. Cabela, G. Richter, and H. Störi, J. Electron Spectrosc. Relat. Phenom. **113**, 127 (2001).
[52] A. Dubus, A. Jabłonski, and S. Tougaard, Prog. Surf. Sci. **63**, 135 (2000).
[53] M. Vos (private communication).
[54] F. Salvat, Phys. Rev. A **68**, 012708 (2003).
[55] F. Yubero and S. Tougaard, Phys. Rev. B **46**, 2486 (1992).
[56] F. Yubero, J. M. Sanz, B. Ramskov, and S. Tougaard, Phys. Rev. B **53**, 9719 (1996).
[57] N. Pauly, S. Tougaard, and F. Yubero, Phys. Rev. B **73**, 035402 (2006).
[58] W. S. M. Werner, M. R. Went, and M. Vos, Surf. Sci. **601**, L109 (2007).
[59] G. Williams, *X-ray Data Booklet* (Lawrence Berkeley National Laboratory, University of California, Berkeley, CA, 2001).
[60] M. R. Went, M. Vos, and W. S. M. Werner, Surf. Sci. **602**, 2069 (2008).
[61] M. Novak, Ph.D. thesis, University of Debrecen, 2008.
[62] H. Winter and J. Burgdörfer, *Slow Heavy Particle Induced Electron Emission from Solid Surfaces*, Springer Tracts in Modern Physics Vol. 225 (Springer, New York, 2007).
[63] D. R. Penn, Phys. Rev. B **35**, 482 (1987).
[64] C. J. Tung, R. H. Ritchie, J. C. Ashley, and V. E. Anderson, Oak Ridge National Laboratory No. Report No. 5188, 1976.
[65] S. Tanuma, C. J. Powell, and D. R. Penn, Surf. Interface Anal. **11**, 577 (1988).
[66] Y. Lin and D. C. Joy, Surf. Interface Anal. **37**, 895 (2005).
[67] L. Reimer, *Scanning Electron Microscopy* (Springer, Berlin, 1985).
[68] A. Jablonski, S. Tanuma, and C. J. Powell, Surf. Interface Anal. **38**, 76 (2005).
[69] S. Tanuma, C. J. Powell, and D. R. Penn, Surf. Interface Anal. **37**, 978 (2005).
[70] W. S. M. Werner, Phys. Rev. B **52**, 2964 (1995).
[71] W. S. M. Werner, T. Cabela, J. Zemek, and P. Jiricek, Surf. Sci. **470**, 325 (2001).
[72] S. Tougaard, Surf. Interface Anal. **25**, 137 (1997).
[73] E. D. Palik, *Handbook of Optical Constants of Solids* (Academic, New York, 1985).
[74] C. J. Powell and M. P. Seah, J. Vac. Sci. Technol. **8**, 735 (1990).
[75] C. J. Powell, W. S. M. Werner, and W. Smekal, Appl. Phys. Lett. **89**, 252116 (2006).
[76] S. Tanuma, C. J. Powell, and D. R. Penn, Surf. Interface Anal. **17**, 927 (1991).
[77] S. Tanuma (private communication).
[78] W. S. M. Werner, C. Tomastik, T. Cabela, G. Richter, and H. Störi, Surf. Sci. **470**, L123 (2000).
[79] Y. F. Chen, Surf. Sci. **519**, 115 (2002).